THE RELATIONS BETWEEN THE X-RAY SPECTRAL PARAMETERS OF GAMMA-RAY BURSTS

by

Ece Kilerci

B.S., Astronomy and Space Sciences, Istanbul University, 2005

B.S., Physics, Istanbul University, 2005

Submitted to the Institute for Graduate Studies in
Science and Engineering in partial fulfillment of
the requirements for the degree of
Master of Science

Graduate Program in Physics

Boğaziçi University

2009

ACKNOWLEDGEMENTS

I am thankful to my thesis advisor Prof. Dr. E. Nihal Ercan for all her help. I am very thankful to Prof. Guido Chincarini who supported me to do my thesis on Gamma-Ray Bursts and to work with him and his colleagues. I thank Raffaella Margutti, Prof. Sergio Campana, Dr. Christiano Guidorzi and all the Italian Swift team for their patience and excellent guidance.

ABSTRACT

THE RELATIONS BETWEEN THE X-RAY SPECTRAL PARAMETERS OF GAMMA-RAY BURSTS

Gamma-Ray Bursts (GRBs) are the most energetic explosions in the universe. They are thought to arise from massive stellar explosions or mergers of compact objects. As a result of these processes a black hole and an acretion disk is formed and their interaction produces a relativistic jet in which gamma-rays are generated. GRB afterglows in X-rays, optics, radio bands are thought to be produced by the interaction between the relativistic jet and the interstellar medium (ISM). X-ray afterglow spectra are generally fit by a photoelectrically absorbed simple power law model (ASPL) that can be modeled using three parameters. These parameters are the Galactic neutral Hydrogen column density (N_H), the intrinsic Hydrogen column density (N_{Hint})and the power law photon index (Γ) (apart from the normalization). In this thesis the X-ray spectral parameters evolution in time and their relations in the ASPL model are studied for a selection of 28 GRBs observed by Swift XRT up to May 2008. In this way we test the efficiency of the ASPL model to adequately fit the GRB X-ray afterglow spectra. In 17 bursts the fits show variations that includes a increasing N_{Hint} with time which is nonphysical. For two burst we found a very significant correlation between the N_{Hint} and the Γ, while for 9 bursts we found a hint for a correlation between the N_{Hint} and the Γ. Finally, for 2 burst we found a hint for anti-correlation between the N_{Hint} and the Γ. We conclude that the increasing N_{Hint} variation is due to a non-physical effect induced by the fitting procedure. We stress that an ASPL model, while able to adequately fit the vast majority of X-ray spectra, induces a spurious relation between the N_{Hint} and the photon index. This is partially due to the limited energy range of the XRT (0.3–10 keV). We remark that the anti-correlation relations are interesting and the possible physical effect during the early phase should be investigated.

ÖZET

GAMA IŞIN PATLAMALARININ X IŞIN TAYFLARI PARAMETRELERİ ARASINDAKİ İLİŞKİLER

Gama ışın patlamaları (GIP) evrendeki en yüksek enerjili patlamalardır. GIP'nın büyük kütleli yıldızların patlamaları veya kompakt nesnelerin birleşmelerinden oluştukları düşünülmektedir. Bu süreçlerin sonucunda bir karadelik ve etrafında yığılma diski oluşmaktadır ve bunların etkileşmesi gama ışınlarını üreten relativistik jeti meydana getirmektedir. GIP X-ışını, optik, radyo bölgelerindeki ardıl ışımaları yıldızlararası ortam ve relativistik jetin etkileşmesiyle oluşurlar. X-ışın ardıl ışıma spektrumları düşük X-ışın enerjilerinde fotoelektriksel soğurmanın olduğu, üç parametresi olan soğurmalı basit güç kanunu (SBGK) ile fit edilir. Bu parametreler, Galaktik Hidrojen kolon yoğunluğu, kaynağın kendi galaksisindeki Hidrojen kolon yoğunluğu (N_{Hesas}) ve güç kanununun indeksidir (Γ) (normalizasyon dışında). Bu tezde Swift uydusunun XRT dedektörü ile Mayıs 2008 ayına kadar gözlenmiş, seçilen 28 GIP için SBGK modelindeki X-ışın spektral parametrelerinin zamanla değişimi ve bu parametreler arasındaki ilişki incelenmiştir. Bu yol ile SBGK modelinin GIP X-ışın ardıl ışımaları için yeterliliği test edilmiştir. 17 GIP için N_{Hesas} değerinde fiziksel olmayan bir artış gözlenmiştir. Dokuz GIP için N_{Hesas} ve Γ arasında korelasyona dair ipucu, iki GIP için N_{Hesas} ve Γ arasında çok güçlü bir korelasyon ve iki GIP için N_{Hesas} ve Γ arasında anti-korelasyona dair ipucu bulunmuştur. Bu tezin sonucunda, artan N_{Hesas} değişimlerinin spektral fit süreciyle ortaya çıkan fiziksel olmayan bir etki olduğu görülmüştür. SBGK GIP X-ışın ardıl ışıma spektrumlarını büyük ölçüde yeterli olarak ifade etsede, N_{Hesas} ve Γ arasında fiziksel olmayan bir korelasyon ortaya çıkardığını vurgulamaktayız. Bunun nedenlerinden biri XRT dedektörünün (0.3-10 keV) sınırlı enerji aralığıdır. Bulunan anti-korelasyon ilişkilerinin ilginç olduğunu ve erken evrede oluşan bir fiziksel etkiyle ilişkisinin araştırılması gerektiğini belirtmekteyiz.

TABLE OF CONTENTS

LIST OF FIGURES

LIST OF TABLES

LIST OF SYMBOLS/ABBREVIATIONS

eV	Electron volt
H_0	Hubble constant
keV	Kilo electron volt
$L_\odot$	Solar luminosity
m	Meter
$M_\odot$	Solar mass
N_H	Neutral Hydrogen Column density
N_{Hint}	Intrinsic Neutral Hydrogen Column density
t	Time
z	Redshift
$Z_\odot$	Metal abundance with respect to Sun
α	Slope of the GRB light curve
β	Photon spectral energy index
ν	Frequency
Γ	Power law photon index
BAT	Burst Alert Telescope
BATSE	Burst And Transient Source Experiment
BeppoSAX	Satellite per Astronomia X, "Beppo"in honor of G. Occhialini
CCD	Coupled Charge Device
GRB	Gamma-ray burst
GRBs	Gamma-ray bursts
CRGO	Compton Gamma-Ray Observatory
HETE	High Energy Transient Explorer
ISM	Interstellar medium
SWIFT	Swift Satellite
XRT	X-Ray Telescope

1. INTRODUCTION

Gamma-ray bursts (GRBs) are bursts of gamma-rays from the distant galaxies. GRBs emit huge amounts of energy (between $10^{52} - 10^{54}$ erg) in very short times (0.1 - 100s). Their energy is equivalent to the total energy that 1.000 sun-like stars produce during their life time. They are seen in random directions, this is related to their extra-galactic nature. Their prompt light curve is quite irregular, different bursts having completely different light curves. Some of them show a unique smooth, fast-rise and exponential decay while others are characterized by different peaks [1]. GRB spectra are non-thermal and well described by a smoothly joint broken power law called as Band function [2]. GRBs have counter part emissions in radio, optic and X-ray band; this is the afterglow emission. Gamma-ray bursts happen at cosmological distances. The highest measured GRB redshift is 8.2. This is the most distant object observed in the universe.

GRBs are believed to be formed either from the collapse of a super massive star or from the merging of compact object binaries. The observed gamma-rays are thought to be formed by shocks inside a highly relativistic jet created by a black hole torus system which is formed by the collapse of the progenitor. The afterglow emission is explained as a result of the interaction between the relativistic shock and the ISM when the relativistic shock enters the surrounding medium. The X-ray emission produced during the interaction with the ISM has a non-thermal spectrum which is generally fit by a power law model which has two absorption contributions, the Galactic and the intrinsic absorption at the sources redshift. When there are enough photons, the time-resolved spectral analysis is a great tool to see the behaviour of these sources. The GRB is expected to ionize the ISM; the neutral N_H is therefore expected to decrease with time. The time scales of this process are very short. From the theoretical point of view the N_H must decrease in a very short time and should be constant later [3]. Nevertheless claims of a decreasing N_H at $t \sim 1000s$ (in the rest frame) can be found in the literature [4]. It is interesting to note that claims of an increasing N_H can also be found [5]. We consider such a behaviour nonphysical.

In this work, we investigate the evolution of the best fit X-ray spectral parameters (N_H and Γ) of GRB X-ray afterglows observed by Swift using time-resolved spectral analysis. We show that the spectral fitting procedure induces a spurious positive correlation between two parameters: the N_H and the Γ (Figure 2.30). Since we have a physical constraint on N_H, we look for a correlation between the N_H and the Γ to explain the N_H increase as a spurious effect. We choose 28 (Table 3.3) GRBs detected by Swift with XRT observations and with known redshifts. We require these bursts to have at least five spectra.

In the first chapter, the historical, observational and theoretical background of GRBs are presented. The second chapter is devoted to the physical background of the X-ray spectral parameters (N_H and Γ). In the third chapter, we presented the Swift satellite, together with the methodology to deal with the data and properties of GRBs in our sample. The fourth chapter contains the results of our analysis on N_H variation, Γ variation and N_H and Γ correlation. In the last chapter, the results are discussed.

1.1. Historical Background

1.1.1. Discovery: 1967-1990

GRBs were discovered in the 1960s, when gamma-ray detecting satellites were flown to watch out the Partial Test Ban Treaty by the world superpowers. Treaty was signed to guarantee that nuclear weapons would not be tested in underwater, atmosphere, or outer space. The US Air Force sent into orbit the first of a series of satellites called Vela. Vela had X-ray, Gamma-ray, and neutron detectors on-board. In 1967 Vela discovered unknown Gamma-rays from the outer space (Figure 1.1). In 1973 these unknown signals were announced as Gamma-ray bursts [6]. This announcement is verified by other satellites and GRBs took their place in the astronomy literature. GRBs are named as year-month-day like GRB050904 and for more than one GRBs in a day, a, b, c letter are added to the end, such as GRB080319B.

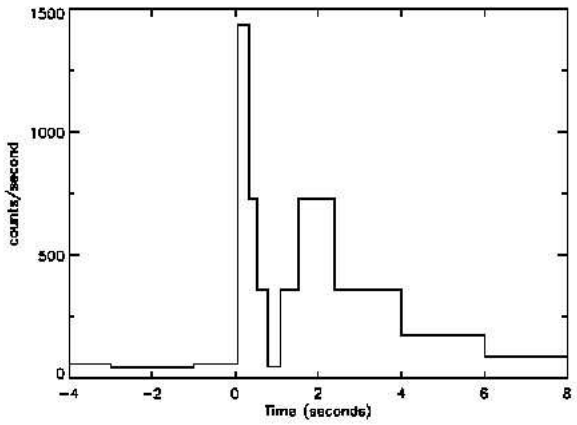

Figure 1.1. The first GRB detected in 1967 [6]

By mid 1990s hundreds of different theories offered to explain this mysteries Gamma-ray emission [7]. Although the number of models were more than the number of detected GRBs during this period GRBs could not be understood in any aspect.

1.1.2. CRGO Era: 1991 - 1996

The BATSE component of the CGRO [8] made crucial observations that showed that the distribution of 2,700 GRBs in the sky was isotropic; they were not simply coming from a specific region (Figure 1.2) [9]. The frequency of BATSE GRBs was roughly two per day [8].

The isotropic distribution of the GRBs in the sky showed that, probably they were not coming from Milky Way or nearby [10]. If they were coming from our own galaxy, they would be expected to be seen in the disk of Milky Way which has the highest stellar population.

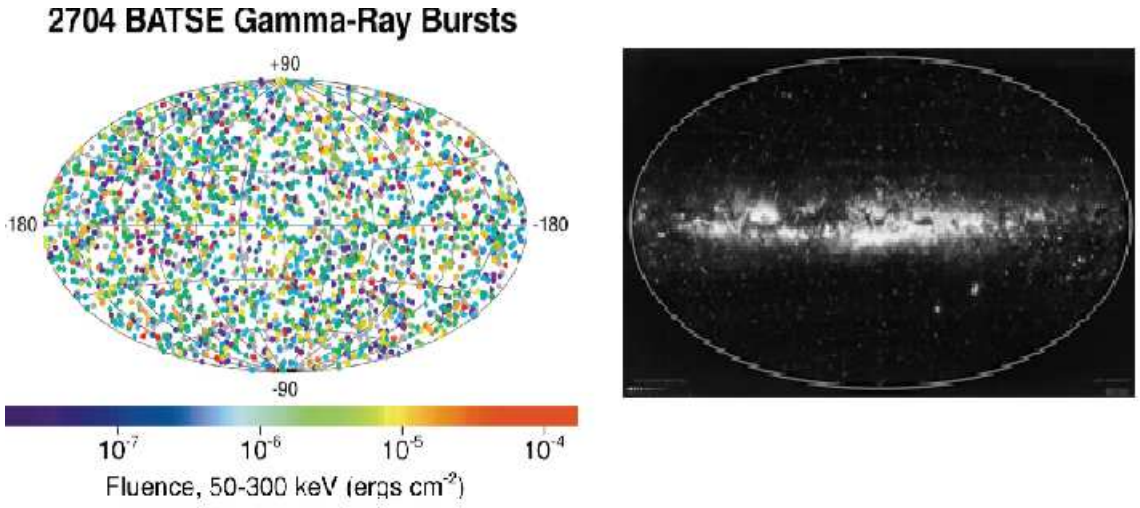

Figure 1.2. BATSE GRB distribution on the sky (left) and the Milky Way (right) [9]

At that time there were debates on distances of GRBs. Since the luminosity depends on the distance, the observed GRB luminosity would be $\sim 10^{42}(erg/sec)$ if they were galactic sources and $\sim 10^{51}(erg/sec)$ if they were at cosmological distances [11]. When BATSE showed the first clue for cosmological distance, GRBs become the candidate to be the most luminous object in the universe.

The second major observational result of the CGRO was the bimodal distribution of GRBs in terms of duration (Figure 1.3) and hardness (see section 2.3.1) (Figure 1.4). BATSE team technically defined T_{90} as the time interval within which (90%) of

burst fluence is detected [12] and GRBs are classified as long/soft bursts if they have $T_{90} > 2sec$ and as short/hard bursts if they have $T_{90} < 2sec$ [1, 13].

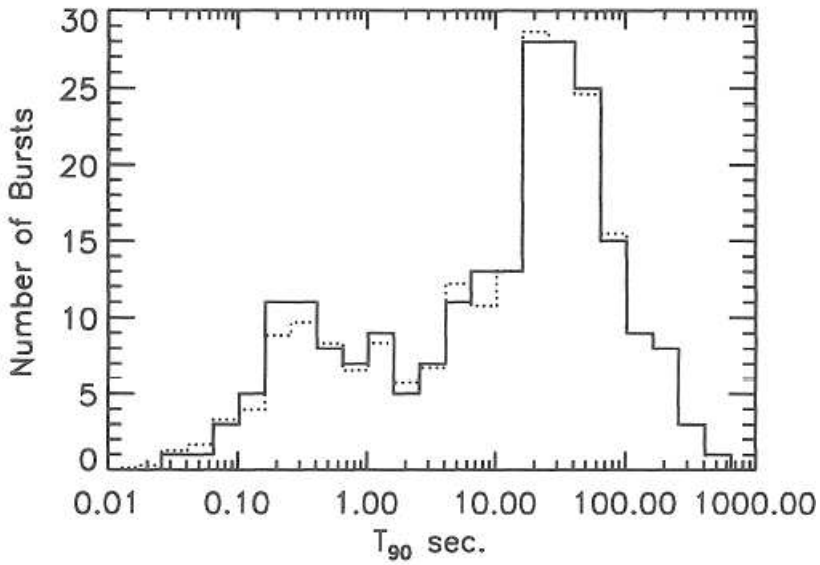

Figure 1.3. T_{90} distribution of 222 GRBs in the first BATSE catalog [13]

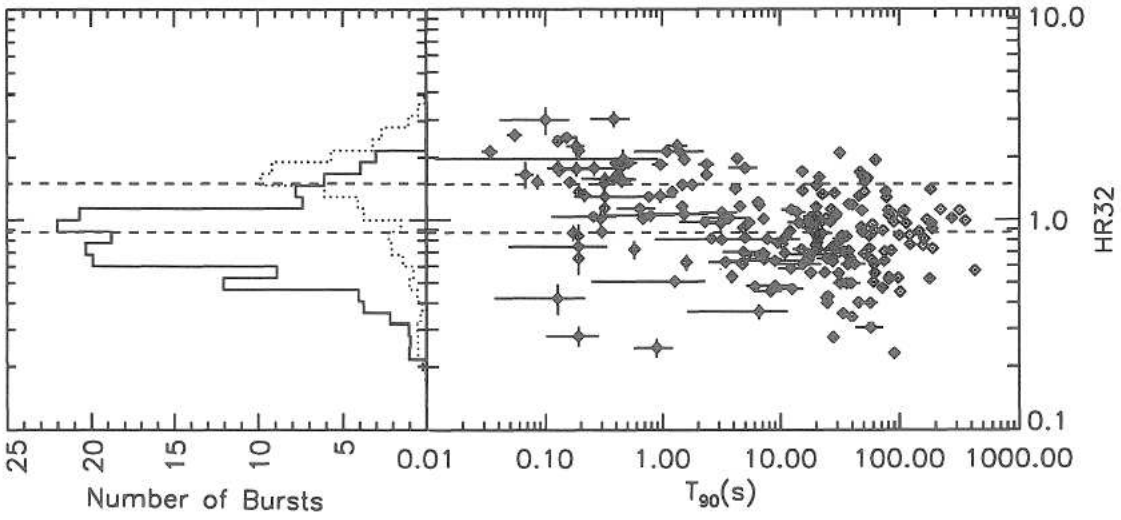

Figure 1.4. Hardness versus duration of BATSE GRBs [13]

At that time only the short domain temporal behavior of GRBs was known. The long term behavior after the Gamma-ray radiation was a big mystery.

1.1.3. BeppoSAX - HETE Era: 1997 - 2003

BeppoSAX satellite [14] was composed of Gamma-ray burst monitor and X-ray cameras that were able to give the first fast and precise position of GRBs. The most important discovery of BeppoSAX is the X-ray (Figure 1.5) [15], optical [16] (Figure 1.6) and radio [17]afterglows of long GRBs which were detected after several hours. The observed afterglows were predicted by the fireball model before their discovery [18–21].

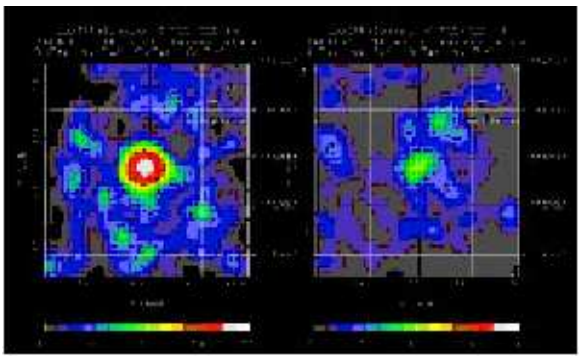

Figure 1.5. Beppo-SAX satellite discovery of the first GRB X-Ray afterglow emission [15]

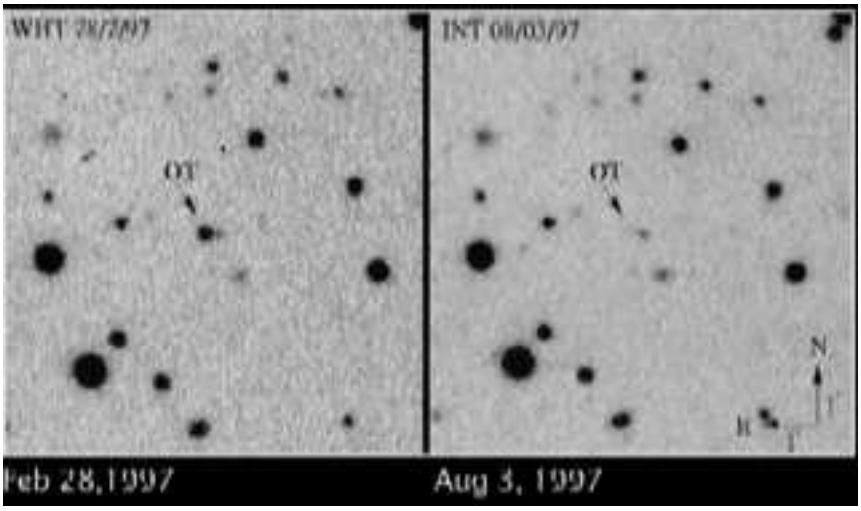

Figure 1.6. First optical afterglow detected by William Herschel Telescope [16]

In the generic fireball shock model, regardless the central engine or the progenitor, a relativistic jet is produced. In this relativistic flow internal shocks produce Gamma-rays while the afterglow is produced by external shocks as the jet enters the interstellar

medium (ISM) [18–21]. In this model synchrotron radiation is the main emission mechanism that produces both Gamma-rays and X-rays [22]. A typical X-ray and optical light curve of a GRB in this era is given in figure 1.7, the afterglows are typically characterized by a power law behavior in time and in frequency, i.e. the observed flux is $F \approx t^{\alpha}\nu^{\beta}$ [23]. Through the spectroscopy of the optical afterglows GRB host galaxy

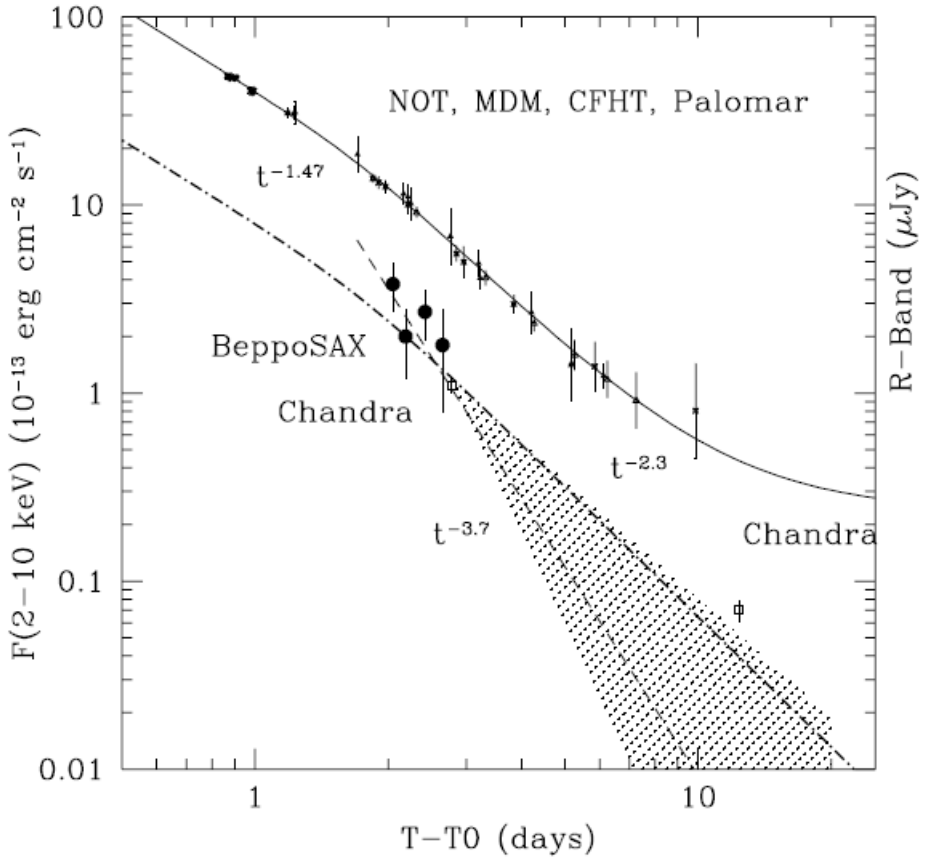

Figure 1.7. The X-ray and optical light curves of GRB 000926 afterglow [23]

detection and redshift measurements (Figure 1.8) became available [24]. The redshift measurement from the host galaxy spectral lines proved that GRBs are at cosmological distances and this pointed out that they are the most violent luminous explosions in the universe after Big Bang. The supernova association seen in optical light curves with some long GRBs is the second major discovery of this period. The first supernova association is seen between GRB980425 and SN1998w [26, 27]. This association is confirmed by the light curve and the spectrum (Figure 1.9) [26]. The feature of the supernova is seen as a bump in the optical afterglow which is called as red supernova

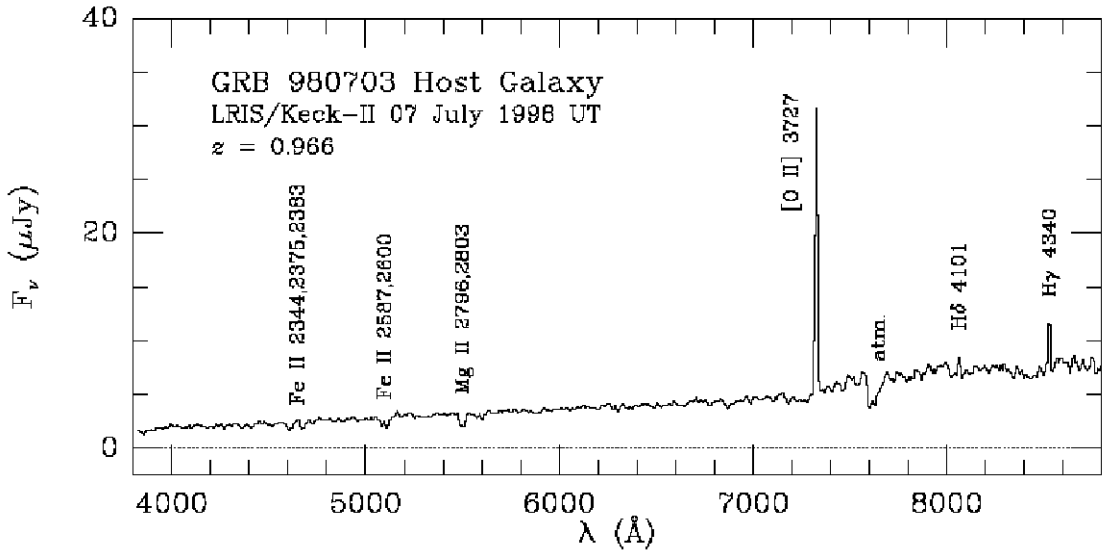

Figure 1.8. Host galaxy spectrum of GRB 980703 [25]

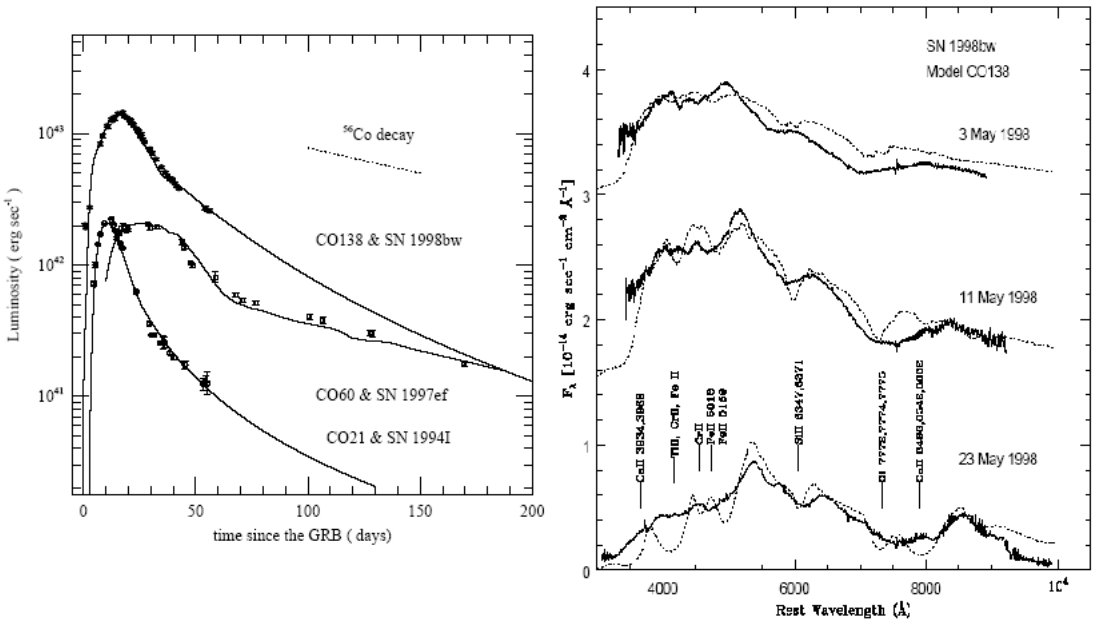

Figure 1.9. Light curve and spectrum of SN 1998bw defines a type Ic supernova [26]

bump (Figure 1.10) and it is used in other GRB optical afterglow light curves to find out the possible supernova connection [28–30]. Supernova association with long GRBs is interpreted as a proof that long duration GRBs are connected to collapses of massive stars [31, 32]. Collapsar model (Figure 1.11) proposed that supernovae are generic to all long GRBs [33, 34]. The third major discovery in the BeppoSAX - HETE era is

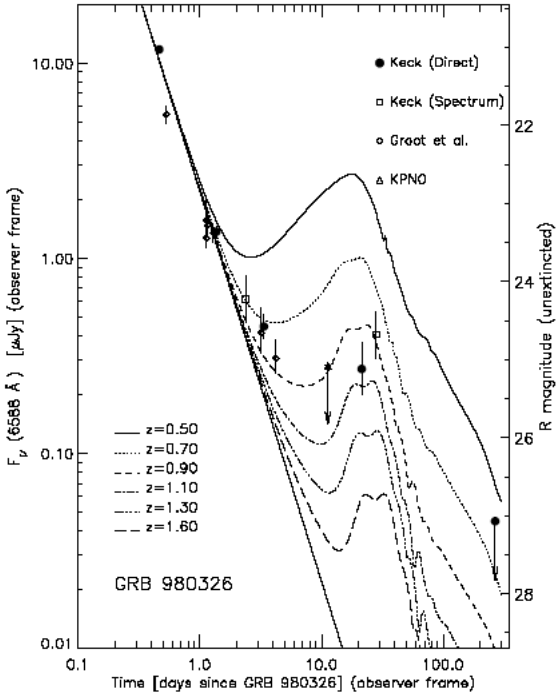

Figure 1.10. GRB 980326 Light curve [28]

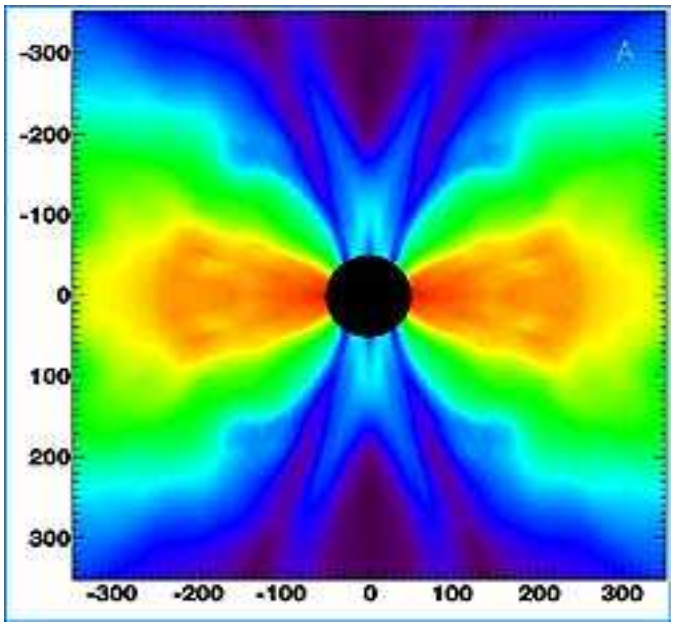

Figure 1.11. Simulation of Collapsar model [34]

the collimation of jet structure in the afterglows [35]. In most of the optical and X-ray afterglow light curves a break or a steepening is seen (Figure 1.12). This feature is explained as being due to a jet-like relativistic outflow with respect to Lorentz factor

(Figure 1.13) [36]. As the outflow slows down the edge of the jet becomes visible and this is seen as a jet break in the light curve [37, 38]. More complex jet models

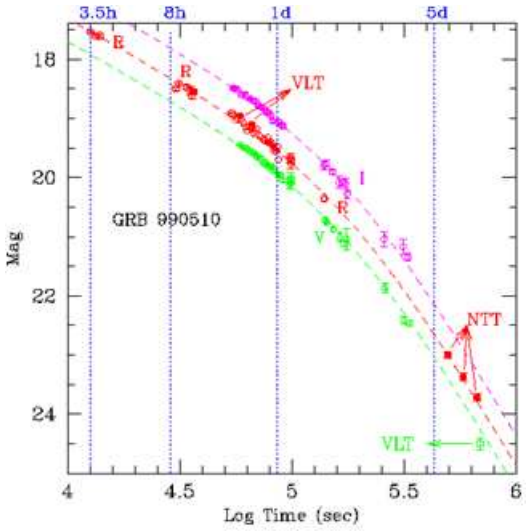

Figure 1.12. Jet break in GRB 990510 optical afterglow [39]

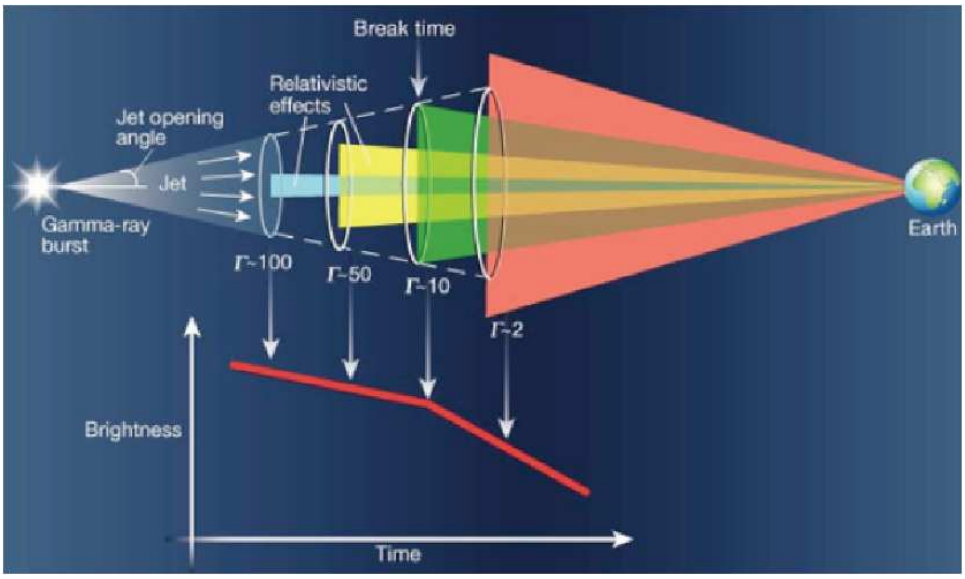

Figure 1.13. Jet break explanation for the light curve [40]

are also discussed which are not completely uniform and have a energy distribution with respect to jet opening angle [41, 42]. During the BeppoSAX-HETE era, the GRB observations became much wider. Both in the spectral and long term temporal domain a very broad band data starting from X-rays to optical and radio became available. In the BeppoSAX-HETE era there was a couple of hours of gap at the starting of

afterglow observations. Confronting data with theory this period was very successful in terms of the light curves. The generic fireball model [18–21] explained the data well. The remaining mysteries were the prompt emission explanation and the properties of the early afterglow phase which starts just a few minutes after the prompt Gamma-ray emission.

1.1.4. SWIFT Era: 2004 -

Swift [43] is a great observatory with major advantages such as sensitivity of the Burst Alert Detector (BAT) [78] and the fast slew capability in less than 100 seconds towards the GRB direction. One of the most important Swift discoveries is the detection of the short GRB X-ray [47] and optical [45, 46] afterglows.

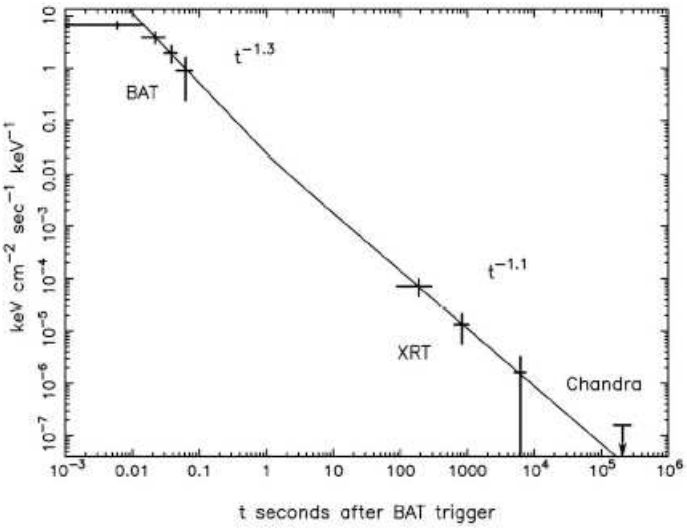

Figure 1.14. The first X-ray afterglow light curve for a short bursts [47]

Short GRBs optical afterglows provided short GRB host galaxies for several bursts (Figure 1.15) (Figure 1.16) [45, 48]. In figure 1.15 on the left, the bright point source in the boxed region is the X-ray afterglow of GRB050709. On the right, red circle is the optical afterglow and the irregular galaxy to its west is the host galaxy. In figure 1.16 host galaxy of GRB050724 is an elliptical galaxy with ellipticity is about 0.17, indicating an E2 Hubble classification [48].

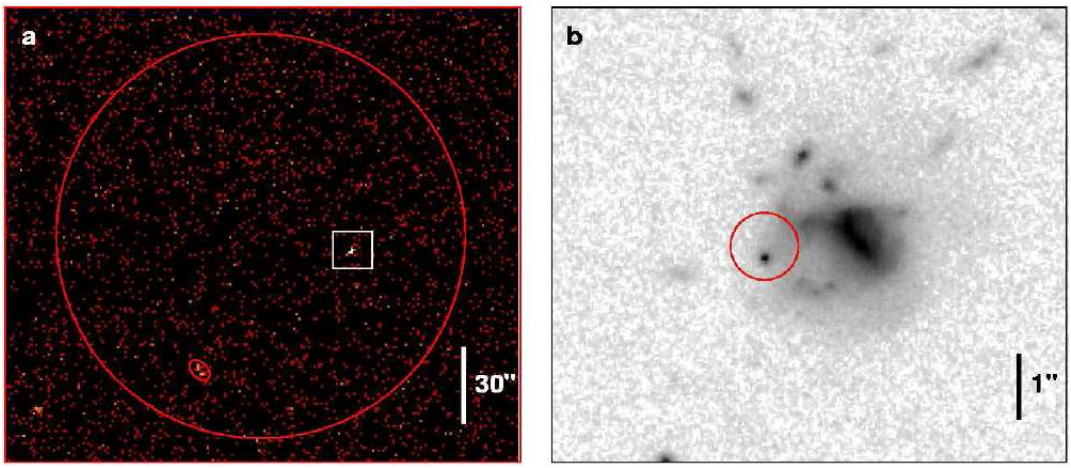

Figure 1.15. Hubble Space Telescope (HTS) and Chandra X-ray Observatory images of the afterglow of GRB050709 [45]

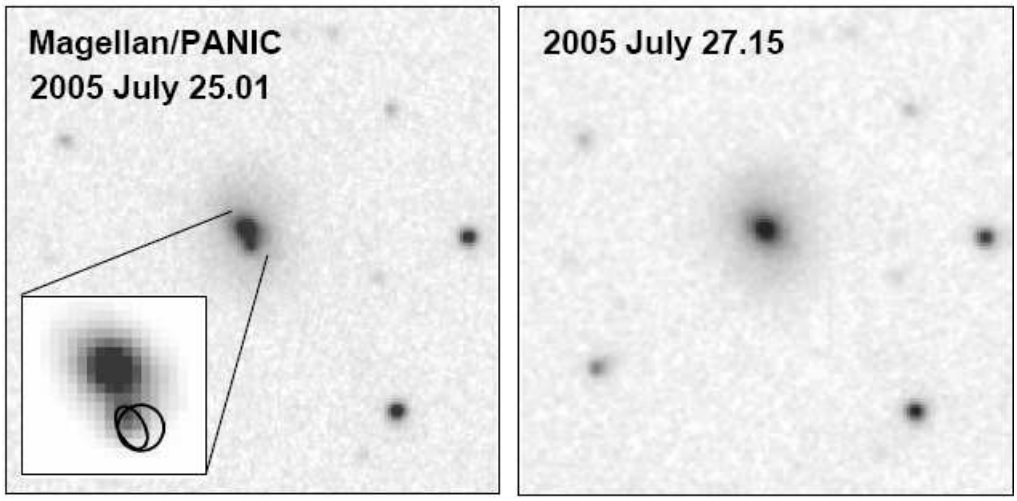

Figure 1.16. Host galaxy of GRB050724 [48]

The short GRB host galaxies mostly defined as elliptical or star forming galaxies [48, 49]. This supported the idea that the origins of short GRBs is different from those of long GRBs [47, 50, 51]. The leading model for short GRBs origin involves two compact objects mergers such a neutron star/neutron star or a black hole/ neutron star binary [52–55]. Although the general properties of short GRB observations were consistent with compact object mergers model, some bursts such as GRB050724 showed different X-ray afterglow features (Figure 1.17) that were challenges to merger model [44].

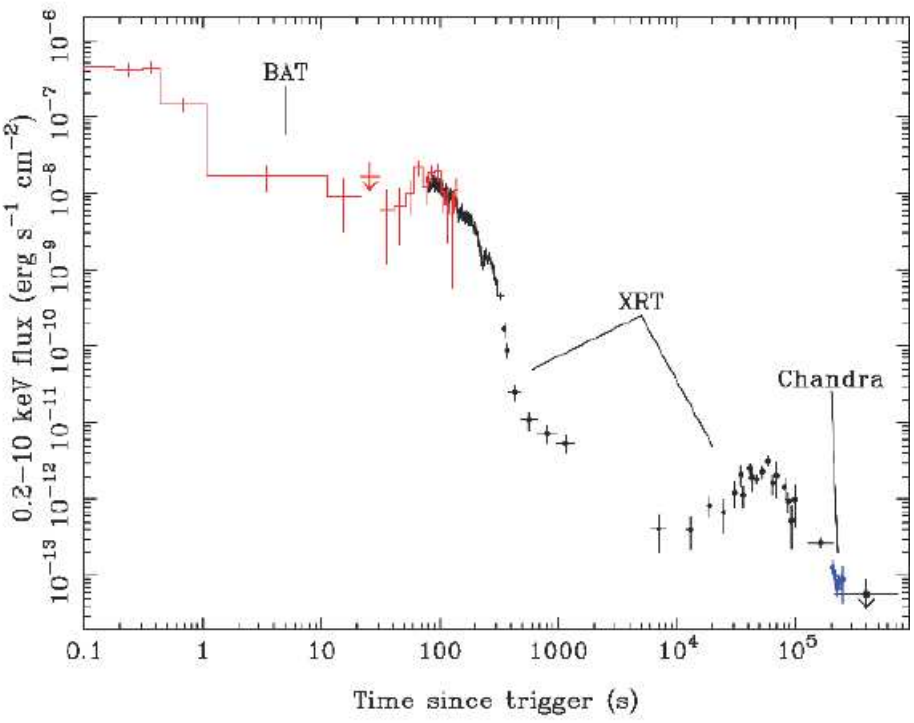

Figure 1.17. Prompt emission and X-ray afterglow light curve of GRB050724 [44]

With the Swift, for the first time, very early afterglow data starting from tens of seconds can be obtained. The second major discovery of the Swift is the early X-ray afterglow that shows new unexpected properties such as a canonical X-ray light curve (Figure 1.18) [56, 57]. The canonical X-ray light curve with several components [57, 58] reveals a more complex afterglow emission with new additions to the standard fireball model [57, 59].

The third important result of the Swift observations is the diversity of GRBs. The previous classification of GRBs was deficient to explain new observations of Swift [61, 62]. One of these observations was the nearby (redshift of 0.125) long burst GRB 060614 that was detected without supernova association [61, 63, 64, 65], while associated supernova had been seen in all other nearby long GRBs [61]. The host galaxy of GRB 060614 has a relatively low star forming rate according to general long GRB hosts [63–65]. This burst has $T_{90} \sim 100s$ and it is defined as a long burst; but GRB 060614 showed some characteristic properties of the short GRBs [61, 66]. The optical, UV and X-ray afterglows of GR060614 agree with standard jetted fireball models [67]. The

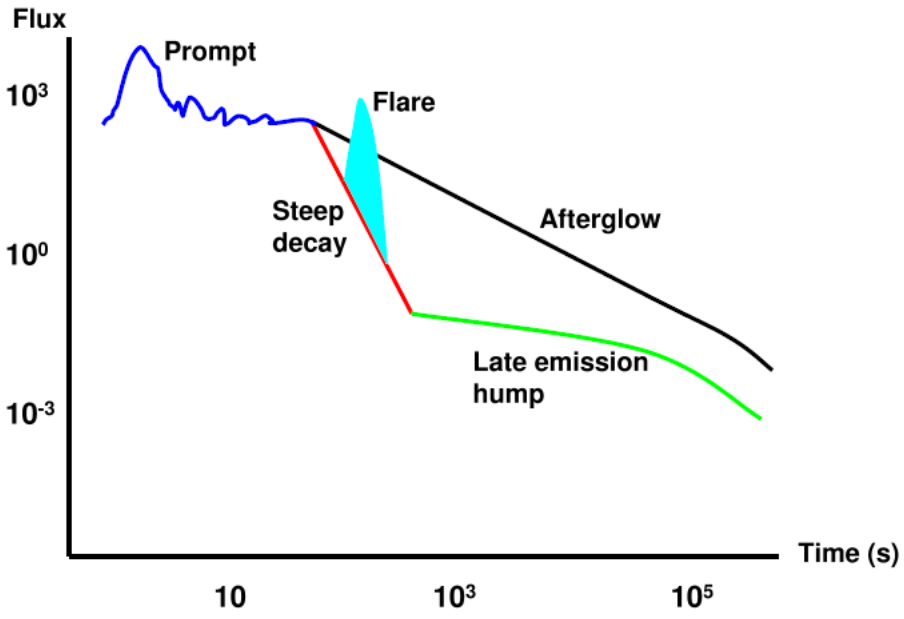

Figure 1.18. Schematic view of typical Swift X-ray light curve [60]

whole observational properties of GRB060614 are not consistent with neither collapsar nor NS-NS merger model but might be consistent with NS-BH merger model; thats why GRB 060614 challenges current progenitor models [62].

GRB 060505 which is nearby (redshift of 0.089) [68] with a duration of 4 seconds without supernova association [64] and also caused a long/short division problem [68–70].

An other important Swift [43] burst is the GRB 080913 which is one of the most distant GRBs with redsifht of 6.7 [71]. GRB 080913 has a 2 seconds of duration and looks like a short/hard GRB [71]. The possible progenitor system of this burst is a question mark [71, 72].

With new observations, it is understood that duration and hardness were no longer enough to understand the physical nature of GRBs [73]. In the Swift era, one of the leading problems is how to understand physical origin of GRBs from the observational properties. To deal with this problem several methods are offered [59, 74, 75, 76]. Instead of long and short classification, Type I and Type II denote the two

physically distinct class of GRBs [75]. The properties of Type I and Type II GRBs depend on multiple observational criteria (Figure 1.19) [73]. GRB observations has

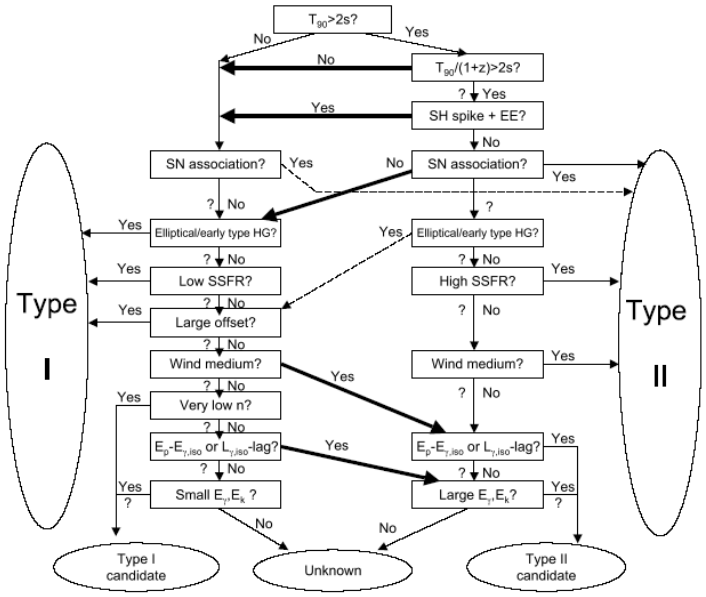

Figure 1.19. GRB classification table for multiple observational criteria [73]

entered a new era with Swift. The early afterglow properties are seen with details and they raised new questions on their physical origins. The classification schema changed with new observations. The very high energy component of the prompt emission and the physics of the prompt emission are the remaining problems to solve.

1.1.5. FERMI Era: 2008 -

The Fermi Gamma-ray Space Telescope (FGST) is launched on 11 June 2008. It's major task is to observe the Gamma-ray universe, including GRBs. The Large Area Telescope (LAT) onboard of the Fermi observatory can measure the energy, direction, and arrival time of Gamma-rays from 20 MeV to more than 300 GeV [77]. The Gamma-ray Burst Monitor (GBM) covers the energy range 10 keV to 30 MeV [77]. The major goal of the Fermi is to solve prompt emission and GRB composition by observing the very high energy emission. Fermi is hoped to improve the knowledge about the energetics and energy mechanisms of GRBs. In the following years GRBs will be one of the most important targets for the upcoming satellites such as SWOM.

1.2. Observational Properties of GRBs

Swift [43] was launched on November 24th 2004. It detects GRBs by the BAT (Burst Alert Telescope) [78]. The X-ray Telescope is able to repoint the source in a few tens of seconds. Swift [43] is detecting nearly 100 bursts per year. In this section, the observational properties of GRBs are described in two sections: the first is denoted to the prompt emission while the second to the afterglow emission. A general view of the phenomenon is offered, following the current leading model of explanation.

1.2.1. Prompt Emission

Prompt emission is the emission detected in Gamma-rays and any lower-energy emission that occurs simultaneously, namely the GRB itself. From the operational point of view the prompt emission is defined as the time period when the Gamma-ray detector detects a signal above the background.

1.2.1.1. Temporal Structure. The duration of the prompt Gamma-ray emission can be very short (like 0.01sec) or it can be long (up to 100sec). Prompt emission light curves are irregular: they do not have exactly common features to be generalized (Figure 1.20). In some prompt emission light curves, at the beginning a small pulse (Figure 1.21) before the main GRB with a lower peak flux is seen and it is called precursor [79]. Among Swift bursts up to March 2008, 15 GRBs have a precursor [79]. In the case of GRB 050820A [80], GRB 060124 [81] and GRB 061121 [82] their precursors triggered BAT and caused BAT to look the real GRB event before it happened. One possible interpretation of GRB precursors, related them to the initially trapped fireball emission in the fireball model [83–86]. Another possibility is that precursors are associated with the relativistic jet interaction with the stellar envelope in the collapsar model of the progenitor [87, 88]. Thirdly, the precursors are thought to be formed by the neutron star that is created by the collapse of the progenitor, afterwards the neutron stars collapse onto a black hole and generates the GRB [89]. The physical origin of the precursors and the relation of the precursor with the GRB event are still not known.

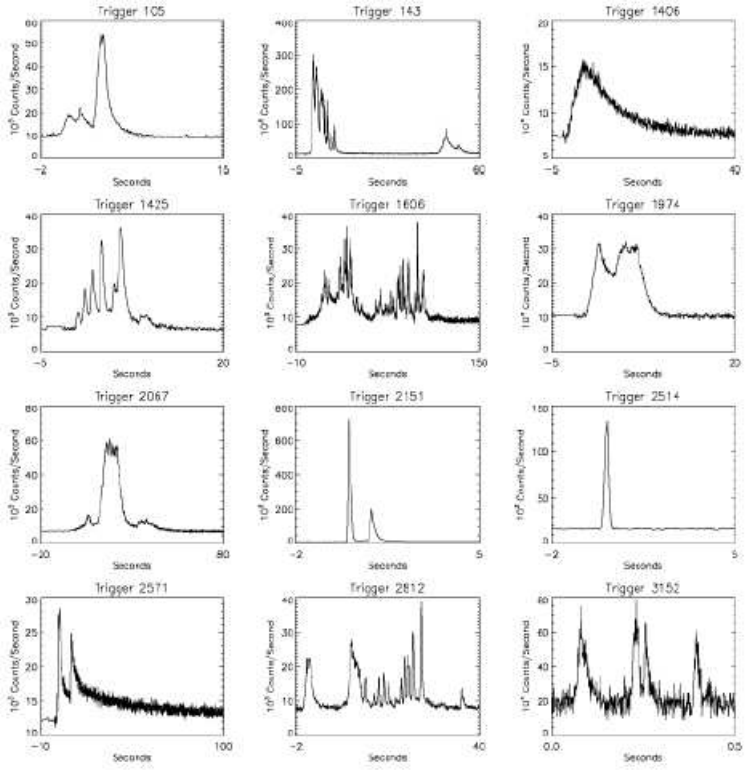

Figure 1.20. Prompt emission light curves. [1]

The light curves of the prompt emission show the change of the flux in time, namely the behavior of the mechanism that produces the gamma-rays.

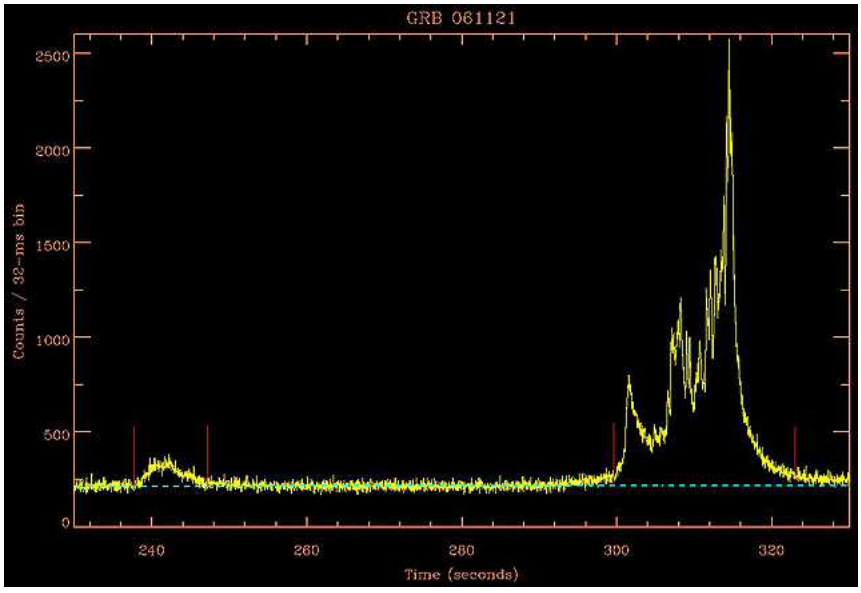

Figure 1.21. GRB 061121 prompt emission lightcurve [90]

1.2.1.2. Spectrum. The GRB Gamma-ray spectra are non-thermal. They are well described by two power laws joined smoothly at a break energy $(\alpha - \beta)E_0$, known as a Band-function (equation 1.1) [2]. Band model represents both the GRB prompt emission and the afterglow emission.

$$N(E) = \begin{cases} A\left(\frac{E}{100keV}\right)^{\alpha} e^{(-E/E_0)} & (\alpha-\beta)E_0 \geq E \\ A\left(\frac{(\alpha-\beta)E_0}{100keV}\right)^{(\alpha-\beta)} e^{(\beta-\alpha)} \left(\frac{E}{100keV}\right)^{\beta} & (\alpha-\beta)E_0 \leq E \end{cases} \tag{1.1}$$

Here α is the low energy photon index, β is the high energy photon index and E_0 is the transition energy of the spectrum (Figure 1.22). An important parameter is the E_{peak}, peak energy of the νF_ν spectrum. Swift BAT observations, showed that most of

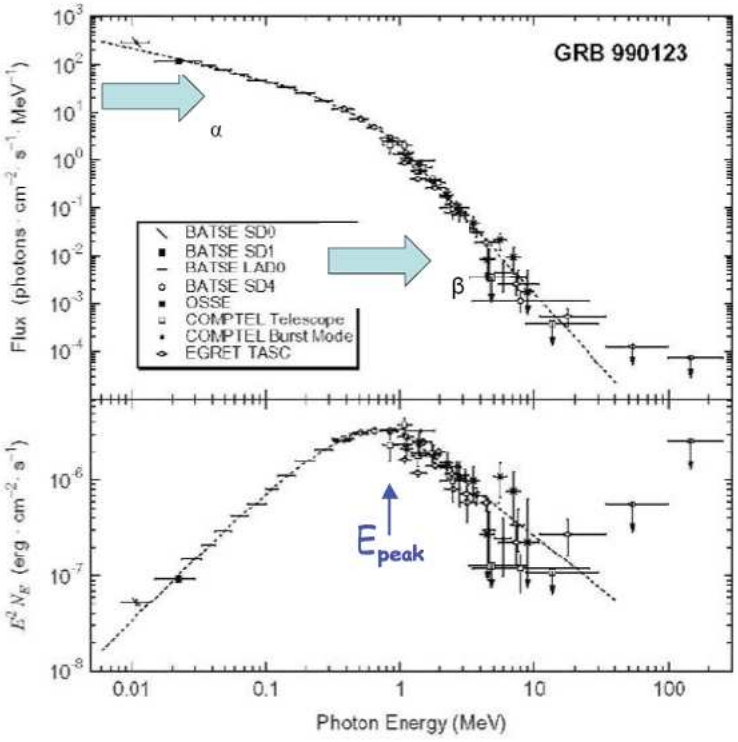

Figure 1.22. GRB spectrum fit Band function [91]

the Gamma-ray spectra can be fit by a simple power-law (PL) (see equation 1.2) and by a cutoff power-law (CPL) (see equation 1.3) model [92]. This is due to the pretty limited energy range (15 - 150 keV) of the BAT. A cutoff power law model is necessary

when the fit is not able to constrain the higher energy index of Band spectrum.

$$f(E) = K_{50}^{PL} \left(\frac{E}{50keV} \right)^{\alpha^{PL}} \tag{1.2}$$

In equation (1.2) α^{PL} is the power-law photon index and K_{50}^{PL} is the normalization at 50 keV in units of photons $cm^{-2}s^{-1}keV^{-1}$.

$$f(E) = K_{50}^{CPL} \left(\frac{E}{50keV} \right)^{\alpha^{CPL}} exp \left(\frac{-E(2+\alpha^{CPL}}{E_{peak}} \right) \tag{1.3}$$

In equation (1.3) α^{CPL} is the power-law photon index, E_{peak} is the peak energy in the νF_ν spectrum and K_{50}^{CPL} is the normalization at 50 keV in units of photons $cm^{-2}s^{-1}keV^{-1}$.

1.2.2. Afterglows

The afterglow emissions of GRBs were first discovered in 1997 by BeppoSAX. It turned out that GRBs have counterpart emissions in radio, optic and X-ray band. However until Swift [43], these afterglow emissions could be observed only after several hours from the trigger; Swift can re-point the source in less than 100s. Swift [43] ushered in a new era, discovering the early properties of GRB afterglows: the steep decay [93] and flares [94]. A brief description of the properties of GRBs afterglow emission is given below: both temporal and spectral characteristic will be discussed.

1.2.2.1. X-Ray Afterglows. The most important Swift discovery in X-ray afterglows is the early X-ray emission and unexpected behaviors [57]. The generic behavior of the light curve (Figure 1.23) is composed of five different power-law segments (with "0"indicates the prompt emission [59]). Most of the afterglows show a steep decay phase ("I"in figure 1.23) around 100-1000 seconds after the burst trigger [44, 93, 95, 96]. This phase is interpreted as the *tail* of the prompt emission [44, 58, 97] since it smoothly connects to the prompt emission light curve extrapolated to the X-rays. The time-averaged spectral index of this phase is different from that of the later phases and this

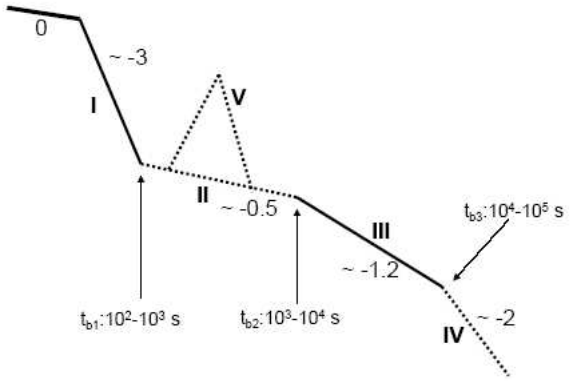

Figure 1.23. X-ray lightcurve based on the Swift XRT observations [59]

is explained as a distinct new component which is not related to the afterglow [59, 98]. The decay slope is given as between 3 - 5 if the GRB trigger time is taken as the zero time point [57, 59, 93]. The characteristic features of the steep decay phase suggest that it is important for the connection between differently originated prompt emission and the afterglow emission. Generally a strong spectral evolution feature is observed in the X-ray *tails* [5, 99].

The steep decay phase is generally followed by a flatter component called shallow decay phase ("II"in Figure 1.23). The shallow decay phase can also be seen directly after the prompt emission [58, 100]. During this phase generally the spectral index does not change [57], but there some cases spectral evolution has been detected [100]. The X-ray afterglow shows sudden re-brightening called X-ray flares (Figure 1.24) at random times between a few hundred seconds up to thousands of seconds [94, 101, 102]. There can be multiple flares in the light curves [103]. Flares have fast rise and decay times [104]. Spectral evolution is always observed during the flares. In some cases X-ray flare fluence is comparable to that of the prompt emission [101]. Flares are seen in both long and short bursts. The normal decay phase ("III"in Figure 1.23) usually has a decay slope of about -1.2. This phase follows the theoretical predictions from the pre-Swift era. After normal decay phase, in some rare cases [105] the post-jet break phase is seen ("IV"in 1.23) which is again a prediction from the pre-Swift era.

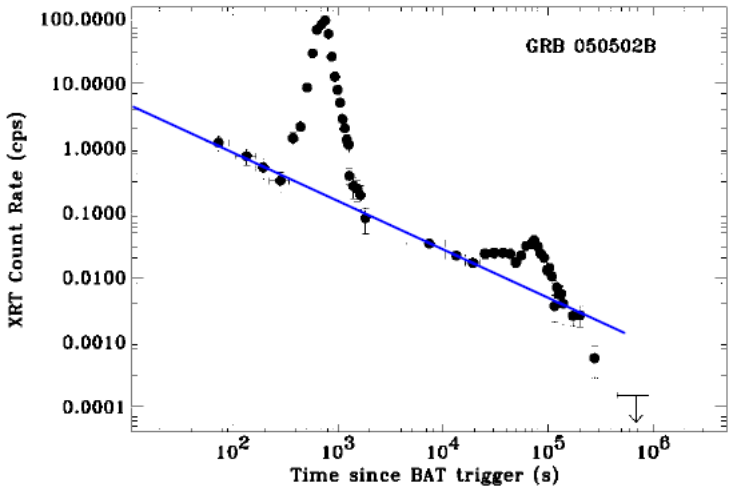

Figure 1.24. X-ray Flares in GRB 050502B light curve [101]

The Band model [2] is thought to represent also the X-ray afterglow spectra but because of the narrow energy range of the (0.3 - 10 keV) XRT we are not able to see the whole Band spectrum. The majority of Swift X-ray afterglows spectra are well modeled by simple power laws in energy, partially absorbed below ~ 1 keV by gas and dust along the line of sight as a contribution from the interaction of X-rays with the matter. A simple absorbed power law model is the general model that gives a good fit to the data and indicates a non-thermal emission mechanism. It is also showed that some spectra can be fitted better with a blackbody model or with emission lines in addition to the absorbed power law model [106].

In the X-ray light curves we see different phases and the spectral properties of these phases are different. When the steep decay phase is fit with a simple power law model, it is seen that the power law photon index tends to increase and gets softer [5, 99]. From the observational point of view this is related to the E_{peak} of the Band model. In this phase as the E_{peak} enters the X-ray range, but in the majority of cases the limited energy range of the XRT does not allow us to determine the E_{peak} and all we see is a part of the Band model in the form of a simple power law model whose power law index increases [5, 107]. In the literature it is mentioned that the early emission in the X-ray afterglows needs a special treatment. Other models apart from the simple power law have been used. For example, in [5], the BAT and the early XRT spectra are

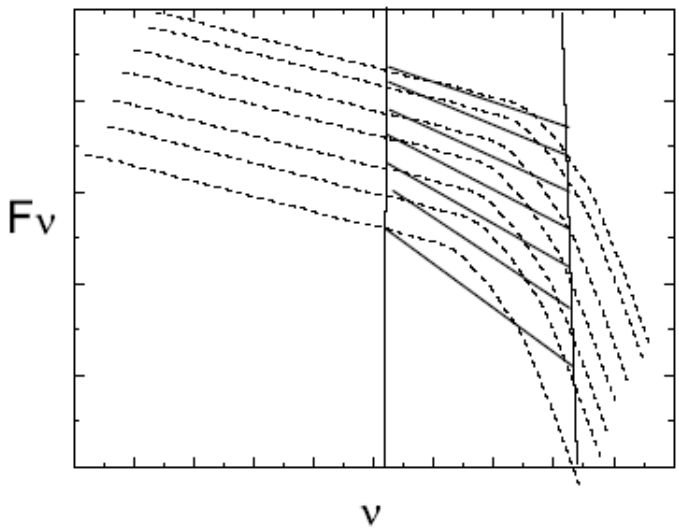

Figure 1.25. A schematic picture showing spectral softening due to the narrow energy band [108]

fit together and from the best-fit model it is seen that the early X-ray spectra look like the GRB spectra which has a characteristic spectral energy E_{peak} in the X-ray band. The same GRB model has proven to be necessary the X-ray flares modelling [5]. X-ray flares spectra are generally fit by a cutt off power-law model or Band model [101, 102]. The exact beginning of the afterglow is one of the major issues at present. Studies in the time and spectral domain propose that up to 1,000 seconds the X-ray emission is related to the main GRB event [104]. After the steep decay phase, if there are no flares in the light curve, then the spectra for the remaining light curve is expected not to evolve. X-Ray afterglow spectra are able to give properties of emission mechanism and absorbing material in line-of-sight. If the absorbed power law model is used to fit the spectra, then the 2 parameters are the power law photon index and the absorbing material in the form of the neutral Hydrogen Column Density. Since the GRBs are extragalactic sources the galactic column density for the given GRB coordinate is known and the redshift also can be obtained from the optical afterglow observations. The excess of the column density seen in the GRB X-ray afterglow spectra is called the intrinsic column density of the GRB. X-ray absorption excess is seen for many bursts in the literature [109, 110].

1.2.2.2. Optical Afterglows. Optical afterglow light curves are generally described with a simple power law (Figure 1.26) or with a multiple power law behavior (Figure 1.27). One of the most important optical light curve feature is the supernova bump (Figure 1.28), seen in almost near GRBs (a very interesting exception is GRB 060614 [65]. The spectral properties of the optical afterglow provides a test of the

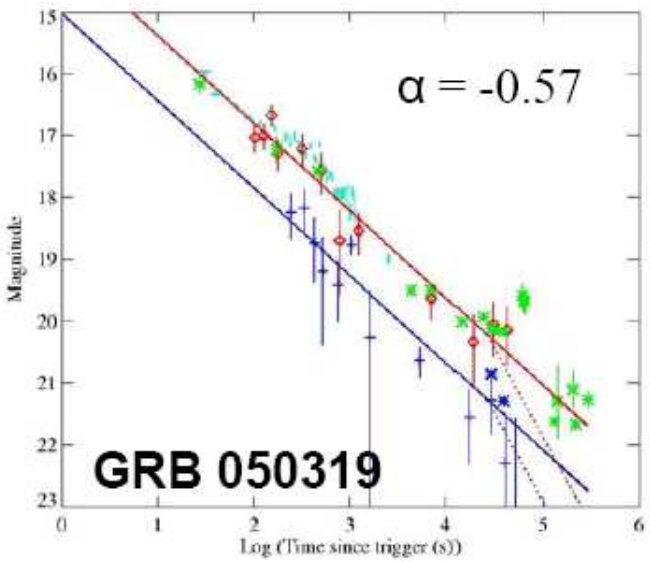

Figure 1.26. GRB050319 optical afterglow [111]

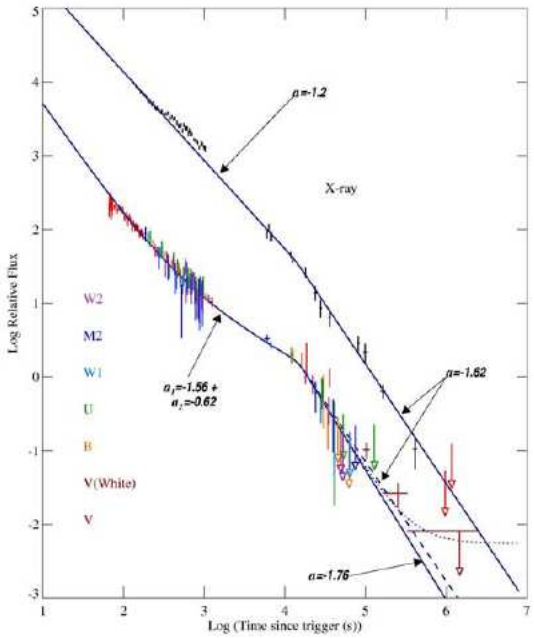

Figure 1.27. Optical and X-ray afterglow light curve [112]

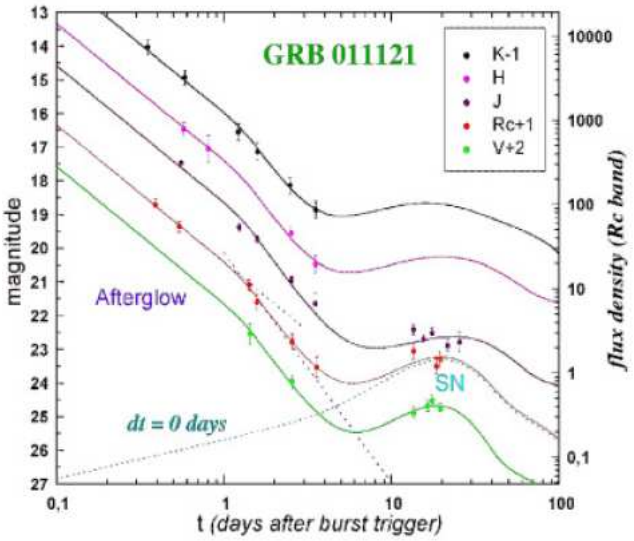

Figure 1.28. GRB 011121 optical light curve [28]

physics that forms the GRBs and the nature of their environment. The most efficient way to obtain the GRB redshift is the optical spectra. GRB-supernova connection is proved in optical afterglow spectra. The GRB related supernovae are in a special class of Type Ic, they are broad-lined with a smooth spectra and very large explosion energy ($E \approx 10^{53}$).

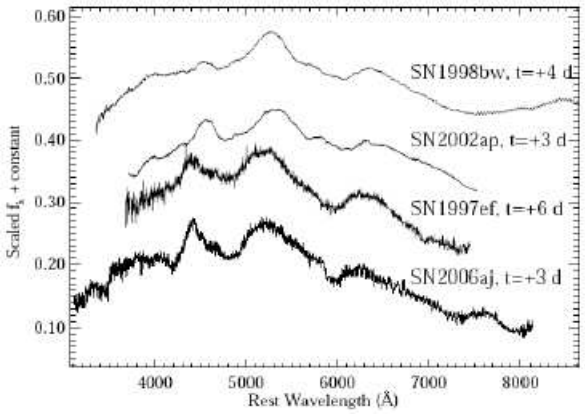

Figure 1.29. Spectrum of SN1998 [113]

1.3. GRB Theoretical Models

After the discovery of GRBs in 1967, they remained as mystery for the following next 25 years. Until the launch of the Compton Gamma-Ray Observatory the number of GRB theories was more than the detected GRBs [114]. After the launch of Swift satellite [43], the theory of the GRBs in all aspects improved but they are not completely understood yet. In this section main theoretical issues are divided in to four parts: GRB prompt emission, GRB afterglows, GRB central engine and the GRB progenitors.

1.3.1. GRB Prompt Emission Model

1.3.1.1. Fireball Model For The Prompt Emission. The Gamma-ray emission seen in the prompt phase should be connected to the progenitor and the central engine, but the theoretical models try to explain how to convert rotational gravitational energy into Gamma-rays regardless the progenitor or the central engine. When the first fireball theory was offered to explain the Gamma-ray emission of GRBs their real distances were unknown. If they were assumed to be at cosmological distances (as we now know they are), their energy could be up to 10^{51} ergs [52]. The problem was to find out the mechanism that produces such amount of energy within a few seconds. The first solutions offered in 1986 by Paczynski and Goodman, related the GRB to a relativistic fireball. A relativistic outflow of electron-positron plasma and photons expands freely and produces Gamma-rays when it becomes transparent [52]. The resultant Gamma-rays of this fireball would form a thermal black body spectrum [52]. At the same time Goodman also discussed the properties of an optically thick relativistic outflow considered of pure radiation that produces Gamma-rays as a thermal spectrum [115]. Then in 1990 Shemi and Piran showed that when some baryonic materials added to the relativistic fireball, most of the radiation energy of the fireball is converted to kinetic energy of the matter and Gamma-rays would be redshifted into the X-ray range or below [116].

The main problem was to generate Gamma-rays from the energy with a non-

thermal spectrum, since the observed Gamma-ray spectra were non-thermal as seen from BATSE observations [2]. In 1993, Paczynski and Xu produced a model that consider a series of shells ejected with different Lorentz factors [117]. The shells with different speeds collide with each other at later times and produces other fireballs that generates Gamma-rays and neutrinos accounting for (2%) of the total energy [117]. This model is not successful to explain the Gamma-ray emission, but it is the first model that uses the idea of the collision between different relativistic shells with different Lorentz factors. In 1994 Rees and Meszaros used the idea of collision between relativistic shells and proposed that an internal shock would be formed when a shell of ejected matter catches up with other material ejected earlier at a lower Lorentz factor in the fireball [18]. According to the internal shock model, the speed of the jet varies with time, and this cause the faster portions of the jet to catch up with slower ones [18]. The collisions between the shells cause an internal shock and as a result, a fraction of the kinetic energy of the jet is converted to thermal energy and into relativistic electrons which produce the Gamma-rays [18]. Before the internal shock model the Gamma-ray producing mechanism the synchrotron emission [118, 119]. In the internal shock model the observed radiation is produced via synchrotron and inverse-Compton processes. For a while, the leading radiation mechanism to generate the prompt emission was believed to be the synchrotron emission [18, 120, 121]. Observed GRB spectra were consistent with the synchrotron emission interpretation [122, 123] although it was not enough to explain several observational facts [124, 125]. The simple synchrotron model improved by some additions [85, 125, 126]. One of these additions was the photospheric emission which is blackbody emission formed when the fireball shell expands to the photospheric radius (Figure 1.30) [85]. The observed Gamma-ray emission is thought to be superposition of the photospheric emission and the internal shock emission [127]. Such a thermal component in the prompt emission is seen and discussed in BATSE observations [128]. We caution the reader that it is still matter of debate, if this component is actually present or not in the GRB spectra. In figure (1.30) the different radii refer to: r_{ph} photospheric radius; r_{is} internal shock radius; r_0 central engine radius. In the standard fireball models the magnetic field does not have any dynamical role [130, 131]. The internal shock model able to explain the Gamma-ray light curves and the spectra. In the previous works the internal shock model thought to be consistent

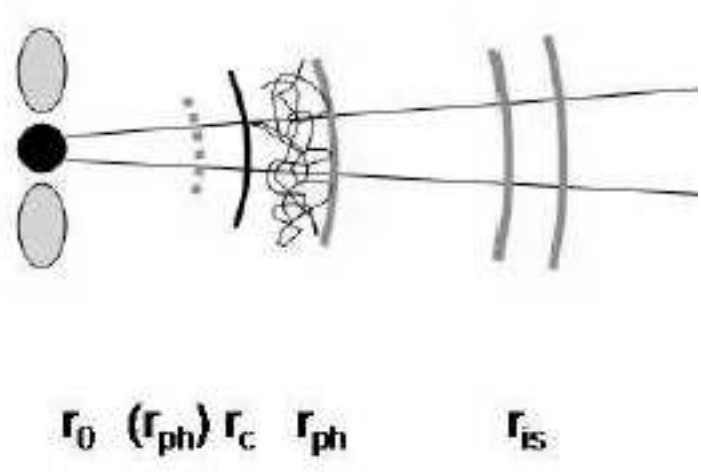

Figure 1.30. Generic fireball model radii [129]

with the GRB light curves [132, 133], although it has several disadvantages such as the low efficiency to convert the jet energy to the radiation energy [134–136]. Also the emission mechanisms of the prompt Gamma-rays pose some problems as described in [137]. With recent Swift observations it is showed that the internal shock model can be ruled for some cases and the alternative models are more consistent with the data [138].

1.3.1.2. Magnetic Field Dominated Prompt Emission Models. The effects of the magnetic fields in GRBs is one of the recent questions. The models containing strong magnetic field are the alternative ways to generate prompt emission [84, 139, 140, 141, 142]. In 1992 Usov presented a new model for GRBs assuming that they were at cosmological distances [139]. This model was based on the formation of a rapidly rotating neutron star with strong surface magnetic field that loses its rotational kinetic energy on a timescale of seconds by a relativistic electron-positron plasma that emits X-rays and Gamma-rays at the photosphere [139]. The source of the non-thermal radiation for GRBs were considered as relativistic electron-positron winds and strong magnetic fields and the Gamma-ray emission mechanism was synchrotron-Compton radiation [140]. In 1994, Thompson introduced a Poynting-flux-dominated, relativistic, Magneto Hydro Dynamic (MHD) wind model to reproduce the basic spectral properties of GRBs [141]. In this model Gamma-rays are produced by Compton scattering by mildly Alfven

turbulence [141]. In 2003, Lyutikov and Blandford introduced the electromagnetic outflow model (Figure 1.31) [84]. In this model as a rotating, relativistic, progenitor loses its rotational energy in the form of a Poynting flux, a electromagnetically-dominated bubble that expands non-relativistically inside the progenitor and becomes highly relativistic after breaking the progenitor surface [84]. Then the electromagnetic energy is concentrated in a thin shell that creates Gamma-rays by accelerated pairs in the magnetic field [84].

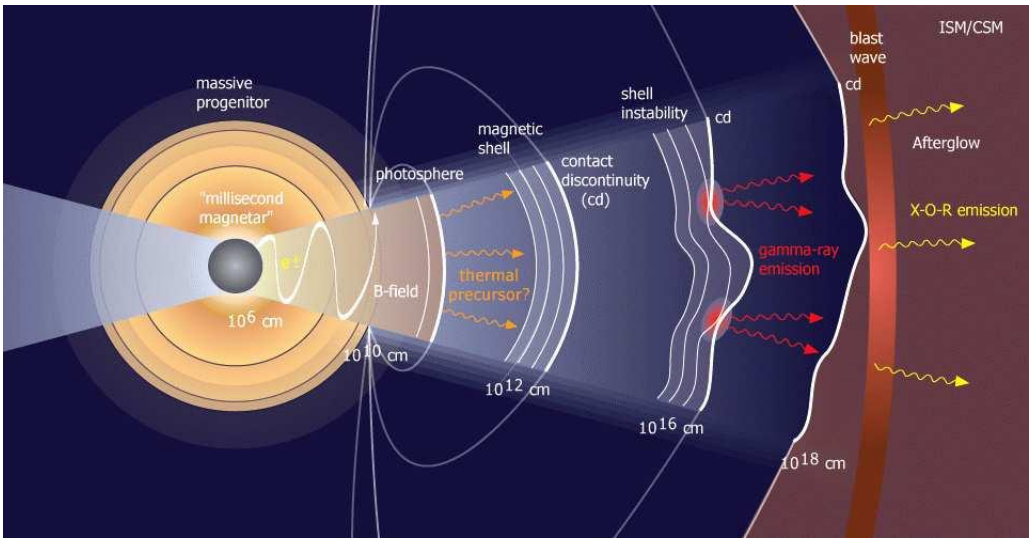

Figure 1.31. Overall view of the electromagnetic outflow model [84]

1.3.1.3. Turbulent and Sub-Jet Model. In recent years the alternative models to the internal shock model is offered to explain the GRBs variable light curves [142, 143]. In the turbulence model, the radiating fluid in the GRB shell is relativistically turbulent [142]. The relativistic turbulence considers a shell that contains randomly distributed emitters that change their direction of motion rapidly and radiate as the shell moves (Figure 1.32) [143]. In the sub-jet model (Figure 1.32), within a highly magnetized relativistically expanding shell relativistic sub-jets are formed that have a constant direction and opening angle [143]. The efficiency of these models to produce the GRB light curves seems highly with proper conditions [143]. For example, a recently work showed that for GRB 080319B can be well explained by the turbulent model of Narayan and Kumar and the internal shock model is ruled out for this burst [142].

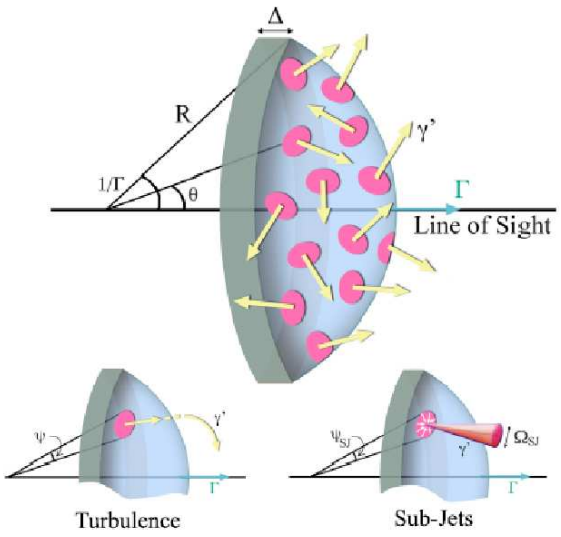

Figure 1.32. Turbulence and Sub-Jet Model [143]

There has been a big effort to explain the Gamma-ray production and the energy transport mechanism that can be via magnetic field, kinetic energy of protons-neutrons or electron-positron pairs. Possible ways to generate the observed Gamma-rays are mentioned above. The Prompt emission theory is a developing topic of the GRB field.

1.3.2. GRB Afterglow Emission Models

1.3.2.1. Fireball External Shock Model. The delayed emission in X-ray, optical and radio wavelengths seen in GRBs is called the afterglow emission. Afterglow emission was predicted theoretically before its discovery [22, 121, 145, 146]. In 1993 Rhoads and Paczynski estimated that the Gamma-ray bursts may be followed by radio transients, as a result of the synchrotron radio [147] emission that is generated when the relativistic ejecta interact with the interstellar matter [145]. Later in 1997 Rees and Meszaros, discussed the evolution of the fireball after the Gamma-ray emission with any swept-up surrounding matter and they predicted an afterglow at X-ray, optical and radio wavelengths whose flux decays as a power of time [22]. This predicted flux decay could show breaks that connects different slopes [22]. The fireball model is confirmed [148, 149] with the detection of X-ray and optical afterglows [16] and the afterglow is described well as synchrotron emission from accelerated electrons when a spherical relativistic shell collides with ISM [149, 150, 151]. To be able to compare the observed

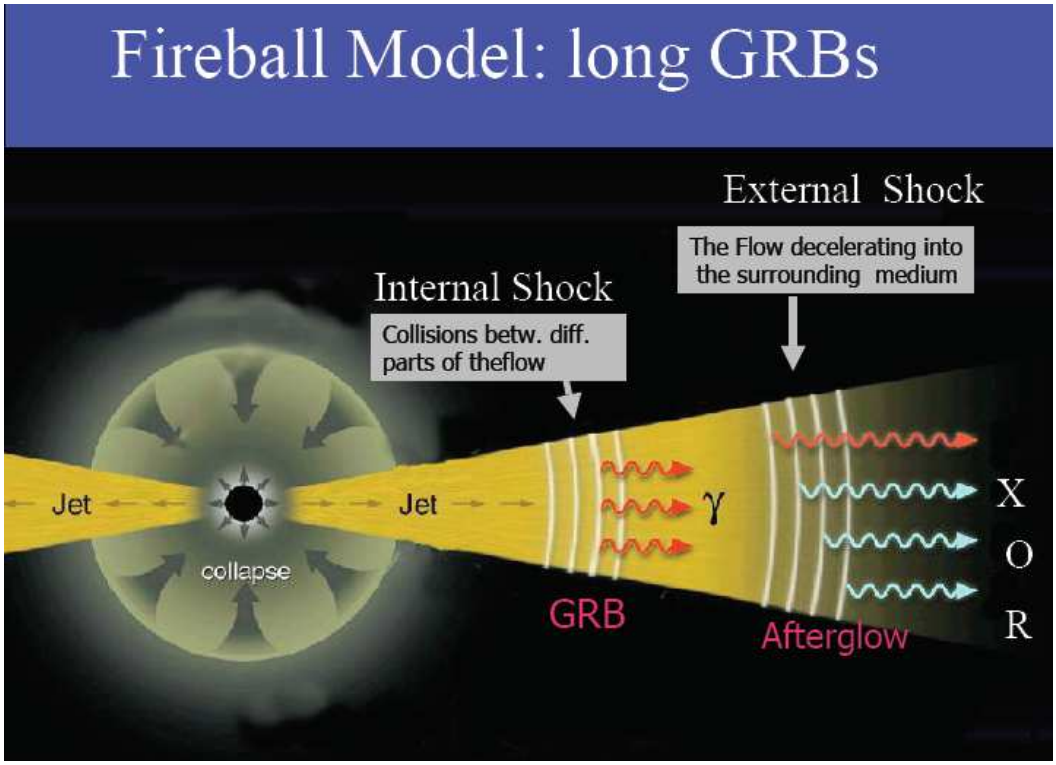

Figure 1.33. Fireball model [144]

afterglow data with the theoretical models, broad-band spectra and the light curves of synchrotron radiation from a power-law distribution of electrons in an expanding relativistic shock are calculated [20]. The spectrum and the light curve is composed of several power-law segments (Figure 1.34) containing a wide range of frequency and time [20]. In this calculation, the theoretical synchrotron radiation spectrum is improved considering the cooling by synchrotron radiation, when the relativistic electron lose a fraction of their energy in radiation [20]. Different electron energies define four important frequencies: the injection frequency, the cooling frequency, the maximum synchrotron frequency and the self-absorption frequency [152]. There are two types of spectra described by the order between the injection frequency and the cooling frequency: *slow cooling case* if $\nu_m < \nu_c$ and *fast cooling case* if $\nu_m > \nu_c$ [20]. The theoretical light curve (Figure 1.35) is constructed according to the hydrodynamical evolution of the shock [20].

The simplest theoretical GRB afterglow models have major assumptions [129]. At the relativistic shocks the electrons are assumed to be Fermi accelerated (see ref. [153])

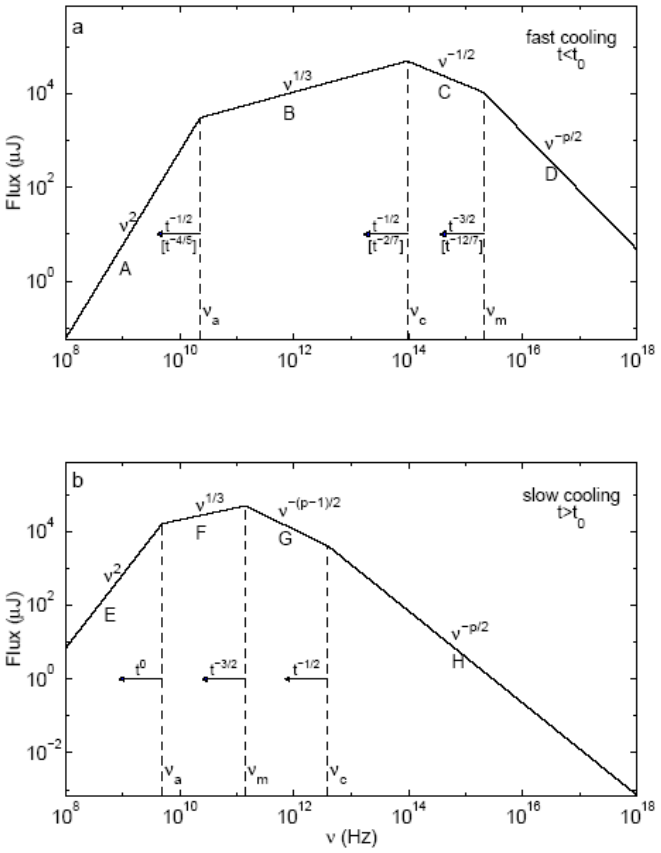

Figure 1.34. Theoretical afterglow synchrotron spectra [20]

and to have a power-law distribution with a power-law index p: $N(E)dE \propto E^{-p}dE_e$. It is also assumed that a fraction ξ_e of the total electrons associated with the baryons in the ISM are accelerated and the total electron energy is a fraction ϵ_e of the total internal energy in the shocked region. Although the strength of the magnetic field is unknown, magnetic energy density is assumed to be a fraction ϵ_B of the internal energy. The model has four basic parameters [129]: the local medium density (n), total energy of burst (E_0), energy portion distributed to the electrons (ϵ_e) and the energy portion distributed to the magnetic fields (ϵ_B). In the standard afterglow model [22], the afterglow flux density changes by a power in time once the synchrotron peak has moved through the bandpass and the relation between the temporal decay index α and the photon spectral energy index β is given as $F_\nu \approx t^\alpha \nu^\beta$ where $\alpha = (3/2)\beta$ [152]. According to current observations the frequency and time dependence of the afterglow spectral energy flux density is consistent only with late time X-ray afterglow phase. For the normal decay phase the theoretical expected spectral energy index is

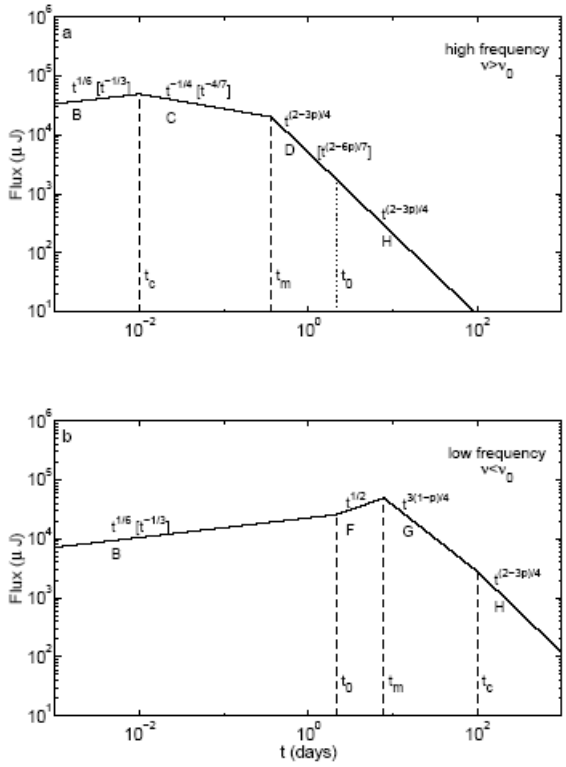

Figure 1.35. Theoretical afterglow synchrotron light curve [20]

in the range between 0.7-1.0 and temporal decay index is in the range of 1.1-1.5 [49]. Before the launch of Swift, the simplest version of the fireball model was enough to explain the data although there were some exceptions that displayed optical variability such as bumps, wiggles and smooth power-law decay []154–156. These variations are discussed theoretically in the literature with different suggestions. These include the inhomogeneities in the surrounding medium [155, 157, 158], refreshed shocks with the surrounding medium [159], angular dependence of the fireball energy [133] and the gravitational lensing [160, 161]. Recent observational properties in X-ray afterglows such as flares, steep decay phase, shallow decay phase [58, 162, 163] challenge fireball shock model [18, 20, 21, 164].

1.3.3. Recent Models For X-Ray Afterglows

1.3.3.1. X-Ray Afterglow Steep Decay Phase. The steep decay phase seen in the most of the Swift [43] X-ray afterglows is a phase between prompt emission and afterglow

emission. This phase is supposed to be dominated by the *curvature effect* (that is the delayed photon emission from high latitudes with respect to the line of sight) [107, 165, 166, 167, 168]. It is proposed that the curvature effect model of a cutoff power-law spectrum is used to model the some X-Ray steep decay phases [59, 97, 108, 169, 170].

Figure 1.36. Curvature effect [171]

1.3.3.2. X-Ray Flares. X-ray flares [94, 101, 102] seen in the Swift [43] afterglows as sudden re-brightening, were a total surprise. They were first interpreted as late-time energy injection into the external shock or a continued internal shocks [101]. It is showed that external shock related processes would produce flares with long time scales [155, 172] which is not always the case in observations [94, 104]. The timescales of flares mainly relate them to a long lasting central engine activity [172]. The internal dissipation model [59, 169, 173] which requires long-lasting central engine activity is the current favorable explanation for the X-ray flares, agrees with the data [97, 174].

1.3.3.3. Shallow Decay Phase. The shallow decay phase can be seen immediately after the prompt emission or after the steep decay phase [58, 163]. This phase is interpreted as energy injection into the fireball [59]. Other models [175, 176] such as dust-scattering-driven emission that offers X-ray scattering by dust can cause shallow decay phase under certain conditions [176, 177].

1.3.4. GRB Progenitors

When GRBs were first discovered, the most popular scenarios for their origins involved galactic nuclei [178] or merging of massive binaries [55]. As the observational progress improved, the afterglows provided the information about the redshift, position of burst and the surrounding environment of the GRBs. GRBs were classified as *long-soft* and *short-hard*. Long GRBs are believed to be related with the death of a massive star and the connected creation of a black hole [26, 32, 179, 180, 181]. Several models were proposed to contain massive stars, such as the *hypernova* [182, 183] that predicts a simultaneous Type Ic supernova with the GRB. Another model is the *Supranova* [31]: it predicts a two-step explosion, were the burst onset follows a supernova after a few months. Optical rebrightening observations [28] supported the hypernova scenario while the detected iron emission and absorption features in the X-ray afterglows suggested the supranova model.

The most favored massive star model for the long GRBs is the *collapsar* [33] [184]: A massive star [33] collapses and forms a black hole after losing its Hydrogen rich envelope. This enables to the jet to go out, while the angular momentum is necessary for the formation of a disk around the black hole [185, 186]. Such a star would have been a Wolf-Rayet star [187] before collapse and its resultant supernova explosion should have matched Type-Ib/c supernovae. These stars have very strong winds, which cause the stars to lose their entire hydrogen envelope [188]. The test of the models depends on mass and the metallicity of the stars [189]. There is also an alternative massive single star model that a rapidly rotating core can develop extensive mixing and burns nearly the entire hydrogen envelope into helium [190, 191]. The link to massive stars is supported by the supernova association [32, 181] and the relations of long GRBs with star-forming galaxies and star-forming regions in galaxies [192]. The supernova association of long GRBs and the Type-Ic supernova progenitors mass knowledge [193] showed that the progenitors of long GRBs should be massive stars. There is strong support for the collapsar model, however; the progenitor of long GRBs is not definitively known and the list of possible progenitors is large and the single massive star is just one of the candidates [189]. Short GRBs are believed to have different progenitors

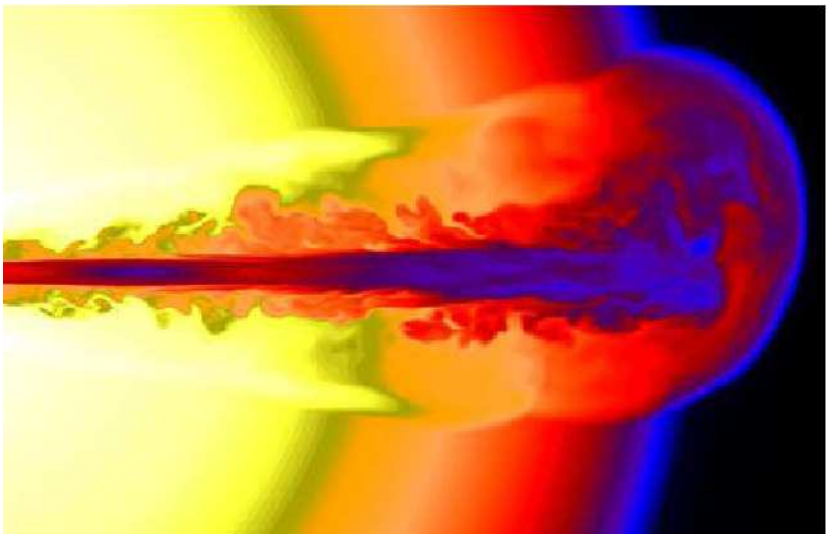

Figure 1.37. Simulation shows GRB jet formed from Wolf-Rayet star. [180]

than long GRBs. The collapsar model don't explain the short GRBs since they are too short. The short GRBs are widely suspected of being two merging compact objects. Two compact objects can be two neutron stars or a neutron star (NS) and a black hole (BH) [52, 54, 194] or a white dwarf (WD) and another compact object [195]. Helium merger progenitor [196] model is one of the favorable models. In this model, in a binary system the more massive star collapses to form a neutron star or black hole and provides a kick to its binary. When the companion star evolves off the main sequence it causes the system to merge and produce a burst. Several observations gradually shows the association of compact-object mergers with short bursts [45, 50, 197]. Binary systems loose angular momentum by gravitational waves and then they merge. As a result, a black hole and a torus around (that carries the angular momentum) can be formed. Observation of gravitational waves from a merger system would be a direct evidence for this model. Alternative models based on a black hole as a central engine have proposed [199, 200]. There are also alternative models without black hole [139, 195]. Consequently, a well explained and tested progenitor scenario is not available yet.

1.3.5. GRB Central Engine Theory

GRB central engine is the mechanism that produce a relativistic outflow with high Lorentz factors in terms of beamed jets [201]. The first idea about the energy

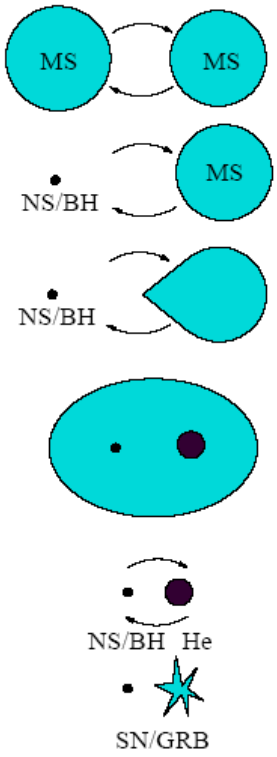

Figure 1.38. An evolutionary pathway to create the NS/BH and He core [198]

source for GRBs was the rotation of a neutron star [203–205]. In such a model GRBs are related to birth of a magnetar [205, 206]. The other possibility for the GRB central engine is an accretion disk which can be formed by collapsar model or by binary merger model. According to collapsar model [34, 182], the acretion disk is formed by the fall back matter from the collapsing envelope of the star and the accretion duration which is on the order of several tens of seconds depends on the dynamical timescale of the collapsing envelope of the star. In the binary merger model [54], the accretion material is formed by the debris of the neutron star which is tidally disrupted. In this case the accretion timescale which is a fraction of seconds, depends disk properties. The accretion timescales make the distinction between the long duration and short duration bursts. The accretion timescale in the binary merger model gives the short duration GRB timescales while the collapsar model accounts for the long GRB timescales. If a black hole and an acretion disk is considered as the central engine, then the next question is how to produce a relativistic outflow from this system. One of the possible mechanisms is the neutrino pairs that are formed in the disk and collide each other along the rotational disk [179, 207, 208, 209]. Other possible mechanisms are magnetic

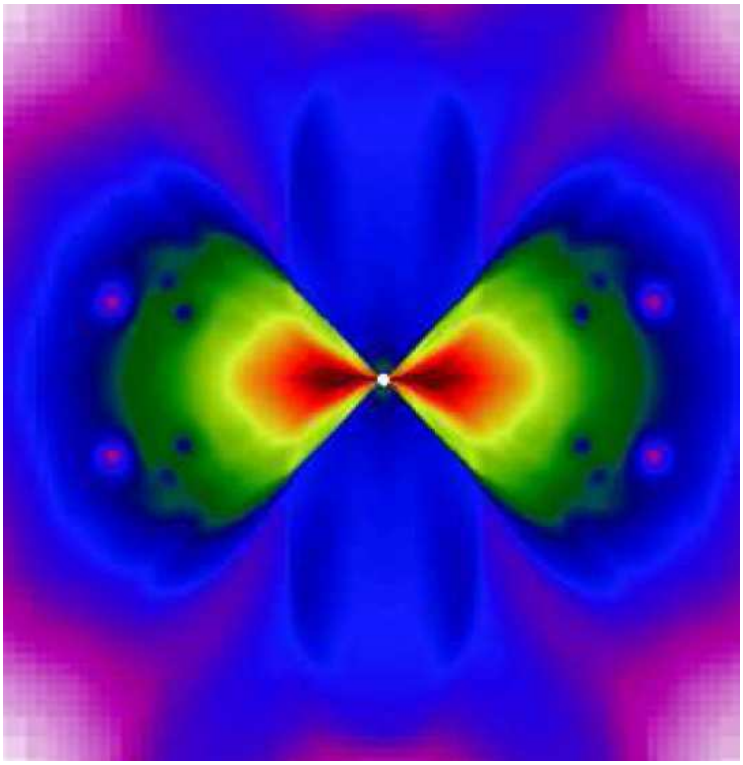

Figure 1.39. Simulation for black hole forming from the core collapse of a Wolf-Rayet star [180]

instabilities in the disk [210, 211] and the MHD extraction of the rotational energy of the black hole [213–215].

1.4. Effects Of GRBs On The Surrounding Medium

GRBs are energetic Gamma-ray, X-ray, optical-UV and radio sources. It is very natural that their surrounding medium is affected by them as they occur. In general the surrounding interstellar medium is composed of gas and dust. However, the X-ray and UV counterpart of the GRBs affect the gas in the ISM by ionizing, heating it and affect the dust grains by vaporizing them. When X-ray afterglow is considered, there is an amount of time dependent X-ray luminosity that ionize the surrounding medium if it is a gas-rich environment that is not ionized initially. The UV afterglow also ionize the gas in such an environment. When the GRB blast wave effects on the ISM (Figure 1.40) are considered, the absorption lines properties are calculated by the bound-free and bound-bound transitions and it is seen that the strength of absorption

lines (in optical band) declines with time [215]. Böttcher et al 1999 focused on time dependent ionization and photoelectric absorption effects mainly in the X-ray regime and they showed the Fe K edge absorption feature temporal evolution [216]. Time

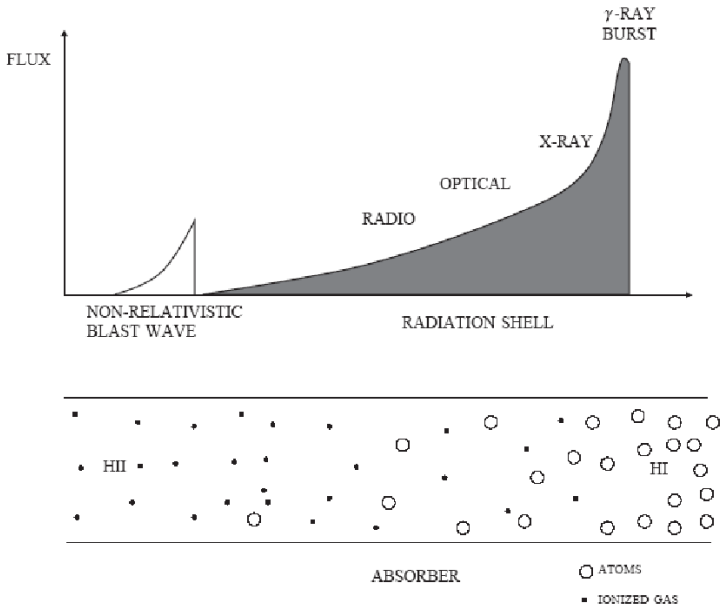

Figure 1.40. Radiation shell and its effect on the ambient absorbing medium [215]

variability of ionization edges depending on the different environments considering the radial profile densities is discussed by [217] and they showed that the required time resolved spectroscopic observations can be done by Swift. The effects of UV flash of the GRB on the surrounding dust [218] and the effects of the X-rays on the dust particles have been discussed [219]. Lazzati and Perna (2002) showed that the time-dependent X-ray extinction is sensitive to the density profile in the close environment of the bursts [3]. They derived the temporal evolution (Figure 1.41) of the measured column density as a function of the density of the medium and the size of the absorbing medium [3]. In figure 1.41 the evolution of the column density is shown for a uniform cloud and a shell. Since in the shell environment case all the material is located at a large distance from the source ionization time is longer. Consequently if we concentrate on the evolution the column density effect of the GRB because of the ionizing, if a first measurement of the intrinsic column density is obtained, the next measurements are expected to be always equal or below this value depending on the distance to the absorbing material. This is due to the fact that there is no physical way to create some matter to increase

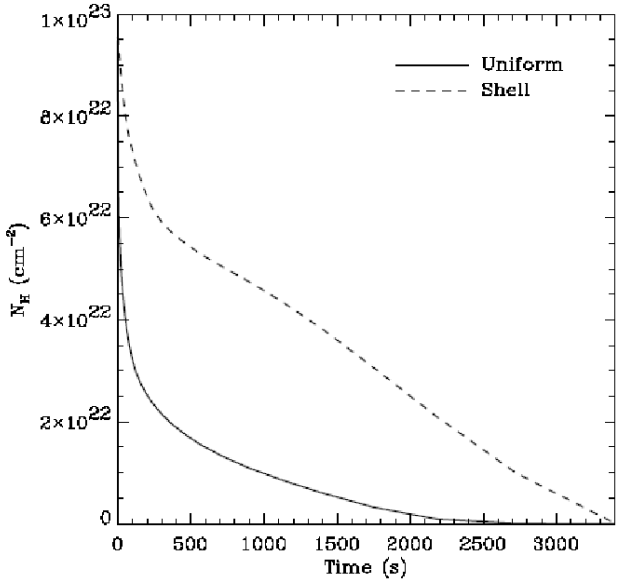

Figure 1.41. Column Density variability density in time according to simulations [3]

column density (since the recombination timescale is much larger than the observing times) [215]. A lower intrinsic column density can be measured since the photons of the GRB can ionize the metals, thus reducing the number of absorbing atoms. In this work, the possible evolution of the neutral Hydrogen column density with time will be analyzed on a sample 28 GRBs.

2. COLUMN DENSITY AND POWER LAW PHOTON INDEX

X-Ray spectral parameters, such as hydrogen column density and power law photon index, are the main focus of this work. The physics behind X-ray spectrum would be introduced in this chapter. After the radiation processes, synchrotron radiation which is related to GRB spectra by the photon index- that produce X-rays would be explained briefly, X-ray absorption processes is summarized to understand the effect of ISM in the observed spectra. A brief introduction to X-ray absorption including the hydrogen column density definition and the photoelectric absorption model that forms the absorption curves would also be given. Consequently, power law model with photoelectric absorption which brings the two parameters, hydrogen column density and the power law photon index, together will be discussed with the illustrated graphs.

2.1. X-Rays

X-rays are form of high energy electromagnetic radiation. They are part of the electromagnetic spectrum. The energy of an X-ray photon is times that of a photon of visible light. X-rays have very short wavelengths, very high frequencies and high energies. X-rays are in the range of $0.1keV - 120keV = 30 \times 10^{15}Hz - 30 \times 10^{18}Hz = 10 - 0.001$ nanometers.

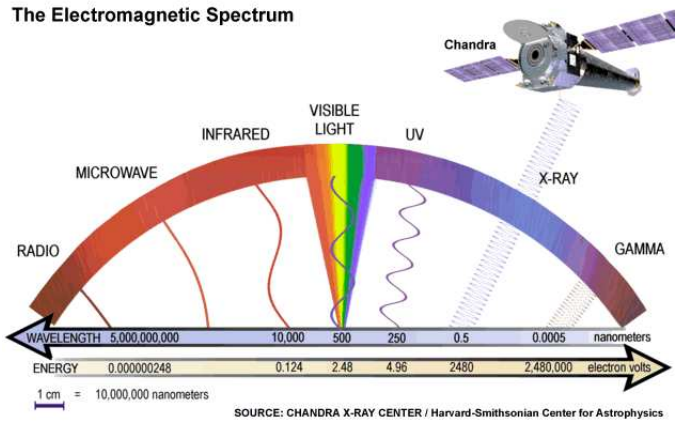

Figure 2.1. Electromagnetic spectrum [220]

2.1.1. Generation Of X-Rays

Radiation processes are divided in two categories which are thermal and non-thermal. In thermal radiation, Maxwell-Boltzmann thermo-dynamic equilibrium [221] conditions relate particle velocities to the temperature of the emitting gas. Conventionally, non-thermal radiation means the continuum radiation from particles whose movement and radiation does not depend on Maxwell-Boltzmann statistics [153]. X-ray producing mechanisms are: bremsstrahlung, black body radiation, synchrotron radiation and inverse Compton.

2.1.1.1. Bremsstrahlung. Radiation due to the acceleration of a charge in the Coulomb field of another charge is called Bremsstrahlung radiation [222]. Thermal bremsstrahlung radiation from an ionized medium is one of the X-ray emission mechanisms. When an electron comes very close to the nucleus and the electromagnetic interaction causes a deviation of the trajectory where the electron looses energy and an X-ray photon is emitted. When the emission of a single electron with single electron velocity is averaged over the Maxwell-Boltzman velocity distributions of electrons the total emission by all particles in this population is called thermal bremsstrahlung [222]. Thermal bremsstrahlung occurs in a hot gas, where many electrons are stripped from their nuclei, leaving a population of electrons and positive ions. If the gas is hot enough (millions of degrees Kelvin), this kind of radiation will primarily take the form of X-rays.

2.1.1.2. Black Body Radiation. Objects at temperature above absolute zero emit electromagnetic radiation with a characteristic distribution over energy (spectrum) determined by their temperature this radiation is called the black body radiation [222]. If the temperature of the object is extremely high (between $3 \times 10^6 - 3 \times 10^8$ K) then its radiation will be predominantly in X-ray band. Black body radiation spectrum is represented by Planck Law [222]. The intensity $I\ (\lambda, T)$ is the energy radiated per unit area per unit solid angle per unit time per unit wavelength (λ) at a given temperature

(T) is given by the Planck law (equation 2.1).

$$I(\lambda, T) = \left(\frac{2hc^2}{\lambda^5}\right) \frac{1}{\left(exp\left(\frac{hc}{\lambda kT}\right)\right) - 1} \tag{2.1}$$

Since the frequency $\nu = c/\lambda$ the intensity $I\ (\lambda, T)$ is the energy radiated per unit area per unit solid angle per unit time per unit frequency (ν)at a given temperature (T) is given in equation (2.2)

$$I(\lambda, T) = \left(\frac{2h\nu^3}{c^2}\right) \frac{1}{\left(exp\left(\frac{h\nu}{kT}\right)\right) - 1} \tag{2.2}$$

Planck Law can be written in terms of energy using the $E = h\nu = hc/\lambda$ relation,where h is the Planck's constant ($6.6260693 \times 10^{-34} J.s = 4.136 \times 10^{-18} keV.s$). Since $I(E)dE = I(\nu)d\nu$ then $I(E) = \frac{d\nu}{dE} I(\nu) = \frac{1}{h} I(\nu)$. Using this Planck Law in terms of energy is given in equation (2.3).

$$I(E, T) = \left(\frac{2E^3}{h^3c^2}\right) \frac{1}{\left(exp\left(\frac{E}{kT}\right)\right) - 1} \tag{2.3}$$

If kT is taken as kT=keV and if the energy is in the unit of keV, then the Planck law in terms of energy becomes as shown in equation (2.4).

$$I(E, T) = \frac{2E^3(keV)^3}{(4.1 \times 10^{-18} kev.s)^3 (2.9 ms^{-1})^2} \frac{1}{\left(exp\left(\frac{E(keV)}{(keV)}\right)\right) - 1} = \frac{3.14 \times 10^{35} E^3}{\left(exp\left(\frac{E}{kT}\right)\right) - 1} \tag{2.4}$$

The spectrum of black body radiation at kT=1 keV is given in Figure (2.2) and the spectrum of black body radiation at kT=0.1 keV, 1 keV and 2 keV is given in Figure (2.3).

2.1.1.3. Synchrotron Radiation. The emission of very relativistic electrons gyrating in a magnetic field is called the synchrotron radiation. This process is responsible for the non-thermal Gamma-ray emission of the prompt emission and optical, X-ray emission observed in GRB afterglows. In any radiation process, to obtain the power of the radiation it is necessary to use the Larmors formula [223] that gives the radiation rate

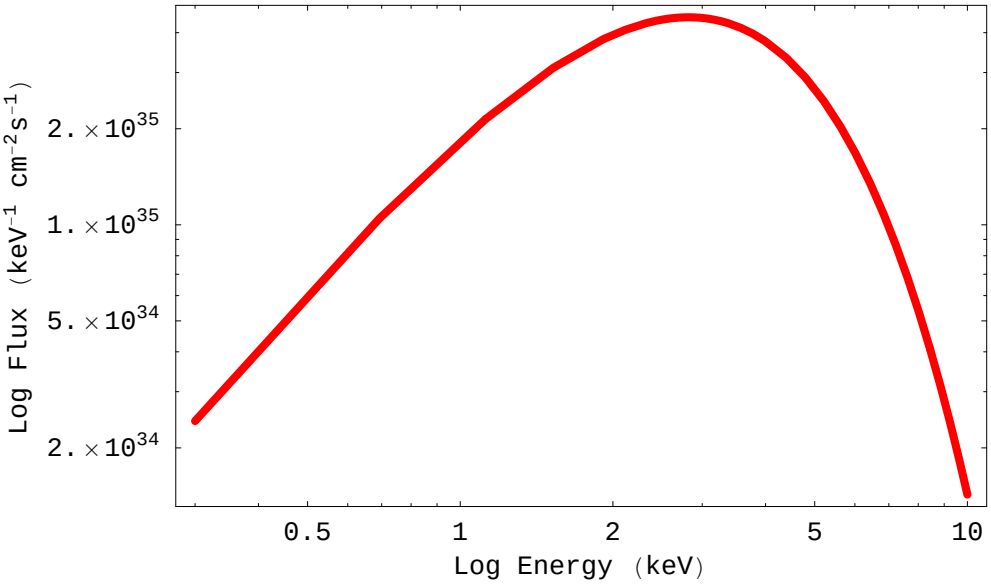

Figure 2.2. Log-log plot of blackbody spectrum at $kT = 1keV$

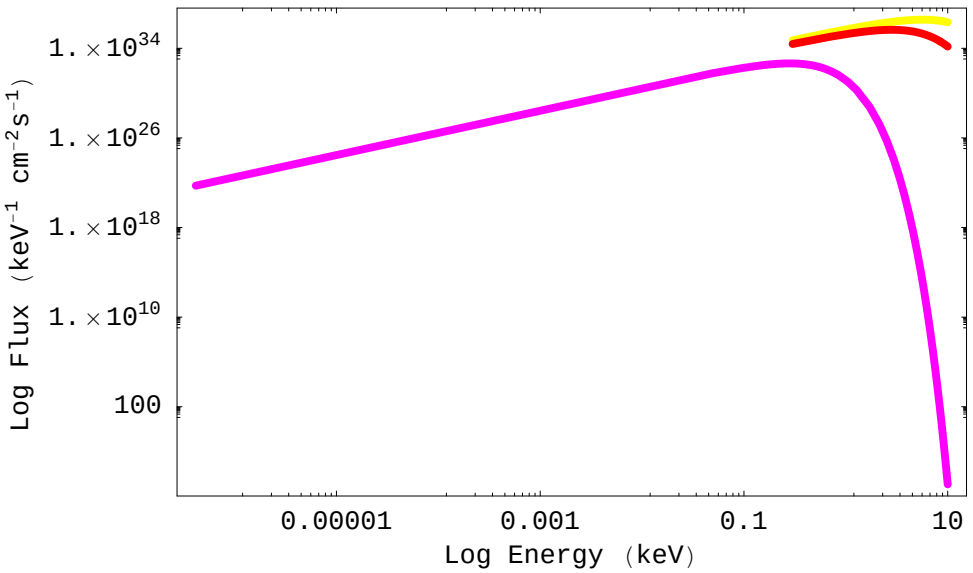

Figure 2.3. Log-log plot of blackbody spectrum for different energies

of an accelerated charged particle. Larmors formula is given by equation (2.5 [222]) where a is the proper acceleration of the particle, P is the power, q is the charge, and c is the speed of light.

$$P = -\left(\frac{dE}{dt}\right)_{rad} = \frac{q^2 a^2}{6\pi\varepsilon_0 c^3} \tag{2.5}$$

The energy loss rate by radiation dE/dt is a Lorents invariant between inertial frames since both the energy and the time interval transform in the same way between inertial frames of reference [224]. If the motion of an electron in a uniform, static magnetic field is considered as a spiral path (Figure 2.4). If we equate the forces on the electron

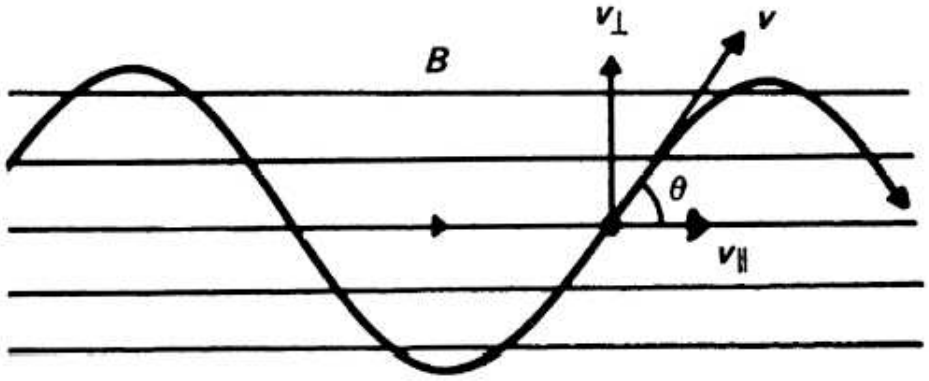

Figure 2.4. Motion of an electric field in a uniform magnetic field [153]

we obtain equation (2.6) where P is the momentum and the $\gamma = \left(1 - \frac{v^2}{c^2}\right)^{-1/2}$ is the Lorentz factor.

$$\vec{F_B} = e(\vec{v} \times \vec{B}) = \left(\frac{dP}{dt}\right) = \left(\frac{d(\gamma m_e v)}{dt}\right) = m_e\gamma\frac{d\vec{v}}{dt} + m_e\gamma^3\vec{v}\frac{(\vec{v}.\vec{a})}{c^2} \tag{2.6}$$

Since in a magnetic field the three-acceleration is always perpendicular to velocity, the $(\vec{v}.\vec{a}) = 0$. So, the equation becomes $e(\vec{v} \times \vec{B}) = m_e\gamma\frac{d\vec{v}}{dt}$. As seen by the figure (2.4) the particles velocity has two components that are parallel (v_{par}) and perpendicular (v_{per}) to the magnetic field. There is an angle (θ) between velocity and magnetic field vectors which is given by $\tan\theta = \frac{v_{per}}{v_{par}}$. $v_{per} = v\sin\theta$ and it can be seen that the v_{par} is constant since $\vec{v_{par}} \times \vec{B} = 0$. The acceleration is perpendicular to the magnetic field direction and to v_{par}. So, the motion is composed of a circular motion with radius r around the magnetic field and a constant velocity along the magnetic field and can be described as $e(\vec{v} \times \vec{B}) = m_e\gamma\frac{d\vec{v}}{dt} = m_e\gamma\vec{a}$. Since only the $\vec{v_{per}}$ changes with time the acceleration is $m_e\gamma\frac{dv}{dt} = ev_{per}B(i_{per} \times i_{par})$ where i_{per} abd i_B are the unit vectors in velocity and magnetic field directions respectively. So the acceleration is

$a = \frac{eBv_{per}}{\gamma m_e}$. The angular frequency of the electron that moves through the spiral is given as $\omega_{gyration} = \frac{v_{per}}{r} = \frac{eB}{\gamma m_e c}$ and the frequency is $\nu_{gyration} = \frac{\omega_{gyration}}{2\pi}$. Since v_{par} is constant, a_{par}=0. If we consider acceleration as $\vec{a} = a_{par}i_{par} + a_{per}i_{per}$ then the radiation becomes as in equation (2.7).

$$\frac{dE}{dt} = \frac{e^2\gamma^4}{6\pi\varepsilon_0 c^3}(|a_{per}|^2 + \gamma^2|a_{par}|^2) \tag{2.7}$$

If the expression for the acceleration of the electron in its orbit is used and inserted into the expression for the radiation rate of a relativistic electron, the total radiation loss rate of the electron is given in equation (2.8).

$$-\frac{dE}{dt} = \frac{e^2\gamma^4}{6\pi\varepsilon_0 c^3}|a_{per}|^2 = \frac{e^2\gamma^4}{6\pi\varepsilon_0 c^3}\frac{e^2v^2B^2\sin^2\theta}{\gamma^2 m_e^2} = \frac{e^2B^2}{6\pi\varepsilon_0 c m_e^2}\frac{v^2}{c^2}\gamma^2\sin^2\theta \tag{2.8}$$

If we use $c^2 = (\varepsilon_0\mu_0)^{-1}$ we can rewrite the equation (2.8) as equation (2.9).

$$-\frac{dE}{dt} = 2\frac{e^4}{6\pi\varepsilon_0^2 c^4 m_e^2}\left(\frac{v}{c}\right)^2 c\frac{B^2}{2\mu_0}\gamma^2\sin^2\theta \tag{2.9}$$

The quantity in the first set of the round brackets on the right-hand side of equation (2.9) is the *Thompson cross-section* and it is defined as ($\sigma_T = \frac{e^4}{6\pi\varepsilon_0^2 c^4 m_e^2}$). Then we can write the total emitted power as equation (2.10) where $U_{mag} = \frac{B^2}{2\mu_0}$ is the energy density of the magnetic field.

$$-\frac{dE}{dt} = 2\sigma_T c U_{mag}\left(\frac{v}{c}\right)^2\gamma^2\sin^2\theta \tag{2.10}$$

This result is for electrons with a specific pitch angle theta. For an isotropic distribution of velocities this formula can be averaged over all angles for a given speed to obtain the average energy loss. If the pitch angle distribution is $P(\theta)d\theta = \frac{1}{2}\sin\theta d\theta$ then the average energy loss rate (total emitted power per electron) becomes as in equation (2.11).

$$-\frac{dE}{dt} = 2\sigma_T c U_{mag}\left(\frac{v}{c}\right)^2\gamma^2\frac{1}{2}\int_0^\pi \sin^3\theta d\theta = \frac{4}{3}\sigma_T c U_{mag}\left(\frac{v}{c}\right)^2\gamma^2 \tag{2.11}$$

Since the velocity and acceleration are perpendicular, the synchrotron radiation is beamed along the velocity vector with an opening angle $\Delta\theta \sim \gamma^{-1}$ [222]. The ob-

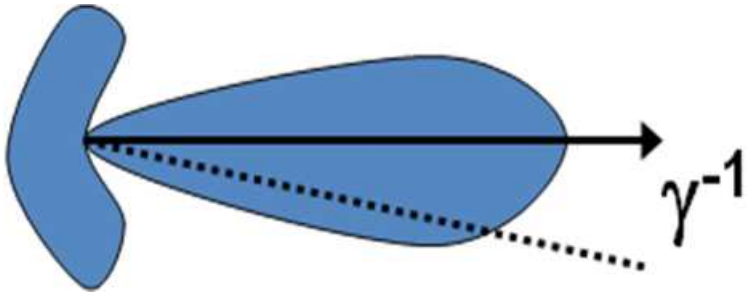

Figure 2.5. Angular distribution of radiation emitted by a particle with perpendicular velocity and acceleration [222]

server sees radiation for duration smaller than the gyration period, this means that the spectrum includes higher harmonics of $\omega_{gyration}$ The maximum harmonic is at a characteristic frequency which is $\omega_c \sim \frac{1}{\Delta t} \sim \frac{\gamma^2 e B_{per}}{m_e c}$. Because of the aberration effect, the radiation is decomposed by Fourier analysis into a sum of equivalent dipoles radiating at harmonics of the relativistic gyration frequency. Since the electron is relativistic, the energy radiated in the higher harmonics contributes to radiation. Electrons energy is $E = \gamma mc^2$ during its spiral motion the pitch angle will change and the radiation will be composed different frequencies. The resultant emission is a series of harmonics at well defined frequencies which broadened and forms continuous emission. The spectrum can be approximated by assuming that all the radiation of an electron of energy E is radiated at the critical frequency $\nu \approx \nu_c \approx \gamma^2 \nu_g$. The number of radiating electrons can be assumed as a power law in the form of $N(E) = KE^{-p}$, that relates the energy radiated in the frequency range ν-$d\nu$ to electrons with energies in the range E-E+dE. Each electron will lose energy via synchrotron emission thus, the emissivity (total emitted power per unit volume) can be written as in equation (2.12).

$$J_\nu d\nu = -\frac{dE}{dt} N(E) dE \tag{2.12}$$

Since $E = \gamma m_e c^2 = \left(\frac{\nu}{\nu_g}\right)^{1/2} m_e c^2$, $dE = \frac{m_e c^2}{2\sqrt{\nu_g}} \nu^{-1/2} d\nu$ and the derivative of energy with respect to time is $-\frac{dE}{dt} = \frac{4}{3}\sigma_T c \frac{v^2}{c^2} \left(\frac{B^2}{2\mu_0}\right) \left(\frac{E}{m_e c^2}\right)^2$, so emissivity can be written as in

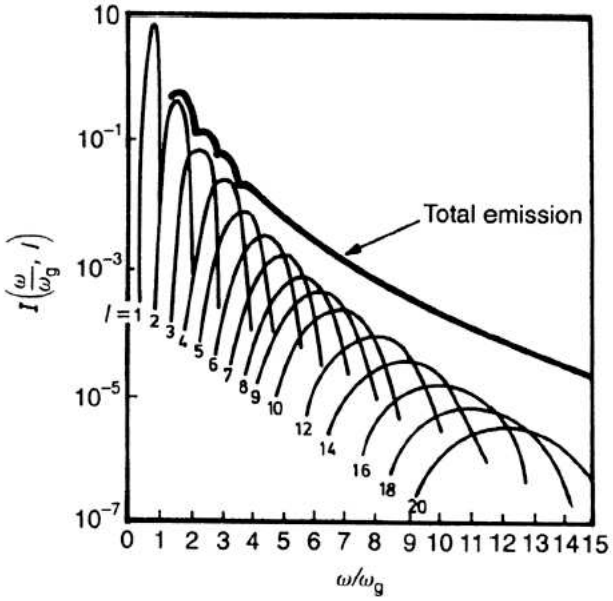

Figure 2.6. Synchrotron radiation is generated by the total harmonics spectra [153]

equation (2.13).

$$J(\nu) = (constants) K B^{\frac{p+1}{2}} \nu^{-(p-1)/2} \tag{2.13}$$

If the electron energy spectrum has power law index p, the spectral index of the synchrotron emission given by $j(\nu) \propto \nu^{-\beta}$ where $\beta = \frac{p-1}{2}$. Spectral index is the negative slope on a log-log plot of the spectrum.

2.1.1.4. Inverse Compton. Inverse compton scattering is an important radiative process to generate high energy photons. In this process, relativistic electrons scatter by low energy photons and they transfer part of their kinetic energy to low energy photons, by that means high energy photons are created. This case is treated by assuming that the energy of photons in the center of the momentum frame of the interaction is much less than $m_e c^2$ and the probability of the scattering is given by Thomson scattering cross-section [153]. In this process the net energy transferred per second from electron to photon can be derived by using kinematics of electron-photon scattering and the Lorentz transformation between electron rest frame and the observer's frame since the

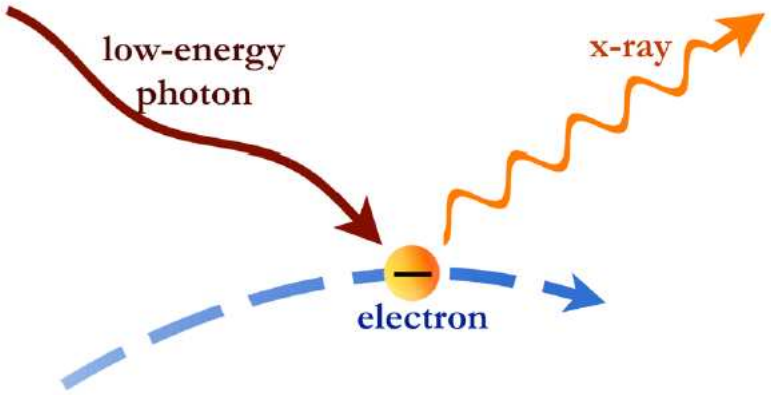

Figure 2.7. Inverse Compton Process [226]

electrons move relativistically in the observer's frame. The electron will extract from

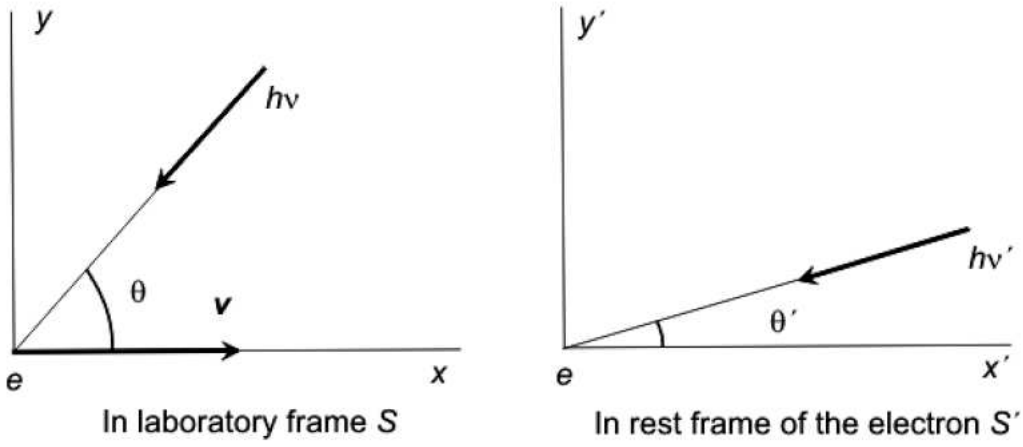

Figure 2.8. Inverse Compton scattering geometry [153]

the incident radiation the amount of power flowing through the area σ_T and radiate this power. As given by [225], the energy loss rate by the electron is $-\left(\frac{dE}{dt}\right)' = \sigma_T c U'_{rad}$, where U_{rad} is the energy density of radiation in the rest frame of the electron. The detailed derivation of the energy density in the electron rest frame and net power lost by the electron for inverse Compton scattering in the astrophysical regime can be found in [222] and [225]. The net power lost by the electron which is equal to the radiation increase is given by equation (2.14).

$$\frac{dE}{dt} = \frac{4}{3}\sigma_T c U_{mag} \left(\frac{v}{c}\right)^2 \gamma^2 \tag{2.14}$$

The spectrum of the resultant radiation from inverse Compton process is given in [227] (Figure 2.9). If the electron energy distribution in the inverse Compton process is a

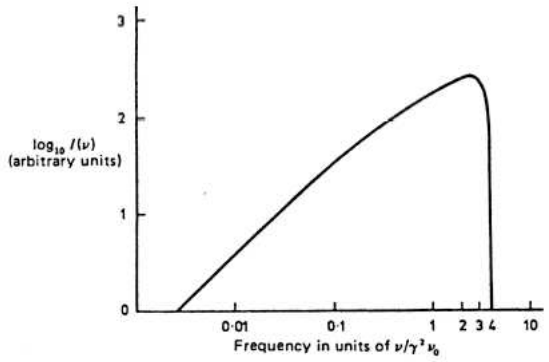

Figure 2.9. Compton Scattering Spectrum [227]

power law distribution, $dN = E^{-p}dE$ the scattered spectrum will also be a power law with $I(\nu) \propto \nu^{-\frac{p-1}{2}}$ [227].

2.1.2. X-Ray Absorption Processes

The main absorption mechanisms of the X-ray absorption seen in the X-ray spectra are, synchrotron self absorption, photo-ionization and Compton scattering.

2.1.2.1. Synchrotron Self Absorption. In the synchrotron discussion it is assumed that the all the photons that are emitted by the synchrotron mechanism can escape the system. This is not always the case and some amount of photons will be absorbed by the system and the normal synchrotron spectrum is modified by the re-absorption of some of the radiation by the relativistic electrons. The effect is called as synchrotron self absorption [222]. In the resultant spectrum there is a absorption in the lower frequency shown in figure (2.10).

2.1.2.2. Photo-Ionization. When an incoming photon with enough energy ($\hbar\omega$) to take an electron and lift it out the atom, ionization [228] occurs. The electron that leaves the atom is called the photoelectron. When the electron is taken out into the continuum

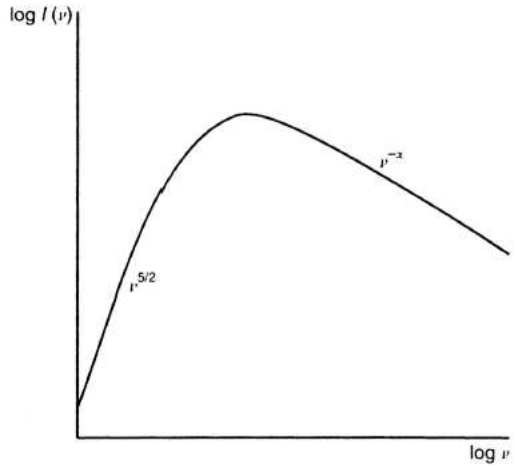

Figure 2.10. Synchrotron spectrum with self absorption [153]

by the incoming photon, there is a left over kinetic energy. In the figure (2.11) nucleus

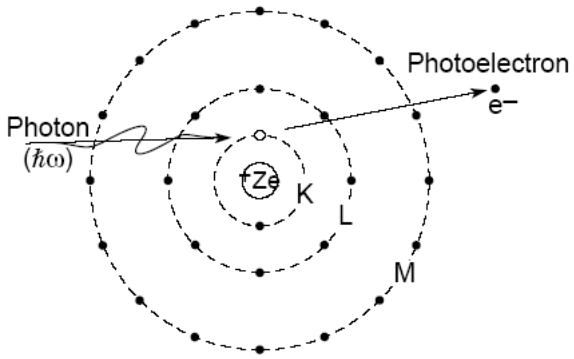

Figure 2.11. Photo-Ionization [228]

of charge $+Ze$ and surrounding it are the principle shells K,L,M. For K principle quantum number n=1, for L n=2 and for M n=3. Corresponding energy diagram for n=1,2,3,4 level is showed in the figure (2.12), the dashed line is the continuum level. The energy required to take out the core electron in the n=1 quantum number just to the continuum is called K-absorption edge.

2.1.2.3. Compton Scattering. Compton scattering process [225] occurs when a photon collides with a stationary electron. In this process photons scatter from lower to higher energies or higher to lower energies in interactions with electrons of higher (or lower) energies. For example, X-ray or Gamma-ray photons decrease in energy when they

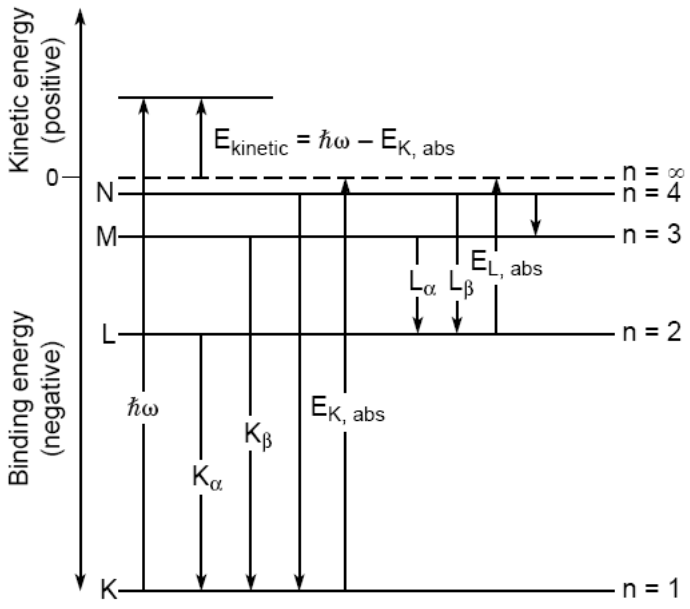

Figure 2.12. Atomic Energy Diagram [228]

interact with electrons.

2.2. Hydrogen Column Density

2.2.1. Interstellar Medium

The interstellar medium is consist of both gas and dust particles. Dust grains are solid, macroscopic particles composed of dielectric and refractory materials. The particles are irregularly shaped, and are composed of silicates, carbon, ice, *and/or* iron compounds.

The dust tends to scatter and absorb the *UV/optical* radiation from the source, the combination of these effects is called as *interstellar extinction* [229]. Extinction is more effective in shorter wavelength so the blue light is blocked more than the red light. As a result if there is extinction, the images appear redder than they should be, this is called *interstellar reddening* [230]. Dust grains can also absorb and scatter X-rays, although to an X-ray photon, a dust grain looks like a dense cloud of atomic gas, with the energies of the edges modified by being in solid materials rather than in

the gas phase.

Extinction is quantified as the difference between the observed and the real magnitude. It is conventional at ultraviolet wavelengths to express the interstellar extinction in units of magnitudes, A_λ, normalized in terms of a color excess that represents the selective extinction is $E(B-V) = A_B - A_V$. A_B and A_V are the absorption in magnitudes in the photometric B and V band but, in general they represent any particular wavelength.

There is a simple relation between the selective extinction, expressed in terms of color excess, and the total extinction, expressed in terms of the extinction at a specific wavelength, usually A_V. This is defined by the ratio of total to selective extinction by $R_V = \frac{A_V}{E(B-V)}$. Observationally, R_V expressed in terms of one of two specific values $R_V = 3.1$ [231], which is typical of the Diffuse ISM and $R_V = 5$ which is typical of dense clouds. The larger value of R_V is thought to be a consequence of different distributions of grain sizes in high-density versus low-density environment, in the sense that larger R_V indicates larger grains on average. In fact, R_V is an empirical factor introduced to account for observed differences in the universal extinction law seen in different environments. The physics behind it is not understood fully yet.

Approximately 99 per cent of the interstellar medium is composed of interstellar gas, and of its mass, about 75 per cent is in the form of hydrogen (either molecular or atomic), with the remaining 25 per cent as helium. The interstellar gas consists partly of neutral atoms and molecules, as well as charged particles, such as ions and electrons. This gas is extremely dilute, with an average density of about 1 atom per cubic centimeter. The interstellar gas is typically found in two forms: cold clouds of neutral atomic or molecular hydrogen and hot ionized hydrogen. The neutral and molecular forms emit radiation in the radio band of the electromagnetic spectrum. The ionized hydrogen is produced when large amounts of ultraviolet radiation. The atoms and ions of the different elements that make up the gas in the intervening ISM material can absorb the background sources radiation at specific wavelengths corresponding to different electronic transitions in the gas atoms giving interstellar absorption lines

superimposed on the intrinsic stellar spectrum. X-rays remove electrons from atoms and ions, and those photoelectrons can provoke secondary ionizations.

2.2.2. X-Ray Absorption

Among X-ray absorption processes, we will deal with photoelectric absorption [225] since it is dominant at low energies $(0-100keV)$. Basic features of the absorption can be derived by considering a beam of light with an initial intensity I_0, travelling in the x direction along our line of sight and passing through an idealized slab of intergalactic gas of thickness L (Figure 2.13). Number density of absorbers of element

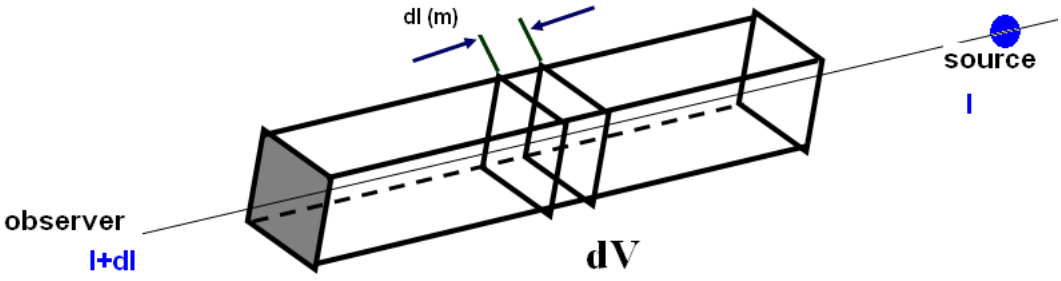

Figure 2.13. Light travelling to the observer passing through a slab of intergalactic gas

Z (particles per unit volume, m^{-3}) is $n_z(x)$ and each absorber has cross-sectional area σ_λ (cm^2). Cross-section offered by element Z at energy E is $\sigma_z(E)$ (m^2). If the beam travels through dx, total area of absorbers is the fraction of volume dV which is locked by the presence of element Z is $number of absorbers \times cross-section = n_z(x) \times \sigma_{z,\lambda}$. The rate of change of the intensity $I(x)$ along x is negative and is proportional to both the number density $n_z(x)$ of absorbing atoms and the intensity itself is given by equation (2.15).

$$\frac{dI_\lambda}{I_\lambda} = -n_z(x)dx\sigma_{z,\lambda} = -n_z(x)\sigma_{z,\lambda}dx \Longrightarrow dI_\lambda = -n_z(x)\sigma_{z,\lambda}I_\lambda dx \equiv a_\lambda I_\lambda(x)dx \quad (2.15)$$

In equation (2.15) a_λ is the line absorption coefficient of the medium, it represents then the cross-section of the absorbing atoms and has units of area. To solve $I(x)$, we

integrate over length from source along x, from 0 to L (equation 2.16 and 2.17).

$$\int_0^L \frac{dI_\lambda}{I_\lambda} = \int_0^L -n_z(x)dx\sigma_{z,\lambda} = -\sigma_{z,\lambda}(E)\int_0^L n_z(x)dx \tag{2.16}$$

$$\ln\frac{I_\lambda}{I_{\lambda,0}} = -\sigma_{z,\lambda}(E)\int_0^L n_z(x)dx \Longrightarrow I_\lambda(x) = I_{\lambda,0}\exp\left(-\sigma_{z,\lambda}(E)\int_0^L n_z(x)dx\right) \tag{2.17}$$

If all elements in the line of sight is included then the intensity is given as in equation (2.18).

$$I_\lambda(x) = I_{\lambda,0}\exp\left(-\sum_z \sigma_{z,\lambda}(E)\int_0^L n_z(x)\frac{n_H}{n_H}dx\right) \tag{2.18}$$

$$\sigma_{eff}(E) = \sum_z \sigma_{z,\lambda}(E)\frac{n_z(x)}{n_H}dx \tag{2.19}$$

If we define $\sigma_{eff}(E)$ (equation 2.19) the effective cross-section, weighted over the abundance of hydrogen element with respect to hydrogen, then the intensity is given by equation (2.20).

$$I_\lambda(x) = I_{\lambda,0}\exp\left(-\sigma_{eff}(E)N_H\right) \tag{2.20}$$

When the absorption of the light from a X-ray source by the interstellar medium is considered, the cross section multiplied by the Hydrogen density N_H defines the optical depth τ_λ,to a source at a distance x. It is a dimensionless quantity as $\tau_\lambda = \sigma_{eff}N_H$. Absorption over the considered path reduces the intensity to $e^{-\tau}$ relative to the initial value. N_H is defined as the hydrogen column density which is the integral of the number density along the line of sight; $N_H = \int n_H dx$. N_H is the number of H-atoms per m^2 column. It is measured from the 21cm atomic hydrogen line. N_H is the number of equivalent hydrogen atoms in line o sight. Although N_H is used as the parameter, virtually none of the absorption is due to hydrogen in soft X-rays region.

The threshold for hydrogen ionization is 13.6 eV, for any X-ray photon hydrogen is completely ionized. When dealing with X-ray spectra the hydrogen column density is used to build absorption curves in photoelectric absorption model.

2.2.2.1. Photoelectric Absorption Model. The radiation observed from a source passes through the interstellar medium while reaching the observer. When the energy of the radiation is in X-ray range, the effects of the interstellar gas are seen as an absorption curve in the soft X-rays. This absorption curve is due to the photo-ionization of the interstellar gas (C, N, O, Fe-L, Ne, Mg, Si, S, Ar, Ca, Fe, Ni). Hydrogen and Helium don't absorb X-ray photons, but all the other elements absorb X-rays. A given pattern of other abundances for these elements with respect to Hydrogen is assumed. Usually, the distribution of elements within Sun is used. The photoelectric absorption cross-section [225] for photons with energy greater than the electron binding energy and $h\nu \ll m_e c^2$ is given by equation (2.21) where a is the fine structure constant and σ_T is the Thompson cross section [225].

$$\sigma_K = 4\sqrt{2}\sigma_T a^4 Z^5 (m_0 c^2/\nu)^{7/2} \tag{2.21}$$

Figure (2.14) shows the absorption cross-section for the interstellar gas assuming typical abundances. The K-shell absorption edges of the elements forms the discontinuities in the figure (2.14). One of the most widely used X-ray absorption model is calculated by the effective absorption cross section given in [233]. They use the element abundances given in the figure (2.15) and obtain the absorption curve using the analytical fit coefficients (Figure 2.16) between 0.25 keV and 10 KeV. The photoelectric absorption cross section per hydrogen atom, $\sigma(E)$, is given by $\sigma(E) = (C_0 + C_1 E + C_2 E^2) E^{-3} \times 10^{-24} cm^2$ where the energy E is in terms of keV [233]. The cross section coefficients in [233] are obtained for the analytic fit according to given abundances (Figure 2.15) where all elements are taken as in neutral atomic form in gas phase. We obtain the same absorption curve (Figure 2.17) by evaluating the given cross section coefficients for the related energy range. In this model, the X-ray absorption is independent of the physical state of the elements, the optical thickness of the grains and the scattering

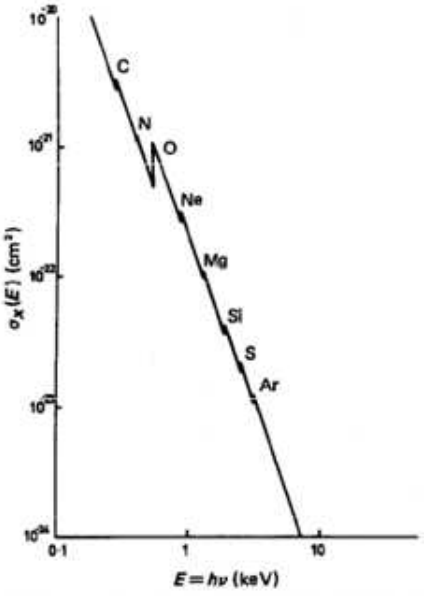

Figure 2.14. The absorption cross-section for interstellar gas assuming typical abundances [232]

ELEMENTAL ABUNDANCES

Element	Abundance[a]	Fraction in Grains[b]
H	12.00	0.
He	11.00	0.
C	8.65	1.
N	7.96	1.
O	8.87	0.25
Ne	8.14	0.
Na	6.32	1.
Mg	7.60	1.
Al	6.49	1.
Si	7.57	1.
S	7.28	1.
Cl	5.28	1.
Ar	6.58	0.
Ca	6.35	1.
Cr	5.69	1.
Fe	7.52	1.
Ni	6.26	1.

Figure 2.15. Element abundances used by Morrison and McCammon (1983) [234]

due to the grains can be neglected [233]. The effect of molecular form of the hydrogen and the absorption corresponding to UV range is also neglected [235]. Figure (2.17) shows the photoelectric absorption cross section which is scaled by $\left(\frac{E}{keV}\right)^3$ just for the appearance of the plot. A photoelectric absorption model of the radiation for a given

COEFFICIENTS OF ANALYTIC FIT TO CROSS SECTION

Energy Range (keV)	c_0	c_1	c_2
0.030–0.100[a]	17.3	608.1	−2150.
0.100–0.284	34.6	267.9	−476.1
0.284–0.400	78.1	18.8	4.3
0.400–0.532	71.4	66.8	−51.4
0.532–0.707	95.5	145.8	−61.1
0.707–0.867	308.9	−380.6	294.0
0.867–1.303	120.6	169.3	−47.7
1.303–1.840	141.3	146.8	−31.5
1.840–2.471	202.7	104.7	−17.0
2.471–3.210	342.7	18.7	0.0
3.210–4.038	352.2	18.7	0.0
4.038–7.111	433.9	−2.4	0.75
7.111–8.331	629.0	30.9	0.0
8.331–10.000	701.2	25.2	0.0

Figure 2.16. Analytic fit coefficients used by Morrison and McCammon (1983) [233]

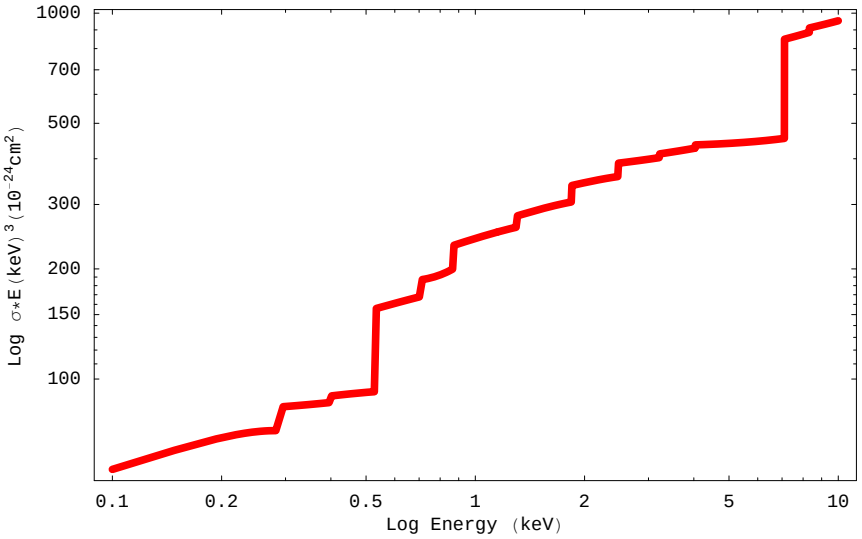

Figure 2.17. A log-log plot of the net photoelectric absorption cross section per hydrogen atom as a function of energy

energy E, is in the form of $Photoelectric\ Absorption(E) = e^{-\sigma(E)N_H}$ (where $\sigma(E)$ does not include Thomson scattering) [236]. The photoelectric absorption depends on the low intermediate atomic number (Z) atoms along the line of sight that cause soft X-ray absorption. This absorption is quantified N_H, the column density of neutral material with solar metallicity that would cause the absorption. When N_H is obtained from a given spectra this measurement can be model dependent since it is performed by

computing the difference of the observed soft X-ray flux with respect to a model in the same energy range. We illustrated the N_H dependence of the photoelectric absorption model. Figure (2.18 and 2.19) shows the photoelectric absorption for different N_H values; $0.4 \times 10^{22} cm^{-2}$ (pink line), $1 \times 10^{22} cm^{-2}$ (blue line), $2 \times 10^{22} cm^{-2}$. As a result we see that as the N_H increases, the corresponding photoelectric absorption tends to increase.

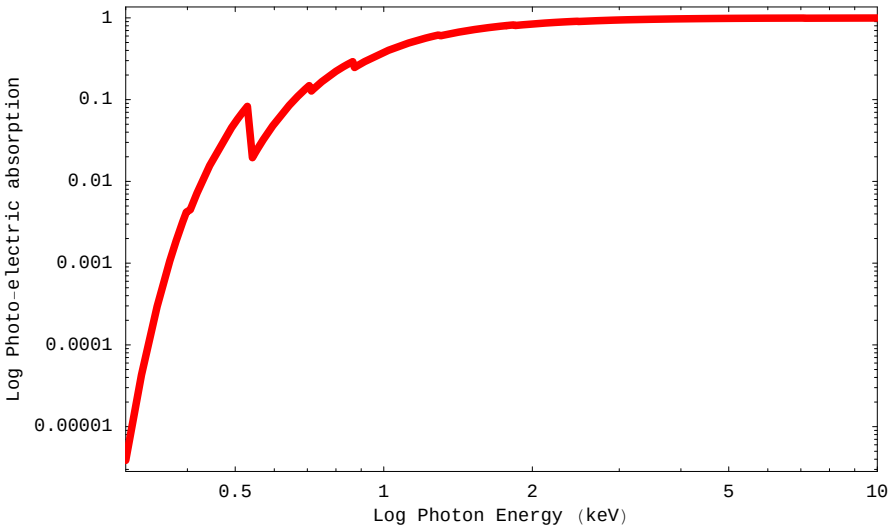

Figure 2.18. Photoelectric absorption for $N_H = 0.4 \times 10^{22} cm^{-2}$

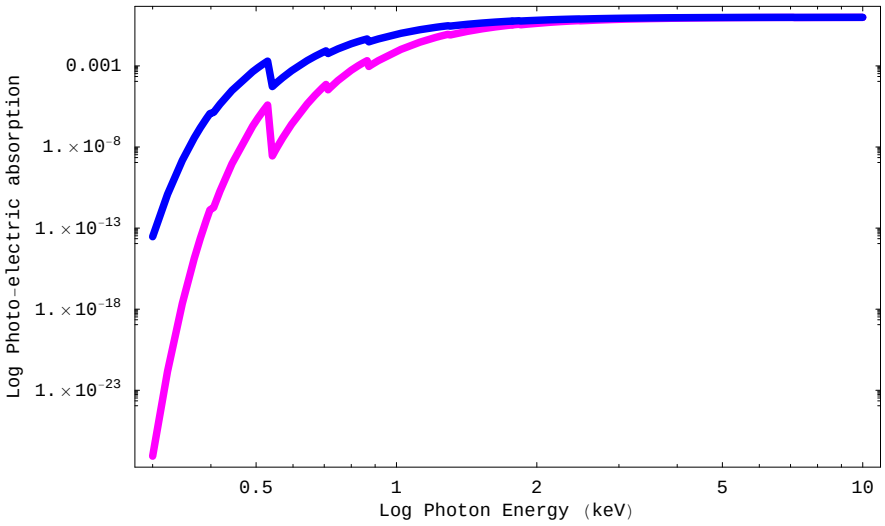

Figure 2.19. Photoelectric absorption for different N_H values

2.2.2.2. Photoelectric Absorption Model for a Specific Redshift. When an extragalactic source is observed, the radiation first passes through the host galaxy interstellar medium of the source, and then it passes through the intergalactic medium and reaches the Milky Ways interstellar medium. The intergalactic medium does not absorb unless there are cosmic objects in the line of sight. The interstellar medium (ISM) of the sources host galaxy causes a photoelectric absorption as Milky Way does. The host galaxy Hydrogen Column Density which is the intrinsic Hydrogen Column Density (N_{Hint}) refers to the medium beyond Milky Way on radiations way through the observer. When a spectrum of a source in a specific redshift is considered, the redshift affects the energy due to the Doppler Effect. The redshift of the source cause the observed energy range to be redshifted. The photoelectric absorption model of the radiation in a given energy E for a specific redshift (z) is in the form of $Photoelectric\ Absorption(E,z) = e^{-\sigma(E(1+z))N_H}$ [236]. For instance, for an observation in the 0.3-10 keV energy range if the source is in $z = 1$, what is observed is not the true spectrum at this band. The true spectrum of the source is seen between 0.6 20 keV which is redshifted. Figure (2.20) shows the photoelectric absorption for a source at $z = 1$. Figure (2.21) shows the photoelectric absorption for a source at z=1 and

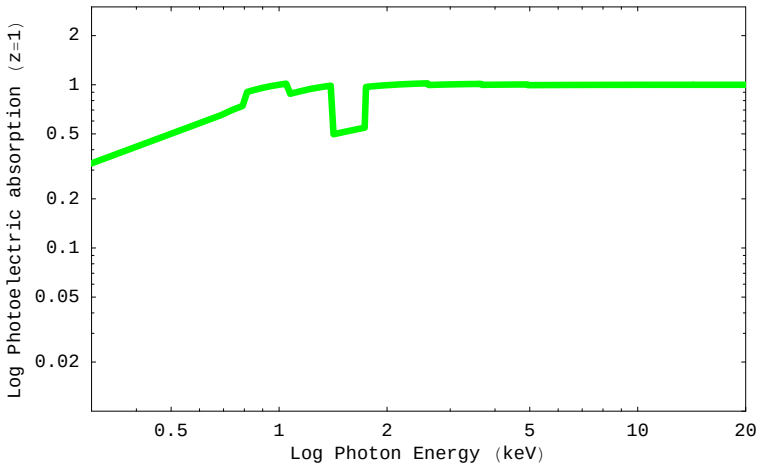

Figure 2.20. Photoelectric absorption for $N_H = 1 \times 10^{22} cm^{-2}$ at $z = 1$

at z=0 for the same $N_H = 1 \times 10^{22} cm^{-2}$. The absorption at z=1 is lower (green line) than the absorption at z=0 (blue line) as seen in the figure (2.21).

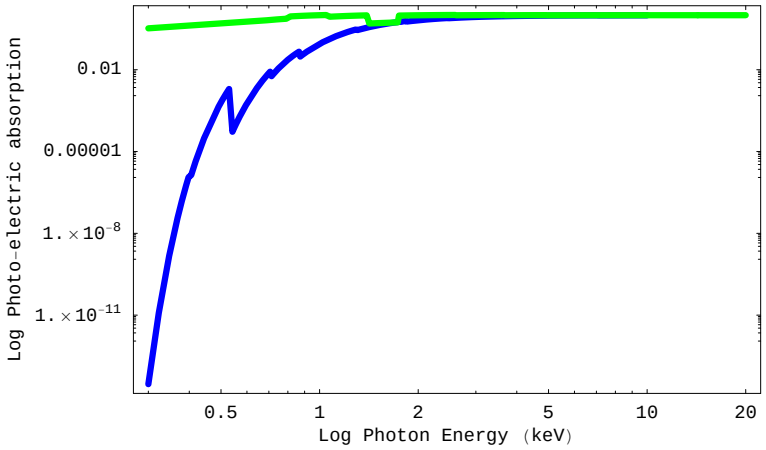

Figure 2.21. The photoelectric absorption for different redshifts

2.2.2.3. Photoelectric Absorption Model for Black Body Radiation. In general, X-ray spectral distributions are modeled with the flux f(E) given as equation (2.22).

$$f(E) = Ce^{-\sigma(E)N_H} f(S,E) photons cm^{-2} s^{-1} keV - 1 \tag{2.22}$$

In equation (2.22) C is the normalization constant, N_H is the neutral Hydrogen column density to, $\sigma(E)$ is the photoelectric cross-section per Hydrogen atom for absorption of photons of energy E by interstellar medium and S is a parameter in the intrinsic spectral shape. For the black body radiation, parameter in the intrinsic spectral shape is the temperature (T). The X-ray spectrum for a black body (where Energy E and kT are in keV) is modeled with equation (2.23).

$$f(E,T) = Ce^{-\sigma(E)N_H} \frac{3.14491 \times 10^{35} E^3}{\left(exp\left(\frac{E(keV)}{keV}\right)\right) - 1} \tag{2.23}$$

Figure (2.22) shows the black body radiation for kT=1 (red line) and the black body radiation for kT=1 with the photoelectric absorption with $N_H = 0.4 \times 10^{22} cm^{-2}$ (black line). Figure (2.22) shows log-log plot of the black body radiation with kT=1kev (red line) and the black body radiation with absorption (black line) $kT = 1keV$.

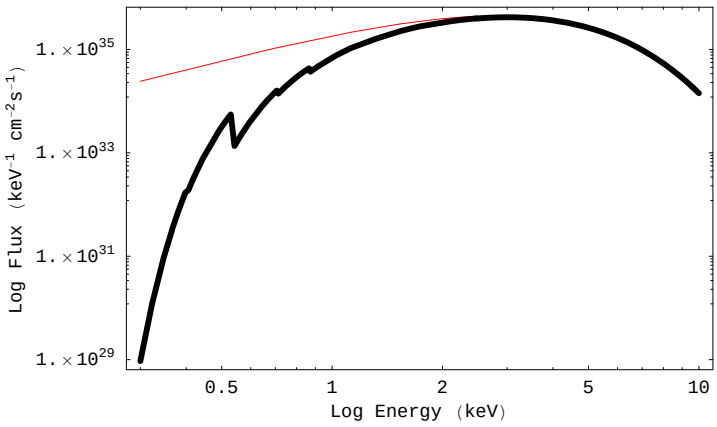

Figure 2.22. Photoelectric absorption model for black body radiation

2.3. Power Law Models

2.3.1. Simple Power Law Model

Synchrotron spectra typically have a power law shape. The flux is proportional to photon energy to some power. The power law photon index is defined as the constant, Γ, in the expression $f(\Gamma, E) = NE^{-\Gamma}$ where N is the normalization and E is the energy. Power law photon index (Γ) is the negative slope on a $\log f(\Gamma, E)$- $\log(E)$ spectrum. The relation between the power law photon index and the spectral index is given as $\Gamma = \beta + 1$. Figure (2.23) shows a $\log f(\Gamma, E)$- $\log(E)$ spectrum which is $f(E_{min}, E_{max}) = \int_{E_{min}}^{E_{max}} N \left(\frac{E}{keV}\right)^2$ for $\Gamma = 2$. Figure (2.24) shows $\log f(\Gamma, E)$- $\log(E)$ spectrum for different power law photon indexes; $\Gamma = 1$ (green line), $\Gamma = 2$ (yellow line), $\Gamma = 3$ (turquoise line), $\Gamma = 4$ (pink line). The hardness ratio of the spectrum is generally defined as equation (2.24).

$$Hardness\,ratio = \frac{Flux\,in\,Soft\,Energies}{Flux\,in\,Hard\,Energies} \tag{2.24}$$

If the power law photon index increases, namely the slope gets larger, the ratio of the soft energy flux to the hard energy flux is larger and the spectrum is called to be softer. If the power law photon index decreases, the ratio of the soft energy flux to the hard energy flux is lower and the spectrum is called to be harder.

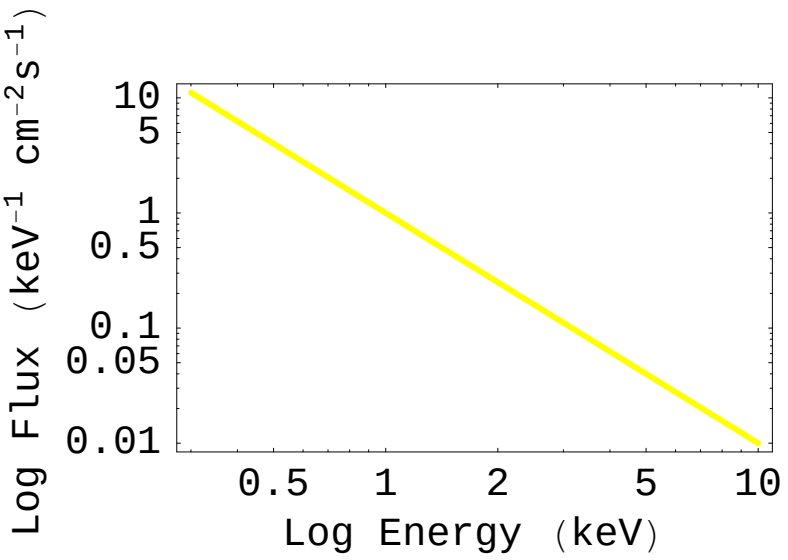

Figure 2.23. $\log f(\Gamma, E)$- $\log(E)$ plot for power law model where energy is in terms of keV and $N = 1$

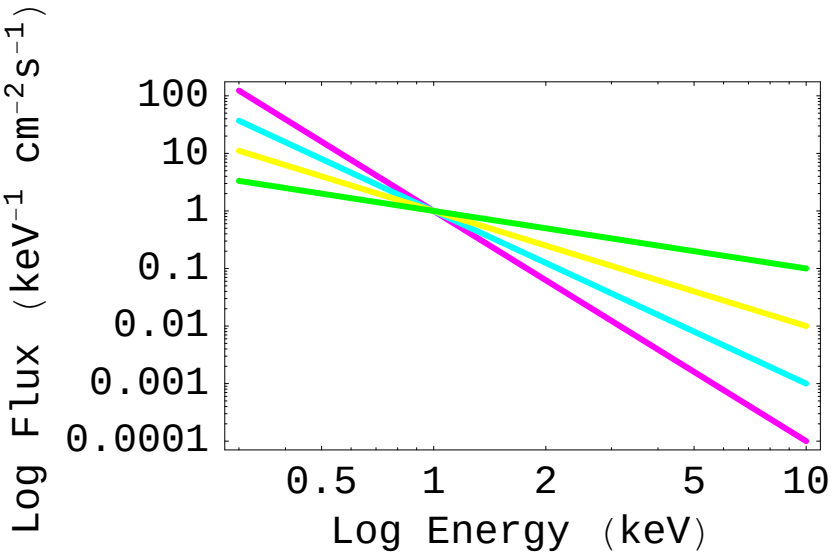

Figure 2.24. $\log f(\Gamma, E)$- $\log(E)$ plot for power law model with different indexes

2.3.1.1. Photoelectric Absorption Model For Simple Power Law Model. For the synchrotron radiation, parameter in the intrinsic spectral shape is the power law photon index (Γ). The X-ray spectrum for a power law is modeled with $f(\Gamma, E) = Ce^{-\sigma(E)N_H}E^{-\Gamma}$. C is the normalization constant, N_H is the neutral Hydrogen column density to source, $\sigma(E)$ is the photoelectric cross-section per Hydrogen atom for absorption of photons of energy E by interstellar medium and Γ is the power law pho-

ton index. Figure (2.25) shows the photoelectric absorption model (red line) for the power law index $\Gamma = 2$, where $N_H = 0.4 \times 10^{22} cm^{-2}$ yellow line represents $\Gamma = 2$ with $N_H = 0$. Figure (2.26) shows the photoelectric absorption model for the simple power law with different power law photon indexes ($\Gamma = 2$ red line, $\Gamma = 3$ blue line, $\Gamma = 4$ green line) where the Hydrogen column density is the same ($N_H = 0.4 \times 10^{22} cm^{-2}$). It can be seen from the figure (2.26) that the power law photon index changes the shape of the photoelectric absorption curve. Figure (2.27) shows the photoelectric absorption model for the same power law photon index ($\Gamma = 2$) with different Hydrogen column density values ($N_H = 0.4 \times 10^{22} cm^{-2}$ red line, $N_H = 1 \times 10^{22} cm^{-2}$ green line, $N_H = 2 \times 10^{22} cm^{-2}$ pink line). Figure (2.27) shows that as the Hydrogen column density increases, the observed flux is decreases due to the increase of the absorption. Figure (2.28) shows $\log f(\Gamma, E)$- $\log(E)$ absorbed power law model with $\Gamma = 1$, $N_H = 0.4 \times 10^{22} cm^{-2}$ (turquoise line) and $\Gamma = 2$, $N_H = 2 \times 10^{22} cm^{-2}$ (pink line) . It can be seen from the model that a higher power law photon index corresponds to a higher column density.

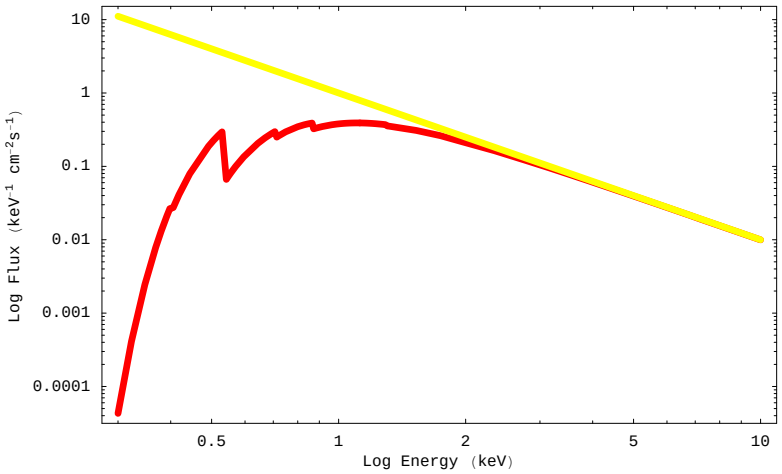

Figure 2.25. $\log f(\Gamma, E)$- $\log(E)$ absorbed power law model for $\Gamma = 2$

2.3.2. Cut Off Power Law Model

Cut of power law model is a power law with high energy exponential roll off. The model is in the form of $f(\Gamma, E) = N(E/1keV)^{-\Gamma} e^{-E/E_{cutoff}}$ where, Γ is the power law photon index. N is the normalization in units of photons/keV/cm^2/s at 1 keV and

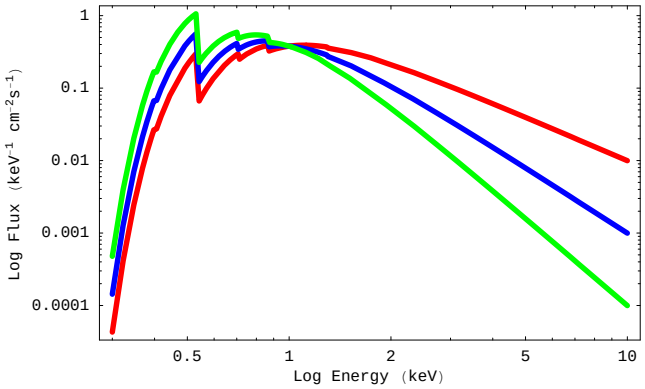

Figure 2.26. $\log f(\Gamma, E) - \log(E)$ photoelectric absorption model for the different power law photon indexes

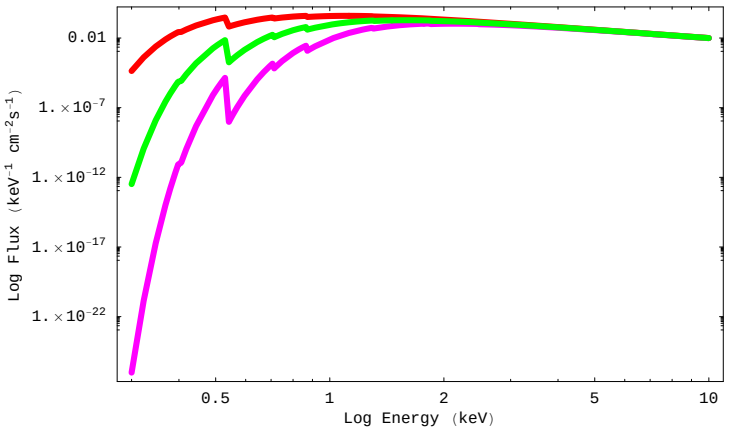

Figure 2.27. $\log f(\Gamma, E) - \log(E)$ photoelectric absorption model for the different column density values

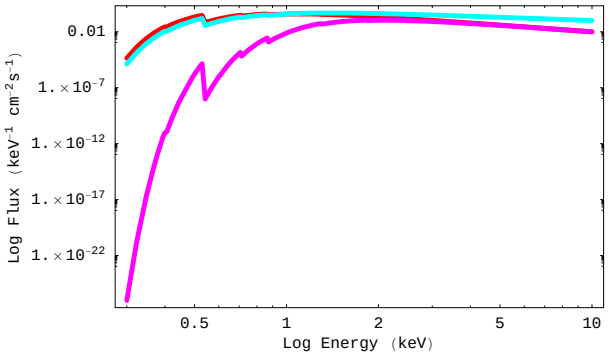

Figure 2.28. $\log f(\Gamma, E) - \log(E)$ photoelectric absorption model for different Γ and N_H values

E_{cutoff} is the electron-folding energy of exponential roll off in keV. Figure (2.29) shows the cut off power law model for $\Gamma = 1$ and $E_{cutoff} = 3keV$

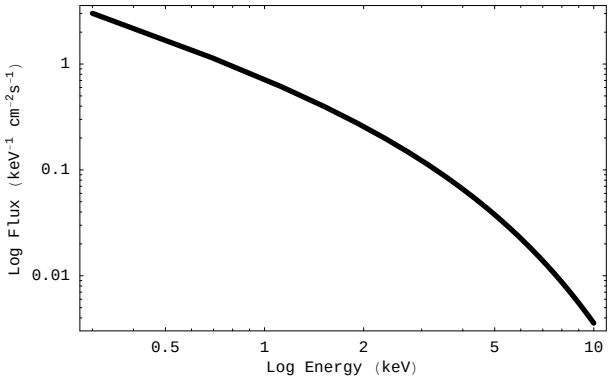

Figure 2.29. Cutoff Power law model

2.4. Hydrogen Column Density and Power Law photon Index Correlation

Hydrogen column density and the power law photon index are the two parameters of the simple absorbed power law model. To investigate the relation between the Hydrogen column density and the power law photon index we created fake spectra in Xspecv.14 [237]. We used *fakeit none* command and use the instructions in [238]. Those fake spectra represent the simple absorbed power law model (wabs*zwabs*pow) [236] with a sum of two absorptions, the intrinsic and the Galactic, as in the case of GRB spectra. Our aim is to show how the power law photon index variations affect the intrinsic Hydrogen column density during the spectral fitting procedure. We created 6 different spectra with different power law photon indexes and in each spectra we used the same fixed galactic column density $0,01.10^{22}cm^{-2}$, same fixed intrinsic column density $0,1.10^{22}cm^{-2}$, same fixed redshift 0.3 and a fixed normalization that corresponds to 1,000 counts in 0.3-10 keV band. When we fix the normalization we used the count rate energy relation given in [239] which is $1count/sec = 5.10^{1}1$ $erg/cm^2/count$. We fit each fake spectrum with simple absorbed power law model to obtain the model parameters and see how the real parameters modified with the spectral fitting procedure. In each fit we fixed redshift and galactic column density and set N_{Hint} and Γ as free parameters. We get the parameters from the fits that are statistically acceptable (*null hypothesis probability value* > 0.05). To see if there is a

correlation between the intrinsic column density and power law photon index obtained from this procedure, we plotted N_{Hint} versus Γ and performed Pearson's correlation test [240]. We obtained the Person index r=0.88 with a chance probability 0.02 that indicates a possible correlation (since the probability of the correlation is not by chance by 98 per cent. An other way to see the correlation between the two parameters is

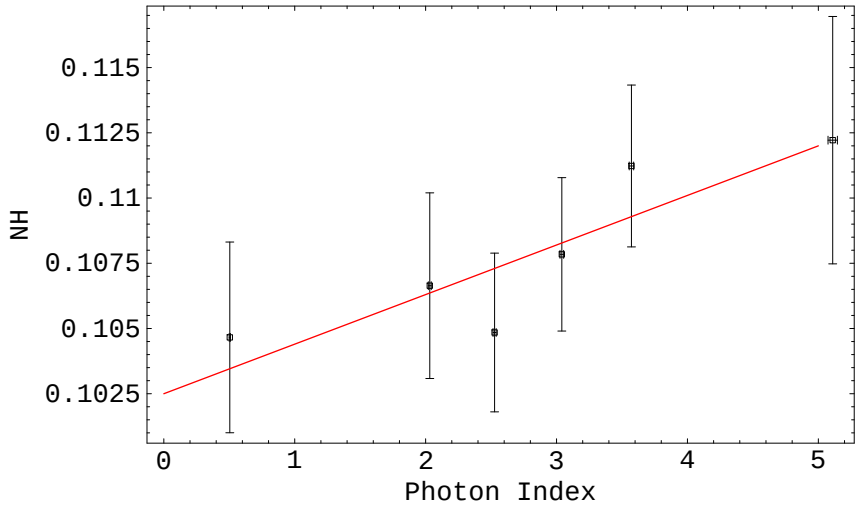

Figure 2.30. N_{Hint}-Γ correlation

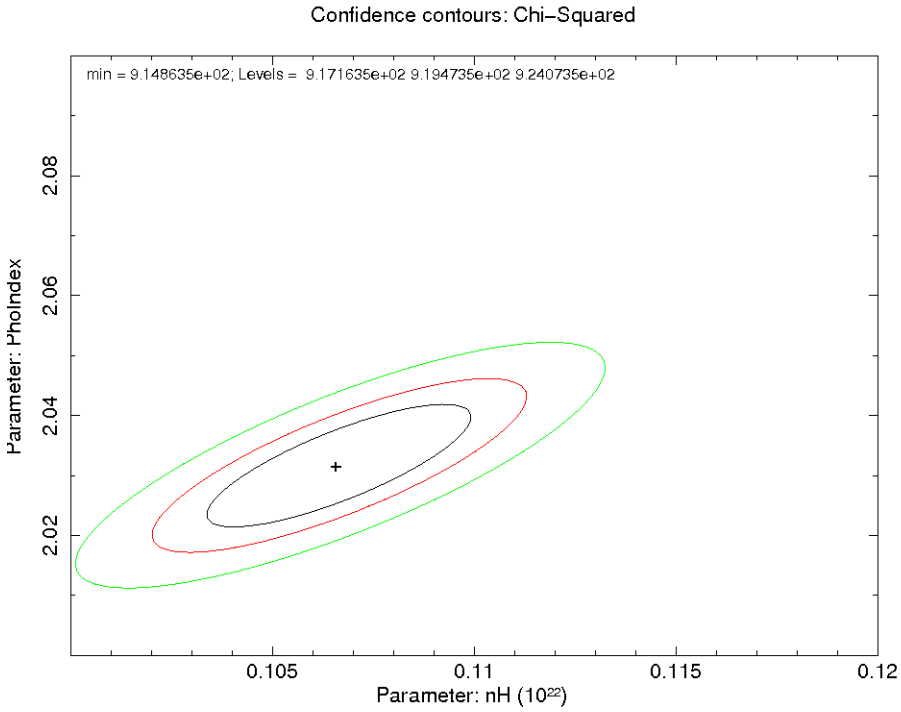

Figure 2.31. N_{Hint}-Γ contour plot

the contour plot of the confidence contour of the fit. For example for one of the fake spectra (the one with $\Gamma = 2$) when we fit the spectra and get the errors for the Γ and N_{Hint} we used *steppar* command to have the contour plot. The point and the inner contour are the best fit and each contour represent 1,2,3, sigma (from inside to outside respectively) confidence contour of the fit on one spectrum (Figure 2.31). We found that due to the spectral fitting procedure, there is a positive correlation between the two parameters. This means that if the spectra are fit by a larger photon index, a larger column density is obtained in order to hide huge number of photons of lower energies. In this work since we deal with GRB X-ray afterglows which are generally fit by an absorbed simple power law model, we expect to see a positive correlation between the N_{Hint} and the Γ which is a spurious effect coming from the spectral fitting procedure due to the power law photon index variations.

3. DATA AND METHODOLOGY

In this chapter, first a brief introduction about the Swift satellite is given. Then our methodology and the data is introduced. The data analysis about the spectral data used in this work is summarized. Then how the X-ray spectral parameters treated for the variation and correlation searches is given in the data processing section. At the end of this section, the light curves and important properties of the GRBs in our sample is given.

3.1. Swift

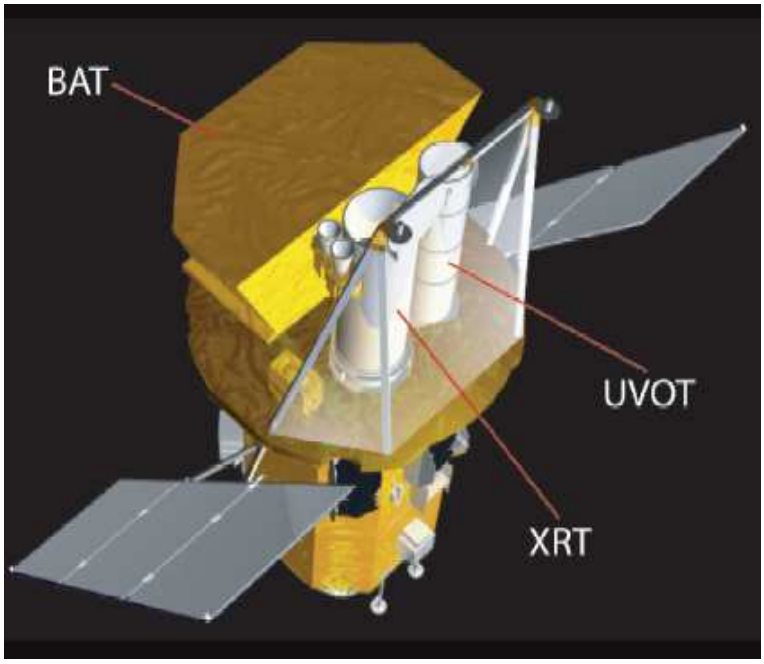

Figure 3.1. Swift satellite. Image courtesy of NASA Swift Team

Swift [43] satellite is built to the study of Gamma-ray burst. Swift was launched on November 20, 2004. The main mission objectives of Swift are to determine the origin of GRBs, to classify GRBs, to determine how the blast wave evolves and interacts with the environment, to use GRBs to study the early universe and to perform a sensitive survey of the sky in the hard X-rays. Swift has three instruments that work together to observe GRBs. These are Burst Alert Telescope (BAT) [78] ,Ultraviolet/Optical Telescope(UVOT) [241] and X-Ray Telescope (XRT) [243]. BAT is the largest instrument

on-board that can view nearly a sixth of the entire sky at one time. When it detects a GRB, in a few seconds the spacecraft autonomously repoints itself to aim the XRT and UVOT at the GRB to get high-precision X-ray and optical positions and spectra. The highprecision positions are announced to the ground for use by a network of observers. By its quick response Swift provides redshifts and detailed multi-wavelength light curves for the afterglows. Swift data is relayed to the ground in real-time and is immediately shared with the world through GRB Coordinate Network (GCN). Swift data is available for everyone via three different data centers located in the United States (the High Energy Astrophysics Science Archive Research Center, HEASARC), the UK (the UK Swift Science Data center, UKSSDC) and Italy (the Italian Swift Achieve Center, ISAC).

Table 3.1. Time table of Swift observational process [242]

Time	*S/CEvent*	*Time*	*GroundEvent*
0s	GRB	|	|
10s	Slew begins	20s	BAT location distributed
$\sim 50s$	GRB acquired	|	|
55s	XRT image	70s	XRT location distributed
150s	UVOT finding chart	240s	Optical finding chart distributed
1200s	XRT spectrum	1210s	XRT spectra distributed
7200s	UVOT filters complete	|	|
$\sim 10^4 s$	Ground station pass	|	All burst data, new observing program uploaded

3.1.1. Swift's X-ray Telescope (XRT)

The XRT [243] is a focusing X-ray telescope with a 110 cm^2 effective area at 1.5 keV 23 arcmin field of view, 18 arcsec resolution (half-power diameter), and 0.2-10 keV energy range. The instrument parameters can be summarized as in table (3.2). More information on the XRT is given by [245] and [246]. The XRT can pinpoint GRBs to 5-arcsec accuracy within 10 seconds and can observe GRBs X-Ray counterparts in 20-70 seconds from burst discovery. The XRT has three readout modes which are

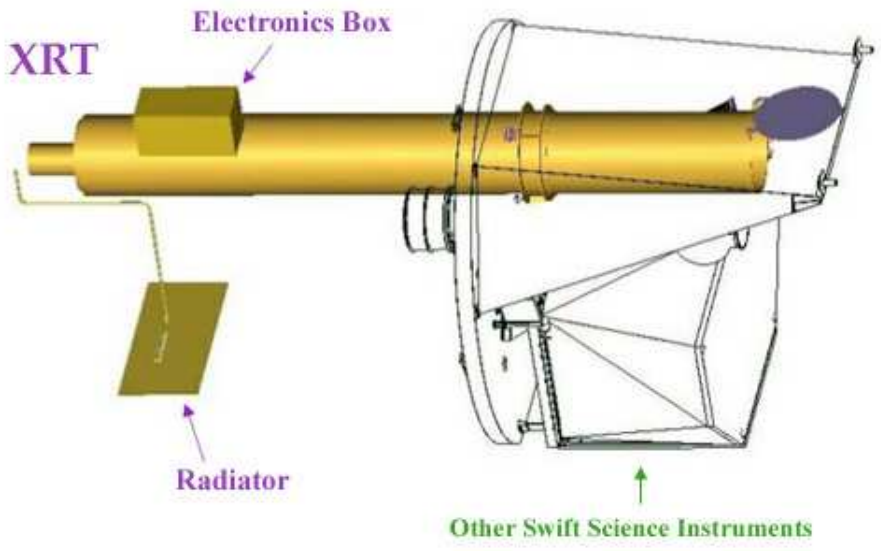

Figure 3.2. Swift's X-Ray Telescope XRT layout [244]

Table 3.2. Properties of XRT [244]

Time	*S/CEvent*
Telescope	JET-X Wolter I
Focal Length	3.5m
Effective Area	110 cm^2@1.5keV
Telescope PSF	18 arcsec HPD @ 1.5 keV
Detector	EEV CCD-22, 600 x 600 pixels
Detector Operation	Imaging, Timing, and Photon-counting
Detection Element	40 x 40 micron pixels
Pixel Scale	2.36 arcsec/pixel
Energy Range	0.2-10 keV
Sensitivity	$2x10^{-14}ergcm^{-2}s{-}1in104seconds$

autonomously determined. Imaging Mode gives an integrated image measuring the total energy deposited per pixel and it is not used spectroscopy. Timing Mode give high time resolution without position information. Timing Mode allows bright source spectroscopy through rapid CCD readouts. Photon-counting Mode gives spectral and spatial information for source fluxes ranging from the XRT sensitivity limit of 2×10^{-14} to 9×10^{-10} erg cm^{-2}/s.

3.2. Methodology

3.2.1. Data Analysis

Swift X-ray Telescope (XRT) observes X-ray emission from Gamma-ray bursts and their afterglows in the energy band 0.2-10 keV. The XRT data used in this work are taken from Brera Observatory Swift Team Archive. The GRB XRT archives have been prepared by Raffaella Margutti and Francesco Pasotti.

The analysis starts from cleaned, calibrated event lists which are produced by Swift data center (NASA/GSFC). At this stage the data are calibrated for Earth limb contribution and CCD defects. The software package XSPEC 12 [237] is used for the analysis. Swift has different observation modes; imaging, two timing modes and photon-counting [247]. The treated data contains only WT (Window Timing) and PC (Photon Counting) modes.

The difference of the two modes is basically due to the configuration of the CCD. WT mode is a unique rod of pixels. In this mode the coordinate information is absent. The collected photons are read in 1.8 milliseconds, and this gives an opportunity to analysis the signal in a very short timescale. WT mode is used when the count rate is higher than 5 count/seconds. It is usually used in the very first part of the observation, depending on burst strength.

PC mode CCD configuration gives a two dimensional map. This gives the coordinates of the observed object in the sky. The read out time of PC mode is 2.5 seconds. Since the read out time is long, the information for shorter time scales is lost. Events files are cleaned selecting only special grades for incoming photons. If a photon is recorded just on a single pixel, it is called single pixel event and it is grade is 0. If a photon is recorded on two pixels its charge is split onto the two pixels. This change can be reconstructed and the photon is called a two pixels event. There are different kinds of two pixels events: horizontal, vertical and two different diagonal events. Each of them has a different grade. It can be shown that cosmic ray events (i.e. not due

to X-ray sources) have typical grade pattern. Cosmic rays can then be efficiently filtered through an appropriate grade filtering. WT data are filtered using only 0-2 grade events, PC data 0-12 (out to 32). The photons that are not coming from the interested object are eliminated by filtering.

Exposure maps are constructed for each observation (by superposition of different frames of the same observation) in order to record the effective time sky region has been producing photons. If a given region is falling on a bad pixel or a dead CCD column its exposure time would be low (usually zero if the satellite is perfectly pointing, which is not the case). So exposure maps collect the information on the sky exposure of the CCD and are used to correct any source extraction region. For each X-ray source of interest, X-ray photons are extracted from a region centered on source. Its extension will depend on source strength. Photons collected in this region (and corrected for CCD defects and loss of exposure using the exposure map) will consist of true source photons and background photons (i.e. due to measured emission from distant AGN). There is no way to disentangle them. What is usually done is to extract photons from a close by region, free of sources, in order to statistically evaluated and level (and the spectrum) of this background emission. The background corrected Light curves are obtained by plotting count rate versus time.

Using the temporal evolution of the count rate time resolved spectral analysis is done by using XSPEC 12 [237]. First, from the derived light curves five different times are chosen according to detector mode and count rate. For each of the five time intervals, a number of spectra are extracted. Each spectrum is binned at least using 2,000 number of photons before background subtraction. Spectra consisting of 2,000 photons are chosen to reduce statistical fluctuations. To calibrate the distribution of photon energies first the ancillary response files (ARF) are generated. The ARF files give the response of the instrument for a perfect detector. In an ideal case, the detector would assign to each photon a change linearly related to its energy. In reality the detector distribution of each detected photon has a probability of each photon centered of the photon energy and with a low energy tail. Updated Swift redistribution matrices (CALDB) give the probability that photon of a particular energy is actually

detected at a given energy. Spectra are rebinned in order to have at least 20 counts per energy bin for using Gaussian statistics (χ^2). Photons with energy below 0.3 keV come in great number from CCD noise and from optical photons and only rarely from X-ray sources scattered from Earth's atmosphere. For this reason, the energy channels below 0.3 keV are ignored. On the other hand, above 10 keV the instrument is not sensible and the energy channels above 10 keV are also ignored.

3.2.1.1. Spectral Fit With Absorbed Simple Power Law Model. Using XSPEC 12 [237] spectra are fitted by using an absorbed simple power law model ((tabs)*(pow)) [236] with three parameters: global normalization, neutral Hydrogen column density and power law index. While fitting the model, these parameters are free to vary. For the GRBs with known redshift, the model is multiplied for an extra neutral absorber at the GRB redshift. Since there are two absorbers at different energy scales due to redshift, the total absorption is separated. Then the model is used as ((tbabs)(ztbabs)*(pow)) [236]. For this model the Galactic Column density is frozen to the value from Dickey & Lockman (1990) [248]. Redshift is also fixed since it is known. Global normalization, host galaxy neutral Hydrogen column density N_{Hint} and power law index (Γ) are set as free parameters. For the redshift known GRBs, the rest frame time can be obtained by cosmological time dilation; $rest\,frame\,time = \frac{observed\,time}{(1+z)}$. For each GRB the same procedure is applied for the spectral analysis. The best spectral fit values in terms of chi-square are obtained. The spectral information and light curve obtained in the count rate per second unit is combined to have a light curve in physical units $erg/(sec\,cm^2)$.

3.2.2. DATA PROCESSING

For each spectrum of burst reduced chi-square, degrees of freedom, null hypothesis probability (p-value), initial time in rest frame, final time in rest frame, intrinsic N_{Hint} value (Milky Ways effect extracted column density), Photon index, upper and lower values of the errors in host galaxy column density and photon index, normalization value, upper and lower values of the errors in normalization were obtained. Since the starting and ending of time is known, the mean of them is used as the time value.

Asymmetric errors for normalization and N_{Hint} are also seen, the mean value of the upper and lower errors are used as error.

Mathematica 5 is used for statistical tools and plots. For each burst the same procedure is followed. For a specific burst, the P-value of each spectrum is checked at first. The ones which are less than 0.05 are eliminated to have only spectral information coming from good spectral fitting.

To see if the N_{Hint} has any kind of evolution with time the N_{Hint} is plotted versus time, including the errors for both values. First a constant is fitted to see if the N_{Hint} is varying. Then a linear variation is checked. The statistical results are given in Table (4.1) and Table (4.2).

The same method is also applied for the photon index. Photon index is plotted versus time, including the errors for both values. A constant and a linear variation were fitted alternately. The statistical results are given in Table (4.3) and (4.4).

For correlation calculations tools from 'Numerical Recipes in C'in C programming language are used [249]. First a linear fit is tried to correlate column density and photon index. The results are given in Table (4.5).The strength and the direction of a linear relationship between the N_{Hint} and the Γ as a Pearsons correlation coefficient [240] is measured. Correlation is also tested without making a linear distribution assumption between two parameters by Spearmans rank correlation coefficient [250] and Kendall tau rank correlation coefficient [251]. These are given in Table (4.6).

From the spectral analysis for each burst the rest frame time, error of the rest frame time, luminosity and the upper-lower limits of luminosity errors are known (luminosity is obtained by standard Λ cosmology; $\Omega_M = 0.3$, $\Omega_\lambda = 0.7$, $H_0 = 70 km.s^{-1}Mpc^{-1}$). A logarithmic plot of luminosity versus time is generated to have the light curve of the GRBs.

3.3. GRB Sample

Up to May 2008 Swift has observed 81 X-ray afterglows with redshift [252]. We choose 28 bursts with known redshift to study, the list of bursts are given in Table (3.3). The redshift values in the table are taken from [252] and the references for all the redshifts are given in [252]. These were the ones which have at least 5 spectra. Number of spectra is limited as 5 to have significant statistical results.

Table 3.3. GRB Sample

GRB	Number of spectra	Number of Photons in each Spectrum	Redshift
060218	103	2000	0.033
080319B	100	2000	0.937
061007	33	2000	1.261
080310	24	2000	2.4300001
060124	23	2000	2.296
060202	18	2000	0.783
060814	17	2000	0.84
060729	17	2000	0.54
060614	17	2000	0.125
060510B	14	2000	4.9000001
071031	13	2000	2.6919999
061121	13	2000	1.314
060526	12	2000	3.221
060210	12	2000	3.9100001
050730	11	2000	3.967
060418	10	2000	1.489
060607A	9	2000	3.082
050820A	9	2000	2.612
060904B	8	2000	0.703
050904	8	2000	6.29
050724	7	2000	0.258
061110A	6	2000	0.758
060714	6	2000	2.711
050401	6	2000	2.9000001
080411	5	2000	1.03
070318	5	2000	0.836
060604	5	2000	2.6800001
051109A	5	2000	2.346

3.3.1. GRBs In Our Sample

- GRB 051109A

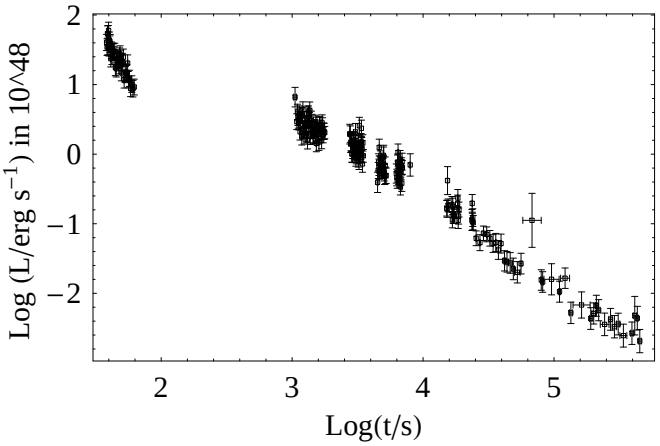

Figure 3.3. GRB 051109A light curve

- GRB 060604

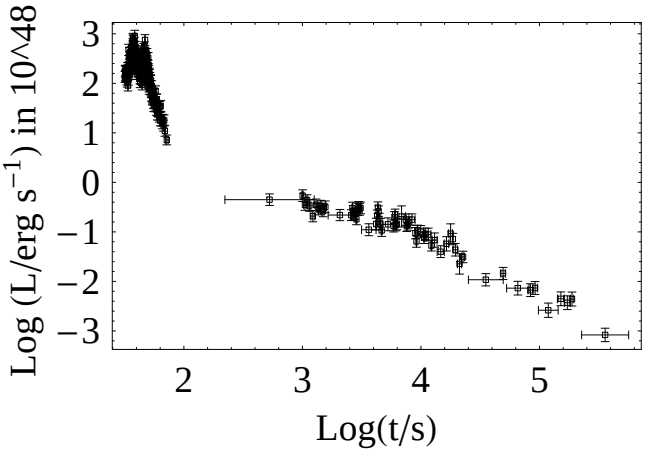

Figure 3.4. GRB 060604 light curve

- GRB 070318 has a X-ray flare in the light curve at the early phase.

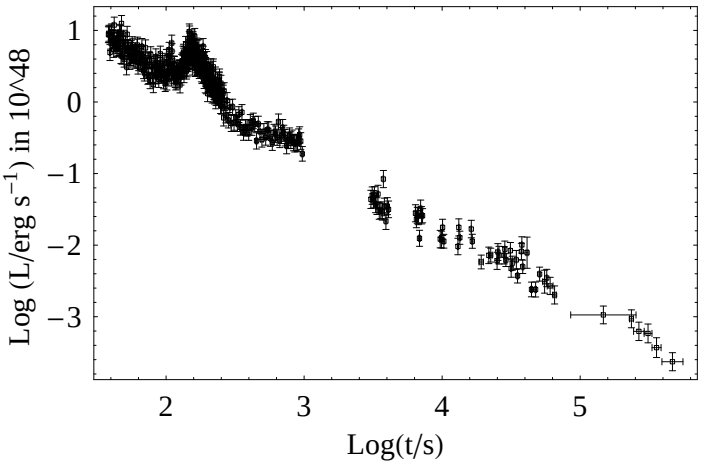

Figure 3.5. GRB 070318 light curve

- GRB 080411

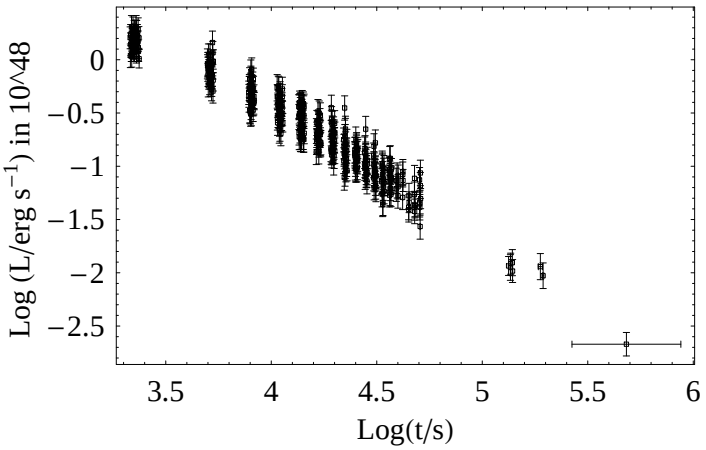

Figure 3.6. GRB 080411 light curve

- GRB 050401

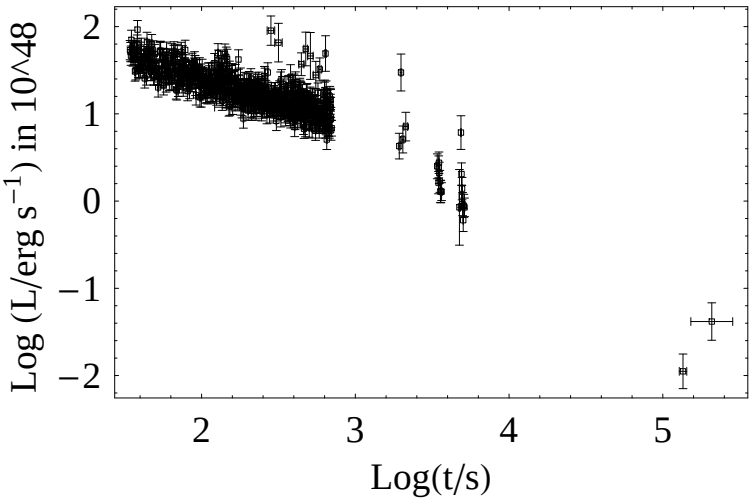

Figure 3.7. GRB 050401 light curve

- GRB 060704 light curve shows a steep decay phase with significant flare contamination. When the spectra fit by absorbed power law with a fixed Galactic N_H and a fixed N_{Hint}, for the steep decay phase a clear hard to soft spectral evolution is found [99].

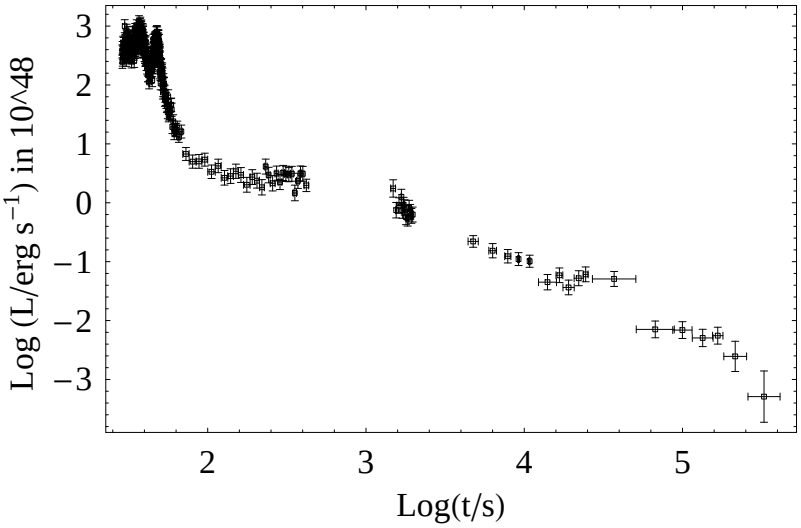

Figure 3.8. GRB 060714 light curve

- GRB 061110A light curve shows a steep decay phase without flares.When the spectra fit by absorbed power law with a fixed Galactic N_H and a fixed N_{Hint}, for the steep decay phase a clear hard to soft spectral evolution is found [99].

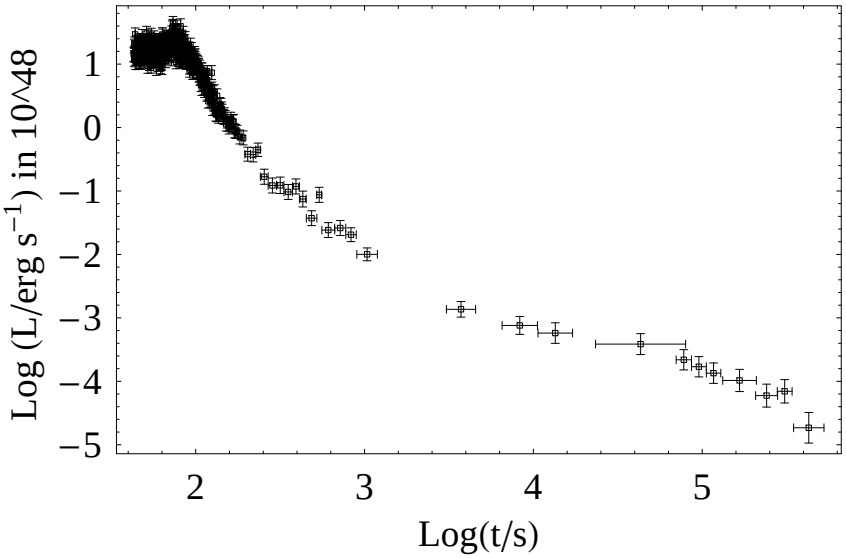

Figure 3.9. GRB 061110A light curve

- GRB 050724 light curve shows a steep decay phase without flares.When the spectra fit by absorbed power law with a fixed Galactic N_H and a fixed N_{Hint}, for the steep decay phase a clear hard to soft spectral evolution is found [99]. The XRT spectral analysis also done considering the first part of the light curve using the absorbed power law model [253] and the N_{Hint} is found to be constant and the power law photon index is found to be softening [253]. GRB 050724 light curve shows flares at late times. When the last part of the light curve is fit with an absorbed (Galactic plus local) power law power law photon index is found to be getting harder [253].

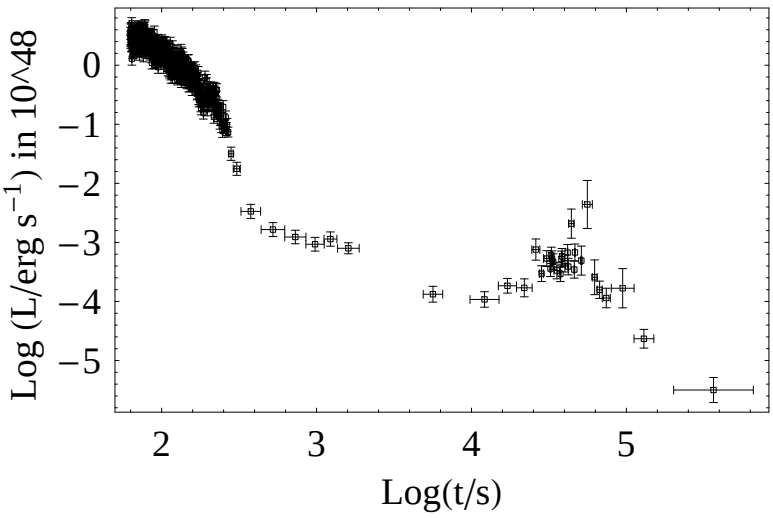

Figure 3.10. GRB 050724 light curve

- GRB 050904 light curve shows a steep decay phase with significant flare contamination. When the spectra fit by absorbed power law with a fixed Galactic N_H and a fixed N_{Hint}, for the steep decay phase a clear hard to soft spectral evolution is found [99]. The light curve shows flares also at late times. GRB 050904 BAT and XRT spectral analysis is also done by [254], they modeled the XRT spectra with absorbed power law model with intrinsic absorption and a fixed Galactic absorption. For the flare interval they found a spectral evolution and after that they did not see a spectral evolution [254]. They report a decreasing intrinsic absorption column density until $T = T + 67.1$ and after that time due to the decreased statistics they only measure the upper limits [254]. In the analysis done by [4], they fit the spectra of the flare interval by a power-law model with a high energy cutoff with different cutoff energies and different power-law spectral indices for each flare. Their results shows that the spectrum gets softer and they found a significant intrinsic column density decrease which is interpreted by them as a physical result.

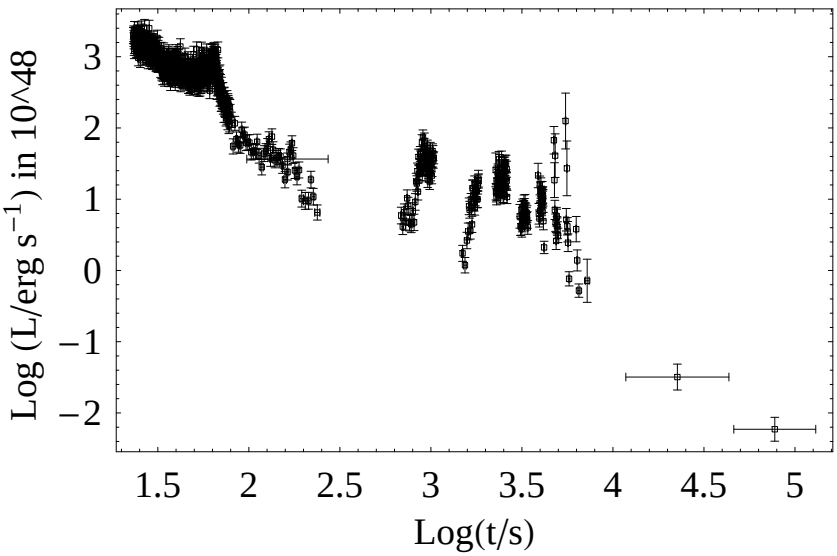

Figure 3.11. GRB 050904 light curve

- GRB 060904B light curve has a X-ray flare at the early phase. For this burst when the spectra are fit with simple power-law Γ tends to increase in the early phase and also model N_H and variations seen [5].

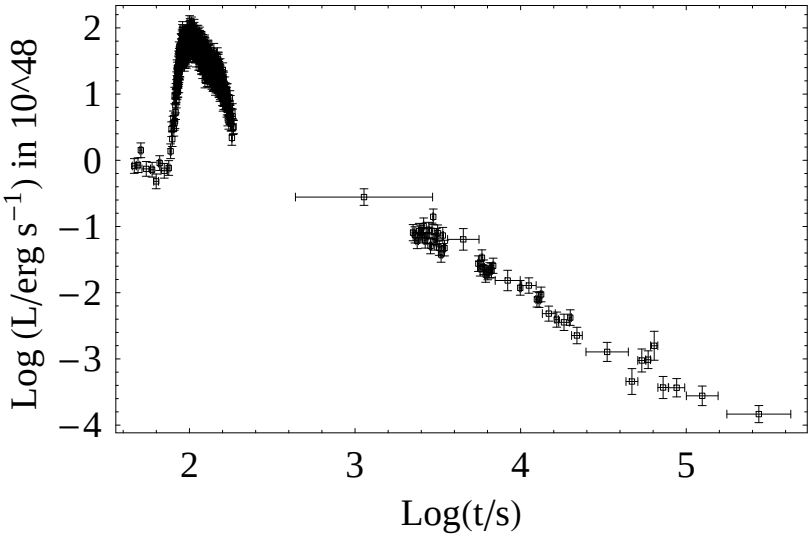

Figure 3.12. GRB 060904B light curve

- GRB 050820A

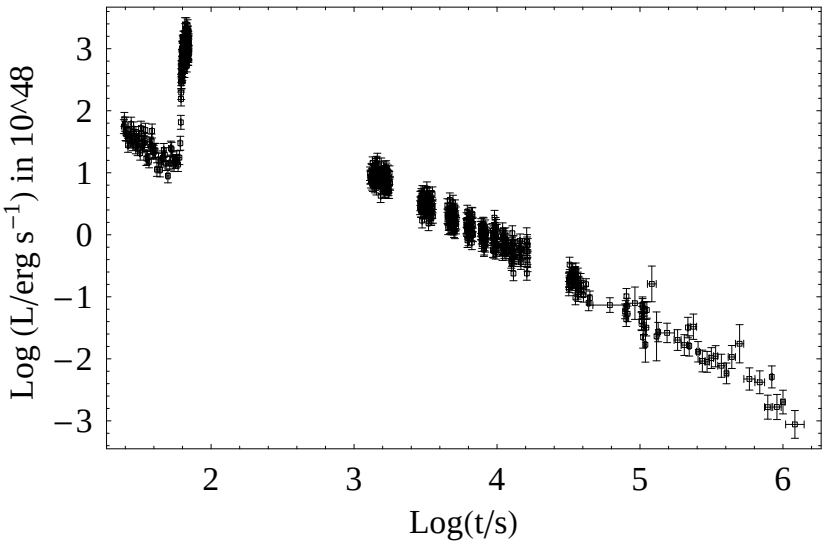

Figure 3.13. GRB 050820A light curve

- GRB 060607A light curve presents X-ray flares at the early phase.

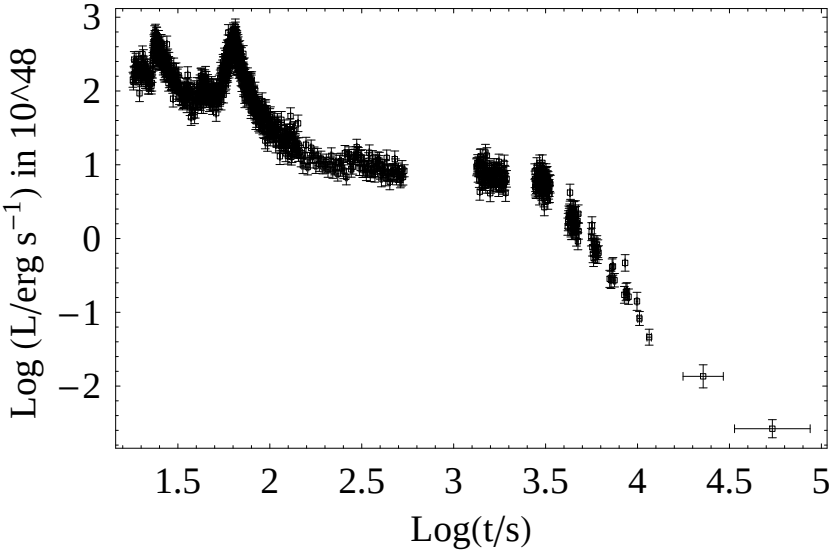

Figure 3.14. GRB 060607A light curve

- GRB 060418 light curve shows a steep decay phase with significant flare contamination. When the spectra fit by absorbed power law with a fixed Galactic N_H and a fixed N_{Hint}, for the steep decay phase a clear spectral evolution is found [99].

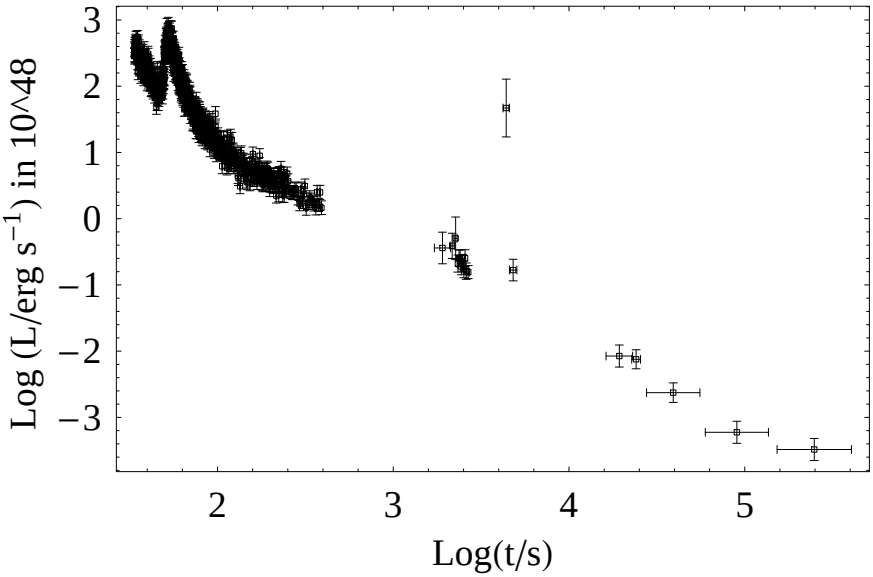

Figure 3.15. GRB 060418 light curve

- GRB 050730 light curve shows a steep decay phase with significant flare contamination. When the spectra fit by absorbed power law with a fixed Galactic N_H and a fixed N_{Hint}, for the steep decay phase a clear hard to soft spectral evolution is found [99].

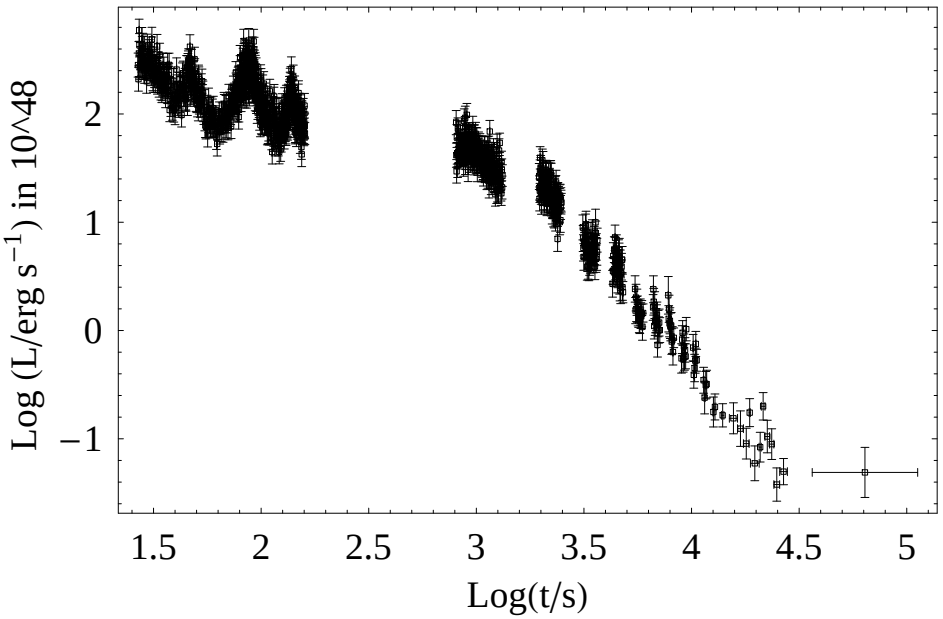

Figure 3.16. GRB 050730 light curve

- GRB 060210 light curve shows flares at early phase.

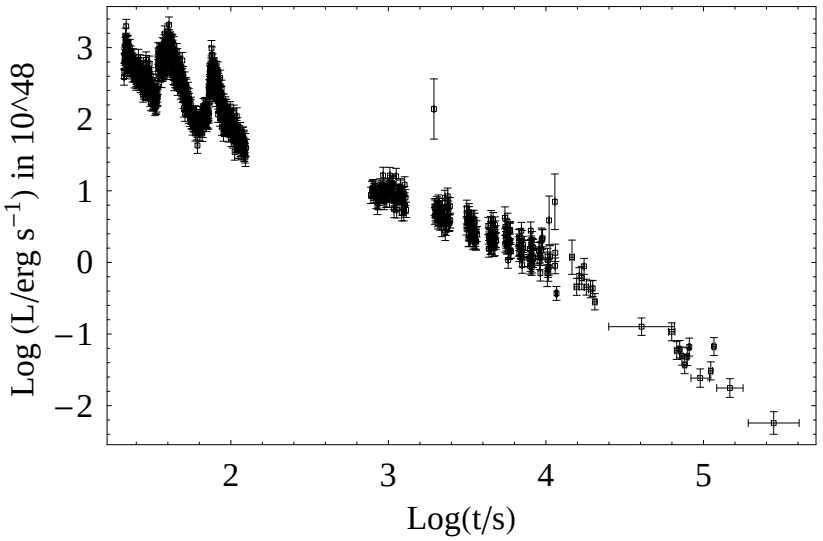

Figure 3.17. GRB 060210 light curve

- The GRB 060526 light curve shows a flare. When the XRT spectra are fit by the power-law model Hydrogen column density and power-law index variations are found (power law photon index increases at the early phase) [5].

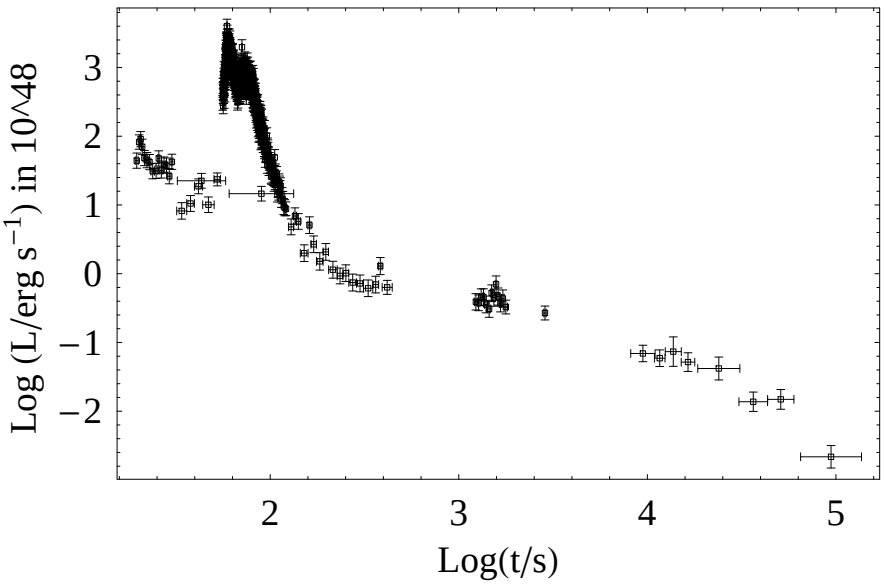

Figure 3.18. GRB 060526 light curve

- GRB 061121 is a special burst because BAT triggered the precursor and observations began before the main GRB event and this lead simultaneous detections in the BAT and XRT bands. GRB 061121 light curve shows a steep decay phase with significant flare contamination. When the spectra fit by absorbed power law with a fixed Galactic N_H and a fixed N_{Hint}, for the steep decay phase a clear hard to soft spectral evolution is found [99]. When the XRT spectra are fit by the power-law model a hard to soft evolution of the photon index and column density variations are found [5].

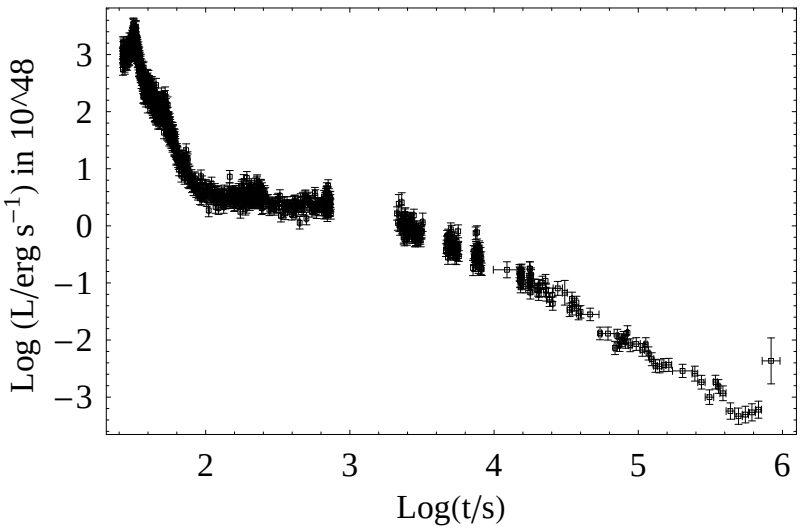

Figure 3.19. GRB 061121 light curve

- GRB 071031 light curve shows a steep decay phase with significant flare contamination. When the spectra fit by absorbed power law with a fixed Galactic N_H and a fixed N_{Hint}, for the steep decay phase a clear hard to soft spectral evolution is found [171].

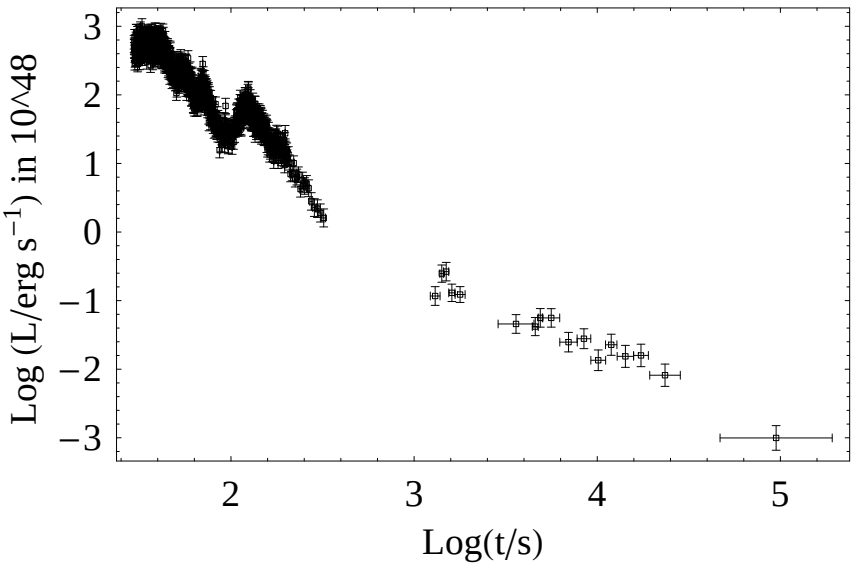

Figure 3.20. GRB 071031 light curve

- GRB 060510B light curve shows a steep decay phase with significant flare contamination. When the spectra fit by absorbed power law with a fixed Galactic N_H and a fixed N_{Hint}, for the steep decay phase a clear hard to soft spectral evolution is found [99].

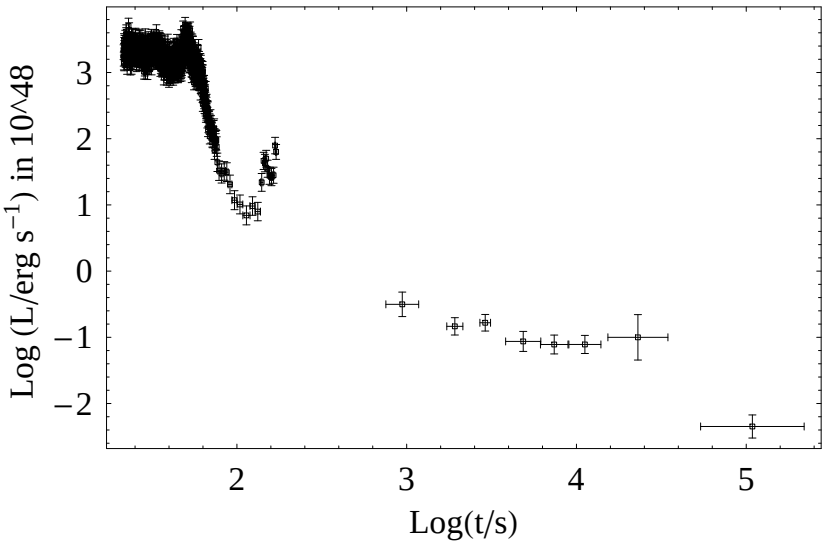

Figure 3.21. GRB 060510B light curve

- GRB 060614 light curve shows a steep decay phase without flares.When the spectra fit by absorbed power law with a fixed Galactic N_H and a fixed N_{Hint}, for the steep decay phase a clear hard to soft spectral evolution is found [99]. When the XRT spectra are fit by the power-law model a hard to soft evolution of the photon index and column density variations are found [5].

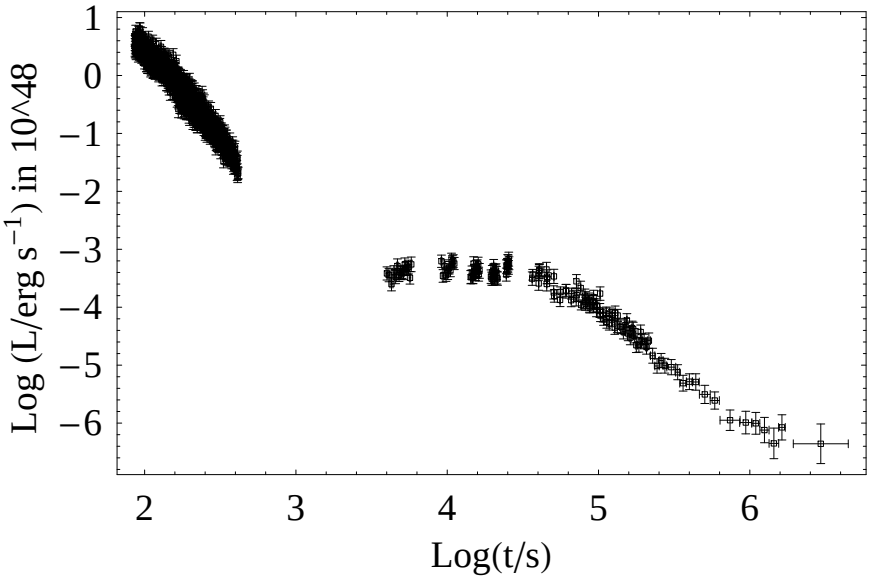

Figure 3.22. GRB 060614 light curve

- GRB 060729 light curve shows a steep decay phase with flare contamination. When the spectra fit by absorbed power law with a fixed Galactic N_H and a fixed N_{Hint}, for the steep decay phase a clear hard to soft spectral evolution is found [99]. When the X-ray spectra are fit with the power-law model, Γ is found to increase at the early phase and N_H is also found to increase during this phase [5]. A correlation between the N_H and the Γ is also given in [255].

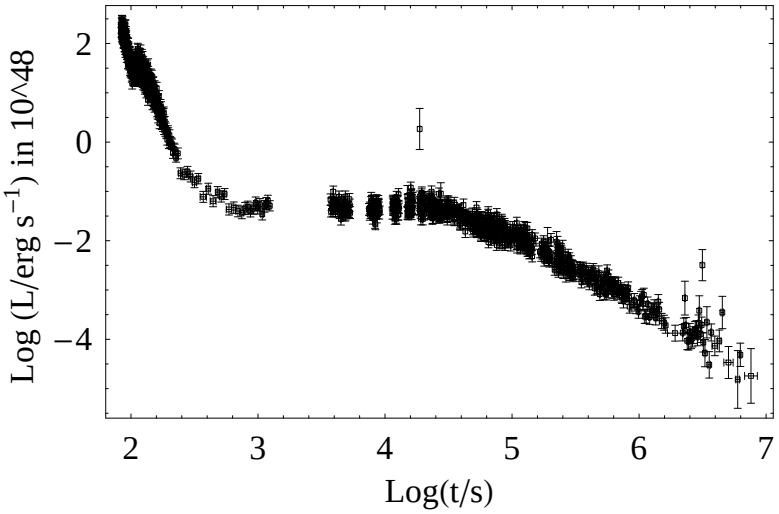

Figure 3.23. GRB 060729 light curve

- GRB 060814 light curve shows a steep decay phase with flare contamination. When the spectra fit by absorbed power law with a fixed Galactic N_H and a fixed N_{Hint}, for the steep decay phase a clear hard to soft spectral evolution is found [99].

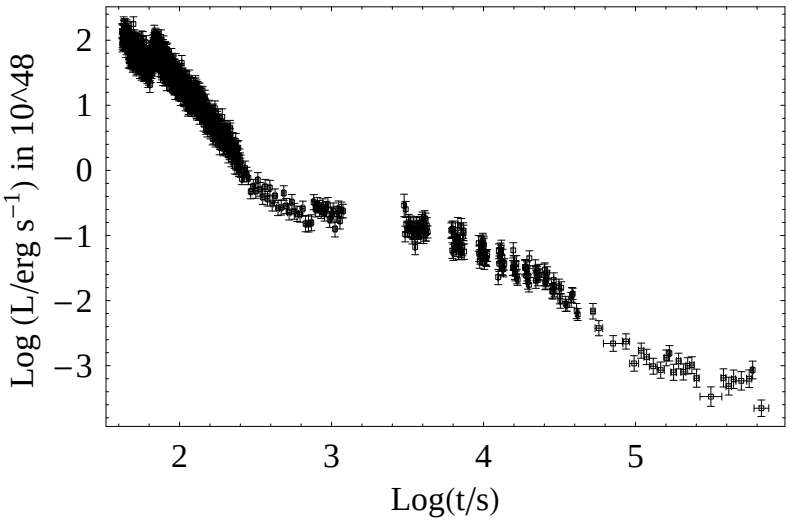

Figure 3.24. GRB 060814 light curve

- GRB 060202 light curve shows a steep decay phase with flare contamination. For the steep decay phase a clear soft to hard spectral evolution is found and this is noted as a unusual feature [99].

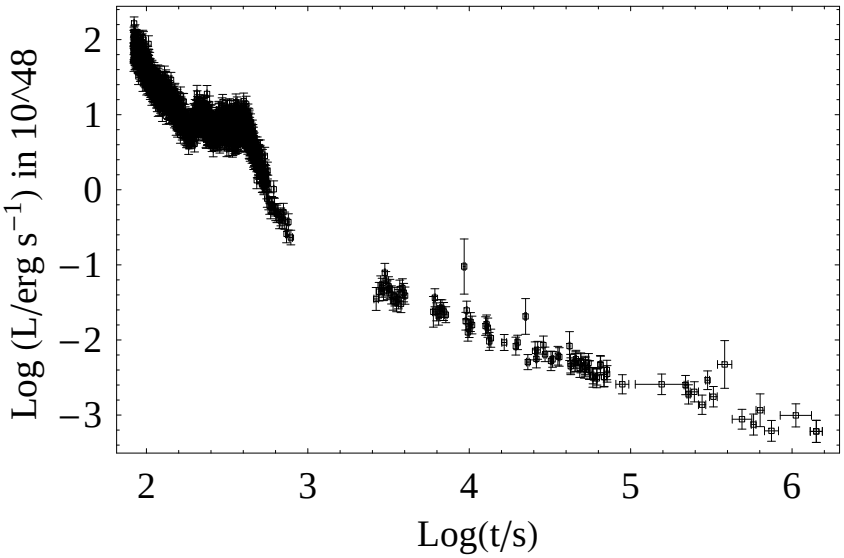

Figure 3.25. GRB 060202 light curve

- Precursor of the GRB 060124 triggered Swift-BAT allowing simultaneous detections with BAT and XRT. In the light curve there is flare at the early phase. The flare interval found to show spectral evolution [171]. The spectral analysis given [5] shows, N_H and Γ variations when the power-law model is used.

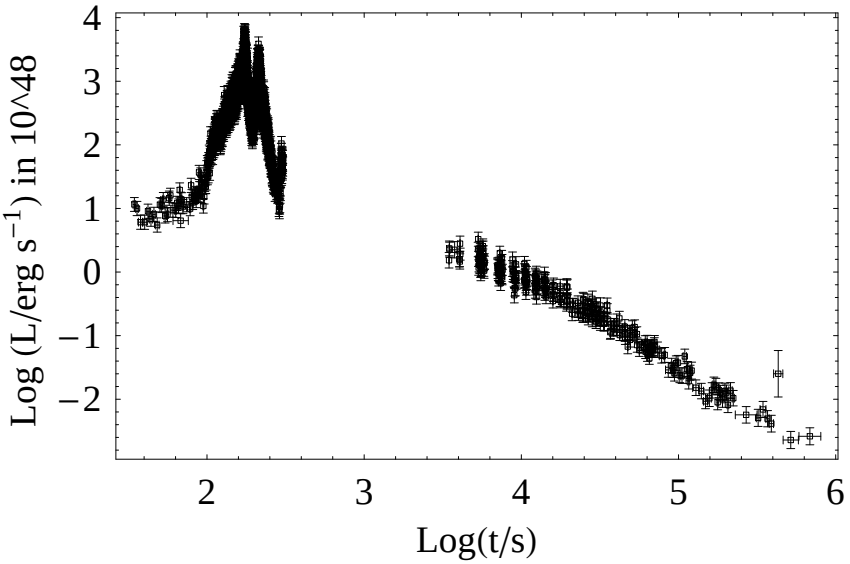

Figure 3.26. GRB 060124 light curve

- GRB080310 light curve shows a flare at the early phase.

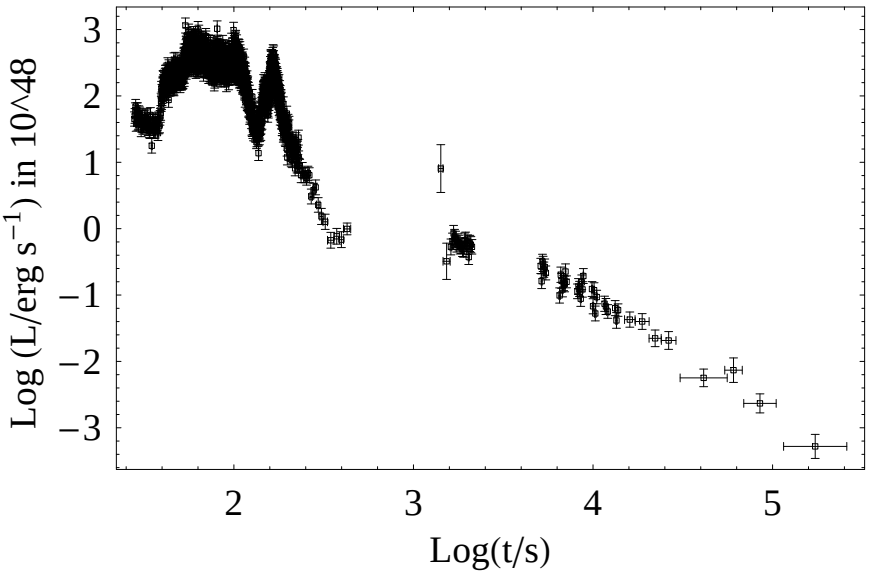

Figure 3.27. GRB 080310 light curve

- GRB 061007 light curve shows a steep decay phase without flare contamination. For the steep decay phase a clear soft to hard spectral evolution is found and this is noted as a unusual feature [99].

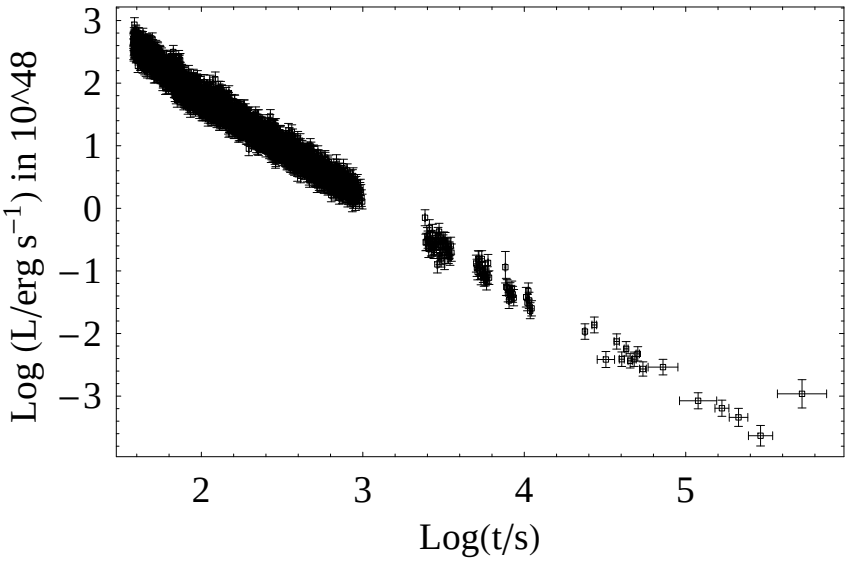

Figure 3.28. GRB 061007 light curve

- GRB 080319B is one of the most energetic Swift bursts and in our analysis it has 100 spectra.

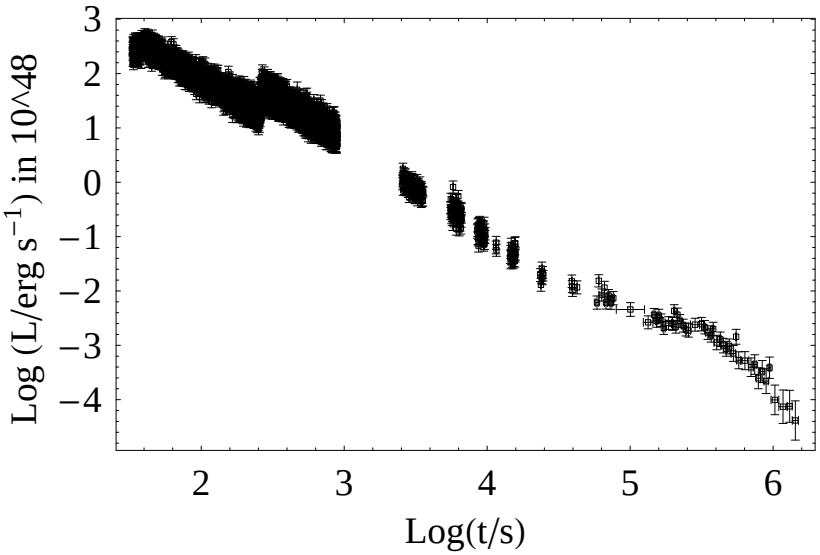

Figure 3.29. GRB 080319B light curve

- GRB 060218 is one of the most energetic Swift bursts and it has the highest number of spectra in our sample. GRB 060218 light curve early phase does not show flares.When the spectra fit by absorbed black body and power law with a fixed Galactic N_H and a fixed N_{Hint}, for the steep decay phase a clear hard to soft spectral evolution is found [99]. When the spectra fit by absorbed simple power law model, a correlation between N_{Hint} and Γ is showed in [256].

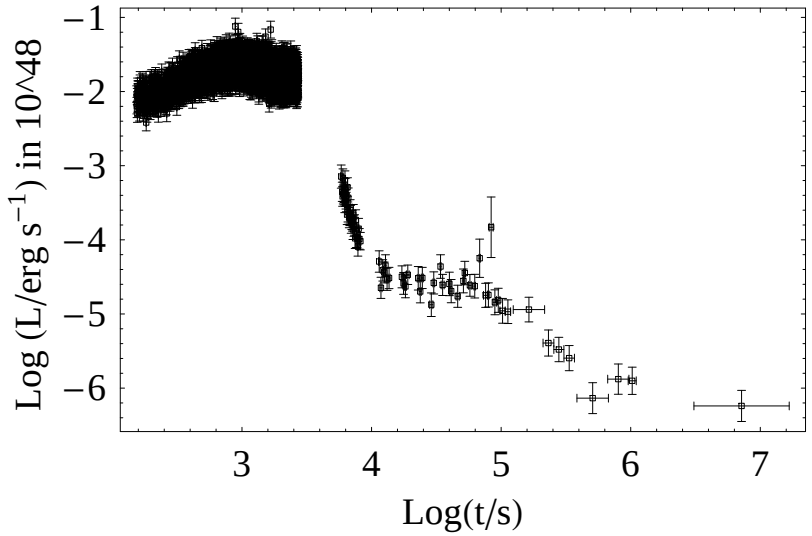

Figure 3.30. GRB 060218 light curve

4. RESULTS

In this chapter the results of this work are given by related graphs and statistical properties. This chapter is divided in three parts which are focusing in N_{Hint} and Γ variations and N_{Hint} - Γ correlations respectively.

4.1. Intrinsic Neutral Hydrogen Column Density Variability

4.1.1. Intrinsic Neutral Hydrogen Column Density Variability Graphs

The graphs show the N_{Hint} versus rest frame time for the related GRB. The N_{Hint} values are obtained by absorbed simple power law model while Γ is as a free parameter in the model. To see the details some graphs are also shown in the logarithmic scale. This could only be done for the cases where it is possible to have the logarithm of the given value. All the N_{Hint} values are in units of $10^{22} cm^{-2}$.

- GRB 051109A

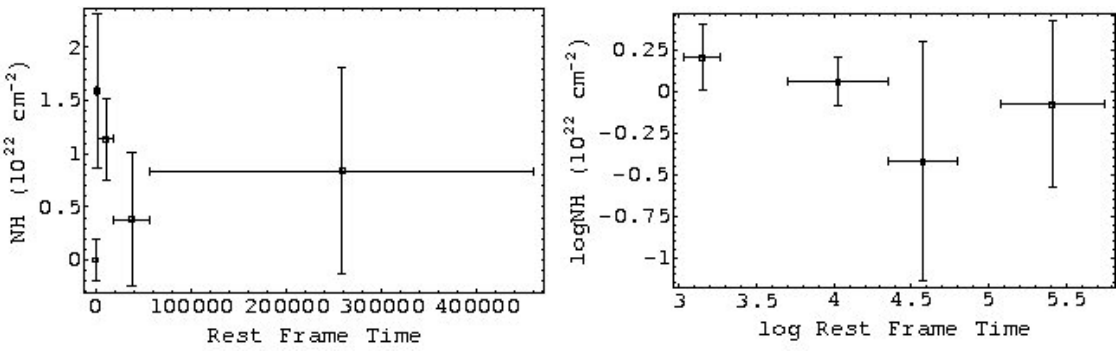

Figure 4.1. GRB 051109A N_{Hint} variation

- GRB 060604

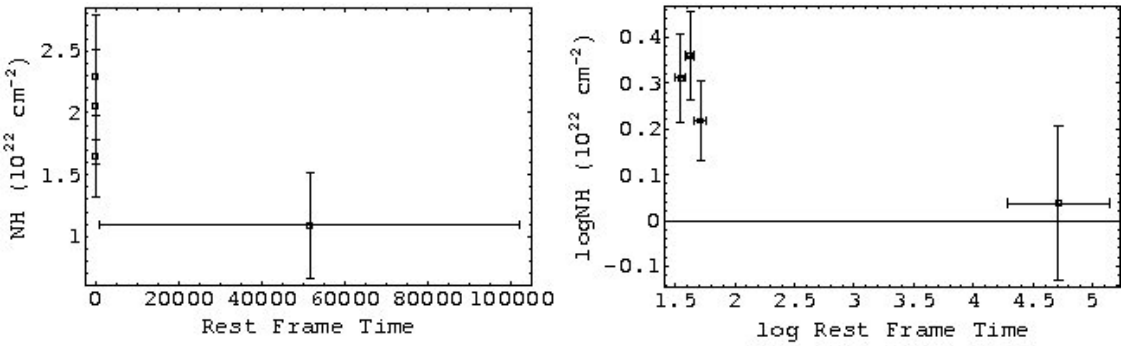

Figure 4.2. GRB 060604 N_{Hint} variation

- GRB 070318

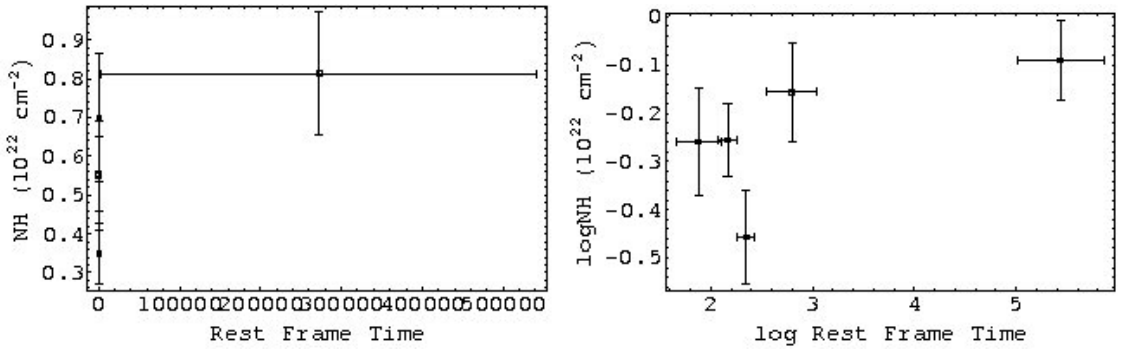

Figure 4.3. GRB 070318 N_{Hint} variation

- GRB 080411

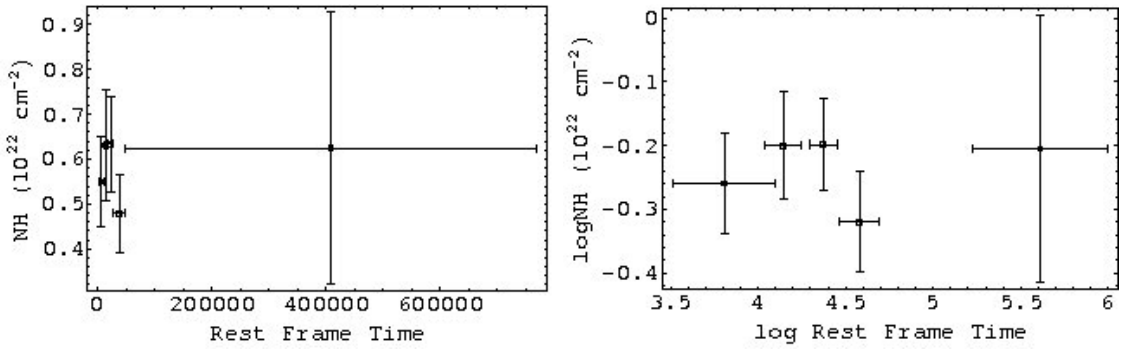

Figure 4.4. GRB 080411 N_{Hint} variation

- GRB 050401

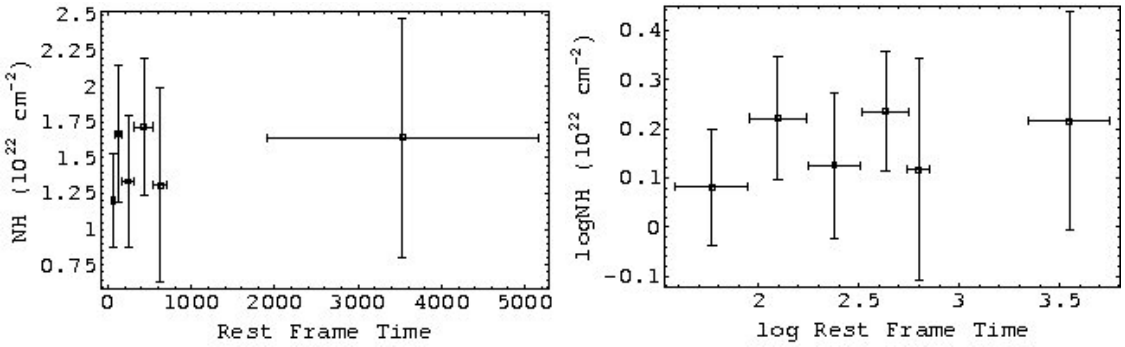

Figure 4.5. GRB 050401 N_{Hint} variation

- GRB 060714

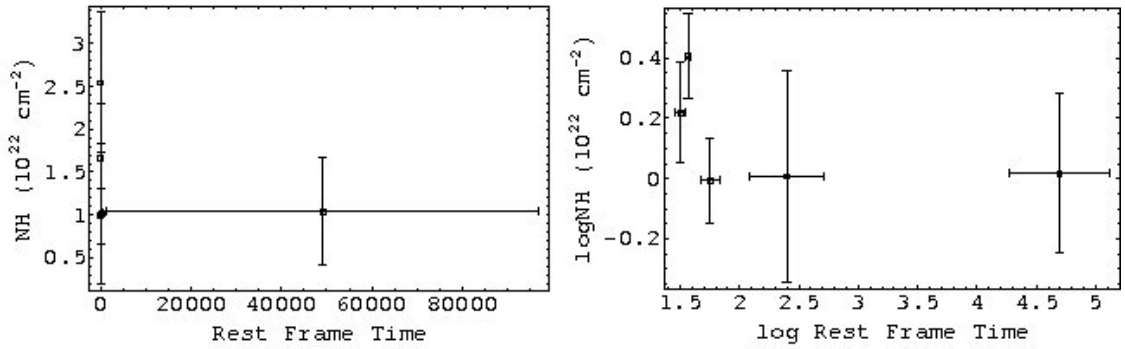

Figure 4.6. GRB 060714 N_{Hint} variation

- GRB 061110A

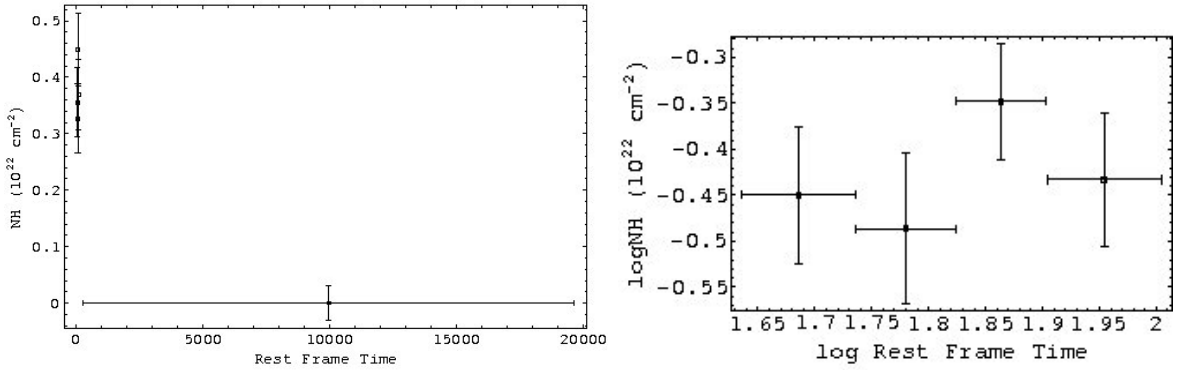

Figure 4.7. GRB 061110A N_{Hint} variation

- GRB 050724

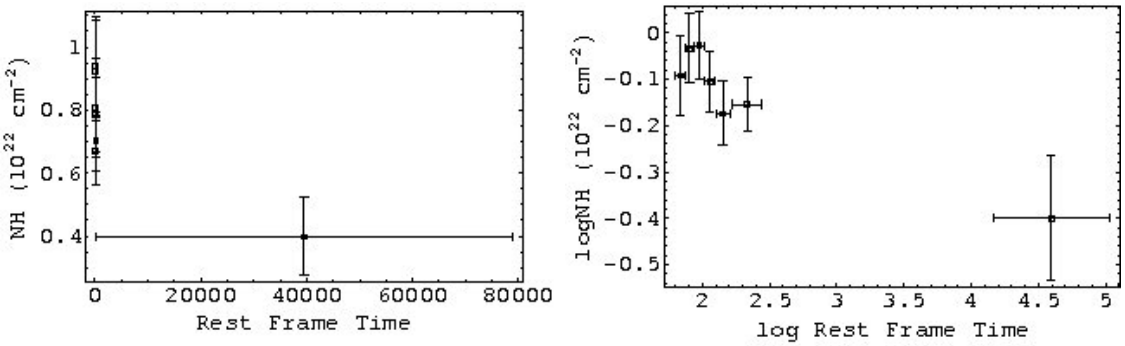

Figure 4.8. GRB 050724 N_{Hint} variation

- GRB 050904

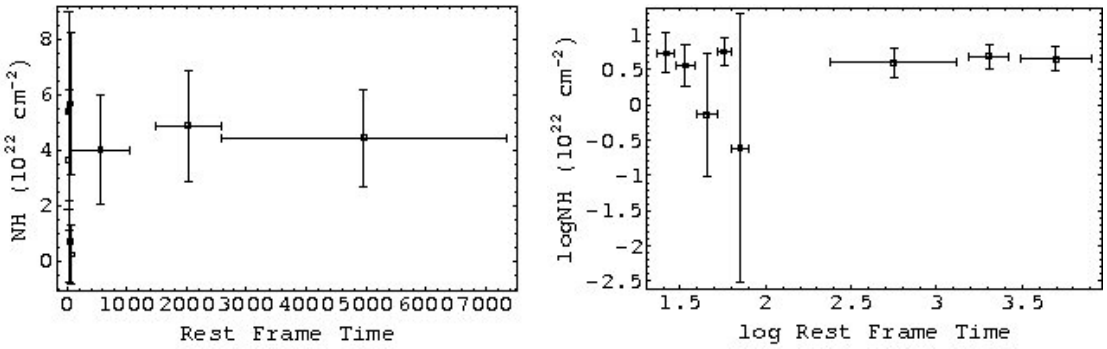

Figure 4.9. GRB 050904 N_{Hint} variation

- GRB 060904B

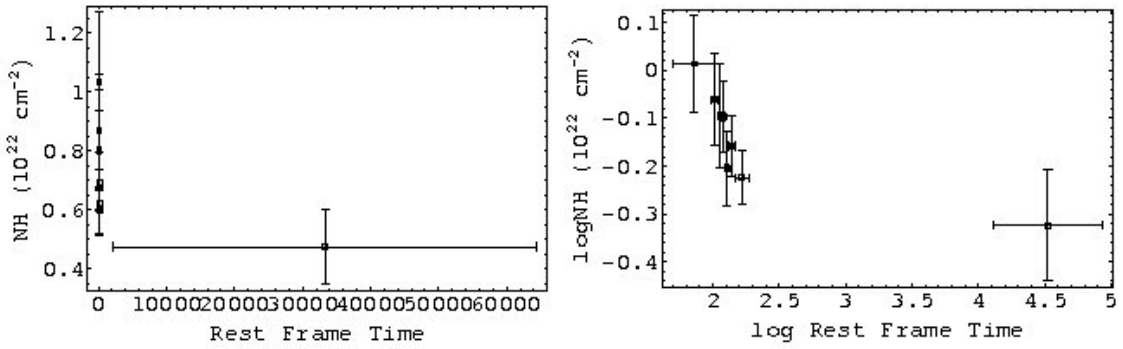

Figure 4.10. GRB 060904B N_{Hint} variation

- GRB 050820A

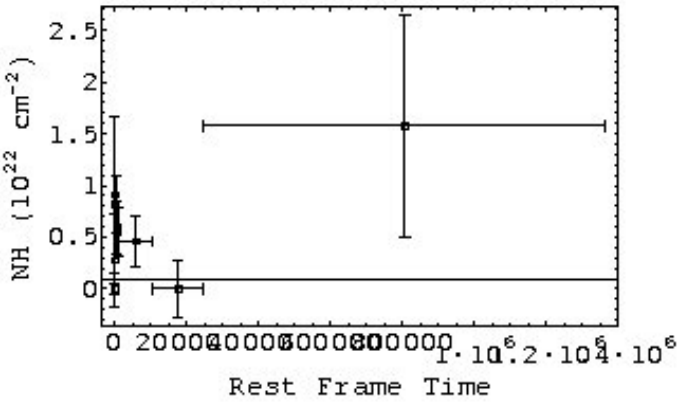

Figure 4.11. GRB 050820A N_{Hint} variation

- GRB 060607A

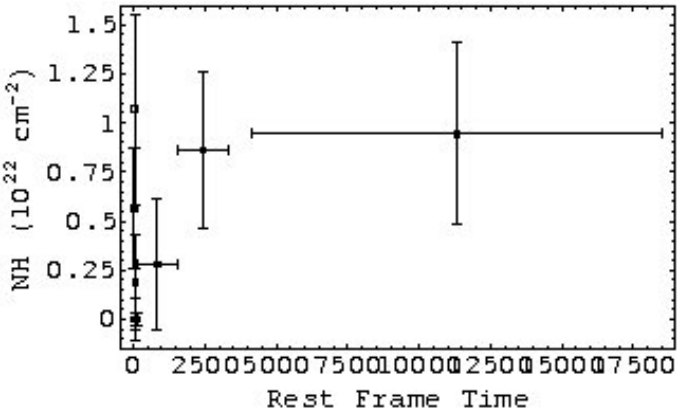

Figure 4.12. GRB 060607A N_{Hint} variation

- GRB 060418

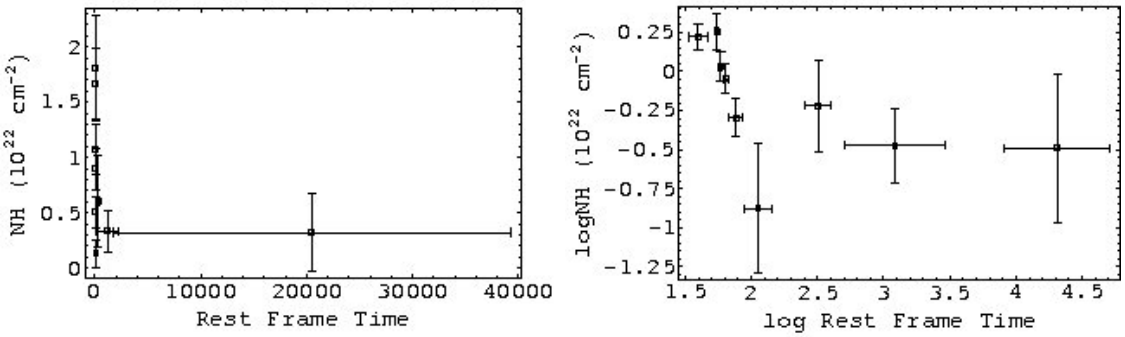

Figure 4.13. GRB 060418 N_{Hint} variation

- GRB 050730

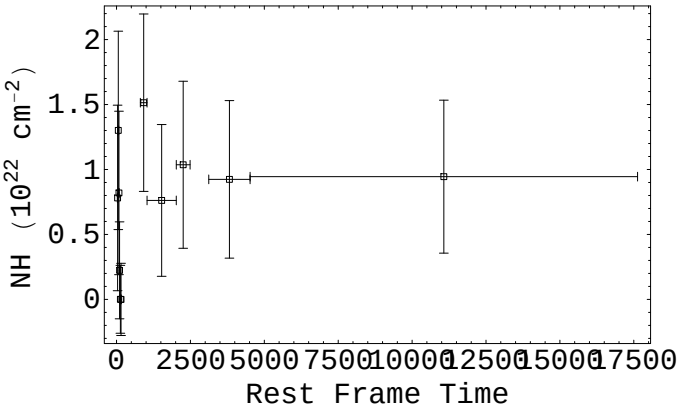

Figure 4.14. GRB 050730 N_{Hint} variation

- GRB 060210

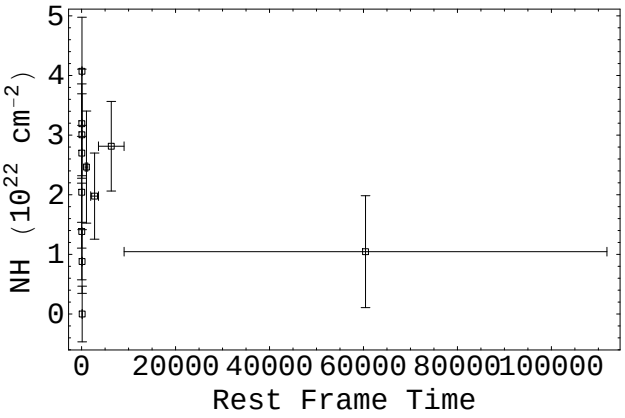

Figure 4.15. GRB 060210 N_{Hint} variation

- GRB 060526

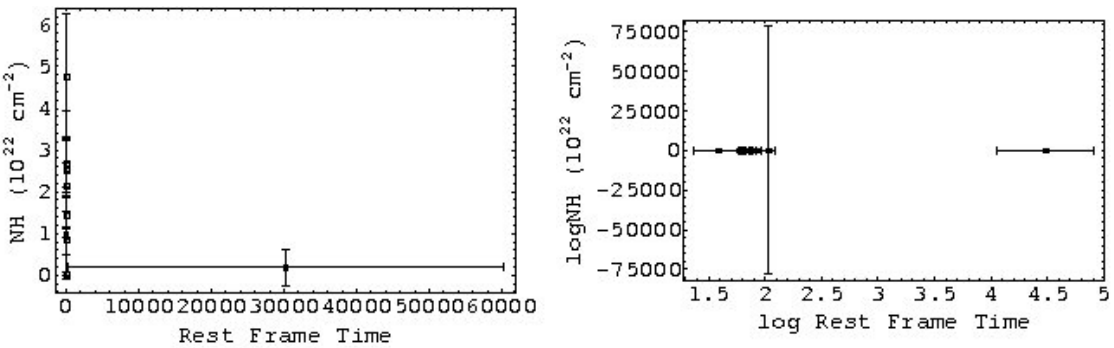

Figure 4.16. GRB 060526 N_{Hint} variation

- GRB 061121

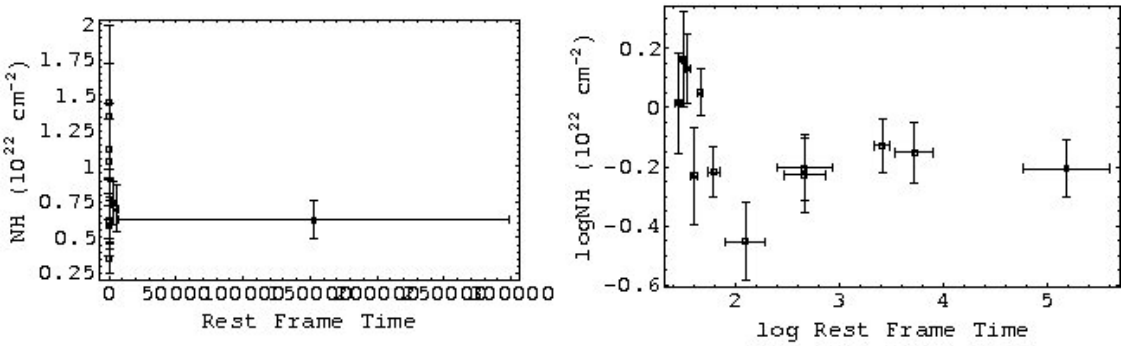

Figure 4.17. GRB 061121 N_{Hint} variation

- GRB 071031

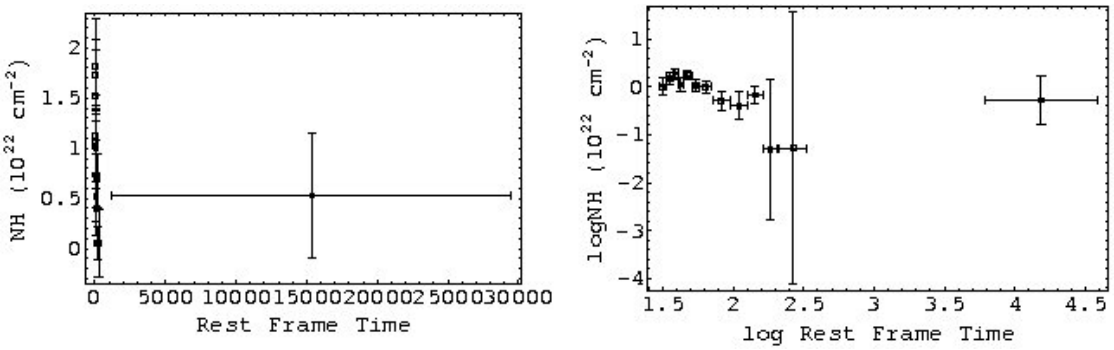

Figure 4.18. GRB 071031 N_{Hint} variation

- GRB 060510B

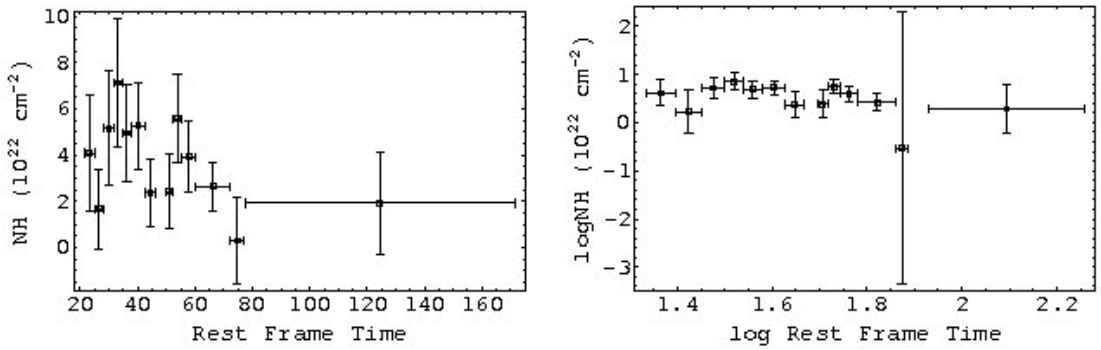

Figure 4.19. GRB 060510B N_{Hint} variation

- GRB 060614

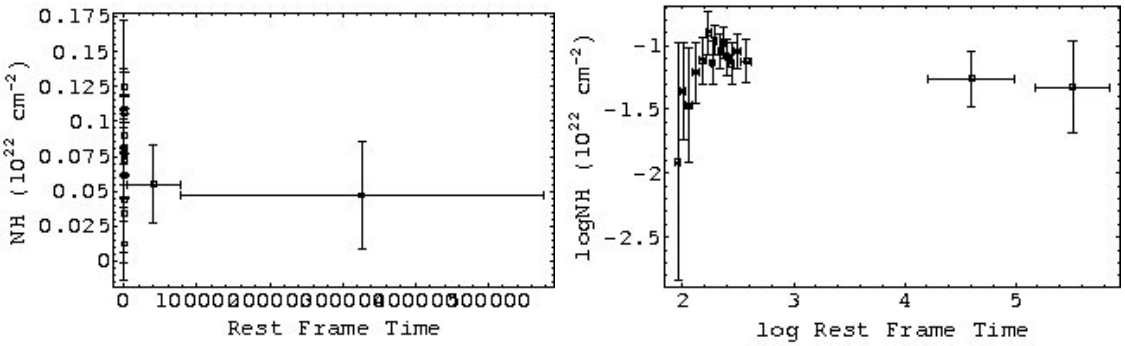

Figure 4.20. GRB 060614 N_{Hint} variation

- GRB 060729

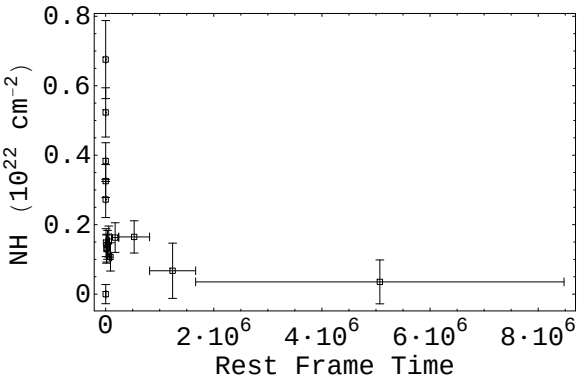

Figure 4.21. GRB 060729 N_{Hint} variation

- GRB 060814

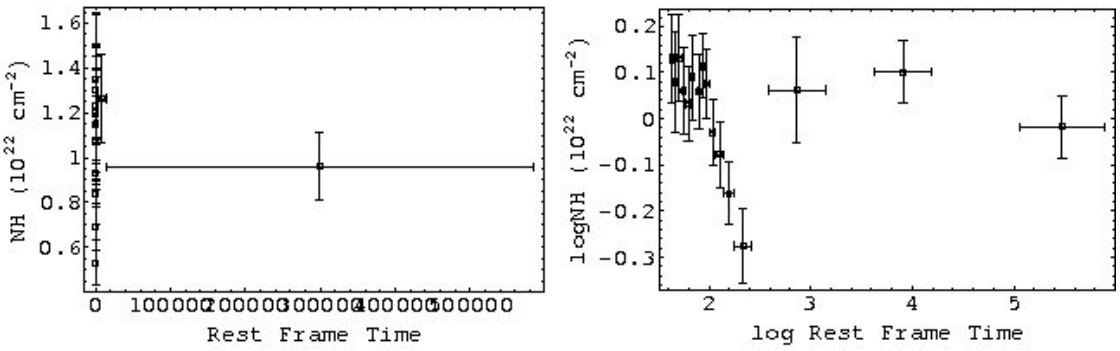

Figure 4.22. GRB 060814 N_{Hint} variation

- GRB 060202

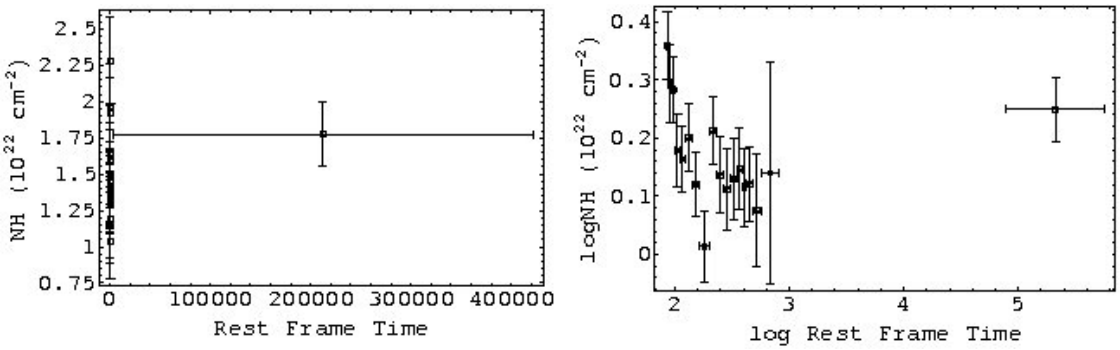

Figure 4.23. GRB 060202 N_{Hint} variation

- GRB 060124

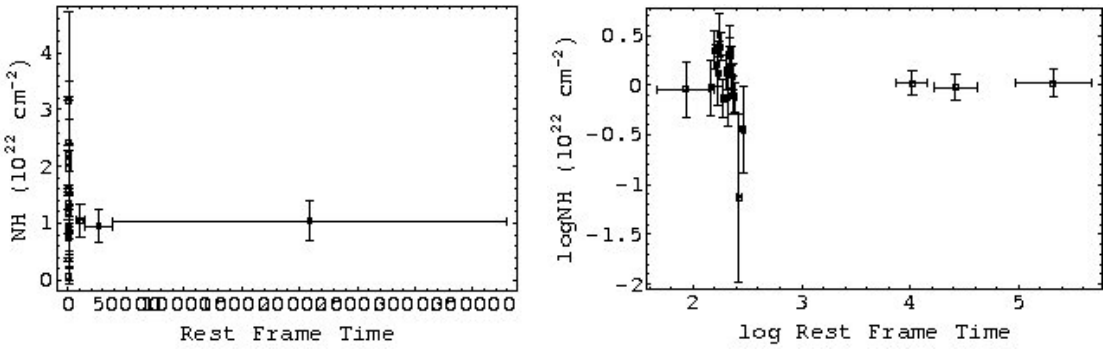

Figure 4.24. GRB 060124 N_{Hint} variation

- GRB 080310

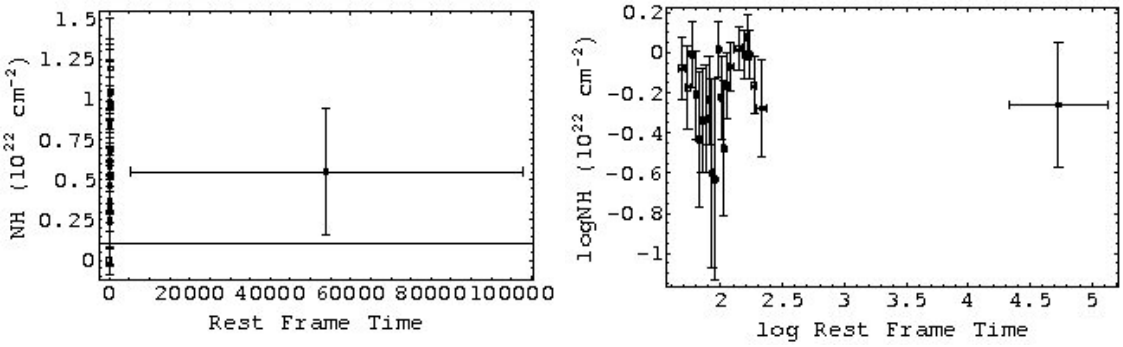

Figure 4.25. GRB 080310 N_{Hint} variation

- GRB 061007

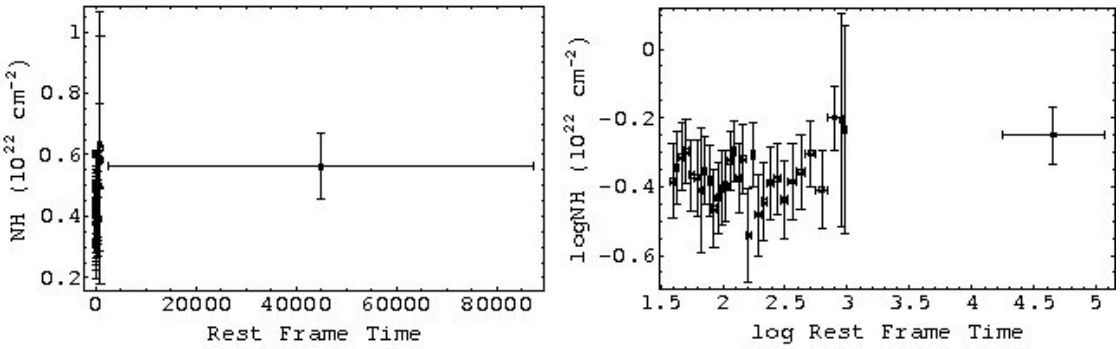

Figure 4.26. GRB 061007 N_{Hint} variation

- GRB 080319B

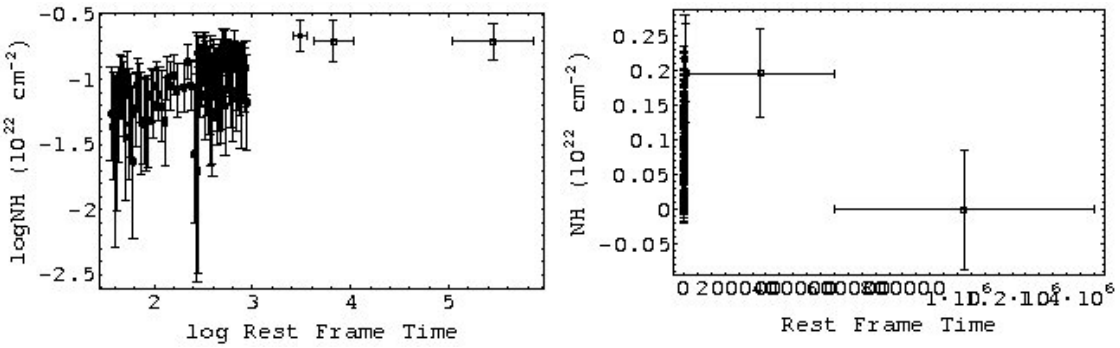

Figure 4.27. GRB 080319B N_{Hint} variation

- GRB 060218

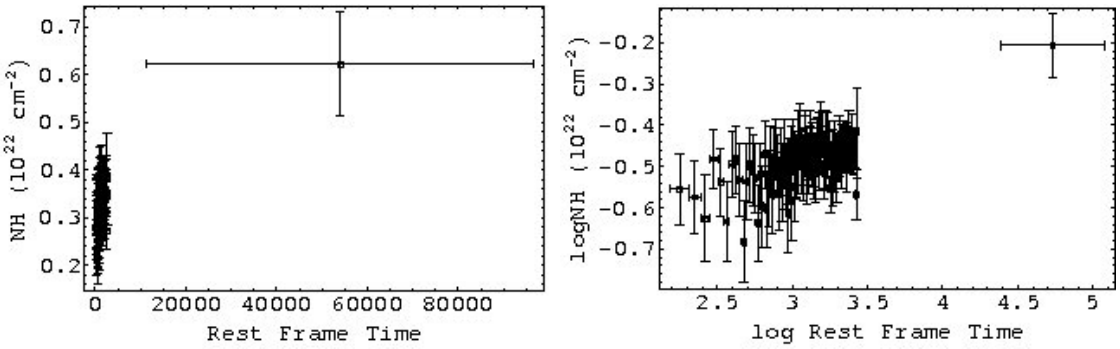

Figure 4.28. GRB 060218 N_{Hint} variation

4.1.2. Intrinsic Neutral Hydrogen Column Density Variability Fit Results

4.1.2.1. Constant Variable Fit. To see if the intrinsic Hydrogen column density is constant in time a constant variable fit is applied. Table (4.1) shows the constant variable fit results where a is the constant variable, χ^2 is the $chi-square$, $d.o.f$ is the degree of freedom, $P-value$ is the null hypothesis probability value.

4.1.2.2. Linear Variable Fit. A linear fit is applied to intrinsic column density change. Table (4.2) shows the linear variable fit results where a is the linear variable, b is the slope, $d.o.f$ is the degree of freedom, $P-value$ is the null hypothesis probability value, χ^2 is the $chi-square$.

4.1.3. Interpretation of the N_{Hint} variability

Time resolved spectral analysis is used for our sample and all the spectra are fitted by absorbed simple power law model. Intrinsic Hydrogen column density variability in time is examined for each burst by constant and linear fits. The statistical results are given in Table (4.1) and in Table (4.2). When 0.05 is chosen as the threshold for one tail probability value ($p-value$), the smaller values than 0.05 certainly give the ones that reject the applied fit. Since the chi square p-value test gives only the non compatible ones exactly, all GRBs (p–$value > 0.05$) in our sample can be described as compatible with the applied fit (can not be rejected).

Table 4.1. Constant variable fit results for N_{Hint} variation

GRB	a	Error of a	Reduced χ^2	D.o.f	P-value (one-tail)
060218	0.3259	0.0049	0.666463	101	0.00399
080319B	0.0821	0.005	0.727421	90	0.02405
061007	0.423	0.019	0.419932	31	0.00188
080310	0.452	0.05	2.74425	22	0.000019
060124	0.751	0.078	2.55168	21	0.000113
060202	1.434	0.051	1.70942	17	0.0339753
060814	0.911	0.044	2.58318	15	0.0006988
060729	0.156	0.011	8.258	15	0
060614	0.0714	0.0016	0.863886	15	0.39448
060510B	3.24	0.49	0.896049	12	0.449767
071031	0.643	0.084	3.44308	12	0.000043
061121	0.632	0.048	1.85064	11	0.0406783
060526	0.289	0.081	8.15644	10	2.4758×10^{-13}
060210	1.7	0.21	3.02242	11	0.000479
050730	0.38	0.14	1.23629	10	0.2615
060418	0.546	0.068	5.02966	8	2.89×10^{-6}
060607A	0.025	0.031	2.51897	7	0.0137414
050820A	0.068	0.041	2.94484	8	0.002716
060904B	0.664	0.043	1.18497	7	0.307317
050904	2.39	0.62	1.66547	7	0.112372
050724	0.715	0.047	1.89023	6	0.0783815
061110A	0.185	0.022	18.4932	4	3.33067×10^{-15}
060714	1.22	0.24	0.940179	4	0.439357
050401	1.42	0.19	0.240165	5	0.0552017
080411	0.561	0.05	0.435482	4	0.216912
070318	0.511	0.05	2.3639	4	0.0506675
060604	1.71	0.21	1.34229	3	0.258577
051109A	0.32	0.16	2.70975	4	0.0284341

Table 4.2. Linear variable fit results for N_{Hint} variation

GRB	a	Err. of a	b	Err. of b	Reduced χ^2	D.o.f	P-value
060218	0.287	0.011	0.0000255	6×10^{-6}	0.4558	100	5.76×10^{-7}
080319B	0.0822	0.0051	-1×10^{-6}	8×10^{-8}	0.734577	89	0.02833
061007	0.418	0.019	3.3×10^{-6}	3.9×10^{-6}	0.375161	30	0.000751
080310	0.45	0.05	2.2×10^{-6}	7.7×10^{-6}	2.87079	21	0.0000115
060124	0.727	0.082	1.8×10^{-6}	2.2×10^{-6}	2.62403	20	0.00009686
060202	1.415	0.052	1.7×10^{-6}	2×10^{-6}	1.66357	16	0.04594
060814	0.906	0.046	2×10^{-7}	5.6×10^{-7}	2.7574	14	0.0004198
060729	0.162	0.012	-2.7×10^{-8}	2.1×10^{-8}	8.51717	14	0
060614	0.0728	0.0079	-9×10^{-8}	1.4×10^{-7}	0.88656	14	0.4267
060510B	4.8	1.4	-0.03	0.024	0.813872	11	0.373731
071031	0.648	0.085	-0.000015	0.000044	3.74398	11	0.000022
061121	0.633	0.052	0.1	1×10^{-6}	2.03543	10	0.02607
060526	0.293	0.082	-4×10^{-6}	0.000015	9.05499	9	8.14×10^{-14}
060210	1.73	0.22	-8×10^{-6}	0.000017	3.29901	10	0.0002734
050730	0.28	0.15	0.000103	0.000069	1.07234	9	0.379462
060418	0.561	0.07	-0.000014	0.000022	5.6533	7	1.519×10^{-6}
060607A	0.002	0.033	0.000141	0.033	1.83322	6	0.0883976
050820A	0.058	0.042	1.4×10^{-6}	1.2×10^{-6}	3.02214	7	0.003547
060904B	0.69	0.046	-6.5×10^{-6}	7.3×10^{-6}	0.95862	6	0.451569
050904	1.77	0.72	0.00068	0.00048	1.38891	6	0.214678
050724	0.769	0.051	-9×10^{-6}	0.00001	0.0722084	5	0.39325
061110A	0.376	0.031	-0.000038	0.000037	0.679802	3	0.435732
060714	1.25	0.26	-4×10^{-6}	0.000015	1.22091	3	0.300263
050401	1.39	0.22	0.00009	0.00026	0.268029	4	0.101329
080411	0.559	0.056	5×10^{-8}	7.8×10^{-7}	0.579136	3	0.371351
070318	0.4766	0.053	1.2×10^{-6}	1.4×10^{-6}	1.77115	3	1.77115
060604	1.9	0.24	-0.000016	0.000018	0.639	2	0.47218
051109A	0.29	0.16	3×10^{-6}	4.4×10^{-6}	3.39303	3	0.0171035

4.2. Power Law Photon Index Variability

4.2.1. Power Law Photon Index Variability Graphs

The graphs show the power law photon index versus rest frame time for the related GRB. The power law photon index values are obtained by absorbed simple power law model while N_{Hint} is as a free parameter in the model. To see the details some graphs are also shown in the logarithmic scale. This could only be done for the cases where it is possible to have the logarithm of the given value.

- GRB 051109A

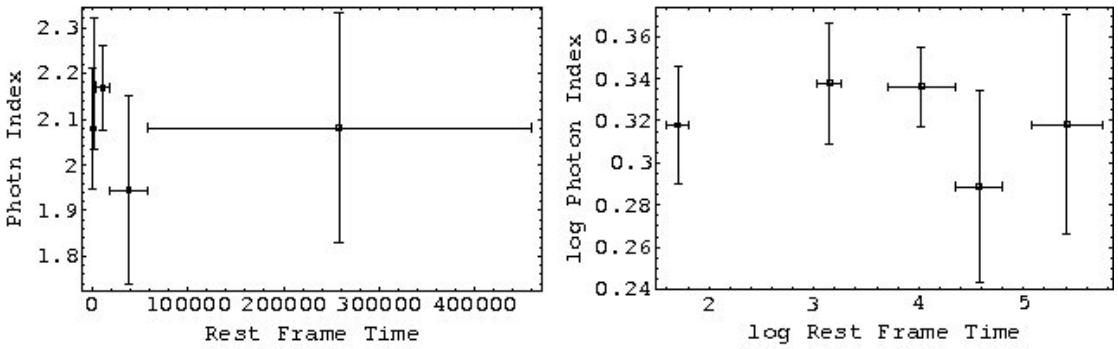

Figure 4.29. GRB 051109A Γ variation

- GRB 060604

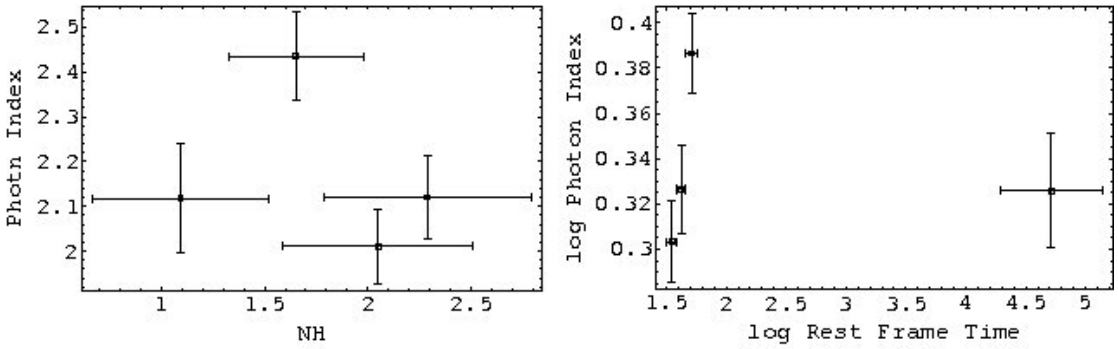

Figure 4.30. GRB 060604 Γ variation

- GRB 070318

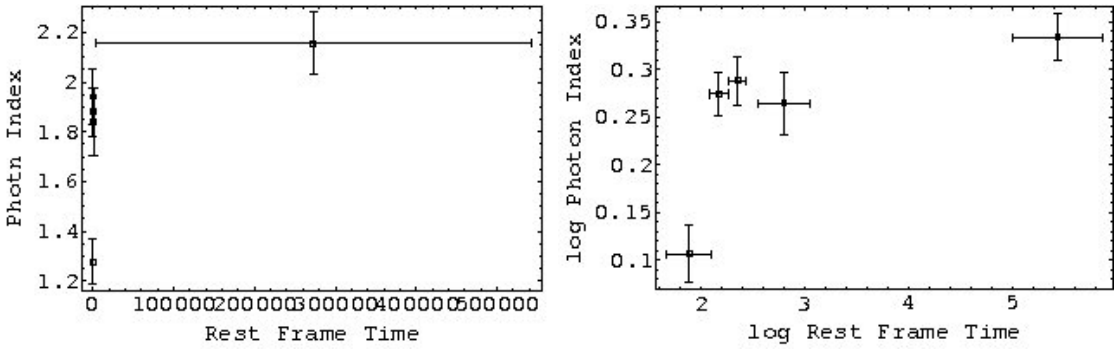

Figure 4.31. GRB 070318 Γ variation

- GRB 080411

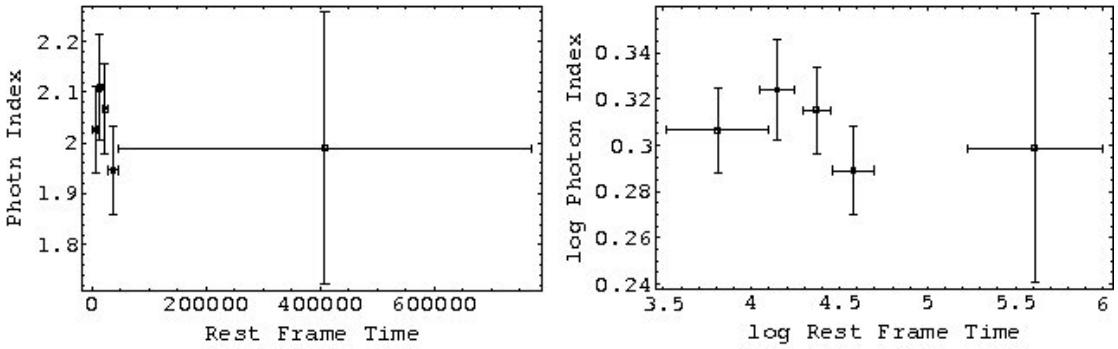

Figure 4.32. GRB 080411 Γ variation

- GRB 050401

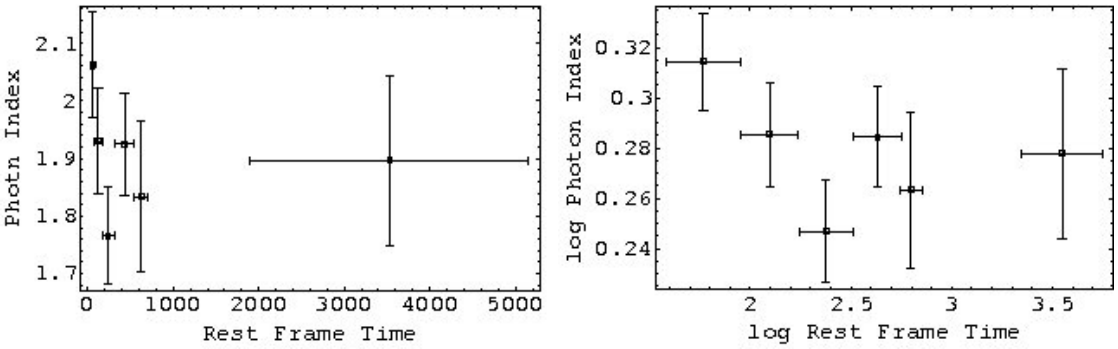

Figure 4.33. GRB 050401 Γ variation

- GRB 060714

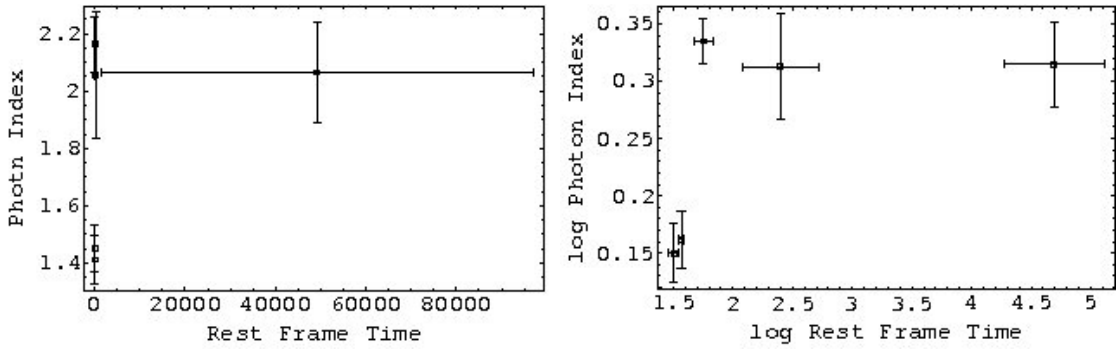

Figure 4.34. GRB 060714 Γ variation

- GRB 061110A

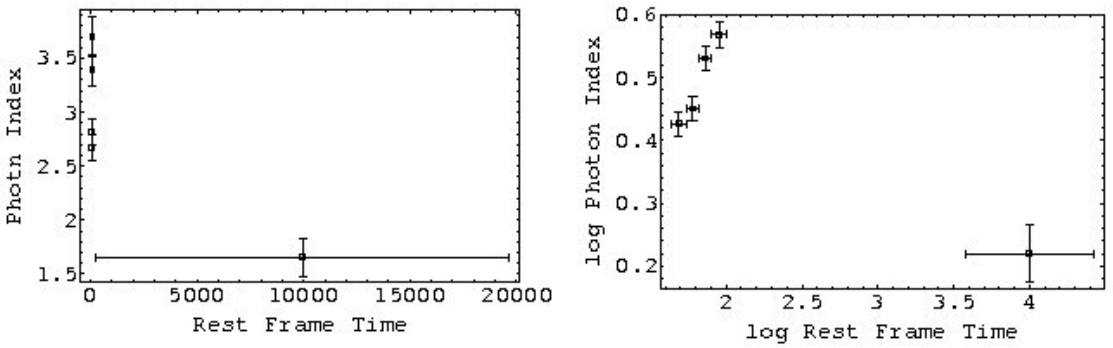

Figure 4.35. GRB 061110A Γ variation

- GRB 050724

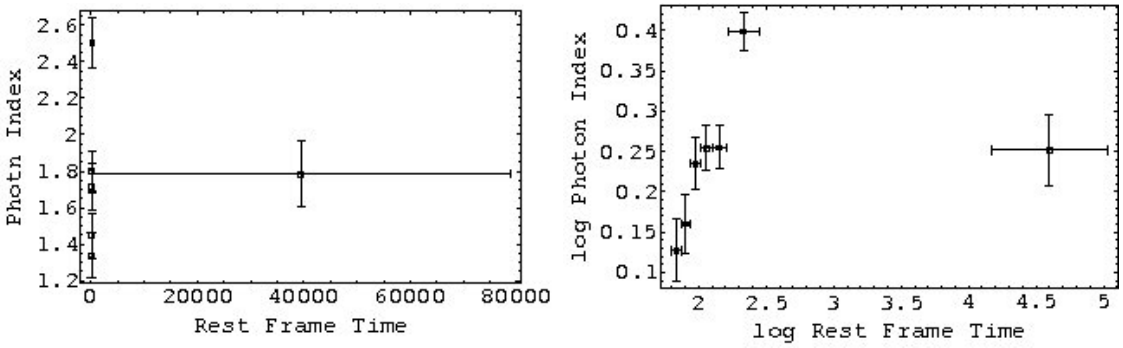

Figure 4.36. GRB 050724 Γ variation

- GRB 050904

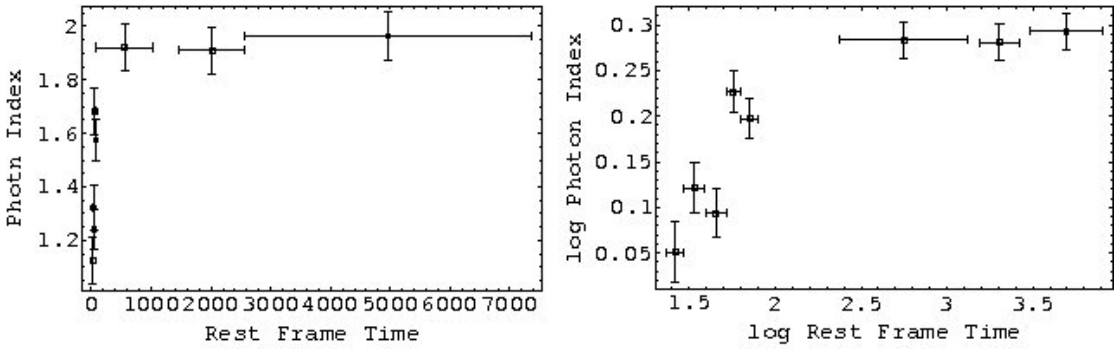

Figure 4.37. GRB 050904 Γ variation

- GRB 060904B

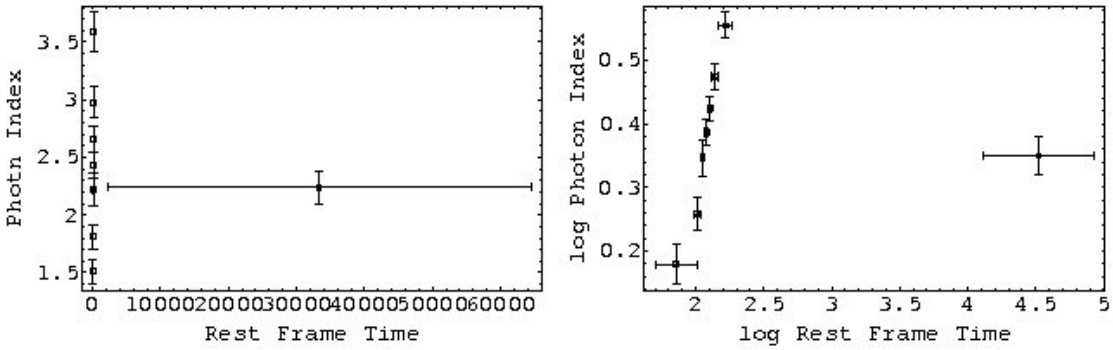

Figure 4.38. GRB 060904B Γ variation

- GRB 050820A

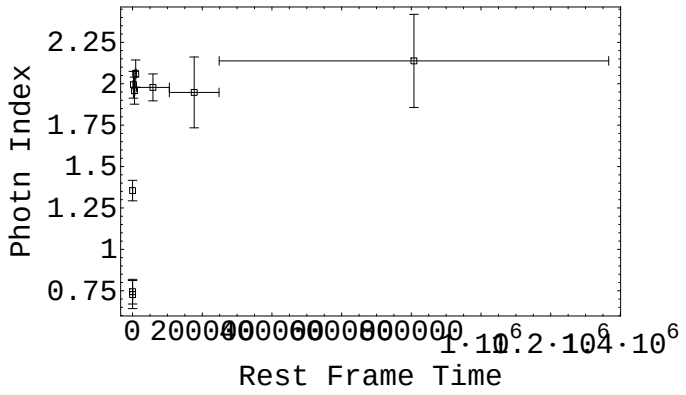

Figure 4.39. GRB 050820A Γ variation

- GRB 060607A

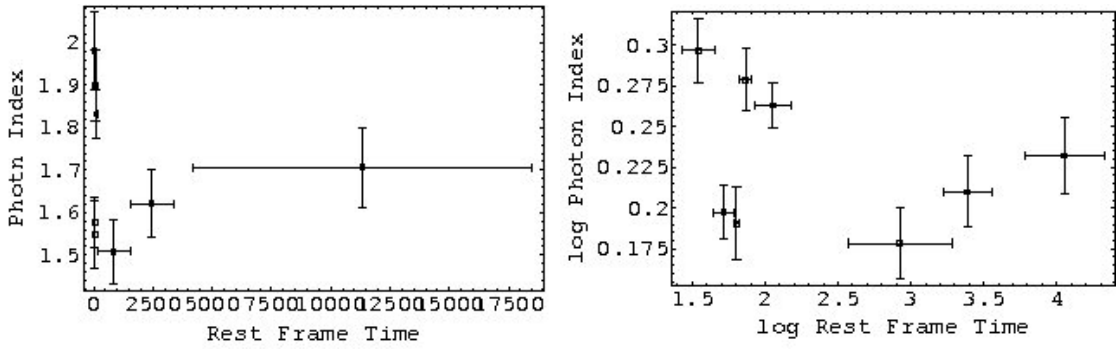

Figure 4.40. GRB 060607A Γ variation

- GRB 060418

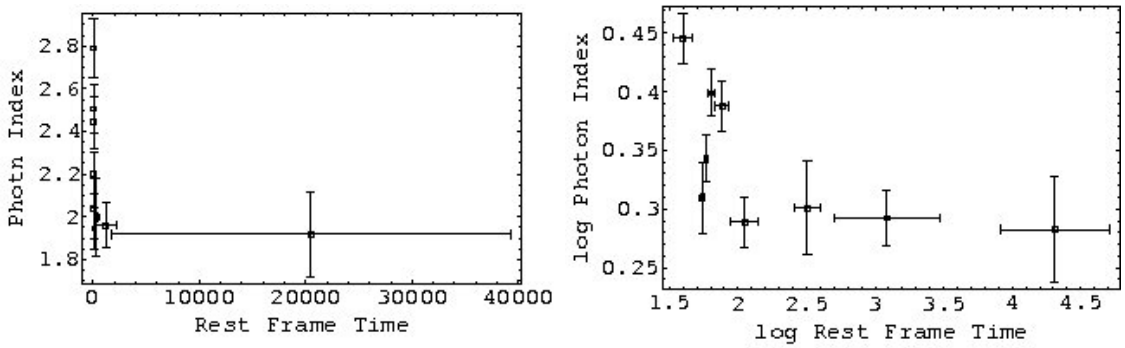

Figure 4.41. GRB 060418 Γ variation

- GRB 050730

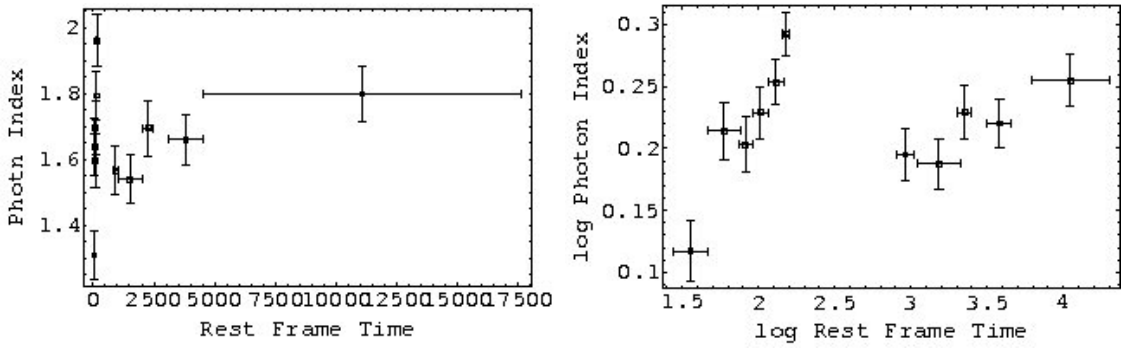

Figure 4.42. GRB 050730 Γ variation

- GRB 060210

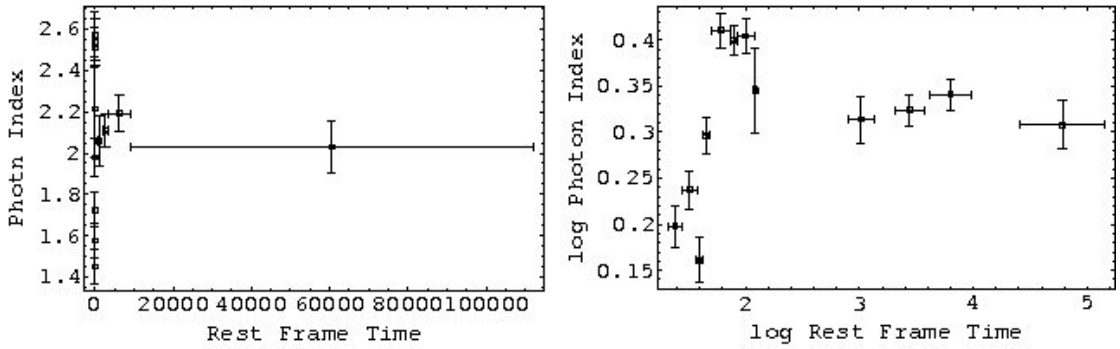

Figure 4.43. GRB 060210 Γ variation

- GRB 060526

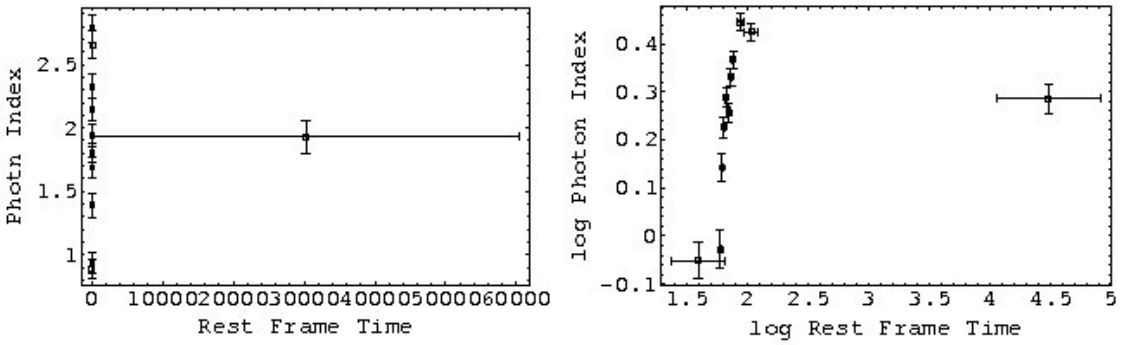

Figure 4.44. GRB 060526 Γ variation

- GRB 061121

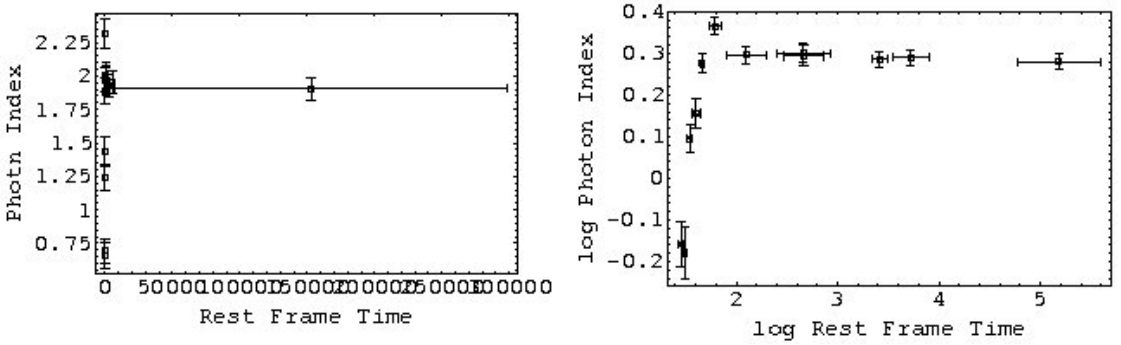

Figure 4.45. GRB 061121 Γ variation

- GRB 071031

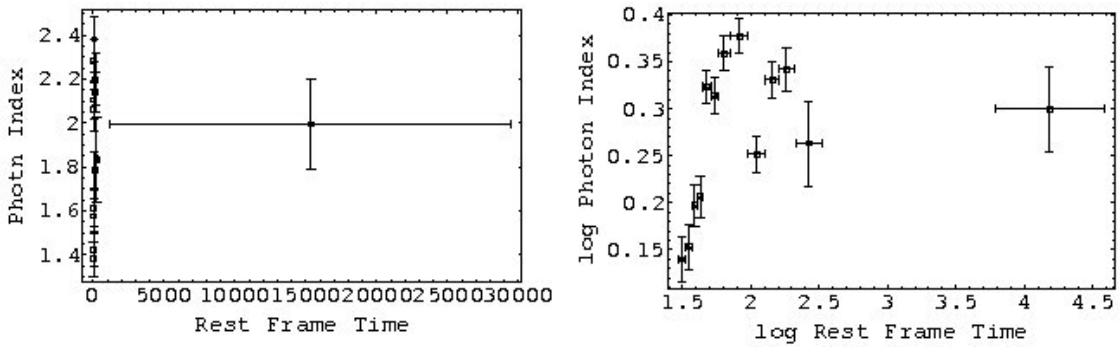

Figure 4.46. GRB 071031 Γ variation

- GRB 060510B

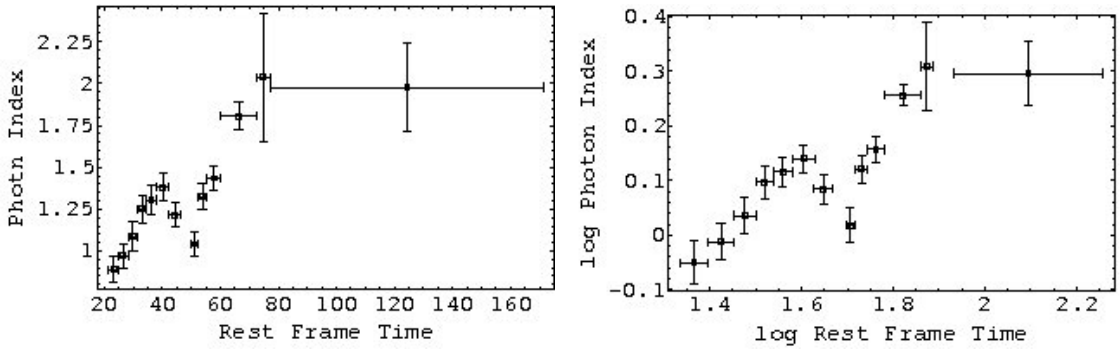

Figure 4.47. GRB 060510B Γ variation

- GRB 060614

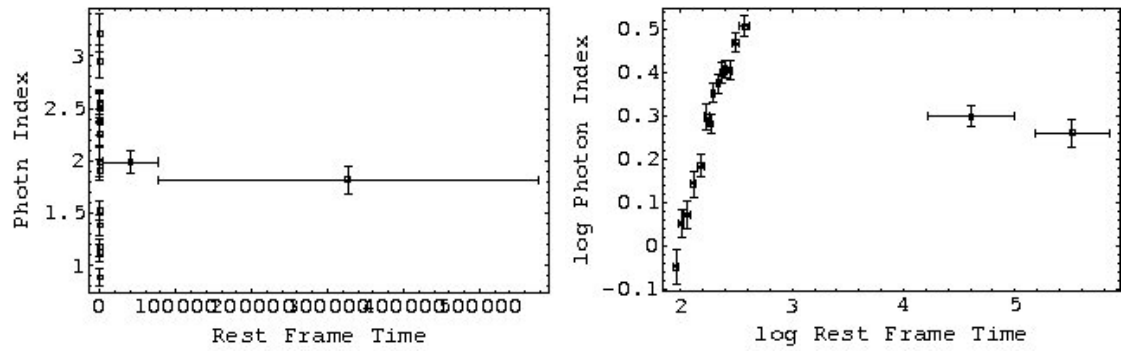

Figure 4.48. GRB 060614 Γ variation

- GRB 060729

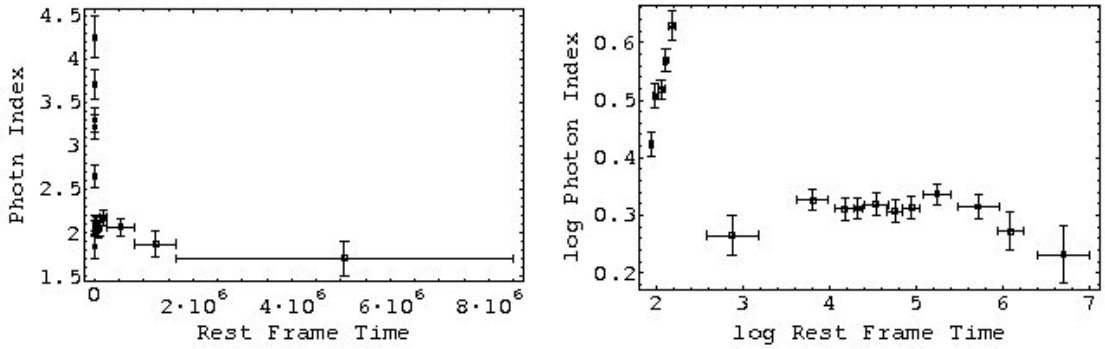

Figure 4.49. GRB 060729 Γ variation

- GRB 060814

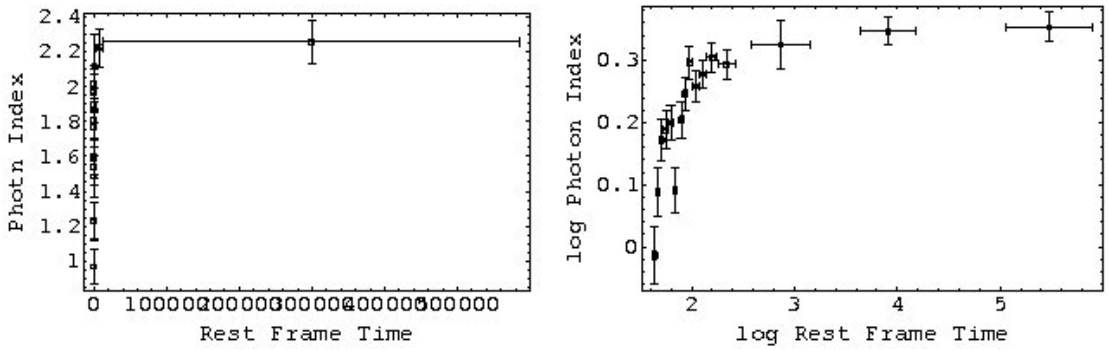

Figure 4.50. GRB 060814 Γ variation

- GRB 060202

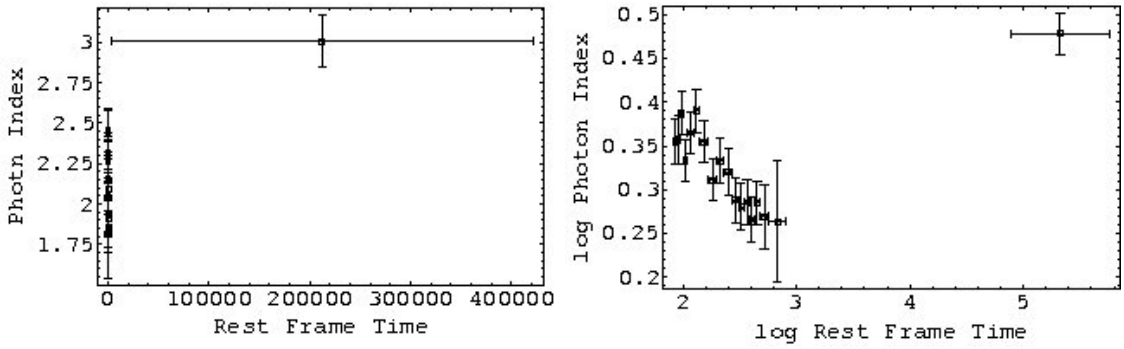

Figure 4.51. GRB 060202 Γ variation

- GRB 060124

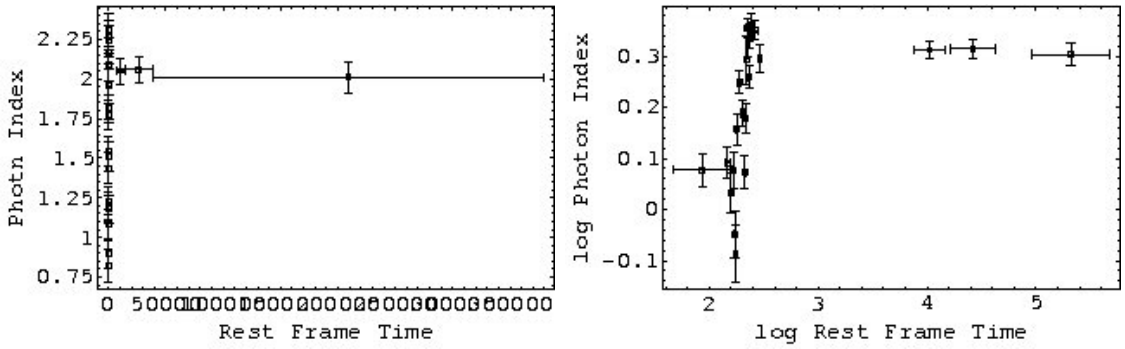

Figure 4.52. GRB 060124 Γ variation

- GRB 080310

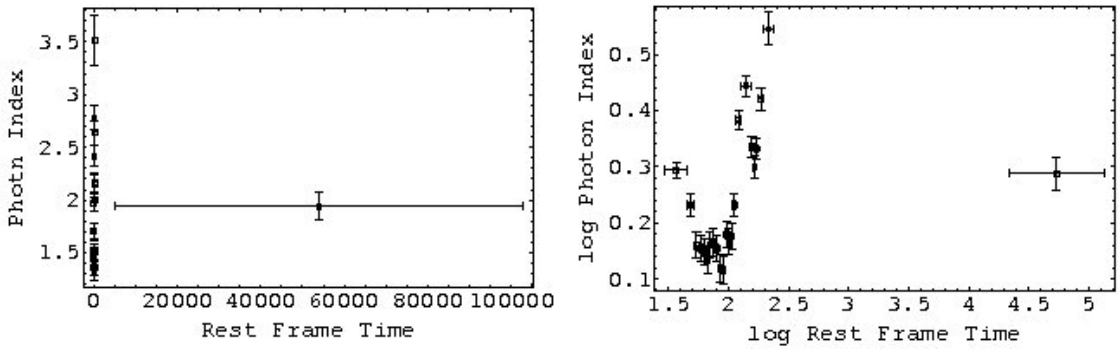

Figure 4.53. GRB 080310 Γ variation

- GRB 061007

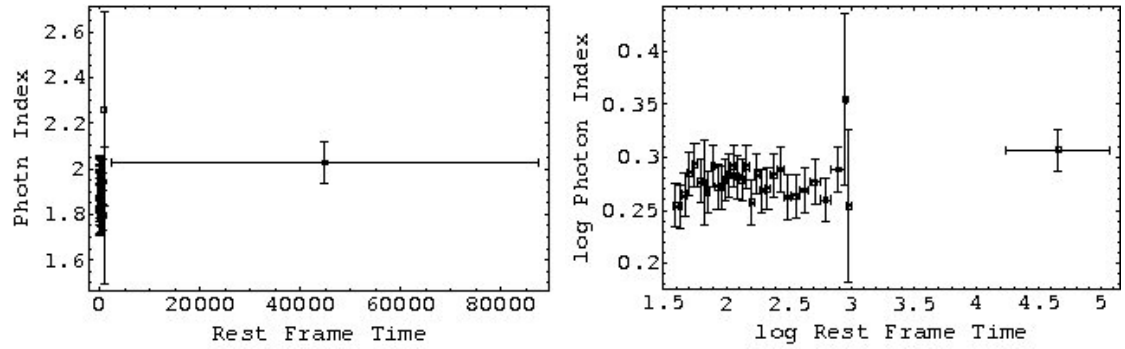

Figure 4.54. GRB 061007 Γ variation

- GRB 080319B

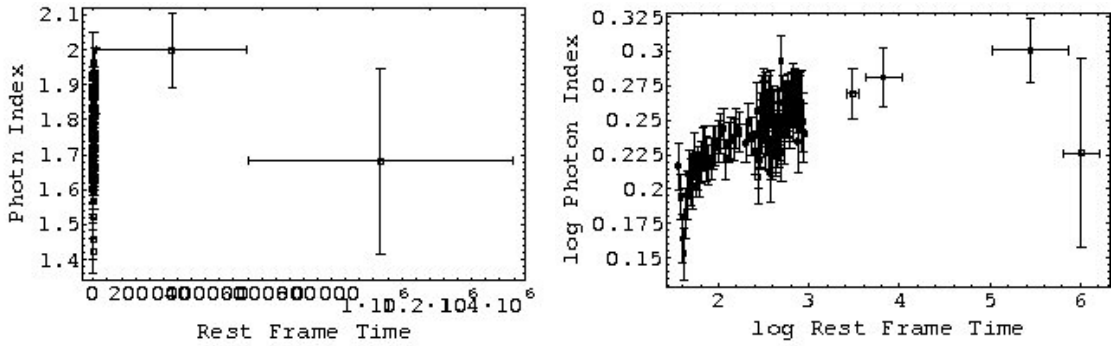

Figure 4.55. GRB 080319B Γ variation

- GRB 060218

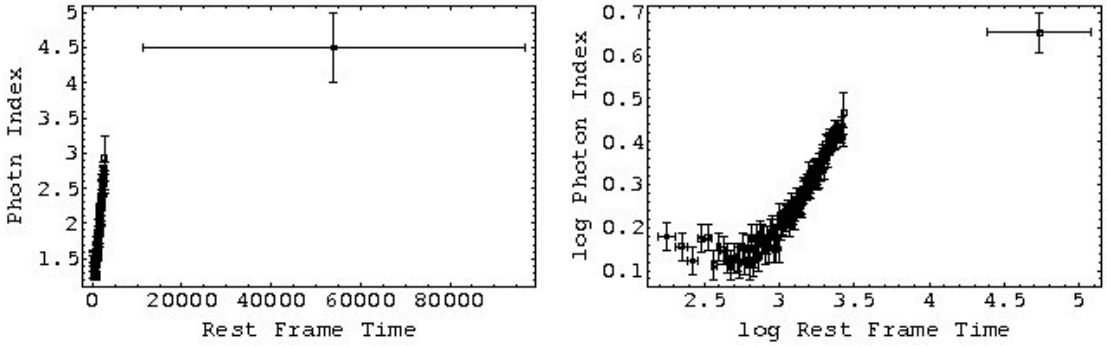

Figure 4.56. GRB 060218 Γ variation

4.2.2. Power Law Photon Index Variability Fit Results

4.2.2.1. Constant Variable Fit. To see if the power law photon index is constant in time, a constant variable fit is applied. Table (4.3) shows the constant variable fit results where a is the constant variable, χ^2 is the $chi-square$, $d.o.f$ is the degree of freedom, $P-value$ is the null hypothesis probability value.

4.2.2.2. Linear Variable Fit. A linear fit is applied to power law photon index change. Table (4.4) shows the linear variable fit results where a is the linear variable, b is the slope, $d.o.f$ is the degree of freedom, $P-value$ is the null hypothesis probability value, χ^2 is the $chi-square$.

Table 4.3. Constant variable fit results for Γ variation

GRB	a	Error of a	Reduced χ^2	D.o.f	P-value (one-tail)
051109A	2.125	0.062	0.316512	4	0.132891
060604	2.161	0.048	3.78297	3	0.00998138
070318	1.751	0.049	10.9203	4	7.47×10^{-9}
080411	2.029	0.044	0.42862	4	0.211914
050401	1.905	0.04	1.23897	5	0.287718
060714	1.688	0.047	12.6817	4	2.54×10^{-10}
061110A	2.832	0.064	21.0064	4	0
050724	1.745	0.048	8.30799	6	5.04×10^{-9}
050904	1.578	0.03	15.3053	7	0
060904B	2.305	0.044	23.4231	7	0
050820A	1.53	0.029	43.734	8	0
060607A	1.698	0.026	5.0726	7	8.97×10^{-6}
060418	2.204	0.041	5.86611	8	1.58×10^{-7}
050730	1.653	0.024	4.75619	10	7.46×10^{-7}
060210	2.012	0.028	15.0633	11	0
060526	1.759	0.028	45.3369	10	0
061121	1.651	0.027	32.209	11	0
071031	1.836	0.026	13.7261	12	0
060510B	1.25	0.024	9.34221	12	0
060614	1.77	0.027	34.8564	15	0
060729	2.252	0.028	20.6732	15	0
060814	1.699	0.028	11.2822	15	0
060202	2.126	0.03	4.0469	17	3.47×10^{-8}
060124	1.649	0.021	23.9609	21	0
080310	1.671	0.018	23.0168	22	0
061007	1.888	0.016	0.406624	31	0.00138397
080319B	1.716	0.0076	1.75954	90	0.0000116381
060218	1.799	0.011	13.5365	101	0

Table 4.4. Linear variable fit results for Γ variation

GRB	a	Err. of a	b	Err. of b	Reduced χ^2	D.o.f	P-value
051109A	2.132	0.067	-3×10^{-7}	1×10^{-6}	0.39359	3	0.24238
060604	2.169	0.053	-1×10^{-6}	2.8×10^{-6}	5.6021	2	0.00369012
070318	1.675	0.053	1.8×10^{-6}	1.8×10^{-6}	10.2483	3	9.6×10^{-7}
080411	2.035	0.05	-2.1×10^{-7}	7.1×10^{-7}	0.540901	3	0.345747
050401	1.912	0.047	-0.000013	0.000046	1.52812	4	0.190905
060714	1.658	0.049	8.4×10^{-6}	8.9×10^{-6}	15.263	3	6.2×10^{-10}
061110A	3.023	0.07	-0.00014	0.00014	10.4155	3	7.5×10^{-7}
050724	1.742	0.049	1.2×10^{-6}	5×10^{-6}	9.95707	5	1.5×10^{-9}
050904	1.4	0.037	0.000253	0.000069	6.30337	6 ,	1.21×10^{-6}
060904B	2.311	0.046	-2.1×10^{-6}	5×10^{-6}	28.4614	6	0
050820A	1.431	0.032	6.1×10^{-6}	2.1×10^{-6}	41.1901	7	0
060607A	1.702	0.029	-3.1×10^{-6}	8.9×10^{-6}	5.89471	6	3.65×10^{-6}
060418	2.226	0.042	-0.000025	0.000019	6.20701	7	2.7×10^{-7}
050730	1.631	0.028	0.000013	0.00001	4.9861	9	9.7×10^{-7}
060210	2.007	0.03	1.2×10^{-6}	2.1×10^{-6}	16.5382	10	0
060526	1.75	0.028	6.1×10^{-6}	7.5×10^{-6}	50.1609	9	0
061121	1.617	0.029	2×10^{-6}	2×10^{-6}	34.2933	10	0
071031	1.831	0.027	0.000013	0.000018	14.8941	11	0
060510B	0.681	0.085	0.0129	0.0019	3.10101	11	0.00034686
060614	1.765	0.028	3×10^{-7}	4.7×10^{-7}	37.3047	14	0
060729	2.308	0.031	-3×10^{-7}	1.2×10^{-7}	20.33	14	0
060814	1.666	0.029	2.1×10^{-6}	2×10^{-6}	10.3968	14	0
060202	2.094	0.031	4.3×10^{-6}	4.3×10^{-6}	2.43318	16	0.00111286
060124	1.61	0.022	7.5×10^{-6}	3.5×10^{-6}	22.7844	20	0
080310	1.666	0.018	5.3×10^{-6}	5.4×10^{-6}	23.9009	21	0
061007	1.883	0.017	3.2×10^{-6}	3.7×10^{-6}	0.338691	30	0.000267015
080319B	1.7149	0.0077	2.8×10^{-7}	2.6×10^{-7}	1.73173	89	0.0000226255
060218	1.027	0.025	0.000616	0.000018	0.947953	100	0.371741

4.2.3. Interpretation of the Γ variability

Photon index variability is searched for each burst. In the first applied absorbed power law model all N_{Hint} is set as a free parameter. First the simplest model, a constant variable fit is examined. The statistical results are given in Table (4.3). When 0.05 is chosen as the threshold for one tail probability value (p-value), the bigger values than 0.05 give the ones that the constant variable fit can not be rejected. These are GRB 051109A, GRB 080411 and GRB 050401. For all the other GRBs in our sample, the P-value is smaller than 0.05, the constant variable fit can be rejected. The results for photon index linear variability are given in Table (4.4) for the whole GRB sample. Since the constant variable fit can not be rejected for GRB051109A, GRB080411, GRB050401, we will examine the results for the others in Table (4.4). Only GRB 060218 has a P-value greater than 0.05, a linear variability for photon index cant be rejected in this case. For P-value smaller than 0.05 the linear variability of photon index can be rejected.

4.3. N_{Hint} and Γ Correlation

4.3.1. N_{Hint} and Γ Correlation Graphs

The graphs show the power law photon index versus intrinsic Hydrogen column density for the related GRB. Both parameter values are obtained by absorbed simple power law model.

- GRB 051109A

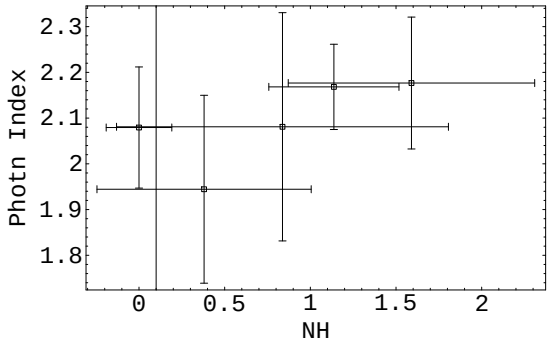

Figure 4.57. GRB 051109A N_{Hint} and Γ Correlation

- GRB 060604

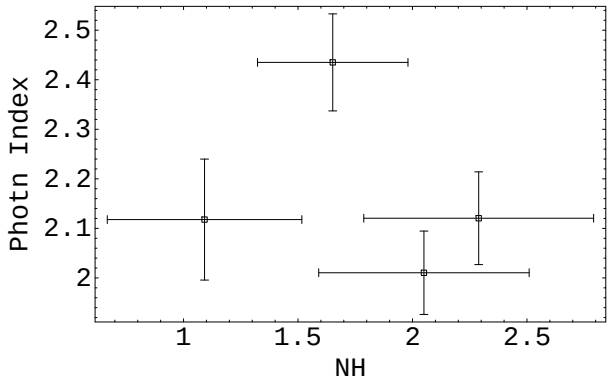

Figure 4.58. GRB 060604 N_{Hint} and Γ Correlation

- GRB 070318

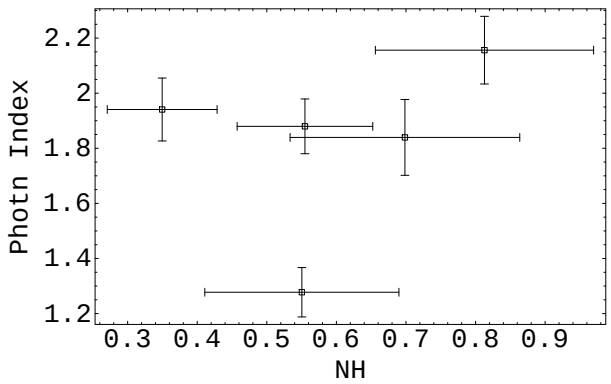

Figure 4.59. GRB 070318 N_{Hint} and Γ Correlation

- GRB 080411

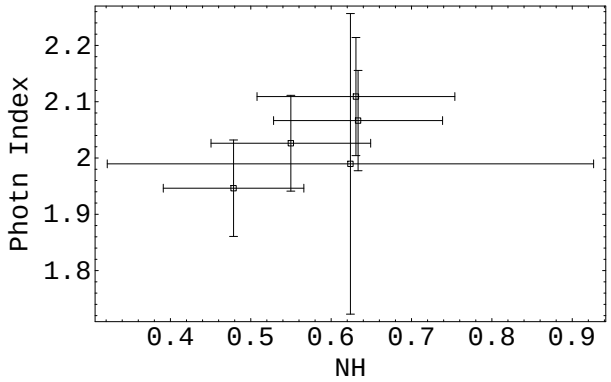

Figure 4.60. GRB 080411 N_{Hint} and Γ Correlation

- GRB 050401

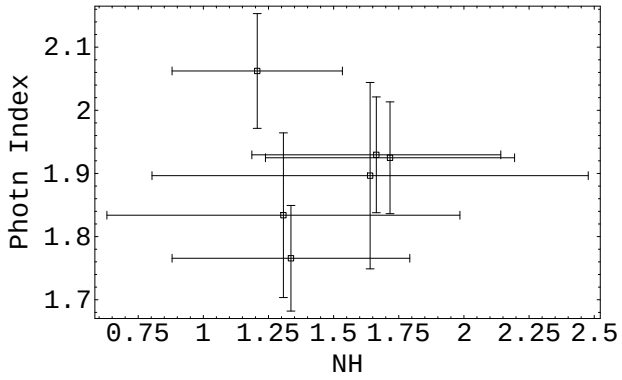

Figure 4.61. GRB 050401 N_{Hint} and Γ Correlation

- GRB 060714

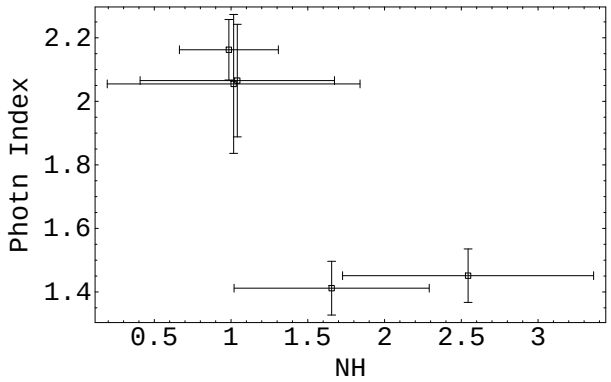

Figure 4.62. GRB 060714 N_{Hint} and Γ Correlation

- GRB 061110A

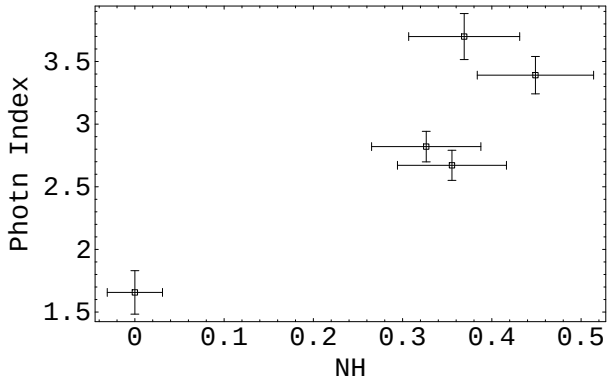

Figure 4.63. GRB 061110A N_{Hint} and Γ Correlation

- GRB 050724

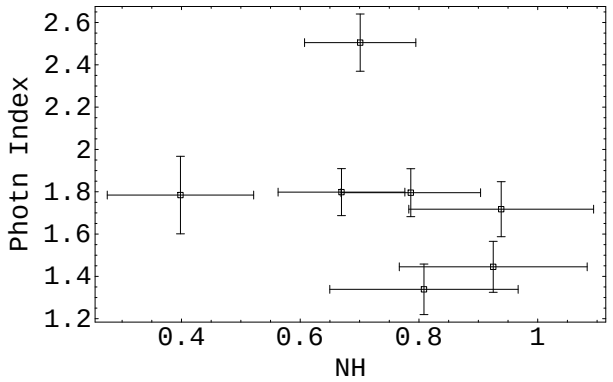

Figure 4.64. GRB 050724 N_{Hint} and Γ Correlation

- GRB 050904

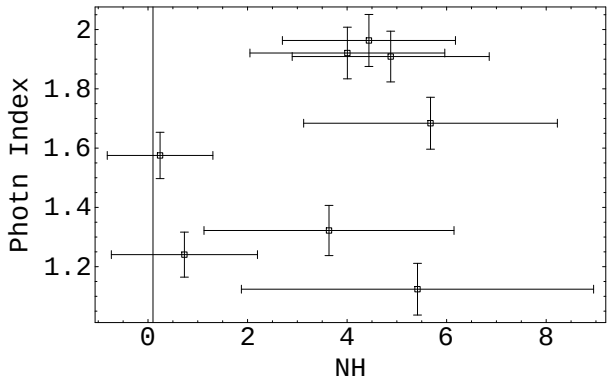

Figure 4.65. GRB 050904 N_{Hint} and Γ Correlation

- GRB 060904B

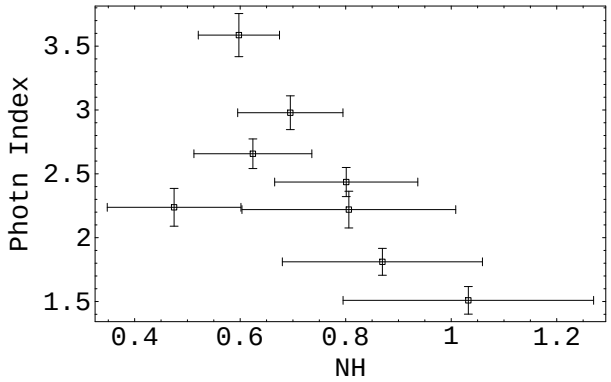

Figure 4.66. GRB 060904B N_{Hint} and Γ Correlation

- GRB 050820A

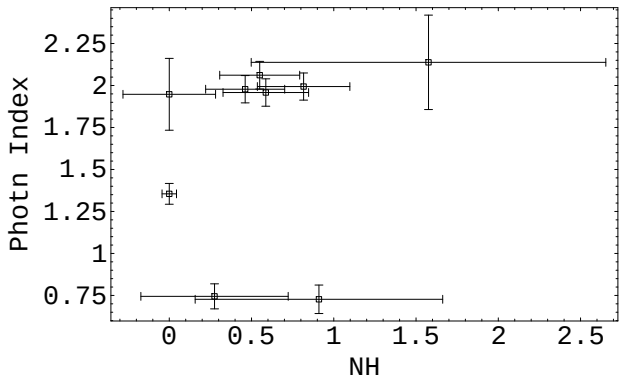

Figure 4.67. GRB 050820A N_{Hint} and Γ Correlation

- GRB 060607A

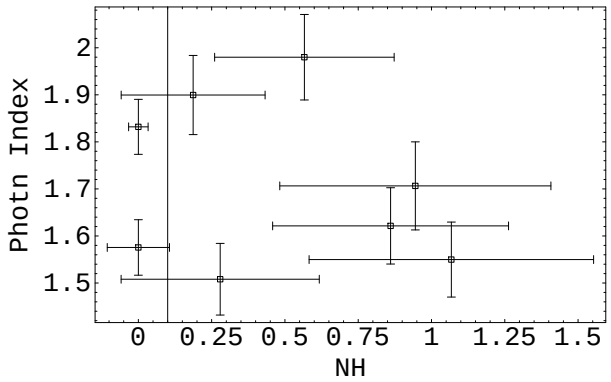

Figure 4.68. GRB 060607A N_{Hint} and Γ Correlation

- GRB 060418

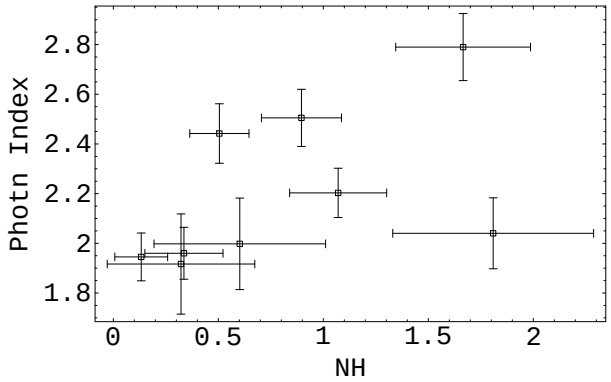

Figure 4.69. GRB 060418 N_{Hint} and Γ Correlation

- GRB 050730

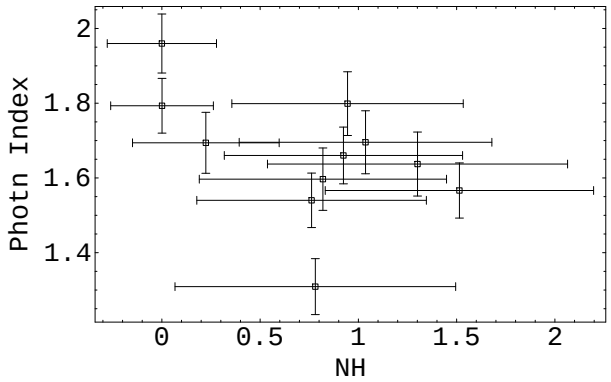

Figure 4.70. GRB 050730 N_{Hint} and Γ Correlation

- GRB 060210

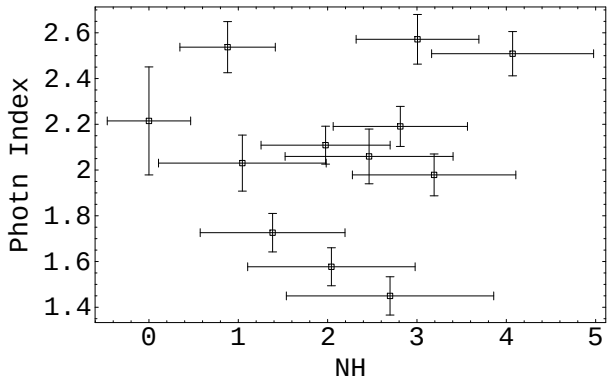

Figure 4.71. GRB 060210 N_{Hint} and Γ Correlation

- GRB 060526

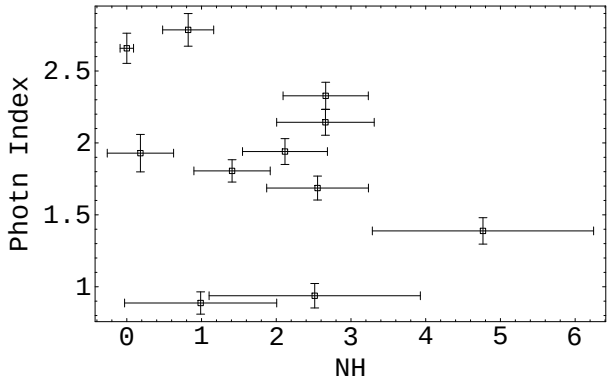

Figure 4.72. GRB 060526 N_{Hint} and Γ Correlation

- GRB 061121

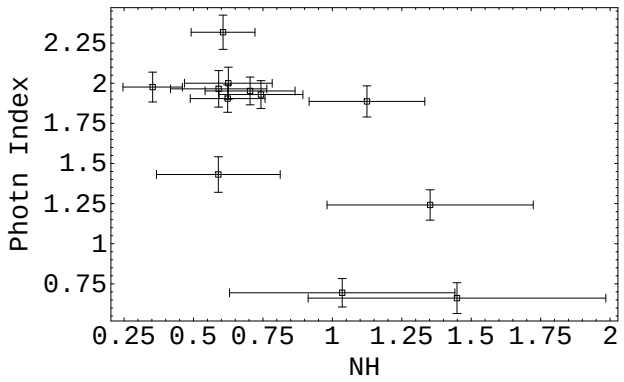

Figure 4.73. GRB 061121 N_{Hint} and Γ Correlation

- GRB 071031

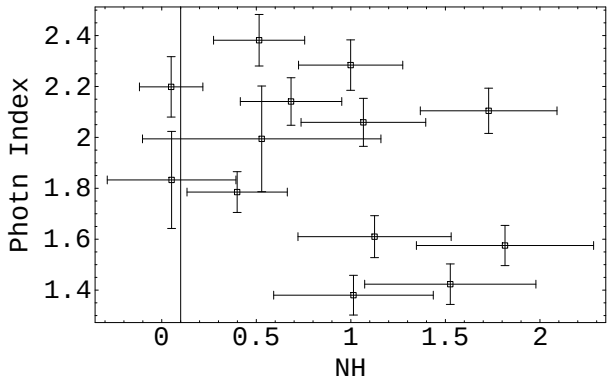

Figure 4.74. GRB 071031 N_{Hint} and Γ Correlation

- GRB 060510B

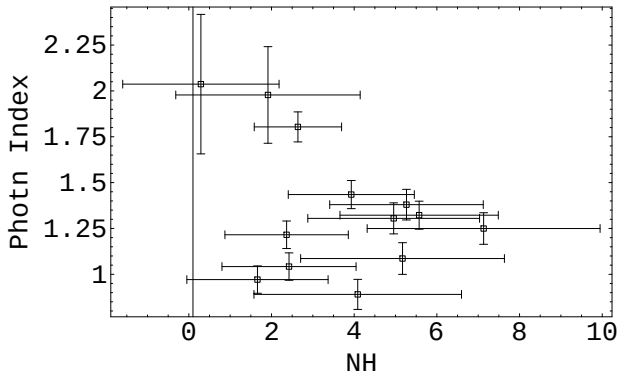

Figure 4.75. GRB 060510B N_{Hint} and Γ Correlation

- GRB 060614

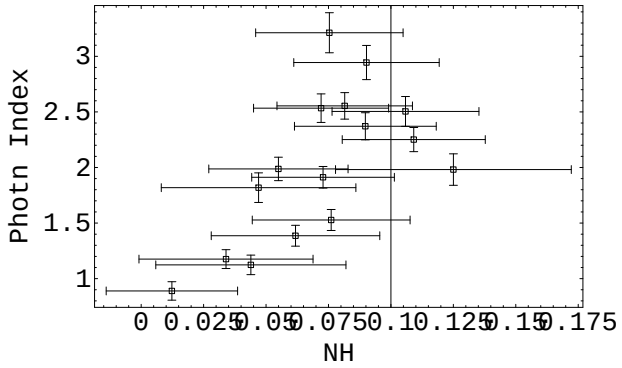

Figure 4.76. GRB 060614 N_{Hint} and Γ Correlation

- GRB 060729

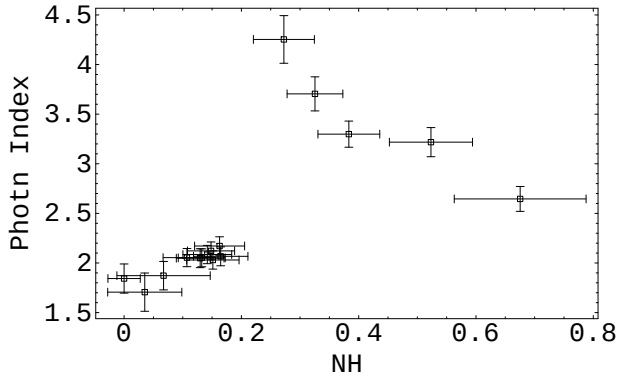

Figure 4.77. GRB 060729 N_{Hint} and Γ Correlation

- GRB 060814

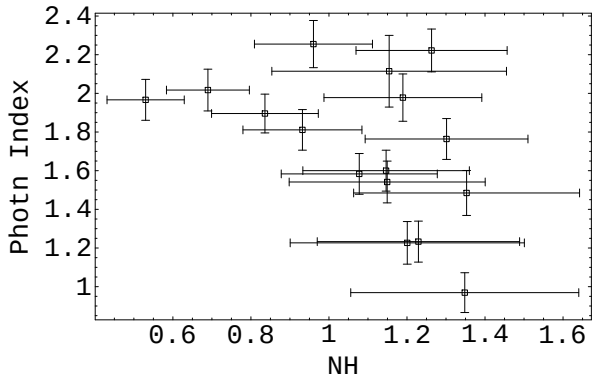

Figure 4.78. GRB 060814 N_{Hint} and Γ Correlation

- GRB 060202

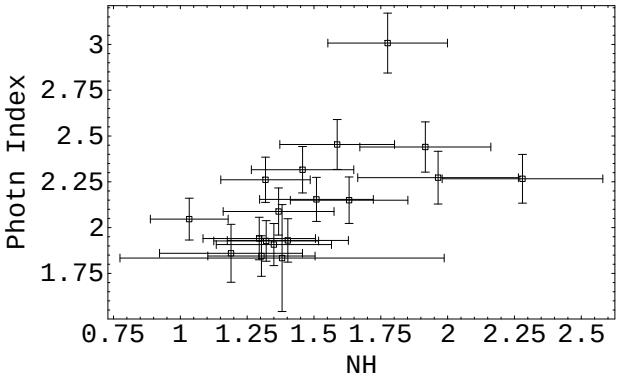

Figure 4.79. GRB 060202 N_{Hint} and Γ Correlation

- GRB 060124

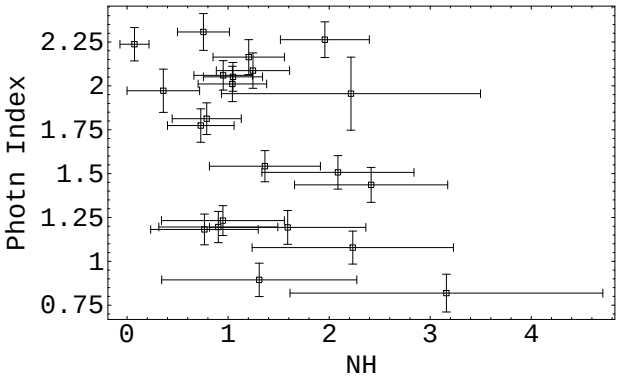

Figure 4.80. GRB 060124 N_{Hint} and Γ Correlation

- GRB 080310

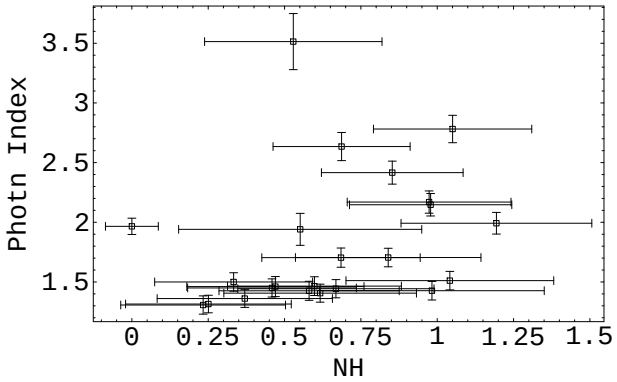

Figure 4.81. GRB 080310 N_{Hint} and Γ Correlation

- GRB 061007

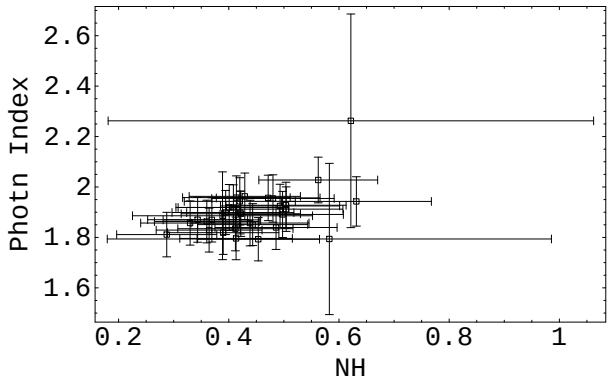

Figure 4.82. GRB 061007 N_{Hint} and Γ Correlation

- GRB 080319B

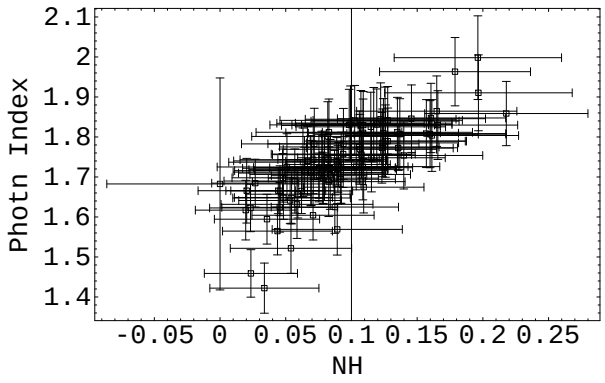

Figure 4.83. GRB 080319B N_{Hint} and Γ Correlation

- GRB 060218

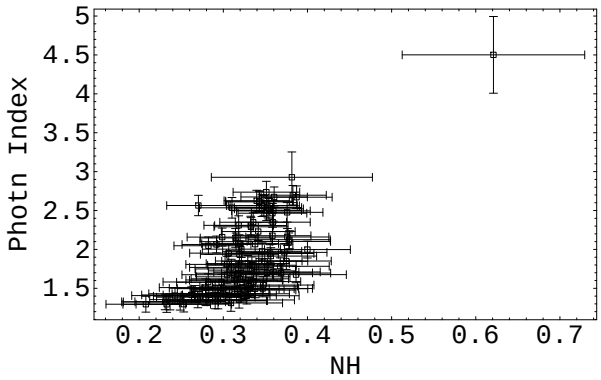

Figure 4.84. GRB 060218 N_{Hint} and Γ Correlation

4.3.2. N_{Hint} and Γ Correlation Fit Results

Multi trail chance probability in Table (4.7) is calculated using Bernoulli Distribution as given in Equation (4.1).

$$probability\ of\ getting\ r\ successes\ in\ 28\ trails = \frac{28}{r!(28-r)!}p^r(1-p)^{28-r} \qquad (4.1)$$

For this calculation we choose the probability p as 0.005. The number of success is 7 for Pearson index, 11 for Kendall and Spearman indexes.

In the Table (4.7) and Table (4.6) Pearson index is shown as r, Sperman index is shown as (ρ) and the Kendall index is shown as τ. In the Table (4.7) single trail chance probability is abbreviated as S.T.C.Prob. and in the Table (4.6) multi trail chance probability is abbreviated as S.T.C.Prob.

Table 4.5. N_{Hint} and Γ Correlation Linear fit results

GRB	a	Err. of a	b	Err. of b	Total χ^2	D.o.f	P-value
051109A	0.096	2.04	0.12	0.118	0.54	3	0.911
060604	-1.38	4.586	2.944	3.511	3.80	2	0.149
070318	31.03	-14.001	277.783	16.281	9.45	3	0.023
080411	0.912	1.511	1.079	1.483	0.12	3	0.989
050401	-1.43	3.97	3.699	2.466	1.06	4	0.899
060714	-0.72	2.86	0.45	0.951	0.83	3	0.841
061110A	4.405	1.529	0.726	0.215	5.49	3	0.139
050724	-7.45	7.322	8.370	41.751	10.52	5	0.061
050904	0.217	1.080	0.117	0.437	8.02	6	0.236
060904B	-9.60	9.21	6.801	10.641	6.23	6	0.397
050820A	1.464	1.307	0.418	0.087	9.95	7	0.1912
060607A	-2.72	1.89	3.319	0.371	16.88	6	0.009
060418	0.635	1.801	0.179	0.118	15.9	7	0.026
050730	-0.42	1.926	0.183	0.111	5.89	9	0.751
060210	-0.72	3.493	0.411	1.414	31.66	10	0.0004
060526	-0.58	2.839	0.098	0.1	37.38	9	2.2×10^{-5}
061121	-2.24	3.377	0.996	0.836	15.13	10	0.127
071031	-0.90	2.660	0.277	0.22	31.04	11	0.001
060510B	-0.59	3.373	0.494	6.835	9.33	11	0.591
060614	33.70	-0.338	13.618	1.251	6.55	14	0.9505
060729	5.909	1.334	0.816	0.146	44.50	14	4.9×10^{-5}
060814	-1.58	3.345	0.446	0.451	26.22	14	0.024
060202	1.319	0.246	0.428	0.682	16.67	16	0.406
060124	-1.01	2.815	0.247	0.221	38.09	20	0.008
080310	5.637	-0.657	3.723	3.559	58.07	21	2.4×10^{-5}
061007	0.862	1.521	0.479	0.232	6.04	30	0.999
080319B	2.638	1.495	0.446	0.041	19.01	89	1
060218	18.6	-4.083	3.730	1.293	41.85	100	1

Table 4.6. N_{Hint}–Γ correlation coefficients with single trail chance probability

GRB	r	S.T.C.Prob.of r	ρ	S.T.C.Prob.of ρ	τ	S.T.C.Prob.of τ
051109A	0.703	0.184	0.9	0.037	0.8	0.005
060604	-0.23	0.769	0	1	0	1
070318	0.295	0.628	0.3	0.623	0.2	0.624
080411	0.741	0.151	0.8	0.104	0.6	0.141
050401	-0.025	0.961	0.028	0.95715	0.06	0.8509
060714	-0.862	0.06	-0.8	0.104	-0.6	0.141
061110A	0.89	0.042	0.8	0.10	0.6	0.141
050724	-0.325	0.475	-0.607	0.14	-0.33	0.293
050904	0.260	0.532	0.142	0.735	0.071	0.804
060904B	-0.65474	0.078	-0.738	0.036	-0.642	0.025
050820A	0.218	0.571	0.393	0.294	0.309	0.244
060607A	-0.217	0.605	-0.203	0.628	-0.109	0.705
060418	0.51566	0.155	0.716	0.029	0.555	0.037
050730	-0.490	0.125	-0.290	0.385	-0.236	0.311
060210	0.079	0.805	0.027	0.931	0	1
060526	-0.369	0.263	-0.263	0.433	-0.127	0.585
061121	-0.726	0.007	-0.650	0.022	-0.515	0.019
071031	-0.390	0.187	-0.434	0.138	-0.282	0.179
060510B	-0.413	0.160	-0.159	0.603	-0.153	0.464
060614	0.643	0.007	0.641	0.007	0.45	0.015
060729	0.621	0.01	0.861	1.78×10^{-5}	0.65	0.000445
060814	-0.472	0.06	-0.464	0.069	-0.35	0.058
060202	0.575	0.01	0.68	0.0015	0.450	0.008
060124	-0.439	0.04	-0.378	0.082	-0.246	0.107
080310	0.287	0.183	0.486	0.018	0.343	0.021
061007	0.525	0.001	0.3977	0.0241	0.282	0.023
080319B	0.791	9.6×10^{-21}	0.83	1.007×10^{-24}	0.636	3.98×10^{-19}
060218	0.710	6.06×10^{-17}	0.656	6.5051×10^{-14}	0.477	1.161×10^{-12}

Table 4.7. N_{Hint}–Γ correlation coefficients with multi trail chance probability

GRB	r	M.T.C.Prob.of r	ρ	M.T.C.Prob.of ρ	τ	M.T.C.Prob.of τ
051109A	0.703	2.89314×10^{-32}	0.9	4.02629×10^{-36}	0.8	4.02629×10^{-36}
060604	-0.23	2.89314×10^{-32}	0	4.02629×10^{-36}	0	4.02629×10^{-36}
070318	0.295	2.89314×10^{-32}	0.3	4.02629×10^{-36}	0.2	4.02629×10^{-36}
080411	0.741	2.89314×10^{-32}	0.8	4.02629×10^{-36}	0.6	4.02629×10^{-36}
050401	-0.025	2.89314×10^{-32}	0.028	4.02629×10^{-36}	0.06	4.02629×10^{-36}
060714	-0.862	2.89314×10^{-32}	-0.8	4.02629×10^{-36}	-0.6	4.02629×10^{-36}
061110A	0.89	2.89314×10^{-32}	0.8	4.02629×10^{-36}	0.6	4.02629×10^{-36}
050724	-0.325	2.89314×10^{-32}	-0.607	4.02629×10^{-36}	-0.33	4.02629×10^{-36}
050904	0.260	2.89314×10^{-32}	0.142	4.02629×10^{-36}	0.071	4.02629×10^{-36}
060904B	-0.65474	2.89314×10^{-32}	-0.738	4.02629×10^{-36}	-0.642	4.02629×10^{-36}
050820A	0.218	2.89314×10^{-32}	0.393	4.02629×10^{-36}	0.309	4.02629×10^{-36}
060607A	-0.217	2.89314×10^{-32}	-0.203	4.02629×10^{-36}	-0.109	4.02629×10^{-36}
060418	0.51566	2.89314×10^{-32}	0.716	4.02629×10^{-36}	0.555	4.02629×10^{-36}
050730	-0.490	2.89314×10^{-32}	-0.290	4.02629×10^{-36}	-0.236	4.02629×10^{-36}
060210	0.079	2.89314×10^{-32}	0.027	4.02629×10^{-36}	0	4.02629×10^{-36}
060526	-0.369	2.89314×10^{-32}	-0.263	4.02629×10^{-36}	-0.127	4.02629×10^{-36}
061121	-0.726	2.89314×10^{-32}	-0.650	4.02629×10^{-36}	-0.515	4.02629×10^{-36}
071031	-0.390	2.89314×10^{-32}	-0.434	4.02629×10^{-36}	-0.282	4.02629×10^{-36}
060510B	-0.413	2.89314×10^{-32}	-0.159	4.02629×10^{-36}	-0.153	4.02629×10^{-36}
060614	0.643	2.89314×10^{-32}	0.641	4.02629×10^{-36}	0.45	4.02629×10^{-36}
060729	0.621	2.89314×10^{-32}	0.861	4.02629×10^{-36}	0.65	4.02629×10^{-36}
060814	-0.472	2.89314×10^{-32}	-0.464	4.02629×10^{-36}	-0.35	4.02629×10^{-36}
060202	0.575	2.89314×10^{-32}	0.68	4.02629×10^{-36}	0.450	4.02629×10^{-36}
060124	-0.439	2.89314×10^{-32}	-0.378	4.02629×10^{-36}	-0.246	4.02629×10^{-36}
080310	0.287	2.89314×10^{-32}	0.486	4.02629×10^{-36}	0.343	4.02629×10^{-36}
061007	0.525	2.89314×10^{-32}	0.3977	4.02629×10^{-36}	0.282	4.02629×10^{-36}
080319B	0.791	2.89314×10^{-32}	0.83	4.02629×10^{-36}	0.636	4.02629×10^{-36}
060218	0.710	2.89314×10^{-32}	0.656	4.02629×10^{-36}	0.477	4.02629×10^{-36}

4.3.3. Interpretation of the N_{Hint}-Γ correlations

Intrinsic column density and photon index correlation is searched for each burst in our sample. First a linear correlation fit is tried. The results for the linear fit parameters are given in Table (4.5). When 0.05 is chosen as the threshold for one trail probability value (p-value), the bigger values than 0.05 give the ones that the linear correlation fit can not be rejected. These are: GRB 051109A, GRB 060604, GRB 080411, GRB 050401, GRB 060714, GRB 061110A, GRB 050724, GRB 050904, GRB 060904B, GRB 050820A, GRB 050730, GRB 061121, GRB 060510B, GRB 060614, GRB 060202, GRB 061007, GRB 080319B, GRB 060218. For P-value smaller than 0.05 the linear correlation fit can be rejected. These are: GRB 070318, GRB 060607A, GRB 060418, GRB 060210, GRB 060526, GRB 071031, GRB 060729, GRB 060814, GRB 060124, GRB 080310.

A possible linear correlation between intrinsic column density and photon index is also checked by Pearsons index. The results for correlation coefficients with related single trail chance probabilities are given in Table (4.6) and the related multi trail chance probabilities are given in Table (4.7). For statistical significance, chance probabilities greater than %5 are interpreted as there is significantly no linear correlation between two parameters. These are: GRB 051109A, GRB 060604, GRB 070318, GRB 080411, GRB 050401, GRB 060714, GRB 050724, GRB 050904, GRB 060904B, GRB 050820A, GRB 060607A, GRB 060418, GRB 050730, GRB 060210, GRB 060526, GRB 071031, GRB 060510B, GRB 060814, GRB 080310, GRB 061110A, GRB 061121, GRB 060614, GRB 060729, GRB 060202, GRB 060124, GRB 061007. For the interval, $10^{-5} < \textit{chance probability} < 0.05$, chance probabilities are interpreted as a hint for a possible linear correlation between two parameters. The cases in which there is a possibility to have a linear correlation between N_{Hint} and Γ are GRB 061110A, GRB 061121, GRB 060614, GRB 060729, GRB 060202, GRB 080310, GRB 061007, GRB 060124. GRB 061121 shows a hint for a linear anti-correlation. Since the chance probability values of GRB 080319B and GRB 060218 lower than 10^{-5}, this can be interpreted as a very strong linear correlation between Γ and N_{Hint}. When multi trial probabilities are considered for the whole sample, the probability to find a correlation

just by chance for Pearson Index is 2.8931410^{-32}; so the linear correlation between Γ and N_{Hint} can not be by chance.

Any possible correlation without assuming a linear correlation is checked with Kendall Index, Spearman Index and related chance probabilities. The statistical results are given in Table (4.6) and in Table (4.7). For both Sperman and Kendall indexes, chance probabilities greater than %5 are interpreted as there is significantly no correlation between two parameters. These are: GRB 060604, GRB 070318, GRB 080411, GRB 050401, GRB 060714, GRB 061110A, GRB 050724, GRB 050904, GRB 050820A, GRB 060607A, GRB 050730, GRB 060210, GRB 060526, GRB 071031, GRB 060510B, GRB 060814, GRB 060124. For the interval $10^{-5} < \textit{chance probability} < 0.05$, chance probabilities are interpreted as a sign for a possible correlation between two parameters: GRB 051109A, GRB 060904B, GRB 060418, GRB 061121, GRB 060614, GRB 060729, GRB 060202, GRB 080310, GRB 061007. Since the chance probability values of GRB 080319B and GRB 060218 lower than 10^{-5}, this can be interpreted as a very strong correlation between N_{Hint} and Γ. When multi trial probabilities are considered for the whole sample, the probability to find a correlation just by chance for Spearman and Kendall Indexes is 4.0262910^{-36}; so any kind of correlation between N_{Hint} and Γ can not be by chance.

5. DISCUSSION

In our sample we have 28 GRBs observed by Swift XRT. All the spectra were fit by a photoelectrically absorbed simple power law model. A time resolved analysis is applied. Intrinsic Hydrogen column density variability with time is examined for each burst by fitting the N_{Hint} evolution with a constant and linear model in time. For GRB 060604, GRB 070318, GRB 080411, GRB 050401, GRB 060714, GRB 050724, GRB 050904, GRB 060904B, GRB 050730, GRB 060510B and GRB 060614, a constant N_{Hint} can not be rejected, consistently with the predictions of photo-ionization models for GRBs [3]. GRB061110A shows a decreasing N_{Hint}. However; we caution this conclusion depends on a single N_{Hint} estimation from the latest interval which is significantly less than the previous values.

GRB 051109A, GRB 050820A, GRB 060607A, GRB 060418, GRB 060210, GRB 060526, GRB0 61121, GRB 071031, GRB 060729, GRB 060814, GRB 060202, GRB 060124, GRB 080310, GRB 061007, GRB 080319B, GRB 060218, GRB 060607A instead show an increasing N_{Hint} in some intervals of time, a behaviour we believe to be nonphysical. In other words it is a spurious effect induced by the fitting procedure (model plus limited energy range spanned by the XRT). For example, when the spectra of the GRB 080319B is fit by a model composed of two broken power laws, N_{Hint} is found to be constant [257]. This strengthens our interpretation.

Photon index variability with time is searched for each burst in the absorbed simple power law model in the 0.3 - 10 keV energy range. GRB 051109A, GRB 080411 and GRB 050401 show a constant power law photon index while in all other cases the power law photon index is found to vary in time.

The non-physical N_{Hint} behavior is probably due to a spurious effect. Unfortunately there is not a precise prediction of the Γ evolution with time in the observed 0.3 - 10 keV energy range. On the other hand, regardless of the source, we expect a positive linear correlation between the Γ and the N_{Hint} (see figure 2.30).

The possible linear correlation between the N_{Hint} and the Γ is tested using the Pearson's Correlation Test. To search for any possible correlation without assuming a linear correlation we used the Kendall Rank Test and the Spearman Rank Test. We found a very significant positive linear correlation in GRB 080319B and in GRB 060218. We explain this significant correlation between intrinsic column density and the power-law photon index as a spurious effect coming from the spectral fitting procedure of the absorbed power law model as shown in figure (2.30).

For GRB 060729, GRB 060614, GRB 060202, GRB 061007, there can be a hint for a positive linear correlation. For GRB 051109A, GRB 060418, GRB 080310 there can be a hint for a positive correlation which is not linear. The chance probability of such correlation is also given in Table (4.6) (the strength of the links in these cases is left for the reader judgment). GRB 080319B and GRB 060218 have the best statistics in our sample. This makes it possible to look for the evolution of their spectral properties with particular attention and prove if the correlation between N_{Hint} and Γ is due to the spectral fitting with absorbed simple power law model. For GRB 061121 there can be a hint for a linear anti- correlation while for GRB 060904B there can be a hint for an anti- correlation which is not linear (the strength of the hints is left for the reader judgment). This anti-correlation can not arise from the fitting procedure. The results of our data analysis are discussed below. Each GRB is discussed separately.

In the case of GRB 051109A Γ and N_{Hint} seem to undergo fluctuations in time for $t < 30000sec$. However; when the total behavior is considered, a constant Γ is found to provide a good explanation of the data. A non–linear Γ–N_{Hint} is also found.

For GRB 060604 and GRB 070318 Γ and N_{Hint} seem to undergo fluctuations in time for $t < 1000sec$. However; when the total behavior is considered, a constant N_{Hint} is found.

For GRB 080411 and GRB 050401 Γ and N_{Hint} shows fluctuations in time for $t < 5000sec$ and $t < 1000sec$ respectively. When the overall manner is considered we interpret Γ and N_{Hint} as constant.

In the analysis of GRB 060714, GRB 050730 and GRB 060510B, we found that the early phase $t < 1000sec$ shows a hard to soft spectral evolution which is consistent with the E_{peak} of the νF_{ν} spectrum shifting to lower energy with time [99] (although they used N_{Hint} as a fixed parameter). While we see fluctuations for the N_{Hint} during the steep decay phase, the total behavior can be fit by a constant.

For GRB 061110A we found that the early phase $t < 1000sec$ shows a hard to soft spectral evolution which is consistent with [99] (although they used N_{Hint} as a fixed parameter). While we see fluctuations for the N_{Hint} during the steep decay phase, the total behavior can be interpreted as decreasing.

In the analysis of GRB 050724 we found that the time interval $t < 1000sec$ shows a hard to soft spectral evolution which is consistent with [253] and [99]. We also found N_{Hint} variations during the early phase $t < 1000sec$, but when we look to the overall manner we interpret N_{Hint} as constant.

In the case of GRB 050904 we found that the early phase $t < 1000sec$ shows a hard to soft spectral evolution that agrees with [99] (in their analysis they took N_{Hint} as a fixed parameter). We don`t see spectral evolution after the early phase which is consistent with [254]. For the time interval $t < 1000sec$, we found that the N_{Hint} is decreasing which agrees with [254], but when we look to the total behavior we interpret N_{Hint} as constant in contrast with [4] (since they used improved spectral models).

Analysis of GRB 060904B showed that up to 1,000 there ia a hard to soft spectral evolution which is consistent with [5]. While N_{Hint} is decreasing during the early phase ($t < 1000sec$) the total behavior of N_{Hint} with time can be interpret as constant. We found a hint for a non-linear anti-correlation between the N_{Hint} and the Γ which is dominated by the early phase behavior. This anti-correlation can not be interpreted as spurious, since a positive correlation would be expected in that case. That's why this anti-correlation effect is important to investigate. We stress that we showed an unpredicted relation between the Γ and the N_{Hint} : The dependence of this correlation on the spectral model used will be investigated in as forthcoming work.

For GRB 050820A, GRB 060607A, GRB 060210 and GRB 071031, we found that the early phase ($t < 200000sec$, $t < 1000sec$, $t < 8000sec$, $t < 1000sec$ respectively)shows N_{Hint} and Γ variations.

In the case of GRB 060418 we found that during the steep decay ($t < 1000sec$) both the Γ and the N_{Hint} decreases and than flattens to a constant behaviour afterward. We found a hint for a positive non-linear correlation between the Γ and the N_{Hint} mainly due to the early phase behavior. Here we can explain the N_{Hint} decrease as an artifact of the Γ decrease. (However, we can also think that if Γ should increase at early phase, than maybe we see Γ decrease as an effect of physical N_{Hint} decrease.). In this case the presence of the flaring activity makes any conclusion difficult.

Analysis of GRB 060526 showed that during the early phase ($t < 1000sec$) there is a hard to soft spectral evolution which is consistent with [5]. We found N_{Hint} variations during the early phase.

For GRB 061121 we found that the early phase ($t < 1000sec$) shows a hard to soft spectral evolution which is consistent with [5] and [99]. We found that the N_{Hint} is decreasing during the early phase, while the total behavior is consistent with a constant N_{Hint}. We found a hint for a linear anti-correlation between the N_{Hint} and the Γ which is dominated by the early phase behavior. In [5] they give the explanation to the Γ variation and interpret the N_{Hint} variation as an artificial effect, but they don't explain how the Γ affects the N_{Hint}. Regardless of the nature of the Γ variations, a positive Γ–N_{Hint} correlation is expected.

In the case of GRB 060614 we found that the early phase ($t < 100sec$) shows soft to hard spectral evolution with Γ is nearly constant afterwards for $t > 100sec$. We see fluctuations for the N_{Hint} during the steep decay phase, but a constant N_{Hint} is a satisfactory explanation for $t > 100sec$. We found a hint for a positive linear correlation between the Γ and the N_{Hint} which is mainly due to the early phase behavior and consistent with our prediction.

For GRB 060729 we found that during the early phase ($t < 50000sec$) Γ increases which is consistent with [99] (although they used N_{Hint} as a fixed parameter). We found that the N_{Hint} increases during the early phase. We found a hint for a positive linear correlation between the Γ and the N_{Hint} which agrees with [255]. This correlation is mainly due to the early phase and consistent with our prediction.

The analysis of GRB 060814 showed that during the early phase ($t < 20000sec$) Γ gets softer which is consistent with [99] (although they used N_{Hint} as a fixed parameter). We found that the N_{Hint} shows variations during the early phase.

For GRB 060202 we found that the early phase ($t < 1000sec$) shows a soft to hard spectral evolution which is consistent with [99] (although they used N_{Hint} as a fixed parameter). We found that the N_{Hint} is decreasing during the early phase. We found a hint for a positive linear correlation between the Γ and the N_{Hint} which is due to the early phase. This correlation is consistent with our prediction if the N_{Hint} is affected by the Γ. However, we should interrogate the behavior of the N_{Hint} during the early phase.

In the case of GRB 060124 we found Γ and N_{Hint} variations during the early phase ($t < 1000sec$) that agrees with [171] and [5].

For GRB 080310 we found Γ and N_{Hint} variations during the early phase ($t < 500sec$) which is dominated by important flaring activity. We found a hint for a positive non-linear correlation between the Γ and the N_{Hint} which is due to the early phase and consistent with our prediction.

The analysis of GRB 061007 showed Γ and N_{Hint} fluctuations at the early phase ($t < 1000sec$). We found a hint for a positive linear correlation between the Γ and the N_{Hint} that originates from the early phase which is consistent with our prediction.

For GRB 080319B we found that the early phase shows a hard to soft spectral evolution and N_{Hint} fluctuations. We found a very significant positive linear correlation

between the Γ and the N_{Hint} that mainly from the early phase ($t < 1000sec$) data points and consistent with our prediction.

In the case of GRB 060218 we found that the early phase ($t < 2500sec$) shows a hard to soft spectral evolution which is consistent with [99] (although they used N_{Hint} as a fixed parameter). We see fluctuations for the N_{Hint} for $t < 2500sec$. We found a very significant positive linear correlation between the Γ and the N_{Hint} that rises from the early phase attitude and consistent with our prediction.

To sum up, we found that the spectral evolution and the N_{Hint} variations are seen during the early phase and that the correlations we found mainly originates from the early phase. As discussed in the literature, the spectral evolution seen during the early phase has both observational and theoretical reasons [5, 99, 107]: while it is generally a hard to soft evolution, the soft to hard evolution is also detected. In this work we showed that a positive linear correlation naturally arises between the Γ the N_{Hint}, when a absorbed simple power law is used to fit XRT data. We stress that a negative correlation is found for GRB 061121 and GRB 060904B. For these two cases a spurious origin is ruled out. A physical interpretation is required. A possibility is that the photoelectrically absorbed simple power law does not represent the intrinsic model of emission as Band [2] model has proven to give a better description of the XRT data when flaring activity is present [103]. This is beyond the scope of the present work and is left as material of investigation of a forthcoming work. We also note that we should interrogate the N_{Hint} behavior during the early phase since the decreasing Γ can also be affected by the possible (physical) N_{Hint} change during this phase.

6. CONCLUSION

X-ray afterglows spectra of the GRBs are one of the most important sources of information about the GRB environment. Intrinsic Hydrogen column density can be inferred from the X-ray spectra when the redshift of the GRB is known. While the obtained value of the intrinsic Hydrogen column density is model dependent, an accurate intrinsic Hydrogen column density value is fundamental to constrain the GRB environment. When fitting the X-ray afterglow spectra, one of the most widely used model is the absorbed power-law model . In this work we have investigated the relations between the X-ray spectral parameters of the GRB X-ray afterglows by assuming only absorbed power-law model. First we search for the evolution of these parameters with time and then we looked for a correlation between them. As a result of this work we can conclude that the determination of the N_{Hint} within the 0.3 - 10 keV energy range must be done with care and we stress that it is model dependent. Nonphysical behaviors may arise from the fitting procedure.

By the correlation analysis we show that the intrinsic Hydrogen column density variations are due to a spurious effect coming from the spectral fitting procedure of the absorbed power-law model. When the spectra become softer, the fit tend to prefer higher values of the N_{Hint}, to account for the observed emission. Additionally, we remark that the anti-correlations may be related to the physics during the early afterglow phase.

This work is the first detailed correlation search between the Γ and the N_{Hint} of the GRB X-ray afterglow spectra. The next step of this work can be to constraint the N_{Hint} with a multi spectra fitting.

REFERENCES

1. Fishman, G. and C. Meegan, "Gamma-Ray Bursts", *Annual Review of Astronomy and Astrophysics*, Vol. 33, pp. 415–458, January 1985.

2. Band, D., J. Matteson, L. Ford, B. Schaefer, D. Palmer, B. Teegarden, T. Cline, M. Briggs, W. Paciesas, G. Pendleton, G. Fishman, C. Kouveliotou, C. Meegan, R. Wilson, P. Lestrade, "BATSE observations of gamma-ray burst spectra. I - Spectral diversity", *Astrophysical Journal*, Vol. 413, No. 1, pp. 281–292, August 1993.

3. Lazzati, D., R. Perna, "Determining the location of gamma-ray bursts through the evolution of their soft X-ray absorption", *Monthly Notices of the Royal Astronomical Society*, Vol. 330, pp. 383–389, February 2002.

4. Campana, S., D. Lazzati, E. Ripamonti, R. Perna, S. Covino, G. Tagliaferri, A. Moretti, P. Romano, G. Cusumano, G. Chincarini, "A Metal-rich Molecular Cloud Surrounds GRB 050904 at Redshift 6.3 ", *The Astrophysical Journal*, Vol. 654, pp. L17–L20, January 2007.

5. Butler, N. R. and D. Kocevski, "X-Ray Hardness Evolution in GRB Afterglows and Flares: Late-Time GRB Activity without N_H Variations", *The Astrophysical Journal*, Vol. 663, pp. 407–419, July 2007.

6. Klebesadel, R. W., I. B. Strong, R. A. Olson, "Observations of Gamma-Ray Bursts of Cosmic Origin", *Astrophysical Journal*, Vol. 182, p. L85, June 1973.

7. Nemiroff R.J., "A Century of Gamma-Ray Burst Models", *American Institute of Physics (AIP) Conference Proceedings of the Second Workshop on Gamma-Ray Bursts*, Huntsville, Alabama, October 1993, Vol. 307, p. 730, New York, January 1994.

8. Meegan, C. A., G. J. Fishman, R. B. Wilson, J. M. Horack, M. N. Brock, W. S. Paciesas, G. N. Pendleton, C. Kouveliotou, "Spatial distribution of gamma-ray bursts observed by BATSE", *Nature*, Vol. 355, pp. 143–145, January 1992.

9. Fenimore, E. E., R. I. Epstein, C. Ho, R. W. Klebesadel, C. Lacey, J. G. Laros, M. Meier, T. Strohmayer, G. Pendleton, G. Fishman, C. Kouveliotou, C. Meegan, "The

Intrinsic Luminosity of Gamma-Ray Bursts and Their Host Galaxies", *Nature*, Vol. 366, p. 40, November 1993.

10. Paczyński, B., "How Far Away Are Gamma-Ray Bursters?", *Publications of the Astronomical Society of the Pacific*, Vol. 107, p. 1167, December 1995.

11. Piran, T., "The implications of the Compton (GRO) observations for cosmological gamma-ray bursts", *Astrophysical Journal*, Vol. 389, pp. L45–L48, April 1992.

12. Koshut, T. M., W. S. Paciesas, C. Kouveliotou, J. van Paradijs, G. N. Pendleton, G. J. Fishman, C. A. Meegan, "T_{90} as a Measurment of the Duration of GRBs", *American Astronomical Society*, Vol. 27, p. 886, May 1995.

13. Kouveliotou, C., C. A. Meegan, G. J. Fishman, N. P. Bhat, M. S. Briggs, T. M. Koshut, W. S. Paciesas, G. N.Pendleton, "Identification of two classes of gamma-ray bursts", *Astrophysical Journal*, Vol. 413, pp. L101–L104, August 1993.

14. Piro, L., "SAX observers' handbook", *Rome: Agenzia Spaziale Italiana*, Issue 1.0, July 1995.

15. Costa, E., F. Frontera, J. Heise, M. Feroci, J. Zand, F. Fiore, M. N. Cinti, D. Dal Fiume, L. Nicastro, M. Orlandini, E. Palazzi, et al., "Discovery of an X-ray afterglow associated with the $\gamma - ray$ burst of 28 February 1997", *Nature*, Vol. 387, pp. 783–785, June 1997.

16. van Paradijs, J., P. J. Groot, T. Galama, C. Kouveliotou, R. G. Strom, J. Telting, R. G. M. Rutten, G. J. Fishman, C. A. Meegan, M. Pettini, N. Tanvir, J. Bloom, et al., "Transient optical emission from the error box of the $\gamma - ray$ burst of 28 February 1997", *Nature*, Vol. 386, pp. 686–689, April 1997.

17. Frail D.A., S. R. Kulkarni, S. R. Nicastro, M. Feroci, G. B. Taylor, "The radio afterglow from the $\gamma - ray$ burst of 8 May 1997", *Nature*, Vol. 389, pp. 261–263, September 1997.

18. Rees, M. J., P. Mészáros, "Unsteady outflow models for cosmological gamma-ray bursts", *The Astrophysical Journal*, Vol. 430, pp. L93–L96, August 1994.

19. Piran, T. and R. Sari, "The Internal-External Grb-Afterglow Model", *American Institute of Physics (AIP) Conference Proceedings of the Fourth Huntsville Symposium on Gamma-Ray Bursts*, Huntsville, September 1997, Vol. 428, p. 662, New York, January 1998.

20. Sari, R., T. Piran, R. Narayan, "Spectra and Light Curves of Gamma-Ray Burst Afterglows", *Astrophysical Journal Letters*, Vol. 497, p. L17, April 1998.

21. Wijers, R. A. M. J. and T. J. Galama, "Physical Parameters of GRB 970508 and GRB 971214 from Their Afterglow Synchrotron Emission", *The Astrophysical Journal*, Vol. 523, pp. 177–186, September 1999.

22. Mészáros, P. and M. J.Rees, "Optical and Long-Wavelength Afterglow from Gamma-Ray Bursts", *Astrophysical Journal*, Vol. 476, p. 232, Feburary 1997.

23. Piro, L., G. Garmire, M. R. Garcia, L. A. Antonelli, E. Costa, M. Feroci, D. A. Frail, F. Harrison, K. Hurley, P. Mészáros, E. Waxman, "The X-Ray Afterglow of GRB 000926 Observed by BeppoSAX and Chandra: A Mildly Collimated Fireball in a Dense Medium?", *The Astrophysical Journal*, Vol. 558, pp. 442–447, September 2001.

24. Metzger, M. R., S. G. Djorgovski, S. R. Kulkarni, C. C. Steidel, K. L. Adelberger, D. A. Frail, D. A., E. Costa, F. Frontera, "Spectral constraints on the redshift of the optical counterpart to the $\gamma - ray$ burst of 8 May 1997", *Nature*, Vol. 387, pp. 878–880, June 1997.

25. Djorgovski, S. G., S. R. Kulkarni, J. S. Bloom, R. Goodrich, D. A. Frail, L. Piro, E. Palazzi, "Spectroscopy of the Host Galaxy of the Gamma-Ray Burst 980703", *The Astrophysical Journal*, Vol. 508, pp. L17–L20, November 1998.

26. Galama, T. J., P. M. Vreeswijk, J. van Paradijs, C. Kouveliotou, T. Augusteijn, H. Böhnhardt, J. P. Brewer, V. Doublier, J. -F. Gonzalez, B. Leibundgut, et al., "An unusual supernova in the error box of the $\gamma - ray$ burst of 25 April 1998", *Nature*, Vol. 395, pp. 670–672, October 1998.

27. Kulkarni, S. R., D. A. Frail, M. H. Wieringa, R. D. Ekers, E. M. Sadler, R. M. Wark, J. L. Higdon, E. S. Phinney, J. S. Bloom, "Radio emission from the unusual

supernova 1998bw and its association with the $\gamma - ray$ burst of 25 April 1998", *Nature*, Vol. 395, pp. 663–669, October 1998.

28. Bloom, J. S., S. R. Kulkarni, S. G. Djorgovski, A. C. Eichelberger, P. Côté, J. P. Blakeslee, S. C. Odewahn, F. A. Harrison, D. A. Frail, A. V. Filippenko, "The unusual afterglow of the $\gamma - ray$ burst of 26 March 1998 as evidence for a supernova connection", *Nature*, Vol. 401, pp. 453–456, September 1999.

29. Bloom, J. S., S. R. Kulkarni, P. A. Price, D. Reichart, T. J. Galama, B. P. Schmidt, D. A. Frail, E. Berger, P. J. McCarthy, R. A. Chevalier, "Detection of a Supernova Signature Associated with GRB 011121 ", *The Astrophysical Journal*, Vol. 572, pp. L45–L49, June 2002.

30. Cobb, B. E., C. D. Bailyn, P. G. van Dokkum, M. M. Buxton, J. S. Bloom, "The Supernova Associated with GRB 031203: SMARTS Optical-Infrared Light Curves from 0.2 to 92 Days", *The Astrophysical Journal*, Vol. 608, pp. L93–L96, June 2004.

31. Vietri, M. and L. Stella, "A Gamma-Ray Burst Model with Small Baryon Contamination", *The Astrophysical Journal*, Vol. 507, pp. L45–L48, November 1998.

32. Hjorth, J., J. Sollerman, P. Møller, J. P. U. Fynbo, S. E. Woosley, C. Kouveliotou, N. R. Tanvir, J. Greiner, M. I. Andersen, A. J. Castro-Tirado, et al., "A very energetic supernova associated with the $\gamma - ray$ burst of 29 March 2003", *Nature*, Vol. 423, pp. 847–850, June 2003.

33. Woosley S. E., "Gamma-Ray Bursts from Stellar Collapse to a Black Hole?", *American Astronomical Society*, Vol. 25, p. 894, May 1993.

34. MacFadyen, A. I. and S. E. Woosley, "Collapsars: Gamma-Ray Bursts and Explosions in ″Failed Supernovae‶", *The Astrophysical Journal*, Vol. 524, pp. 262–289, October 1999.

35. Sari, R., T. Piran, J. P. Halpern, "Jets in Gamma-Ray Bursts", *The Astrophysical Journal*, Vol. 519, pp. L17–L20, July 1999.

36. Rhoads, J. E., "How to Tell a Jet from a Balloon: A Proposed Test for Beaming

in Gamma-Ray Bursts", *Astrophysical Journal Letters*, Vol. 487, p. L1, September 1997.

37. Rhoads, J. E., "The Dynamics and Light Curves of Beamed Gamma-Ray Burst Afterglows", *The Astrophysical Journal*, Vol. 525, pp. 737–749, November 1999.

38. Mészáros, P. and M. J. Rees, "GRB 990123: reverse and internal shock flashes and late afterglow behaviour", *Monthly Notices of the Royal Astronomical Society*, Vol. 306, pp. L39–L43, July 1999.

39. Harrison, F. A., J. S. Bloom, D. A. Frail, R. Sari, S. R. Kulkarni, S. G. Djorgovski, T. Axelrod, J. Mould, B. P. Schmidt, M. H. Wieringa, et al., "Optical and Radio Observations of the Afterglow from GRB 990510: Evidence for a Jet", *The Astrophysical Journal*, Vol. 523, pp. L121–L124, October 1999.

40. Woosley, S., *Invited Talk*, http://www.batse.msfc.nasa.gov∼santorini/Santorini2005 /Talks/woosley/santorini05.ppt, 2005.

41. Zhang, B. and P. Mészáros, "Gamma-Ray Burst Beaming: A Universal Configuration with a Standard Energy Reservoir?", *The Astrophysical Journal*, Vol. 571, pp. 876–879, June 2002.

42. Rossi, E., D. Lazzati, M. J. Rees, "Afterglow light curves, viewing angle and the jet structure of $\gamma - ray$ bursts", *Monthly Notices of the Royal Astronomical Society*, Vol. 332, pp. 945–950, June 2002.

43. Gehrels, N., G. Chincarini, P. Giommi, K. O. Mason, J. A. Nousek, A. A. Wells, N. E. White, S. D. Barthelmy, D. N. Burrows, L. R. Cominsky, et al., "The Swift Gamma-Ray Burst Mission", *The Astrophysical Journal*, Vol. 611, pp. 1005–1020, August 2004.

44. Barthelmy, S. D., G. Chincarini, D. N. Burrows, N. Gehrels, S. Covino, A. Moretti, P. Romano, P. T. O'Brien, C. L. Sarazin, C. Kouveliotou, et al., "An origin for short $\gamma - ray$ bursts unassociated with current star formation", *Nature*, Vol. 438, pp. 994–996, December 2005.

45. Fox, D. B., D. A. Frail, P. A. Price, S. R. Kulkarni, E. Berger, T. Piran, A. M. Soderberg, S. B. Cenko, P. B. Cameron, A. Gal-Yam, et al., "The afterglow of GRB 050709 and the nature of the short-hard $\gamma - ray$ bursts", *Nature*, Vol. 437, pp. 845–850, September 2005.

46. Hjorth, J., D. Watson, J. P. U. Fynbo, P. A. Price, B. L. Jensen, U. G. Jørgensen, D. Kubas, J. Gorosabel, P. Jakobsson, J. Sollerman, et al., "The optical afterglow of the short $\gamma - ray$ burst GRB 050709", *Nature*, Vol. 437, pp. 859–861, September 2005.

47. Gehrels, N., C. L. Sarazin, P. T. O'Brien, B. Zhang, L. Barbier, S. D. Barthelmy, A. Blustin, D. N. Burrows, J. Cannizzo, J. R. Cummings, et al., "A short $\gamma - ray$ burst apparently associated with an elliptical galaxy at redshift $z = 0.225$", *Nature*, Vol. 437, pp. 851–854, October 2005.

48. Berger, E., P. A. Price, S. B. Cenko, A. Gal-Yam, A. M. Soderberg, M. Kasliwal, D. C. Leonard, P. B. Cameron, D. A. Frail, S. R. Kulkarni, et al., "The afterglow and elliptical host galaxy of the short $\gamma - ray$ burst GRB 050724", *Nature*, Vol. 438, pp. 988–990, December 2005.

49. Fox, D. B. and P. Mészáros, "GRB fireball physics: prompt and early emission ", *New Journal of Physics*, Vol. 8, p. 199, September 2006.

50. Bloom, J. S., J. X. Prochaska, D. Pooley, C. H. Blake, R. J. Foley, S. Jha, E. Ramirez-Ruiz, J. Granot, A. V. Filippenko, S. Sigurdsson, et al., "Closing in on a Short-Hard Burst Progenitor: Constraints from Early-Time Optical Imaging and Spectroscopy of a Possible Host Galaxy of GRB 050509b", *The Astrophysical Journal*, Vol. 638, pp. 354–368, Feburary 2006.

51. Lee, W. H. and E. Ramirez-Ruiz, "The progenitors of short gamma-ray bursts ", *New Journal of Physics*, Vol. 9, p. 17, January 2007.

52. Paczyński, B, B., "Gamma-ray bursters at cosmological distances", *Astrophysical Journal*, Vol. 308, pp. L43–L46, September 1986.

53. Paczynski, B., "Cosmological gamma-ray bursts", *Acta Astronomica*, Vol. 41, No. 4, 1991, pp. 257–267, 1991.

54. Eichler, D., M. Livio, T. Piran, D. N. Schramm, "Nucleosynthesis, neutrino bursts and gamma-rays from coalescing neutron stars", *Nature*, Vol. 340, pp. 126–128, July 1989.

55. Narayan, R., B. Paczynski, T. Piran, "Gamma-ray bursts as the death throes of massive binary stars", *Astrophysical Journal*, Vol. 395, pp. L83–L86, August 1992.

56. Chincarini, G., A. Moretti, P. Romano, S. Covino, G. Tagliaferri, S. Campana, M. Goad, S. Kobayashi, B. Zhang, L. Angelini, et al., "Prompt and afterglow early X-ray phases in the comoving frame. Evidence for Universal properties?", *eprint arXiv:astro-ph/0506453*, June 2005.

57. Nousek, J. A., C. Kouveliotou, D. Grupe, K. L. Page, J. Granot, E. Ramirez-Ruiz, S. K. Patel, D. N. Burrows, V. Mangano, S. Barthelmy, et al., "Evidence for a Canonical Gamma-Ray Burst Afterglow Light Curve in the Swift XRT Data", *The Astrophysical Journal*, Vol. 642, pp. 389–400, May 2006.

58. O'Brien, P. T., R. Willingale, J. Osborne, M. R. Goad, K. L. Page, S. Vaughan, E. Rol, A. Beardmore, O. Godet, C. P. Hurkett, et al., "The Early X-Ray Emission from GRBs", *The Astrophysical Journal*, Vol. 647, pp. 1213–1237, August 2006.

59. Zhang, B., Y. Z. Fan, J. Dyks, K. Kobayashi, P. Mészáros, D. N. Burrows, J. A. Nousek, N. Gehrels, "Physical Processes Shaping Gamma-Ray Burst X-Ray Afterglow Light Curves: Theoretical Implications from the Swift X-Ray Telescope Observations", *The Astrophysical Journal*, Volume 642, pp. 354–370, May 2006.

60. O'Brien, Paul T. and R. Willingale, "Using Swift observations of prompt and afterglow emission to classify GRBs", *Philosophical Transactions of the Royal Society A: Mathematical, Physical and Engineering Sciences*, Vol. 365, pp. 1179–1188, May 2007.

61. Gehrels, N., J. P. Norris, S. D. Barthelmy, J. Granot, Y. Kaneko, C. Kouveliotou, C. B. Markwardt, P. Mészáros, E. Nakar, J. A. Nousek, et al., "A new $\gamma - ray$ burst classification scheme from GRB060614 ", *Nature*, Vol. 444, pp. 1044–1046, December 2006.

62. Gehrels, N., J. K. Cannizzo, J. P. Norris, "Gamma-ray bursts in the Swift era", *New Journal of Physics*, Vol. 9, p. 37, Feburary 2007.

63. Gal-Yam, A., D. B. Fox, P. A. Price, E. O. Ofek, M. R. Davis, D. C. Leonard, A. M. Soderberg, B. P. Schmidt, K. M. Lewis, B. A. Peterson, et al., "A novel explosive process is required for the $\gamma - ray$ burst GRB 060614", *Nature*, Vol. 444, pp. 1053–1055, December 2006.

64. Fynbo, Johan P. U., D. Watson, C. Thöne, J. Sollerman, J. S. Bloom, T. M. Davis, J. Hjorth, P. Jakobsson, U. G. Jørgensen, J. F. Graham, et al., "No supernovae associated with two long-duration $\gamma - ray$ bursts", *Nature*, Vol. 444, pp. 1047–1049, December 2006.

65. Della Valle, M., G. Chincarini, N. Panagia, G. Tagliaferri, D. Malesani, V. Testa, D. Fugazza, S. Campana, S. Covino, V. Mangano, et al., "An enigmatic long-lasting $\gamma - ray$ burst not accompanied by a bright supernova", *Nature*, Vol. 444, pp. 1050–1052, December 2006.

66. Mangano, V., S. T. Holland, D. Malesani, E. Troja, G. Chincarini, B. Zhang, V. La Parola, P. J. Brown, D. N. Burrows, S. Campana, et al., "Swift observations of GRB 060614: an anomalous burst with a well behaved afterglow", *Astronomy and Astrophysics*, Vol. 470, pp. 105–118, July 2007.

67. Mangano, V., S. T. Holland, D. Malesani, E. Troja, G. Chincarini, B. Zhang, V. La Parola, D. N. Burrows, M. Della Valle, N. Gehrels, "The Swift view of GRB 060614", *American Institute of Physics (AIP) Conference Proceedings of the Santa Fe Conference on Gamma-Ray Bursts*, Saanta Fe, New Mexico, 2007, Vol. 1000, pp. 323–326, May 2008.

68. Ofek, E. O., S. B. Cenko, A. Gal-Yam, D. B. Fox, D. B., E. Nakar, A. Rau, D. A. Frail, S. R. Kulkarni, P. A. Price, B. P. Schmidt, et al., "GRB 060505: A Possible Short-Duration Gamma-Ray Burst in a Star-forming Region at a Redshift of 0.09", *The Astrophysical Journal*, Vol. 662, pp. 1129–1135, July 2007.

69. Thöne, C. C., J. P. U. Fynbo, G. Östlin, B. Milvang-Jensen, K. Wiersema, D. Malesani, D. Della Monica Ferreira, J. Gorosabel, D. A. Kann, D. Watson, et al.,

"Spatially Resolved Properties of the GRB 060505 Host: Implications for the Nature of the Progenitor", *The Astrophysical Journal*, Vol. 676, pp. 1151–1161, April 2008.

70. McBreen, S., S. Foley, D. Watson, L. Hanlon, D. Malesani, J. P. U. Fynbo, D. A. Kann, N. Gehrels, S. McGlynn, D. Palmer, et al., "The Spectral Lag of GRB 060505: A Likely Member of the Long-Duration Class ", *The Astrophysical Journal*, Vol. 677, pp. L85–L88, April 2008.

71. Greiner, J., T. Krühler, J. P. U. Fynbo, A. Rossi, R. Schwarz, S. Klose, S. Savaglio, N. R. Tanvir, S. McBreen, T. Totani, et al., "GRB 080913 at Redshift 6.7", *The Astrophysical Journal*, Vol. 693, pp. 1610–1620, March 2009.

72. Perez-Ramirez, D., A. de Ugarte Postigo, J. Gorosabel, M. A. Aloy, M. A. Guerrero, J. P. Osborne, K. L. Page, R. S. Warwick, I. Horvath, P. Veres, et al., "Detection of the ultra-high z short GRB 080913 and its implications on progenitors and energy extraction mechanisms", *eprint arXiv:0810.2107*, September 2008.

73. Zhang, B., B.-B Zhang, F. J. Virgili, E. Liang, D. A. Kann, X. Wu, D. Proga, H. Lv, K. Toma, P. Mészáros, et al., "Physical classification scheme of cosmological Gamma-ray bursts and their observational characteristics: on the nature of z=6.7 GRB 080913 and some short/hard GRBs", *eprint arXiv:0902.2419*, Feburary 2009.

74. Donaghy, T. Q., D. Q. Lamb, T. Sakamoto, J. P. Norris, Y. Nakagawa, J. Villasenor, J.-L. Atteia, R. Vanderspek, C. Graziani, N. Kawai, et al., "HETE-2 Localizations and Observations of Four Short Gamma-Ray Bursts: GRBs 010326B, 040802, 051211 and 060121", *eprint arXiv:astro-ph/0605570*, May 2006.

75. Zhang, B, B.-B Zhang, E.-W Liang, N. Gehrels, D. N. Burrows, P. Mészáros, "Making a Short Gamma-Ray Burst from a Long One: Implications for the Nature of GRB 060614", *The Astrophysical Journal*, Vol. 655, pp. L25–L28, January 2007.

76. Bloom, J. S., N. R. Butler, D. A. Perley, "Gamma-ray Bursts, Classified Physically", *American Institute of Physics (AIP) Conference Proceedings of the Santa Fe Conference on Gamma-Ray Bursts*, Saanta Fe, New Mexico, 2007, Vol. 1000, pp. 11–15, New York, May 2008.

77. Atwood, W. B., A. A. Abdo, M. Ackermann, W. Althouse, B. Anderson, M. Axelsson, L. Baldini, J. Ballet, D. L. Band, G. Barbiellini, et al., "The Large Area Telescope on the Fermi Gamma-Ray Space Telescope Mission", *The Astrophysical Journal*, Vol. 697, pp. 1071–1102, June 2009.

78. Barthelmy, S. D., L. M. Barbier, J. R. Cummings, E. E. Fenimore, N. Gehrels, D. Hullinger, H. A. Krimm, C. B. Markwardt, D. M. Palmer, A. Parsons, et al., "The Burst Alert Telescope (BAT) on the SWIFT Midex Mission", *Space Science Reviews*, Vol. 120, pp. 143–164, Septemer 2005.

79. Burlon, D., G. Ghirlanda, G. Ghisellini, D. Lazzati, L. Nava, M. Nardini, A. Celotti, "Precursors in Swift Gamma Ray Bursts with Redshift", *The Astrophysical Journal*, Vol. 685, pp. L19–L22, September 2008.

80. Cenko, S. B., M. Kasliwal, F. A. Harrison, V. Pal'shin, D. A. Frail, P. B. Cameron, E. Berger, D. B. Fox, A. Gal-Yam, S. R. Kulkarni, et al., "Multiwavelength Observations of GRB 050820A: An Exceptionally Energetic Event Followed from Start to Finish", *The Astrophysical Journal*, Vol. 652, pp. 490–506, November 2006.

81. Romano, P., S. Campana, G. Chincarini, J. Cummings, G. Cusumano, S. T. Holland, V. Mangano, T. Mineo, K. L. Page, V. Pal'Shin, et al., "Panchromatic study of GRB 060124: from precursor to afterglow", *Astronomy and Astrophysics*, Vol. 456, pp. 917–927, September 2006.

82. Page, K. L., R. Willingale, J. P. Osborne, B. Zhang, O. Godet, F. E. Marshall, A. Melandri, J. P. Norris, P. T. O'Brien, V. Pal'shin, et al., "GRB 061121: Broadband Spectral Evolution through the Prompt and Afterglow Phases of a Bright Burst", *The Astrophysical Journal*, Vol. 663, pp. 1125–1138, July 2007.

83. Li, L.-X., "Gamma-ray burst precursors as the remnant of the thermal radiation initially trapped in the fireball", *Monthly Notices of the Royal Astronomical Society*, Vol. 380, pp. 621–636., September 2007.

84. Lyutikov, M. and R. Blandford, "Gamma Ray Bursts as Electromagnetic Outflows", *eprint arXiv:astro-ph/0312347*, December 2003.

85. Mészáros, P. and M. J. Rees, "Steep Slopes and Preferred Breaks in Gamma-Ray Burst Spectra: The Role of Photospheres and Comptonization", *The Astrophysical Journal*, Vol. 530, pp. 292–298, Feburary 2000.

86. Daigne, F. and R. Mochkovitch, "The expected thermal precursors of gamma-ray bursts in the internal shock model", *Monthly Notice of the Royal Astronomical Society*, Vol. 336, pp. 1271–1280, November 2002.

87. Ramirez-Ruiz, E., A. I. MacFadyen, D. Lazzati, "Precursors and $e^{+/-}$ pair loading from erupting fireballs", *Monthly Notices of the Royal Astronomical Society*, Vol. 331, pp. 197–202, March 2002.

88. Lazzati, D. and M. C. Begelman, "Universal GRB Jets from Jet-Cocoon Interaction in Massive Stars", *The Astrophysical Journal*, Vol. 629, pp. 903–907, August 2005.

89. Wang, X.-Y. and P. Mészáros, "GRB Precursors in the Fallback Collapsar Scenario", *The Astrophysical Journal*, Vol. 670, pp. 1247–1253, December 2007.

90. GRB 061121 lightcurve, http://swift.gsfc.nasa.gov/docs/swift/results/releases/images/GRB061121/

91. Briggs, M. S., D. L. Band, R. M. Kippen, R. D. Preece, C. Kouveliotou, J. van Paradijs, G. H. Share, R. J. Murphy, S. M. Matz, A. Connors, et. al, "Observations of GRB 990123 by the Compton Gamma Ray Observatory", *The Astrophysical Journal*, Vol. 524, pp. 82–91, October 1999.

92. Sakamoto, T., S. D. Barthelmy, L. Barbier, J. R. Cummings, E. E. Fenimore, N. Gehrels, D. Hullinger, H. A. Krimm, C. B. Markwardt, D. M. Palmer, A. M. Parsons, G. Sato, M. Stamatikos, J. Tueller, T. N. Ukwatta, B. Zhang, "The First Swift BAT Gamma-Ray Burst Catalog", *The Astrophysical Journal Supplement Series*, Vol. 175, pp. 179–190, March 2008.

93. Tagliaferri, G., M. Goad, G. Chincarini, A. Moretti, S. Campana, D. N. Burrows, M. Perri, S. D. Barthelmy, N. Gehrels, H. Krimm, et al., "An unexpectedly rapid decline in the X-ray afterglow emission of long $\gamma - ray$ bursts", *Nature*, Vol. 436, pp. 985–988, August 2005.

94. Chincarini, G., A. Moretti, P. Romano, A. D. Falcone, D. Morris, J. Racusin, S. Campana, S. Covino, C. Guidorzi, G. Tagliaferri, et. al., "The First Survey of X-Ray Flares from Gamma-Ray Bursts Observed by Swift: Temporal Properties and Morphology", *The Astrophysical Journal*, Vol. 671, pp. 1903–1920, December 2007.

95. Cusumano, G., V. Mangano, L. Angelini, S. Barthelmy, A. P. Beardmore, D. N. Burrows, S. Campana, J. K. Cannizzo, M. Capalbi, G. Chincarini, et al., "Swift XRT Observations of the Afterglow of GRB 050319 ", *The Astrophysical Journal*, Vol. 639, pp. 316–322, March 2006.

96. Vaughan, S., M. R. Goad, A. P. Beardmore, P. T. O'Brien, J. P. Osborne, K. L. Page, S. D. Barthelmy, D. N. Burrows, S. Campana, J. K. Cannizzo, et al., "Swift Observations of the X-Ray-Bright GRB 050315", *The Astrophysical Journal*, Vol. 638, pp. 920–929, Feburary 2006.

97. Liang, E. W., B. Zhang, P. T. O'Brien, R. Willingale, L. Angelini, D. N. Burrows, S. Campana, G. Chincarini, A. Falcone, N. Gehrels, et al., "Testing the Curvature Effect and Internal Origin of Gamma-Ray Burst Prompt Emissions and X-Ray Flares with Swift Data", *The Astrophysical Journal*, Vol. 646, pp. 351–357, July 2006.

98. Liang, E.-W., B.-B. Zhang, B. Zhang, "A Comprehensive Analysis of Swift XRT Data. II. Diverse Physical Origins of the Shallow Decay Segment", *The Astrophysical Journal*, Vol. 670, pp. 565–583, November 2007.

99. Zhang, B.-B., E.-W. Liang, B. Zhang, "A Comprehensive Analysis of Swift XRT Data. I. Apparent Spectral Evolution of Gamma-Ray Burst X-Ray Tails", *The Astrophysical Journal*, Vol. 666, pp. 1002–1011, September 2007.

100. Willingale,R., P. T O'Brien,J. P. Osborne,O. Godet,K. L. Page,M. R. Goad,D. N. Burrows,B. Zhang,E. Rol,N. Gehrels, G. Chincarini, "Testing the Standard Fireball Model of Gamma-Ray Bursts Using Late X-Ray Afterglows Measured by Swift", *The Astrophysical Journal*, Vol. 662, pp. 1093–1110, June 2007.

101. Burrows, D. N., P. Romano, A. Falcone, S. Kobayashi, B. Zhang, A. Moretti, P.

T. O'Brien, M. R. Goad, S. Campana, K. L. Page, et. al., "Bright X-ray Flares in Gamma-Ray Burst Afterglows ", *Science*, Vol. 309, pp. 1833–1835, September 2005.

102. Falcone, A. D., D. N. Burrows, D. Lazzati, S. Campana, S. Kobayashi, B. Zhang, P. Mészáros, K. L. Page, J. A. Kennea, P. Romano, et. al., "The Giant X-Ray Flare of GRB 050502B: Evidence for Late-Time Internal Engine Activity", *The Astrophysical Journal*, Vol. 641, pp. 1010–1017, April 2006.

103. Falcone, A. D., D. Morris, J. Racusin, G. Chincarini, A. Moretti, P. Romano, D. N. Burrows, C. Pagani, M. Stroh, D. Grupe, et. al., "The First Survey of X-Ray Flares from Gamma-Ray Bursts Observed by Swift: Spectral Properties and Energetics", *The Astrophysical Journal*, Vol. 671, pp. 1921–1938, December 2007.

104. Kocevski, D., N. Butler, J. S. Bloom, "Pulse Width Evolution of Late-Time X-Ray Flares in Gamma-Ray Bursts", *The Astrophysical Journal*, Vol. 667, pp. 1024–1032, October 2007.

105. Burrows, D. N., A. Falcone, G. Chincarini, D. Morris, P. Romano, J. E. Hill, O. Godet, A. Moretti, H. Krimm, J. P. Osborne, et. al., "X-ray flares in early GRB afterglows", *Philosophical Transactions of the Royal Society A: Mathematical, Physical and Engineering Sciences*, Vol. 365, pp. 1213–1226, May 2007.

106. Butler, N. R., "On the Early-Time X-Ray Spectra of Swift Afterglows. I. Evidence for Anomalous Soft X-Ray Emission", *The Astrophysical Journal*, Vol. 656, pp. 1001–1018, Feburary 2007.

107. Qin, Y.-P., "Temporal and spectral characteristics of GRBs deduced from the curvature effect", *The Astrophysical Journal*, Vol. 683, pp. 900–912, August 2008.

108. Zhang, B.-B., B. Zhang, E.-W. Liang, X.-Y. Wang, "Curvature Effect of a Non-Power-Law Spectrum and Spectral Evolution of GRB X-Ray Tails", *The Astrophysical Journal Letters*, Vol. 690, pp. L10–L13, January 2009.

109. Stratta, G.; F. Fiore, L. A. Antonelli, L. Piro, M. De Pasquale, "Absorption in Gamma-Ray Burst Afterglows", *The Astrophysical Journal*, Vol. 608, pp. 846–864, June 2006.

110. de Luca, A., A. Melandri, P. A. Caraveo, D. Götz, S. Mereghetti, A. Tiengo, L. A. Antonelli, S. Campana, G. Chincarini, S. Covino, et. al, "XMM-Newton and VLT observations of the afterglow of GRB 040827 ", *Astronomy and Astrophysics*, Vol. 440, pp. 85–92, September 2005.

111. Mason, K. O., A. J. Blustin, P. Boyd, S. T. Holland, M. J. Page, P. Roming, M. Still, B. Zhang, A. Breeveld, M. de Pasquale, et al., "Prompt Optical Observations of GRB 050319 with the Swift UVOT ", *The Astrophysical Journal*, Vol. 639, pp. 311–315, March 2006.

112. Blustin, A. J., D. Band, S. Barthelmy, P. Boyd, M. Capalbi, S. T. Holland, F. E. Marshall, K. O. Mason, M. Perri, T. Poole, et. al., "Swift Panchromatic Observations of the Bright Gamma-Ray Burst GRB 050525a ", *The Astrophysical Journal*, Vol. 637, pp. 901–913, Feburary 2006.

113. Modjaz, M., K. Z. Stanek, P. M. Garnavich, P. Berlind, S. Blondin, W. Brown, M. Calkins, P. Challis, A. M. Diamond-Stanic, H. Hao, et. al., "Early-Time Photometry and Spectroscopy of the Fast Evolving SN 2006aj Associated with GRB 060218", *The Astrophysical Journal*, Vol. 645, pp. L21–L24, July 2006.

114. Ruderman, M., "Theories of gamma-ray bursts", *New York Academy of Sciences, Annals*, Vol. 262, pp. 164–180, October 1975.

115. Goodman, J., "Are gamma-ray bursts optically thick?", *Astrophysical Journal*, Vol. 308, pp. L47–L50, September 1986.

116. Shemi, A., T. Piran, "The appearance of cosmic fireballs", *Astrophysical Journal*, Vol. 365, pp. L55–L58, December 1990.

117. Paczynski, B., G. Xu, "Neutrino bursts from gamma-ray bursts", *Astrophysical Journal*, Vol. 427, No. 2, pp. 708–713, June 1994.

118. Mészáros, P. and M. J. Rees, "Relativistic fireballs and their impact on *externalmatter–Models* for cosmological gamma-ray bursts", *Astrophysical Journal*, Vol. 405, pp. 278-284, March 1993.

119. Meszaros, P. and M. J. Rees, "Gamma-Ray Bursts: Multiwaveband Spectral Predictions for Blast Wave Models", *Astrophysical Journal Letters*, Vol. 418, p. L59, December 1993.

120. Mészáros, P., M. J. Rees, H. Papathanassiou, "Spectral properties of blast-wave models of gamma-ray burst sources", *Astrophysical Journal*, Vol. 432, pp. 181–193, September 1994.

121. Katz, J. I., "Low-frequency spectra of gamma-ray bursts", *Astrophysical Journal*, Vol. 432, pp. L107–L109, September 1994.

122. Tavani, M., "A Shock Emission Model for Gamma-Ray Bursts. II. Spectral Properties ", *Astrophysical Journal*, Vol. 466, p. 768, August 1996.

123. Cohen, E. and T. Piran, "The Implications of Direct Redshift Measurement of Gamma-Ray Bursts", *Astrophysical Journal Letters*, Vol. 488, p. L7, October 1997.

124. Preece, R. D., M. S. Briggs, R. S. Mallozzi, G. N. Pendleton, W. S. Paciesas, D. L. Band, "The Synchrotron Shock Model Confronts a ″Line of Death‟in the BATSE Gamma-Ray Burst Data", *The Astrophysical Journal*, Vol. 506, pp. L23–L26, October 1998.

125. Lloyd, N. M., V. Petrosian, "Synchrotron Radiation as the Source of Gamma-Ray Burst Spectra ", *The Astrophysical Journal*, Vol. 543, pp. 722–732, November 2000.

126. Medvedev, M. V., "Theory of ″Jitter‟Radiation from Small-Scale Random Magnetic Fields and Prompt Emission from Gamma-Ray Burst Shocks", *The Astrophysical Journal*, Vol. 540, pp. 704–714, September 2000.

127. Rees, M. J. and Mészáros, P., "Dissipative Photosphere Models of Gamma-Ray Bursts and X-Ray Flashes", *The Astrophysical Journal*, Vol. 628, pp. 847–852, August 2005.

128. Ryde, F., "Is Thermal Emission in Gamma-Ray Bursts Ubiquitous?", *The Astrophysical Journal*, Vol. 625, pp. L95–L98, June 2005.

129. Zhang, B. and P. Mészáros, "Gamma-Ray Bursts: progress, problems & prospects", *International Journal of Modern Physics A*, Vol. 19, pp. 2385–2472, 2004.

130. Mészáros, P., "Theories of Gamma-Ray Bursts", *Annual Review of Astronomy and Astrophysics*, Vol. 40, pp. 137–169, 2002.

131. Piran, T., "Gamma-ray bursts and the fireball model", *Physics Reports*, Vol. 314, pp. 575–667, June 1999.

132. Ramirez-Ruiz, E. and E. E. Fenimore, "Pulse Width Evolution in Gamma-Ray Bursts: Evidence for Internal Shocks", *The Astrophysical Journal*, Vol. 539, pp. 712–717, August 2000.

133. Nakar, E., T. Piran, "Gamma-Ray Burst Light Curves-Another Clue on the Inner Engine", *The Astrophysical Journal*, Vol. 572, pp. L139–L142, June 2002.

134. Kobayashi, S., T. Piran, R. Sari, "Can Internal Shocks Produce the Variability in Gamma-Ray Bursts?", *Astrophysical Journal*, Vol. 490, p. 92, November 1997.

135. Daigne, F., R. Mochkovitch, "Gamma-ray bursts from internal shocks in a relativistic wind: temporal and spectral properties", *Monthly Notices of the Royal Astronomical Society*, Vol. 296, pp. 275–286, May 1998.

136. Panaitescu, A., M. Spada, P. Mészáros, "Power Density Spectra of Gamma-Ray Bursts in the Internal Shock Model", *The Astrophysical Journal*, Vol. 522, pp. L105–L108, September 1999.

137. Kumar, P., E. McMahon, "A general scheme for modelling $\gamma - ray$ burst prompt emission", *Monthly Notices of the Royal Astronomical Society*, Vol. 384, pp. 33–63, Feburary 2008.

138. Kumar, P., R. Narayan, "GRB 080319B: evidence for relativistic turbulence, not internal shocks", *Monthly Notices of the Royal Astronomical Society*, Vol. 395, pp. 472–489, May 2009.

139. Usov, V. V., "Millisecond pulsars with extremely strong magnetic fields as a cosmological source of gamma-ray bursts", *Nature*, Vol. 357, No. 6378, pp. 472–474, June 1992.

140. Usov, V. V., "On the Nature of Nonthermal Radiation from Cosmological Gamma-Ray Bursters", *R.A.S. Monthly Notices*, Vol. 267, p. 1035, April 1994.

141. Thompson, C., "A Model of Gamma-Ray Bursts", *R.A.S. Monthly Notices*, Vol. 270, p. 480, October 1994.

142. Narayan, R., P. Kumar, "A turbulent model of gamma-ray burst variability", *Monthly Notices of the Royal Astronomical Society: Letters*, Vol. 394, pp. L117–L120, March 2009.

143. Lazar, A., E. Nakar, T. Piran, "GRB Light Curves in the Relativistic Turbulence Model", *eprint arXiv:0901.1133*, January 2009.

144. Mészáros, P., *Afterglow theories*, http://www.astro.psu.edu/∼nnp/md05.pdf, November 2005.

145. Rhoads, J. E. and B. Paczynski, "Radio Transients from Gamma-Ray Bursters", *Bulletin of the American Astronomical Society*, Vol. 25, p. 1296, December 1993.

146. Vietri, M., "The Soft X-Ray Afterglow of Gamma-Ray Bursts, A Stringent Test for the Fireball Model", *Astrophysical Journal Letters*, Vol. 478, p. L9, March 1997.

147. Pacholczyk, A. G., "Radio astrophysics. Nonthermal processes in galactic and extragalactic sources", *Series of Books in Astronomy and Astrophysics*, San Francisco: Freeman, 1970.

148. Waxman, E., "Gamma-Ray–Burst Afterglow: Supporting the Cosmological Fireball Model, Constraining Parameters, and Making Predictions", *Astrophysical Journal Letters*, Vol. 485, p. L5, August 1997.

149. Wijers, R. A. M. J., J. M. Rees, P. Mészáros, "Shocked by GRB 970228: the afterglow of a cosmological fireball", *Monthly Notices of the Royal Astronomical Society*, Vol. 288, Issue 4, pp. L51–L56, July 1997.

150. Waxman, E., P. Mészáros, S. Campana, "GRB 060218: A Relativistic Supernova Shock Breakout", *The Astrophysical Journal*, Vol. 667, Issue 1, pp. 351–357, September 2007.

151. Katz, J. I. and T. Piran, Persistent Counterparts to Gamma-Ray Bursts, *Astrophysical Journal*, Vol. 490, p. 772, December 1997.

152. Mészáros, P., "Gamma-Ray Bursts and Bursters", *Nuclear Physics B Proceedings Supplements*, Vol. 80, pp. 63–77, March 2000.

153. Longair, M.S., High Energy Astrophysics Volume 2, Cambridge University Press, pp. 229–346, 1994.

154. Masetti, N., C. Bartolini, S. Bernabei, A. Guarnieri, E. Palazzi, E. Pian, A. Piccioni, A. J. Castro-Tirado, J. M. Castro Cerón, L. Verdes-Montenegro, et al., "Unusually rapid variability of the GRB000301C optical afterglow", *Astronomy and Astrophysics*, Vol. 359, pp. L23–L26, July 2000.

155. Lazzati, D., E. Ramirez-Ruiz, M. J. Rees, "Soft X-Ray Emission Lines in the Early Afterglow of Gamma-Ray Bursts", *The Astrophysical Journal*, Vol. 572, Issue 1, pp. L57-L60, June 2002.

156. Matheson, T., P. M. Garnavich, K. Z. Stanek, D. Bersier, S. T. Holland, K. Krisciunas, N. Caldwell, P. Berlind, J. S. Bloom, M. Bolte, et al., "Photometry and Spectroscopy of GRB 030329 and Its Associated Supernova 2003dh: The First Two Months", *The Astrophysical Journal*, Vol. 599, pp. 394–407, December 2003.

157. Wang, X., A. Loeb, "Variability of Gamma-Ray Burst Afterglows due to Interstellar Turbulence", *The Astrophysical Journal*, Vol. 535, pp. 788–797, June 2000.

158. Heyl, Jeremy S. and R. Perna, "Broadband Modeling of GRB 021004", *The Astrophysical Journal*, Vol. 586, pp. L13–L17, March 2003.

159. Rees, M. J., P. Mészáros, P., "Refreshed Shocks and Afterglow Longevity in Gamma-Ray Bursts", *Astrophysical Journal Letters*, Vol. 496, p. L1, March 1998.

160. Loeb, A. and R. Perna, "Are H i Supershells the Remnants of Gamma-Ray Bursts?", *Astrophysical Journal Letters*, Vol. 503, p. L35, August 1998.

161. Garnavich, P. M., A. Loeb, K. Z. Stanek, "Resolving Gamma-Ray Burst 000301C with a Gravitational Microlens", *The Astrophysical Journal*, Vol. 544, pp. L11–L15, November 2000.

162. Panaitescu, A., P. Mészáros, D. Burrows, J. Nousek, N. Gehrels, P. O'Brien, R. Willingale, "Evidence for chromatic X-ray light-curve breaks in Swift gamma-ray burst afterglows and their theoretical implications", *Monthly Notices of the Royal Astronomical Society*, Vol. 369, pp. 2059–2064, July 2006.

163. Willingale, R., P. T. O'Brien, S. W. H. Cowley, G. H. Jones, D. J. McComas, K. O. Mason, J. P. Osborne, A. Wells, M. Chester, S. Hunsberger, et al., "Swift X-Ray Telescope Observations of the Deep Impact Collision", *The Astrophysical Journal*, Vol. 649, pp. 541–552, September 2006.

164. Sari, R. and T. Piran, "Variability in Gamma-Ray Bursts: A Clue", *Astrophysical Journal*, Vol. 485, p. 270, August 1997.

165. Fenimore, E. E., C. D. Madras, S. Nayakshin, "Expanding Relativistic Shells and Gamma-Ray Burst Temporal Structure", *Astrophysical Journal*, Vol. 473, p. 998, December 1996.

166. Kumar, P., A. Panaitescu, "Afterglow Emission from Naked Gamma-Ray Bursts", *The Astrophysical Journal*, Vol. 541, pp. L51–L54, October 2000.

167. Dermer, C. D., "Curvature Effects in Gamma-Ray Burst Colliding Shells", *The Astrophysical Journal*, Vol. 614, pp. 284–292, October 2004.

168. Dyks, J., B. Zhang, Y. Z. Fan, "Curvature effect in structured GRB jets", *eprint arXiv:astro-ph/0511699*, November 2005.

169. Wu, X. F., Z G. Dai, X. Y. Wang, Y. F. Huang, L. L. Feng, T. Lu, "X-ray flares from late internal and late external shocks", *Meeting Abstract of the 36th COSPAR Scientific Assembly*, Beijing, China, No. 731, July 2006.

170. Yamazaki, R., K. Toma, K. Ioka, T. Nakamura, "Tail emission of prompt gamma-ray burst jets", *Monthly Notices of the Royal Astronomical Society*, Vol. 369, pp. 311–316, June 2006.

171. Zhang, B.-B, *Spectral Evolution of GRB X-ray Tails due to the Curvature Effect of a Non-power-law Spectrum*, http://www.grbhuntsville2008.cspar.uah.edu/content /Talks/BbZhang.pdf, 2008.

172. Lazzati, D. and R. Perna, "X-ray flares and the duration of engine activity in gamma-ray bursts", *Monthly Notices of the Royal Astronomical Society: Letters*, Vol. 375, pp. L46–L50, Feburary 2007.

173. Fan, Y. Z. and D. M. Wei, "Late internal-shock model for bright X-ray flares in gamma-ray burst afterglows and GRB 011121", *Monthly Notices of the Royal Astronomical Society Letters*, Vol. 364, pp. L42–L46, November 2005.

174. Lazzati, D., R. Perna, M. C. Begelman, "X-ray flares, neutrino-cooled discs and the dynamics of late accretion in gamma-ray burst engines", *Monthly Notices of the Royal Astronomical Society Letters*, Vol. 388, pp. L15–L19, July 2008.

175. Panaitescu, A., "Jet breaks in the X-ray light-curves of Swift gamma-ray burst afterglows", *Monthly Notices of the Royal Astronomical Society*, Vol. 380, pp. 374–380, September 2007.

176. Shao, L., Z. G. Dai, N. Mirabal, "Echo Emission from Dust Scattering and X-Ray Afterglows of Gamma-Ray Bursts", *The Astrophysical Journal*, Vol. 675, Issue 1, pp. 507–518, March 2008.

177. Shao, L., Z. G. Dai, "Behavior of X-Ray Dust Scattering and Implications for X-Ray Afterglows of Gamma-Ray Bursts", *The Astrophysical Journal*, Vol. 660, pp. 1319–1325, May 2007.

178. Prilutski, O. F. and V. V. Usov, "On the Nature of $\gamma - Ray$ Bursts", *Astrophysics and Space Science*, Vol. 34, p. 387, May 1975.

179. Woosley, S. E., "Gamma-ray bursts from stellar mass accretion disks around black holes", *Astrophysical Journal*, Vol. 405, No. 1, pp. 273–277, March 1993.

180. Woosley, S. E., J. S. Bloom, "The Supernova Gamma-Ray Burst Connection", *Annual Review of Astronomy & Astrophysics*, Vol. 44, pp. 507–556, September 2006.

181. Stanek, K. Z., T. Matheson, P. M. Garnavich, P. Martini, P. Berlind, N. Caldwell, P. Challis, W. R. Brown, R. Schild, K. Krisciunas, et al., "Spectroscopic Discovery of the Supernova 2003dh Associated with GRB 030329", *The Astrophysical Journal*, Vol. 591, pp. L17–L20, July 2003.

182. Paczyński, B, B., "Are Gamma-Ray Bursts in Star-Forming Regions?", *Astrophysical Journal Letters*, Vol. 494, p. L45, Feburary 1998.

183. MacFadyen, A. and S. Woosley, "Collapsars - Gamma-Ray Bursts and Explosions in ″Failed Supernovae ″", *Bulletin of the American Astronomical Society*, Vol. 30, p. 1311, December 1998.

184. Zhang, W., S. E. Woosley, A. I. MacFadyen, "Relativistic Jets in Collapsars", *The Astrophysical Journal*, Vol. 586, Issue 1, pp. 356–371, March 2003.

185. Langer, N., "Coupled mass and angular momentum loss of massive main sequence stars", *Astronomy and Astrophysics*, Vol. 329, pp. 551–558, January 1998.

186. Maeder, A., G. Meynet, "Stellar evolution with rotation. VI. The Eddington and Omega -limits, the rotational mass loss for OB and LBV stars", *Astronomy and Astrophysics*, Vol. 361, pp. 159–166, September 2000.

187. Mirabal, N., J. P. Halpern, R. Chornock, A. V. Filippenko, D. M. Terndrup, E. Armstrong, J. Kemp, J. R. Thorstensen, M. Tavarez, C. Espaillat, "GRB 021004: A Possible Shell Nebula around a Wolf-Rayet Star Gamma-Ray Burst Progenitor", *The Astrophysical Journal*, Vol. 595, pp. 935–949, October 2003.

188. Fryer, C. L., S. E. Woosley, D. H. Hartmann, "Formation Rates of Black Hole Accretion Disk Gamma-Ray Bursts", *The Astrophysical Journal*, Vol. 526, pp. 152–177, November 1999.

189. Fryer, C. L., P. A. Mazzali, J. Prochaska, E. Cappellaro, A. Panaitescu, E. Berger, M. van Putten, E. P. J. van den Heuvel, P. Young, A. Hungerford, et al., "Constraints on Type Ib/c and GRB Progenitors", *eprint arXiv:astro-ph/0702338*, Feburary 2007.

190. Yoon, S.-C. and N. Langer, "Stabilization of helium shell burning by rotation in accreting white dwarfs", *Astronomy and Astrophysics*, Vol. 443, pp. 643–648, November 2005.

191. Woosley, S. E. and A. Heger, "The Progenitor Stars of Gamma-Ray Bursts", *The Astrophysical Journal*, Vol. 637, Issue 2, pp. 914–921, Feburary 2006.

192. Fruchter, A. S., A. J. Levan, L. Strolger, P. M. Vreeswijk, S. E. Thorsett, D. Bersier, I. Burud, J. M. Castro Cern, A. J. Castro-Tirado, C. Conselice, et al., "Long $\gamma - ray$ bursts and core-collapse supernovae have different environments", *Nature*, Vol. 441, pp. 463–468, May 2006.

193. Hirschi, R., G. Meynet, A. Maeder, "Stellar evolution with rotation. XII. Pre-supernova models", *Astronomy and Astrophysics*, Vol. 425, pp. 649–670, October 2004.

194. Nakar, E., "Short-hard gamma-ray bursts", *Physics Reports*, Vol. 442, Issue 1-6, pp. 166–236, April 2007.

195. King, A., E. Olsson, M. B. Davies, "A new type of long gamma-ray burst", *Monthly Notices of the Royal Astronomical Society: Letters*, Vol. 374, Issue 1, pp. L34–L36, January 2007.

196. Fryer, C. L. and S. E. Woosley, "Helium Star/Black Hole Mergers: A New Gamma-Ray Burst Model", *Astrophysical Journal Letters*, Vol. 502, p. L9, July 1998.

197. Nakar, E., A. Gal-Yam, D. B. Fox, "The Local Rate and the Progenitor Lifetimes of Short-Hard Gamma-Ray Bursts: Synthesis and Predictions for the Laser Interferometer Gravitational-Wave Observatory", *The Astrophysical Journal*, Vol. 650, pp. 281–290, October 2006.

198. Levan, A. J., M. B. Davies, A. R. King, "Neutron star binaries and long-duration gamma-ray bursts", *Monthly Notices of the Royal Astronomical Society*, Vol. 372, pp. 13511–356, November 2006.

199. Ruffini, R., M. G. Bernardini, C. L. Bianco, P. Chardonnet, F. Fraschetti, R. Guida, S. Xue, "GRB 050315: A Step toward Understanding the Uniqueness of the Overall Gamma-Ray Burst Structure", *The Astrophysical Journal*, Vol. 645, pp. L109–L112, July 2006.

200. Dar, A., "The GRB/XRF-SN Association", *eprint arXiv:astro-ph/0405386*, May 2004.

201. Frail, D. A., S. R. Kulkarni, R. Sari, S. G. Djorgovski, J. S. Bloom, T. J. Galama, D. E. Reichart, E. Berger, F. A. Harrison, P. A. Price, et al., "Beaming in Gamma-Ray Bursts: Evidence for a Standard Energy Reservoir", *The Astrophysical Journal*, Vol. 562, pp. L55–L58, November 2001.

202. Wheeler, J. C., I. Yi, P. Höflich, L. Wang, "Asymmetric Supernovae, Pulsars, Magnetars, and Gamma-Ray Bursts", *The Astrophysical Journal*, Vol. 537, pp. 810–823, July 2000.

203. Drenkhahn, G., "Acceleration of GRB outflows by Poynting flux dissipation", *Astronomy and Astrophysics*, Vol. 387, pp. 714–724, May 2002.

204. Lyutikov, M., E. G. Blackman, "Gamma-ray bursts from unstable Poynting-dominated outflows", *Monthly Notices of the Royal Astronomical Society*, Vol. 321, pp. 177–186, Feburary 2001.

205. Qian, Y.-Z. and S. E. Woosley, "Nucleosynthesis in Neutrino-driven Winds. I. The Physical Conditions", *Astrophysical Journal*, Vol. 471, p. 331, November 1996.

206. Blandford, R., "High Energy Emission from Ultrarelativistic Outflows", *American Physical Society*, Meeting Id: APR02, Abstract No: 2A3.007, April 2002.

207. Popham, R., S. E. Woosley, C. Fryer, "Hyperaccreting Black Holes and Gamma-Ray Bursts", *The Astrophysical Journal*, Vol. 518, pp. 356–374, June 1999.

208. Narayan, R., T. Piran, P. Kumar, "Accretion Models of Gamma-Ray Bursts", *The Astrophysical Journal*, Vol. 557, pp. 949–957, August 2001.

209. Di Matteo, T., R. Perna, R. Narayan, "Neutrino Trapping and Accretion Models for Gamma-Ray Bursts", *The Astrophysical Journal*, Vol. 579, pp. 706–715, Novemver 2002.

210. Blandford, R. D., D. G. Payne, "Hydromagnetic flows from accretion discs and the production of radio jets", *Royal Astronomical Society Monthly Notices*, Vol. 199, pp. 883–903, June 1982.

211. Proga, D., A. I. MacFadyen, P. J. Armitage, M. C. Begelman, "Axisymmetric Magnetohydrodynamic Simulations of the Collapsar Model for Gamma-Ray Bursts", *The Astrophysical Journal*, Vol. 599, pp. L5–L8, December 2003.

212. Blandford, R. D., R. L. Znajek, "Electromagnetic extraction of energy from Kerr black holes", *Royal Astronomical Society Monthly Notices*, Vol. 179, pp. 433–456, May 1977.

213. Lee, H. K., G. E. Brown, R. A. M. J. Wijers, "Issues Regarding the Blandford-Znajek Process as a Gamma-Ray Burst Inner Engine", *The Astrophysical Journal*, Vol. 536, pp. 416–419, June 2000.

214. Mizuno, Y., S. Yamada, S. Koide, K. Shibata, "General Relativistic Magnetohydrodynamic Simulations of Collapsars: Rotating Black Hole Cases", *The Astrophysical Journal*, Vol. 615, pp. 389–401, November 2004.

215. Perna, R., A. Loeb, "Identifying the Environment and Redshift of Gamma-Ray Burst Afterglows from the Time Dependence of Their Absorption Spectra", *Astrophysical Journal*, Vol. 501, p. 467, July 2007.

216. Böttcher, M., C. D. Dermer, E. P. Liang, "Time-dependent photoionization and fluorescence line emission in gamma-ray burst environments", Astronomy and Astrophysics Supplement, Vol. 138, pp. 543–544, September 1999.

217. Lazzati, D., R. Perna, G. Ghisellini, "Time-dependent photoionization opacities in dense gamma-ray burst environments", *Monthly Notices of the Royal Astronomical Society*, Vol. 325, pp. L19–L23, August 2001.

218. Draine, B. T. and L. Hao, "Gamma-Ray Burst in a Molecular Cloud: Destruction of Dust and H2 and the Emergent Spectrum", *The Astrophysical Journal*, Vol. 569, Issue 2, pp. 780–791, April 2002.

219. Fruchter, A., J. H. Krolik, J. E. Rhoads, "X-Ray Destruction of Dust along the Line of Sight to $\gamma - Ray$ Bursts", *The Astrophysical Journal*, Vol. 563, pp. 597–610, December 2001.

220. Electromagnetic spectrum, http://chandra.harvard.edu/resources/em_radiation.html

221. Reif, F., Statistical Physics, McGraw-Hill Book Company, New York, p. 343, 1967.

222. Rybicki, G. B. and A. P. Lightman,Radiative Processes in Astrophysics, A Wiley-Interscience publication, pp. 15–167, 1979.

223. Larmor J., "On a dynamical theory of the electric and luminiferous medium", *Philosophical Transactions of the Royal Society*, Vol. 190, pp. 205–300, 1897.

224. Jackson, D., Classical Electrodynamics Third Edition, p. 666, 1925.

225. Longair, M.S., High Energy Astrophysics Volume 1, Cambridge University Press, pp. 86–101, 1992.

226. Inverse Compton Figure, http://heasarc.gsfc.nasa.gov/docs/xrayschool–2005/talks/smith_emissionIII.pdf

227. Blumental., G. R. and R. J. Gould, "Energy Loss of High-Energy Cosmic Rays in Pair-Producing Collisions with Ambient Photons", *Physical Review D*, Vol. 1, pp. 1596–1602, March 1970.

228. Attwood. D., Soft X-Rays and Extreme Ultraviolet Radiation: Principles and Applications, Cambridge University Press, pp. 5-420, 2007.

229. Osterbrock, D. E. and G. J. Ferland, Astrophysics of Gaseous Nebulae and Active Galactic Nuclei, University Science Books, p. 202, 2005.

230. Kutner, M. L., Astronomy A Physical Perpective second edition, Cambridge University Press, p. 240, 2003.

231. Schalen, C., "On the Value of $R = AVIEBV$", *Astronomy and Astrophysics*, Vol. 42, pp. 251, August 1975.

232. Brown, R. L. and Gould, R. J., "Interstellar absorption of cosmic X rays", Phys. Rev. D, Vol. 1, pp. 2252–2256, 1970.

233. Morrison,R. and D. McCammon, "Interstellar photoelectric absorption cross sections, 0.03-10 keV", *Astrophysical Journal*, Vol. 270, pp. 119–122, July 1983.

234. Anders, E., M. Ebihara, "Solar-system abundances of the elements", *Geochimica et Cosmochimica Acta*, Vol. 46, pp. 2363–2380, November 1982.

235. Cruddace, R., F. Paresce, S. Bowyer, M. Lampton, "On the opacity of the interstellar medium to ultrasoft X-rays and extreme-ultraviolet radiation", *The Astrophysical Journal*, Vol. 187, pp. 497–504, Feburary 1974.

236. Arnaud, K., B. Dorman, C. Gordon, "XSPEC Users Guide for version 12.5", http://heasarc.nasa.gov/xanadu/xspec/manual/manual.html, Section 6.3.29, Feburary 2009.

237. Arnaud, K. A., "XSPEC: The First Ten Years", *A.S.P. Conference Series of Astronomical Data Analysis Software and Systems V*, Vol. 101, p. 17., 1996.

238. XRT Spectral Simulation, http://heasarc.gsfc.nasa.gov/docs/swift/proposals/swift_xspec_sim.html

239. Evans, P. A., A. P. Beardmore, K. L. Page, K. L., L. G. Tyler, J. P. Osborne, M. R. Goad, P. T. O'Brien, L. Vetere, J. Racusin, D. Morris, et al., "An online repository of Swift/XRT light curves of $\gamma - ray$ bursts", *Astronomy and Astrophysics*, Vol. 469, pp. 379–385, July 2007.

240. Rodgers J. L. and W. A. Nicewander, "Thirteen ways to look at the correlation coefficient", *The American Statistician*, Vol. 42(1), pp. 59–66, Feburary 1988.

241. Roming, P. W. A., S. D. Hunsberger, J. A. Nousek, M. Ivanushkina, K. O. Mason, A. A. Breeveld, "The Swift Ultra-Violet/Optical Telescope (UVOT)", *American Institute of Physics (AIP) Conference Proceedings of the 30 Years of Discovery: Gamma-Ray Burst Symposium on Gamma-Ray Bursts*, Santa Fe, New Mexico, 8-12 September 2003, Vol. 727, pp. 651–654, New York, September 2004.

242. Swift Observational Process Time Table, http://heasarc.gsfc.nasa.gov/docs/swift /about_swift/mission_flow/observations.html

243. Burrows, D. N., J. E. Hill, G. Chincarini, G. Tagliaferri, S. Campana, A. Moretti, P. Romano, D. Malesani, J. L. Racusin, S. Kobayashi, et al., "Swift X-Ray Telescope and Very Large Telescope Observations of the Afterglow of GRB 041223", *The Astrophysical Journal*, Vol. 622, pp. L85–L88., April 2005.

244. Swift's X-Ray Telescope XRT, http://heasarc.gsfc.nasa.gov/docs/swift/about_ swift/xrt_desc.html

245. Burrows, D. N.; J. E. Hill, J. A. Nousek, A. A. Wells, A. D. Short, R. Willingale, O. Citterio, G. Chincarini, G. Tagliaferri, "Swift X-Ray Telescope", *SPIE Proceedings X-Ray and Gamma-Ray Instrumentation for Astronomy XI*, Vol. 4140, pp. 64–75, December 2000.

246. Hill, J. E., M. E. Zugger, J. Shoemaker, M. E. Witherite, T. S. Koch, L. L. Chou, T. Case, D. Burrows, N. David, "Laboratory x-ray CCD camera electronics: a test bed for the Swift X-Ray Telescope", *SPIE Proceedings X-Ray and Gamma-Ray Instrumentation for Astronomy XI*, Vol. 4140, pp. 87–98 December 2000.

247. Hill, J., D. Burrows, J. Nousek, A. Wells, J. Osborne, K. Mukerjee, G. Chincarini, G.Tagliaferri, S. Campana, "The Swift X-ray Telescope", *American Physical Society*, Meeting Id: APR04, Abstract No:S10.005, May 2004.

248. J. M. and F. J. Lockman, "H I in the Galaxy", *Annual Review of Astronomy and Astrophysics*, Vol. 28, pp. 215–261, 1990.

249. William H. P., P. F. Brian, A. T. Saul, T. V. William, Numerical Recipes in C: The Art of Scientific Computing Second Edition, Cambridge University Press, pp. 100-150, 1992.

250. Spearman, C., "The proof and measurement of association between two things", *American Journal Psychology*, Vol. 15, pp. 72–101, 1904.

251. Kendall, M., "A New Measure of Rank Correlation", *Biometrika*, Vol. 30, pp. 81–89, 1938.

252. Swift GRB Table, http://swift.gsfc.nasa.gov/docs/swift/archive/grb_table/

253. Campana, S., G. Tagliaferri, D. Lazzati, G. Chincarini, S. Covino, K. Page, P. Romano, A. Moretti, G. Cusumano, V. Mangano, et al., "The X-ray afterglow of the short gamma ray burst 050724", *Astronomy and Astrophysics*, Vol. 454, pp. 113–117, July 2006.

254. Cusumano, G., V. Mangano, G. Chincarini, A. Panaitescu, D. N. Burrows, V. La Parola, T. Sakamoto, S. Campana, T. Mineo, G. Tagliaferri, et al., "Swift observations of GRB 050904: the most distant cosmic explosion ever observed", *Astronomy and Astrophysics*, Vol. 462, pp. 73–80, January 2007.

255. Moretti, A., R. Margutti, F. Pasotti, A. P. Beardmore, S. Campana, G. Chincarini, S. Covino, O. Godet, C. Guidorzi, J. P. Osborne, et. al., "When GRB afterglows get softer, hard components come into play", *Astronomy and Astrophysics*, Vol. 478, pp. 409–417, Feburary 2008.

256. Butler N. R., "On the Early-Time X-Ray Spectra of Swift Afterglows. I. Evidence for Anomalous Soft X-Ray Emission", *The Astrophysical Journal*, Vol. 656, pp. 1001–1018, Feburary 2008.

257. Racusin, J. L., S. V. Karpov, M. Sokolowski, J. Granot, X. F. Wu, V. Pal'Shin, S. Covino, A. J. van der Horst, S. R. Oates, P. Schady, et al., "Broadband observations of the naked-eye $\gamma - ray$ burst GRB080319B", *Nature*, Vol. 455, pp. 183–188, September 2008.